

**ADSORPTIVE CHARACTERISTICS OF
AFLATOXIN B1 IN THE PRESENCE OF PURIFIED
CLINOPTILOLITE RICH MINERAL AND
LACTOBACILLUS PLANTARUM S2**

**A Thesis Submitted to
the Graduate School of Engineering and Sciences of
İzmir Institute of Technology
in Partial Fulfillment of the Requirements for the Degree of**

DOCTOR OF PHILOSOPHY

in Chemical Engineering

**by
Çisem BULUT ALBAYRAK**

**January 2012
İZMİR**

We approve the thesis of **Çisem BULUT ALBAYRAK**

Examining Committee Members:

Prof. Dr. Semra ÜLKÜ

Department of Chemical Engineering, İzmir Institute of Technology

Prof. Dr. Rengin ELTEM

Department of Bioengineering, Ege University

Prof. Dr. Fehime ÖZKAN

Department of Chemical Engineering, İzmir Institute of Technology

Assoc. Prof. Dr. Canan TARI

Department of Food Engineering, İzmir Institute of Technology

Assoc. Prof. Dr. Oğuz BAYRAKTAR

Department of Chemical Engineering, İzmir Institute of Technology

13 January 2012

Prof. Dr. Semra ÜLKÜ

Supervisor, Department of Chemical Engineering,
İzmir Institute of Technology

Prof. Dr. H. Şebnem HARSA

Supervisor, Department of Food Engineering,
İzmir Institute of Technology

Prof. Dr. Mehmet POLAT

Head of the Department of Chemical Engineering

Prof. Dr. R. Tuğrul SENGER

Dean of the Graduate School of
Engineering and Sciences

ACKNOWLEDGEMENTS

I would like to express my sincere gratitude to my adviser, Prof Dr. Semra Ülkü for her guidance, support, supervision and encouragement. I am also grateful to my co-advisor Prof. Dr. Şebnem Harsa for her valuable support during the research study. This project was supported by Turkish Government Planning Organization (Project No: IYTE-98 K 122130) and I am also thankful for their financial support. I would like to thank to Assoc. Prof. Dr. Canan Tarı , Assoc Prof. Dr. Oğuz Bayraktar, Prof. Dr. Fehime Özkan and Prof. Dr. Rengin Eltem for their valuable suggestions in thesis comitte.

I also thank to Prof. Dr. Rengin Eltem and Yüksel Gezgin for their valuable technical laboratory supports in the aflatoxin analyses part.

Special thanks to all members of Biochemical Engineering Research Laboratory and Zeolite Research Group. Especially, I would like to express my special thanks to Assist. Prof Dr. Güler Narin for her valuable contributions and discussions. Moreover, special thanks to Assist. Prof Dr. Ayben Top for her support.

Additionally, special thanks to my friends Burcu Okuklu, Zelal Polat, Berna Ülkü, Seda Genç, Seyhun Gemili, Koray Şekeroğlu, , Murat Molva ,Sevdiye Savrık, Başak Özer, Derya Baytak and Dildare Başalp for their friendships and all kinds of supports during my study.

Finally, my special thanks to my husband Hasan Basri Albayrak and my sweet baby girl, Maya Albayrak, for their valuable encouragement, patience and understanding. In addition, special thanks to my cousin Selda Mansour for her all kinds of supports. Lastly, but not leastly, I would like to express my intimate gratitude to my dear father and mother Yonis Bulut and Saadet Bulut and my brother Ali Bulut for their endless encouragements and love.

ABSTRACT

ADSORPTIVE CHARACTERISTICS OF AFLATOXIN B1 IN THE PRESENCE OF PURIFIED CLINOPTILOLITE RICH MINERAL AND *LACTOBACILLUS PLANTARUM* S2

The human diet contains a wide variety of natural carcinogens. Aflatoxin B1 (afB1) is the most toxic and most prevalent compound. Both probiotic lactic acid bacteria and clinoptilolite rich zeolite mineral have potential to eliminate this toxin. This study was planned in order to investigate adsorptive characteristics of afB1 by local purified clinoptilolite rich mineral (PNZ) and probiotic strains which were isolated from different natural sources (fermented cabbage, boza) in the present work. PNZ and isolated strains were characterized by using several physical, chemical and biological techniques. Adsorption characteristics of both probiotic lactobacilli and PNZ were investigated in simulated gastrointestinal solutions. The chosen probiotic strain was identified as *L. plantarum* .The studies indicated that, both *L. plantarum* S2 and PNZ can eliminate afB1 in the phosphate buffer solution. They are more effective when they were used together (45% for *L. plantarum* S2, 32% for PNZ, 86%for *L. plantarum* S2 and PNZ together). AfB1 adsorption equilibrium data were best represented by Sips isotherm model for PNZ, whereas by Langmuir isotherm model for *L. plantarum* S2. Thermodynamic studies implied that afB1 adsorption by mineral and *L. plantarum* S2 was physical adsorption. Experiments with different temperatures showed that afB1 adsorption by PNZ was exothermic but afB1 adsorption by lactobacilli was endothermic. Adsorption kinetics were analysed by diffusional models and reaction models for afB1 adsorption by PNZ mineral. Both film diffusion and /or intra particle diffusion were effective on adsorption kinetics depending on the experimental conditions (Temperature, pH, agitation speed, etc).

ÖZET

SAFLAŞTIRILMIŞ KLİNOPTİLOLİTÇE ZENGİN MİNERAL VE *LACTOBACİLLUS PLANTARUM* S2 VARLIĞINDA AFLATOKSİN B1'İN ADSORPTİF ÖZELLİKLERİ

İnsan beslenmesi çeşitli doğal kanserojenler içermektedir. Aflatoksin B1 (afB1) en zehirli ve en yaygın maddedir. Hem probiyotik laktik asit bakterileri hem de klinoptilolitçe zengin zeolit minerali bu toksini elemine etme potansiyeline sahiptir. Bu çalışma yöresel saflaştırılmış klinoptilolitçe zengin mineral (PNZ) ve bu çalışmada farklı doğal kaynaklardan (fermente lahana, boza) izole edilmiş probiyotik suşların afB1'i adsorbe etme özelliklerini araştırmak için planlanmıştır. Hem *L. plantarum* S2 hem de PNZ' nin adsorpsiyon özellikleri simüle gastrointestinal sıvılarda araştırılmıştır. Çalışmalar *L. plantarum*, S2 ve PNZ nin her ikisinin de fosfat tampon çözelti içinde afB1'i ortadan kaldırabilir olduğunu göstermiştir. Beraber kullanıldıklarında daha etkilidirler (*L. plantarum* S2 için 45% , PNZ için 32% , *L. plantarum* S2 ve PNZ birlikte 86%). AFB1 adsorpsiyon denge verileri klinoptilolitçe zengin mineral için Sips izoterm modeli ile temsil edilirken, *L. plantarum* S2 için Langmuir modeli tarafından temsil edilmiştir. Termodinamik çalışmalar PNZ' nin afB1 adsorpsiyonunun fiziksel adsorpsiyon olduğunu göstermiştir. Adsorpsiyon kinetiği difüzyon ve reaksiyon modelleri ile analiz edilmiştir, film difüzyonun ve parçacık içi difüzyonu deneysel koşullara (Sıcaklık, pH, karıştırma hızı, vb.) bağlı olarak adsorpsiyon kinetiği üzerinde etkili olmuştur.

*Dedicated to
My Father
Yonis BULUT*

TABLE OF CONTENTS

LIST OF FIGURES.....	xii
LIST OF TABLES	xvii
CHAPTER 1. INTRODUCTION	1
CHAPTER 2. PROBIOTIC LACTIC ACID BACTERIA.....	3
2.1. Definition.....	3
2.2. Selection Criteria for Probiotics.....	5
2.3. Probiotic <i>Lactobacillus</i> Isolation and Identification	6
2.4. Beneficial Health Effects of Probiotic Lactobacilli	9
2.5. Mechanism of Probiotic Activity.....	13
CHAPTER 3. NATURAL ZEOLITES	15
3.1. Structure of Zeolites	16
3.2. Properties of Zeolites.....	18
3.3. Natural Zeolites and Clinoptilolite rich Natural Zeolite.....	20
3.4. Natural Zeolites in Health Studies	21
3.4.1. Effect on Aflatoxicosis	22
3.4.2. Removal of Heavy Metals and Organopoisinin	23
3.4.3. Antimicrobial Effects.....	24
3.4.4. Effects on Gastrointestinal Disorders	24
3.4.5. Immunological Consequences.....	25
3.4.6. Effects on Tumor Growth	25
3.4.7. Toxicology of Clinoptilolite.....	26
3.4.8. Drug Studies.....	27
3.4.9. Other Health Related Cases	29
CHAPTER 4. AFLATOXINS	32
4.1. Structure.....	32
4.2. Toxicity and Carcinogenicity of Aflatoxins.....	34

CHAPTER 5. ADSORPTION PHENOMENA.....	37
5.1. Introduction to Adsorption	37
5.1.1. Physical Adsorption.....	38
5.1.2. Chemical Adsorption.....	39
5.2. Adsorption Equilibria	39
5.3. Adsorption Isotherm models.....	39
5.3.1. Langmuir Model.....	40
5.3.2. Freundlich Model	41
5.4. Factors Affecting the Adsorption.....	41
5.5. Adsorption Mechanism and Kinetics	43
5.6. Adsorption Kinetic Models.....	44
5.6.1. Adsorption Reaction Models	44
5.6.2. Adsorption Diffusion Models	46
5.6.2.1. External Film Diffusion	47
5.6.2.2. Particle Diffusion.....	49
5.7. Thermodynamic Properties.....	55
5.8. Adsorption of Aflatoxins by Mineral.....	59
5.9. Adsorption of Aflatoxins by Probiotic Lactic Acid Bacteria	60
 CHAPTER 6. MATERIALS AND METHODS.....	 64
6.1. Materials	64
6.1.1. Chemicals.....	64
6.1.2. Samples Used for Probiotic sources.....	64
6.1.3. Reference Strains.....	64
6.1.4. Natural Zeolite Samples.....	65
6.2. Methods	65
6.2.1. Isolation and Characterization of Organism	65
6.2.1.1. Isolation of Lactobacilli strains from Different Sources.....	65
6.2.1.2. Purification and Preliminary Identification.....	66
6.2.1.3. Catalase Test.....	66
6.2.1.4. Microscopic Examination of the Cell Morphology	66
6.2.1.5. Gram Status	67
6.2.1.6. Long Term Preservation of the Isolates	68

6.2.1.7. Gas Production from Glucose	68
6.2.1.8. Growth at Different Temperatures.....	68
6.2.1.9. Growth at Different Salt Concentrations.....	68
6.2.1.10. Arginine Hydrolyses	69
6.2.1.11. Species Level Identification	69
6.2.2. Test for Probiotic Criteria	69
6.2.2.1. Acid Tolerance.....	69
6.2.2.2. Bile Salt Tolerance.....	70
6.2.2.3. Pancreatic Enzyme Tolerance	70
6.2.2.4. Susceptibility to Antibiotics	70
6.2.3. Characterization of Bacterial Surface.....	71
6.2.3.1. Hydrophobicity	71
6.2.3.2. Surface Charge.....	71
6.2.4. Preparation of Natural Zeolites for Health Studies	72
6.2.4.1. Purification Steps of Natural Zeolites.....	72
6.2.4.2. Preparation of Homogenized Representative PNZ.....	73
6.2.5. Characterization of Purified Natural Zeolite(PNZ).....	73
6.2.5.1. Topographic and Microstructural Examination.....	74
6.2.5.2. Particle Size Distribution Measurement.....	74
6.2.5.3. Mineralogy and Crystallinity of the samples.....	74
6.2.5.4. Thermal analysis	75
6.2.5.5. Pore Volume and Surface Area Analysis.....	75
6.2.5.6. Infrared Spectroscopy	75
6.2.5.7. Zeta-potential Measurements	75
6.2.5.8. Analysis of Major Elements by Inductively Coupled Plasma Atomic Emission Spectroscopy(ICP-AES)	76
6.2.5.9. Minor and Trace Element Analysis by Inductively Coupled Plasma Mass Spectroscopy(ICP-MS).....	76
6.2.6. Aflatoxin Adsorption Experiments.....	77
6.2.6.1. Aflatoxin standards and HPLC quantification	81
 CHAPTER 7. RESULTS AND DISCUSSION	 82
7.1. Isolation and Characterization of the Probiotic Candidates	82
7.1.1. Isolation of Lactobacilli	82

7.1.2. Purification and Preliminary Identification	83
7.1.3. Identification at Species Level	87
7.1.4. Probiotic Properties	88
7.1.5. Characterization of bacterial surface	90
7.2. Purification and Characterization of Clinoptilolite Rich Mineral.....	92
7.2.1. Purification of the Natural Zeolite	92
7.2.2. SEM Examination Results	95
7.2.3. Particle Size Distribution	98
7.2.4. IR Absorption Results.....	99
7.2.5. Surface Area Analysis Results	100
7.2.6. Thermal Gravimetric Analysis (TGA)	102
7.2.7. Elemental Analysis of Clinoptilolite rich PNZ	104
7.2.7.1. Major Element Analysis.....	104
7.2.7.2 Minor and Trace Element Analysis	105
7.2.8. Surface Charge Measurements of the PNZ.....	108
7.3. The Results of the Adsorption Experiments.....	110
7.3.1. Adsorption Experiments with only Clinoptilolite Rich Mineral.....	110
7.3.1.1. Adsorption Equilibrium and Adsorption Isotherms.....	110
7.3.1.2. Effects of Experimental Parameters on Adsorption	120
7.3.2.1.1. Analysis of Experimental Uptake Curves.....	120
7.3.1.3. Thermodynamic Parameters.....	129
7.3.1.4. Adsorption Mechanism and Kinetic Models.....	131
7.3.1.4.1. Analyzing the Adsorption Kinetic Data by Diffusional Models.....	132
7.3.1.4.2. Analyzing the Adsorption Kinetic Data by Reaction Models.....	156
7.3.2. Adsorption Experiments with only Probiotic Bacteria	161
7.3.2.1. Adsorption Equilibrium and Adsorption Isotherms.....	161
7.3.2.2. Parametric Study of afB1 Adsorption by <i>L. plantarum</i> S2	163
7.3.3. Adsorption Experiments by PNZ and <i>L plantarum</i> S2 (together).....	172

CHAPTER 8. CONCLUSION.....	178
REFERENCES.....	180
APPENDICES	
APPENDIX A CHEMICALS.....	194
APPENDIX B. TEST MEDIA RECIPES.....	196
APPENDIX C. HPLC OPERATION SPECIFICATIONS.....	199
APPENDIX D. CALIBRATION CURVES.....	200

LIST OF FIGURES

<u>Figure</u>	<u>Page</u>
Figure 2.1. The dominant microflora in the adult humangastrtointesnal system.....	4
Figure 3.1. Primary and secondary building units of zeolite structure	16
Figure 3.2. (a) Model framework for structure of clinoptilolite (b) Orientation of clinoptilolite structure.....	17
Figure 3.3. Biochemical effects of zeolites	22
Figure 4.1. Chemical structues of majojr dietary aflatoxins(aflatoxin B1,G1, M1 and aflatoxins B2 , G2 and M2).....	32
Figure 7.1. Representative optical microscopy picture of the isolated <i>Lactobacillus</i> strains	85
Figure 7.2. Representative Scanning Electron Microscopy picture of the isolated <i>Lactobacillus</i> strains.	86
Figure 7.3. Antibiotic sensitivities of the isolates and some reference strains.....	89
Figure 7.4. Antibiotic sensitivities of the two Isolated strains(L1 and L4) of <i>L.</i> <i>plantarum</i> which can resistant to gastric environment and bile salts	90
Figure 7.5. The variation of zeta potential of isolated <i>Lactobacillus</i> strain in the different pH values.	91
Figure 7.6. XRD diagram of mineral reference of Idaho	93
Figure 7.7. XRD diagram of mineral reference of California	94
Figure 7.8. X-ray powder diffractograms of the reference clinoptilolite mineral (Idaho) and the different fractions in the purification study	94
Figure 7.9. Elemental analysis results of different fractions during purification	95
Figure 7.10. Scanning electron micrographs of clinoptilolite rich natural zeolite before purification.	96
Figure 7.11. Scanning electron micrographs of reference mineral of clinoptilolite-rich natural zeolite	97
Figure 7.12. Scanning electron micrographs (SEM) of purified local type clinoptilolite- rich natural zeolite mineral.(PNZ).....	97
Figure 7.13. Particle size distributions of purified local type clinoptilolite-rich natural zeolite.(PNZ) and reference mineral of Idaho.....	98
Figure 7.14. Infrared spectra of the reference and local type minerals.	99

Figure 7.15. N ₂ adsorption and desorption isotherms of reference mineral of Idaho and local type mineral (-196 °C).....	100
Figure 7.16. Pore size distribution of the purified local type clinoptilolite-rich natural zeolite.(PNZ) and reference mineral of Idaho.....	102
Figure 7.17. TGA curves of PNZ and refernce mineral of Idaho	103
Figure 7.18. Variations in the zeta potential of zeolite (2.5 mg/ml) at different pH values (potassium phosphate buffer)	109
Figure 7.19 Effect of temperature on adsorption isotherms. (T: 15 °C, 25 °C and 37 °C. agitation speed: 130 rpm, S/L:25mg/10 ml, working solution: PBS pH 7.3, particle size: 8 µm).	111
Figure 7.20. Uptake curves at 37 °C (agitation speed: 130 rpm, S/L:25mg/10 ml, working solution: PBS pH 7.3, particle size: 8 µm).....	111
Figure 7.21. Uptake curves at 25 °C.(agitation speed: 130 rpm, S/L:25mg/10 ml, working solution: PBS pH 7.3, particle size: 8 µm).....	112
Figure 7.22. Uptake curves at 15 °C.(agitation speed: 130 rpm, S/L:25mg/10 ml, working solution: PBS pH 7.3, particle size: 8 µm).....	112
Figure 7.23. Effect of pH on adsorption isotherms. (T:37 °C, co= agitation speed: 130 rpm, S/L:25mg/10 ml, working solution: PBS, particle size: 8 µm).	113
Figure 7.24. Uptake curves for pH 3.0. (T: 37 °C, agitation speed: 130 rpm, S/L:25mg/10 ml, working solution: PBS ,particle size: 8 µm).	113
Figure 7.25. Uptake curves for pH 5.0. (T: 37 °C, agitation speed: 130 rpm, S/L:25mg/10 ml, working solution: PBS ,particle size: 8 µm).	114
Figure 7.26. Experimental isotherm data and isotherm models for afB1 adsorption by PNZ (T:37°C, agitation speed: 130 rpm, S/L:25mg/10 ml, working solution: PBS pH 7.3, particle size: 8 µm).....	117
Figure 7.27. Experimental isotherm data and isotherm models for afB1 adsorption by PNZ(T:25 °C, agitation speed: 130 rpm, S/L:25mg/10 ml,working solution: PBS pH 7.3, particle size: 8 µm)	117
Figure 7.28. Experimental isotherm data and isotherm models for afB1 adsorption by PNZ (T:15 °C. agitation speed: 130 rpm. S/L:25mg/10 ml, working solution: PBS pH 7.3, particle size: 8 µm).....	118
Figure 7.29. Effect of initial adsorbate concentration on adsorption kinetics of afB1 by PNZ (T:37 °C, agitation speed: 130 rpm, S/L:25mg/10 ml, working solution: PBS pH 7.3, particle size: 8 µm).	121

Figure 7.30. Effect of solid liquid ratio on adsorption kinetics of afB1 by PNZ (T:37°C, c ₀ = 0.25 ppm afB1, agitation speed: 130 rpm, S/L:12.5-100 mg/10 ml, working solution: PBS pH 7.3, particle size: 8 μm)	122
Figure 7.31. Effect of solid liquid ratio on adsorbed amount at equilibrium and on the total adsorbed amount of afB1 (T:37°C, c ₀ = 0.25 ppm afB1, agitation speed: 130 rpm, S/L:12.5-100mg/10 ml, working solution: PBS pH 7.3, particle size: 8 μm)	123
Figure 7.32. Effect of particle size on adsorption kinetics of afB1 by PNZ (T:37°C, c ₀ = 0.25 ppm afB1, agitation speed: 130 rpm, S/L:25 mg/10 ml, working solution: PBS pH 7.3)	124
Figure 7.33. Effect of agitation speed on adsorption kinetics of afB1 by PNZ. (T:37°C, c ₀ = 0.25 ppm afB1, S/L:25 mg/10 ml, working solution: PBS pH 7.3, particle size: 8 μm)	125
Figure 7.34. Effect of solution pH on adsorption kinetics of afB1 by PNZ (T:37°C, c ₀ = 0.25 ppm afB1, agitation speed: 130 rpm, S/L:25 mg/10 ml, working solution: PBS particle size: 8 μm)	127
Figure 7.35. Effect of temperature on adsorption kinetics of afB1 by PNZ (T:15°C-37°C, c ₀ = 0.25 ppm afB1, agitation speed: 130 rpm, S/L:25 mg/10 ml, working solution: PBS pH 7.3, particle size: 8 μm).....	128
Figure 7.36. Change of the Langmuir-Freundlich isotherm parameter (K _{LF}) with the adsorption temperature (T: 15 °C, 25 °C and 37 °C, agitation speed: 130 rpm, S/L:25mg/10 ml, working solution: PBS pH 7.3, particle size: 8 μm).	130
Figure 7.37. Arrhenious plot (lnk ₂ vs 1/T and lnk _d vs 1/T) Experiment conditions: T:15 °C,25 °C, 37 °C, c _i = 0.25 ppm afB1, agitation speed: 130 rpm,S/L:25 mg/10 ml, working solution: PBS pH 7.3, particle size: 8 μm.)	131
Figure 7.38. Analysing of kinetic data by Boyd model for different initial concentrations (conditions : c ₀ =0.25-2 ppm afB1, 25 mg PNZ10ml of the PBS pH 7.3 (S/L=1/400), 130 rpm.37 °C, particle size 8μm).....	134
Figure 7.39. Analysing of kinetic data by Boyd model for different experimental parameters (a)Particle size (b)agitation speed (c)temperature (d) PH.....	137
Figure 7.40. Mathew Weber Plot for different afB1 initial concentrations (conditions: c ₀ =0.25-2 ppm afB1 ,25 mg PNZ 10ml of the PBS pH 7.3 (S/L=1/400, 130 rpm,37 °C, particle size 8μm)	139

Figure 7.41. Mathew weber plot for different experimental parameters (a) Particle size (b) agitation speed (c) temperature and (d) pH	140
Figure 7.42. Analyzing external mass transfer coefficient by Mathew-Weber plot for different initial afB1 concentrations ($c_0=0.25-2$ ppm, 25 mg PNZ 10ml of the PBS pH 7.3, (S/L=1/400), 130 rpm, 37 °C, particle size 8 μ m)	141
Figure 7.43. Weber Morris Plot for different initial concentrations (exp conditions : $c_0=0.25-1$ ppm afB1, 25 mg PNZ, 10ml of the PBS pH 7.3, (S/L=1/400), 130 rpm, 37 °C)	145
Figure 7.44. Weber Morris plot for different experimental parameters a) Particle size b) agitation speed c) temperature and d) pH	146
Figure 7.45. Analyzing diffusion constant by Weber Morris plot for different initial afB1 (exp conditions : $c_i=0.25-1$ ppm, 25 mg PNZ 10ml of the PBS pH 7.3 (S/L=1/400), 130 rpm, 37 °C)	147
Figure 7.46. Relationship of intra particle rate constant with square root of particle diameter	149
Figure 7.47. Representative comparison of Boyd (conditions : $c_i=0.25$ ppm afB1 25 mg PNZ 10ml of the PBS pH 7.3 (S/L=1/400). 130 rpm, 37 °C. particle size 8 μ m)	151
Figure 7.48. Boyd plot for different initial afB1 concentrations (exp conditions : $c_i=0.25-2$ ppm afB1, 25 mg PNZ, 10ml of the PBS pH 7.3 (S/L=1/400), 130 rpm, 37 °C, particle size 8 μ m)	152
Figure 7.49. Boyd plot for different experimental parameters a) Particle size b) agitation speed c) temperature and d) pH)	153
Figure 7.50. First order Kinetic plot for the adsorption of afB1 by zeolite ($C_0:0.25- 1.0$ ppm, 37 °C. 130 rpm, S/L: 25 mg/10 ml, pH 7.3, particle size: 8-10 μ m)	156
Figure 7.51. Pseudo second order Kinetic plot for the adsorption of afB1 onto zeolite ($C_0: 0.25- 1.0$ ppm, 37 °C, 130 rpm, S/L: 25 mg/10 ml, pH 7.3. particle size: 8- 10 μ m)	158
Figure 7.52. Transmittance infrared spectra of the PNZ. (a) After adsorption afB1 (b) Original clinoptilolite rich PNZ	160
Figure 7.53. Uptake curves of afB1 adsorption by <i>L. plantarum</i> S2 ($C_0:0.06-0.25$ ppm, 37 °C, 130 rpm, S/L: 10^{10} cell/10 ml, pH 7.3)	161

Figure 7.54. Adsorption isotherms of afB1 by <i>L. plantarum</i> S2 (C_0 :0.06-0.5 ppm,37°C, 130 rpm, S/L:10 ¹⁰ cell /10 ml, pH7.3	162
Figure 7.55. Effect of viability of bacteria on uptake curves of afB1 adsorption by <i>L.plantarum</i> S2	164
Figure 7.56.Effect of bacteria type on afB1 removal (c_0 =0.25ppm,130 rpm, S/L=10 ¹⁰ cell/10ml, pH7.3).....	165
Figure 7.57. Effect of organism amount on uptake curves (10 ml PBS pH 7.3, 130 rpm agitation speed , 37 °C, c_0 =0.25 ppm.).....	166
Figure 7.58. Effect of bacteria amount on total afB1 adsorbed amount (10 ml PBS pH 7.3,130 rpm agitation speed , 37 °C, c_0 =0.25 ppm	167
Figure 7.59. Effect of bacteria amount on afB1 adsorbed per bacteria (10 ml PBS pH 7.3,130 rpm agitation speed , 37 °C, c_0 =0.25 ppm).....	167
Figure 7.60. Effect of agitation speed on afB1 adsorbed per bacteria (10 ml PBS pH 7.3 , 37 °C, c_0 =0.25 ppm)	168
Figure 7.61. Effect of pH on uptake curves (10 ml PBS pH 7.3,130 rpm agitation speed , 37 °C, c_0 =0.25 ppm).....	168
Figure 7.62. Effect of temperature on adsorption isotherms (10 ml PBS pH 7.3, 130 rpm agitation speed , c_0 =0.25 ppm)	169
Figure 7.63. Effect of temperature on uptake curves (10 ml PBS pH 7.3,130 rpm agitation speed , 37 °C, c_0 =0.25 ppm).....	170
Figure 7.64. Van't Hoff's plot for afB1 adsorption by bacteria.	171
Figure 7.65. Effect of presence of PNZ with probiotic bacteria together on adsorbed amounts (25 mg PNZ+10 ¹⁰ cell/10 ml PBS pH 7.3,130 rpm agitation speed ,37 °C, c_0 =0.25 ppm.....	172
Figure 7.66. Effect of initial afB1 concentration on uptake curves (25 mg PNZ+10 ¹⁰ cell/10 ml PBS pH 7.3,130 rpm agitation speed , 37 °C, c_0 =0.25 ppm)....	175
Figure 7.67. Effect of temperature on uptake curves (25 mg PNZ+10 ¹⁰ cell/10 ml PBS pH 7.3,130 rpm agitation speed , c_0 =0.25 ppm).....	176
Figure 7.68. Effect of pH on uptake curves (25 mg PNZ+10 ¹⁰ cell/10 ml PBS pH 7.3,130 rpm agitation speed , c_0 =0.25 ppm)	177

LIST OF TABLES

<u>Table</u>	<u>Page</u>
Table 2.1. Some of lactic acid bacteria used as probiotics for human consumption ...	4
Table 2.2. Selection criteria for probiotic microorganisms.	6
Table 2.3. Recent studies on isolation of probiotics and criteria	7
Table 2.4. Classification schema for Lactobacilli species.....	8
Table 3.1. Channel characteristics and cation sites in clinoptilolite	18
Table 3.2. Properties of Commercial Adsorbents.....	19
Table 3.3. Summary of Clinoptilolite Characteristics	21
Table 4.1. Some chemical end structural properties of afB1	33
Table 5.1. Comparison of physisorption and chemisorption.....	38
Table 5.2. Recent thermodynamic studies.....	57
Table 5.3. Studies on adsorption of AfB1 by several clay minerals	60
Table 5.4. Some of the studies on binding of aflatoxins by lactic acid bacteria.....	63
Table 6.1. Operating parameters, temperature programs, and digestion reagents.....	77
Table 6.2. Experimental conditions of the various kinetic adsorption experiments for the removal of afB1 at constant volume of toxin solution.....	79
Table 6.3. Experimental conditions of the various kinetic adsorption experiments for the removal of afB1 by probiotic lactobacilli alone at constant volume of toxin solution.....	80
Table 6.4. Experimental conditions of the various kinetic adsorption experiments for the removal of afB1 at constant volume of toxin solution.....	80
Table 7.1. Summarized isolation data for lactobacilli organism	83
Table 7.2. Summarized elimination, purification data.....	84
Table 7.3. Physiochemical and biochemical identification results	87
Table 7.4. The results of the resistance of the isolates the pH.....	88
Table 7.5. Screening results for pancreatic enzyme and bile salt tolerance	89
Table 7.6. Adhesion properties to hydrocarbons	91
Table 7.7. Qualitative analysis results of by search-match	92
Table 7.8. Purity determination results.....	95
Table 7.9. Particle size results.....	98
Table 7.10. Surface area and pore properties of PNZ and reference mineral.....	101

Table 7.11. Percent weight losses that indicate the various water contents	103
Table 7.12. Major elements in oxide form for clinoptilolite richPNZ and reference mineral.....	105
Table 7.13. Guide-value and maximum admissible concentration of selected elements in drinking waters	106
Table 7.14. Minor and trace element concentration determined by microwave assisted ICP-MS technique using two different acid digestion	107
Table 7.15. Estimated toxic elements and safe/tolreable exposure levels.....	108
Table 7.16. Applied adsorption isotherm models and the determination of their constants.....	115
Table 7.17. Comparison of applied adsorption isotherm models.. ..	116
Table 7.18. Henry’s modeling of adsorption isotherm for different pH’s.....	118
Table 7.19. Thermodynamic parameters for afB1 adsorption on PNZ.....	130
Table 7.20. Analysing the External Film Mass Transfer and Skin resistance.....	135
Table 7.21. Analyzing the External Film Mass Transfer by Mathew-Weber Model ..	143
Table 7.22. Analysing the kinetic data by Weber-Morris Model	148
Table 7.23. Analysing the kinetic data by Boyd Model.....	154
Table 7.24. Kinetic data analysis using first order model	157
Table 7.25. Analyzing the kinetic data by Pseudo Second order Model.....	159
Table 7.26. Comparison of applied adsorption isotherm models	163
Table 7.27. Some of the studies on binding of Aflatoxins by Lactic Acid Bacteria....	165
Table 7.28. Thermodynamic parameters for afB1 adsorption on <i>Lactobacillus plantarum</i> S2	172
Table 7.29. Viable organism numbers during time Exp 1 g NZ / 9ml cell suspension in PBS pH 7.3.....	173
Table 7.30. Viable organism numbers during time.....	174
Table 7.31. Change in afB1 removal percentages with respect to initial afB1 concentration	175

CHAPTER 1

INTRODUCTION

Although Turkey is the origin of lactic acid bacteria fermented foods since ancient times probiotic lactic acid bacteria has not yet been developed in the industry. Fermented foods are one of the main sources for developing new probiotic strains. In recent times, there have been several limited probiotic studies that indicate our probiotic potential.

In order to introduce the probiotic concept, it is useful to give information about the intestinal system of the human. The intestinal microbial population is a dynamic ecosystem of high complexity, consisting of an estimated number of that around 10^{14} microorganisms including more than 400 bacterial species (Isolouri and Salminen, 2004). It plays a vital role by providing the host with enzymes necessary for assimilation and/or synthesis of certain nutrients, as well as in detoxification of harmful dietary compounds. Aflatoxins are among the harmful toxic compounds that can be eliminated by probiotics. Strains of *Lactobacillus* spp. exist naturally in the human intestine and these strains are used for development of probiotics in general. It is known that our traditional fermented foods are rich sources of this type of *Lactobacillus* strains. When fermented foods like yogurt, cheese, and fermented vegetables are consumed, it helps balance our intestinal ecosystem and has additional beneficial health effects.

It is known that some toxins can be eliminated by zeolites, as well. Zeolites are crystalline hydrated aluminosilicates having a fine network of structural cavities. They have found various applications as adsorbents, ion exchangers and catalysts in industry, agriculture, veterinary medicine, sanitation and environmental protection. In recent years, the use of natural and synthetic zeolites in medical applications has increased due to biological properties, and long-term physical chemical stability in biological environment. Natural zeolite clinoptilolite has been reported to be nutritionally an inert adsorbent and non-toxic to animals (Papaioannou et al., 2002). This part was explained in detail in Chapter 3.

When probiotic lactic acid bacteria and natural zeolites were considered together, some common properties were noticed in the literature. One of them is the binding of aflatoxins and this feature is very important for health studies. Additionally, some heavy metals like cadmium, arsenic, lead and mercury that are harmful to humans can be eliminated by both zeolites and probiotics. The other common property is that both of them can interact in different ways with nitric oxide gases. This characteristic has also significance for health studies.

By considering these findings and ideas, the aims of the thesis were constructed. Isolation of potential probiotic lactobacilli from natural sources and investigation of interaction with zeolites in simulated gastrointestinal solutions were planned. The purification and detailed characterization were aimed for the zeolites in order to provide checking the material for health applications and understand some interactions such as adsorption behavior. The natural zeolite purification studies were conducted to develop material with a high purity for medical applications and these purified materials were characterized. Both probiotic lactobacilli and natural zeolite have ability to bind aflatoxin B1 (afB1) and the thesis research was focused on this property. The adsorption behavior of afB1 by purified natural clinoptilolite rich mineral was investigated and the adsorption phenomena was discussed in detail to provide an explanation about the mechanism. The binding ability of probiotic lactobacilli isolates was also studied. It was considered that the eliminating of afB1 in the presence of both lactobacilli organisms and natural zeolite can provide new research areas in health studies.

CHAPTER 2

PROBIOTIC LACTIC ACID BACTERIA

2.1. Definition

The term probiotic was introduced by Lilly and Stillwell (1965) to describe substances produced by one microorganism that stimulated the growth of other microorganisms. Probiotics have been defined in many different ways, depending on understanding of the mechanisms of their effects on the health and well being of humans. The most common definition currently used is that of Fuller (1989): *Probiotics are live microbial feed supplements which beneficially affect the host animal by improving its intestinal microbial balance.* Havenaar and Huis in't Veld (1992) have expanded the definition to include food and nonfood use and the use of mono and mixed cultures. Recently a European expert group proposed a definition that also included mechanisms not mediated by microflora change (Sanders, 2003).

It is obvious that the common definition suggests that safety and efficacy of probiotics have to be demonstrated for each strain and each product. Selected strains, mainly belonging to the genera *Lactobacillus* and *Bifidobacterium*, are increasingly being used as probiotics (Table 2.1.). After ingestion they must overcome biological barriers, including acid in the stomach and bile in the intestine, to reach their place of action in order to exert their health-promoting effects. The intestine's normal microbiota is as yet an unexplored organ of host defense. Although bacteria are distributed throughout the intestine, the major concentration of microbes and metabolic activity is found in the large intestine. The mouth harbours a complex microbiota consisting of facultative and strict anaerobes including streptococci, Bacteroides, lactobacilli and yeasts. The upper bowel is sparsely populated, and from the ileum on bacterial concentrations gradually increases, reaching 10^{11} – 10^{12} colony-forming units (CFU)/g in the colon (Figure 2.1). Up to 500 species of bacteria may be present in the adult human large intestine; it has been estimated that bacteria account for 35–50% of the volume of the contents of the human colon (Isolauri and Salminen, 2004).

Table 2.1. Examples of lactic acid bacteria used as probiotics for human use
(Source: Fooks et al., 1999)

Lactobacilli	Bifidobacteria	Streptococci	Enterococci
<i>L. delbrueckii</i> subsp. <i>bulgaricus</i>	<i>B. bifidum</i>	<i>S. thermophilus</i>	<i>E. faecalis</i>
<i>L. acidophilus</i>	<i>B. longum</i>		<i>E. faecium</i>
<i>L. rhamnosus</i>	<i>B. breve</i>		
<i>L. reuteri</i>	<i>B. Infantis</i>		
<i>L. casei</i>			

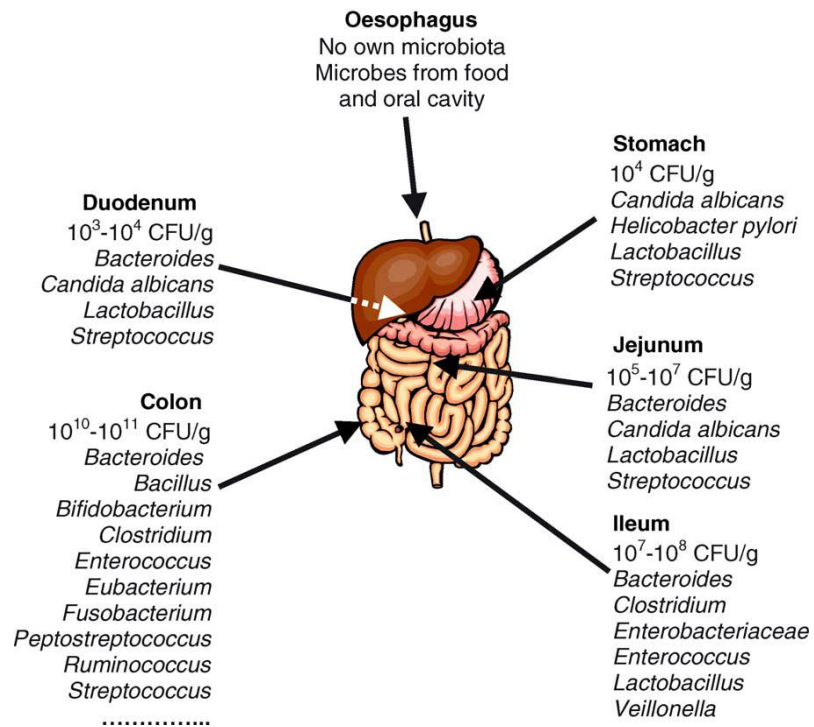


Figure 2.1. The dominant microflora in the adult human gastrointestinal system
(Source: Isolauri and Salminen, 2004).

To produce therapeutic benefits, a sufficient number of viable microorganisms must be present throughout the entire shelf life of the product. However, these organisms often show poor viability in market preparations (Gueimonde and Salminen, 2006). Acting either themselves or by influencing the host flora, probiotics may enhance various defense mechanisms, modulate innate and adaptive immunity, eliminate toxins, carcinogens and pathogens, release antioxidants and stimulate gastrointestinal motility. The molecular mechanisms governing these activities are currently the subject of intense investigation. It seems clear that both agents secreted by metabolically active viable probiotics (bactericins, short-chain fatty acids and peptides) and components from nonviable bacteria (DNA, protein constituents) can mediate protective pathways, but for many of these effects the exact mechanism of action still remains to be elucidated.

2.2. Selection Criteria for Probiotics

A potentially successful probiotic strain is expected to have several desirable properties in order to be able to exert its beneficial effects. The selection criteria that have been considered to be relevant for any potential probiotic microorganism are listed in Table 2.2. Because of their general importance, some of these selection criteria will be discussed in more detail from a mechanistic viewpoint. Depending on the desired outcome, a probiotic may need to have additional properties such as cholesterol metabolism, bioavailability of vitamins and minerals, faecal carcinogen and mutagen levels, immune response, coaggregation with pathogens. However, a potential probiotic does not need to fulfill all such selection criteria.

Table 2.2. Selection Criteria for Probiotic Microorganisms
(Source: Ouwehand et al., 1999)

Probiotic Strain Properties	Remarks
Human origin, if intended for human use	May be important for species-dependent health effects although, for example, the human probiotic <i>Saccharomyces boulardii</i> is not of human origin.
Acid and bile stability	Important for oral administration, may not be relevant for other applications; for survival through the intestine, retaining cell integrity, maintaining adhesiveness and metabolic activity.
Adhesion to mucosal surfaces	Immune modulation, competitive exclusion of pathogens, prevention of pathogen adhesion, transient colonization
Safe for food and clinical use	Accurate strain identification and characterization. Documented safety. No degradation of intestinal mucus. No invasion.
Clinically validated and documented health effects	Dose-response data for minimum effective dosage for each particular strain and in different products. Double blind, placebo-controlled, randomized studies.
Good technological properties	Strain stability, phage resistance, survival in product (if viable organisms are required), culturable at large scale, no negative effect on product flavour, oxygen resistance.

2.3. Probiotic *Lactobacillus* Isolation and Identification

Several probiotic studies were summarized in Table 2.3. and selection criteria of probiotic strains were presented. Martin et al. (2006) reported that *Lactobacillus salivarius* is considered as one of the potential probiotic bacteria and can be found in a number of commercial probiotic products. They had originally isolated this strain from feces of a one month old breast fed and they investigated if this specific strain was present in breast milk of the respective mother. RAPD and PFGE analysis revealed the presence of the strain *L. salivarius* CECT 5713 in this biological fluid.

Todarav et al. (2007) studied on the probiotic properties of the strains from Boza. Boza is a traditional beverage produced from cereals fermented with lactic acid bacteria of the genera *Lactobacillus*, *Lactococcus*, *Pediococcus*, *Leuconostoc* and Yeast. They concluded that Boza is a rich source of probiotic lactic acid bacteria. They

reported that all strains survived conditions simulating the gastrointestinal tract and produced bacteriocins active against a number of pathogen.

Table 2.3. Recent studies on different sources of probiotics and screening criteria

Bacteria	Source	Screening Criteria	Reference
<i>L. salivarius</i> CECT 5713	Feces of a one-month-old breast-fed infant	Antimicrobial spectrum Production of bacteriocin Production of hydrogen peroxide Production of lactic acid Survival on gastrointestinal passage Adherence to HT-29 and Caco-2 cells Degradation of gastric mucin	Martin et al., 2006
<i>Lactobacillus</i> spp.	Traditional fermented milk products and children's faeces	Resistance to gastrointestinal conditions Screening for antagonistic activity Bile salt hydrolase activity Production of β -galactosidase Determinations of antibiotic resistance	Pinto et al., 2006
<i>L. plantarum</i>	Fermented green olive	Testing for resistance to antibiotics Bile tolerance Lactic acid production Acidifying activity Tolerance to acidic pH values Proteolytic activity Exopolysaccharide production Haemolytic activity	Mourad and Nour-Eddine et al., 2006
<i>L. gasseri</i> , <i>L. fermentum</i> , <i>L. vaginalis</i> , <i>L. reuteri</i> <i>L. salivarius</i>	Human stomach	Antimicrobial activity, Acid bile tolerance Bile tolerance	Ryan et al., 2008
<i>Lactobacillus</i> spp.	Regional yogurts	NaCl Tolerance Quantification of Organic Acid Bile Tolerance and Gastric juice Tolerance Sensitivity to Antibiotic	Hoque et al., 2010

In traditional identification, most commonly used characteristics are morphology, staining reactions, nutritional requirements, cell wall chemistry, ability to use different energy sources, fermentation byproducts, gas requirements, temperature and pH tolerance, antibiotic sensitivity, pathogenicity, immunological characteristics and habitat (Morata et al., 1999). Some of these characters are used to identify specific bacterium or a group of bacteria but the difficulty here is to determine which attribute should be used for the identification of a given organism. In the following table some discriminative characteristics of Lactobacilli species were presented.

Table 2.4. Classification schema for Lactobacilli species.
(Source: Nair and Surendran, 2004)

<i>Lactobacillus</i> spp.	Morphology	Growth at			Acid and gas from glucose	NH ₃ from arginine	Sugar fermentation																			
		15 °C only	45 °C only	15 and 45 °C			Arabinose	Cellobiose	Mannitol	Mannose	Melebiose	Raffinose	Ribose	Salicin	Lactose	Melezitose	Rhamnose	Sorbitol	Xylose	Trehalose						
<i>L. plantarum</i>	S R	+	-	+	-	-		+	+	+	+	+	+	+	+											
<i>L. brevis</i>	S R	+	-	+	+	+	+							+		+	-	-	-	+						
<i>L. divergens</i>	S R	+	-		+	+		+		+	-	-		+	-							+	+			
<i>L. gasseri</i>	S R	-	+		-	-	-	+		+				-	+				-	+						+
<i>L. rhamnosus</i>	S R	-	-	+	-	-		+	+	+	-			+	+	+				+	+	+				+
<i>L. fermentum</i>	S R			+	+	+	+	+	+	+	+	+	+	+	+	+	-	-	+	+	+	+				+
<i>L. viridescens</i>	S R			+			-	+	+	+	-	-	-	-	+	+	-	-	-	+	+					+
<i>L. farciminis</i>	S R			+		+	-	+	+	+	+	-	+	+	-	+	-	-	+	+	+	+				+
<i>L. buchneri</i>	S R	+			+	+	-	+	-	-	+	-	+	-	+	-	-	-	-	-	-	+	-			-
<i>L. acidophilus</i>	S R	-	-				+	+	+	+	-	-	-	+	+	+	-	-	-	+	+	+				+
<i>L. animalis</i>	C	-	-				+	+	+	+	+	+	-	+	+	-	+	+	+	+	+	-	-			+
<i>L. reuteri</i>	R			+	+	+	+	-	-	-	+	-	+	-	+	-	-	-	-	-	-	+	-			-

Legend: 80% or more strains are positive(+);80% or more strains are positive(-).

C: Cocci shaped
SR: Short rod

2.4. Beneficial Health Effects of Probiotics

A number of benefits in the ingestion of probiotics have been reported. While a number of reported effects have been only partially established, some can be regarded as well established and clinically well documented for specific strains. These health-related effects are given below (Fooks et al., 1999) and some of them are presented in detail.

- Managing lactose intolerance
- Improving immune system
- Prevention of colon cancer
- Reduction of cholesterol and triacylglycerol plasma concentrations (weak evidence)
- Lowering blood pressure
- Reducing inflammation
- Reduction of allergic symptoms
- Beneficial effects on mineral metabolism, particularly bone density and stability
- Reduction of *Helicobacter pylori* infection
- Suppression of pathogenic microorganisms (antimicrobial effect)
- Prevention of osteoporosis
- Prevention of urogenital infections

Lactose Malabsorption

Lactose malabsorption results from insufficient activity of lactase in the human gut and causes abdominal distension, excessive flatulence and/or diarrhea. Over half of the world's population is unable to utilise lactose effectively. It has been established that lactose administered in yoghurt can be utilised more efficiently than the same amount given in untreated milk (Fooks et al., 1999). Moreover, probiotic strains can produce β -galactosidase which improves tolerance to lactose.

Intestinal Infections

Gibson et al., 1997 reviewed the use of probiotics to treat intestinal infections. One of the most popular areas is that of antibiotic associated diarrhea (AAD). The effect of *Saccharomyces boulardii* treatment in reducing incidence of AAD has been confirmed in several studies (Surawicz et al., 1989; McFarland et al., 1995).

S. boulardii has also been studied for *Clostridium difficile* related infections. It has been found that recurrence of this infection was significantly reduced in a group given *S. boulardii* with antibiotic treatment, as compared to the antibiotics alone (McFarland et al., 1994). Overgrowth of candida in the gut is also a frequent consequence of antibiotic use. Studies in hamsters have shown that the gut microflora is involved in suppression of *Candida albicans* (Kennedy and Volz, 1985). In gnotobiotic mice, *S. boulardii* protected against colonisation of the gut by this organism (Ducluzeau and Bensaada, 1982). A human trial showed that milk containing *L. acidophilus* and a *Bifidobacterium* was effective in reducing *Candida* occurrence in faeces (Tomoda et al., 1983). There is also evidence that *Lactobacillus* GG can influence the cause of diarrhoea in children (Isolauri et al., 1991).

The mechanism by which protection is offered by these probiotics has not yet been fully established. However, one or more of the following are possible (Fooks et al., 1999).

- Competition for nutrients
- Secretion of antimicrobial substances
- Reduction of gut pH through SCFA formation
- Blocking of adhesion sites
- Attenuation of virulence
- Blocking of toxin receptor sites
- Immune stimulation
- Suppression of toxin production

Suppression of Cancer

Epidemiological studies have suggested that an increase in the consumption of saturated fats has contributed towards the increased incidence of colon cancer in the Western world. However, no definitively successful clinical trials using probiotics in cancer therapy have been carried out. Animal models have shown that dietary intake of lyophilised cultures of *Bifidobacterium longum* significantly suppressed the development of azoxymethane induced aberrant cryptic foci (ACF) formation in the colon (Kulkarni and Reddy, 1994). Again, the same group elucidated the ability of the same strain to inhibit IQ-induced incidence of colon tumours in rats (Reddy, 1998). This

was confirmed by another group, which used animal models to determine that a combination of *B. longum* and the prebiotic inulin was effective in generating beneficial changes related to tumour risk (Rowland et al., 1998). Moreover, other researchers found that culture supernatants of *L. acidophilus* and *B. adolescentis* suppressed ileal ulcer formation by using animal models (Kinouchi et al., 1998). However, the problems of transposing observations from rodents or in vitro cell lines, to humans should be considered. Bacterial enzymes which convert precarcinogens to active carcinogens are produced in the gut, but their involvement in the pathogenesis of cancer is unclear. However, *L. acidophilus* when fed to healthy volunteers has been shown to significantly decrease β -glucuronidase, nitroreductase and azoreductase activities (Goldin and Gorbach, 1984).

Although mechanisms for the anti-tumour actions of probiotics have not yet been confirmed, some proposals are as follows (McIntosh, 1996):

- Suppression of the carcinogen/procarcinogen by binding, blocking, or removal
- Suppression of bacteria with enzyme activities that may convert procarcinogens to carcinogens
- Reducing the intestinal pH, thereby altering microflora
- Activity and bile solubility
- Altering colonic transit time to remove faecal mutagens more effectively
- Stimulation of the immune system

The precise mechanisms by which lactic acid bacteria may inhibit colon cancer are presently unknown. Such mechanisms might include enhancing the host's immune response, binding and degrading potential carcinogens, quantitative and/or qualitative. The faecal stream is a rich source of cancer inducing agents, and also substances that may protect against cancer. Bacterial transformation of components in the lumen is associated with carcinogen production and the bacterial conversion of other compounds in the lumen (e.g. glucosinolates) may increase anti-carcinogenic activity.

Certain probiotics are immunogenic and regular consumption of these microorganisms leads to contact with the immune components of the gastrointestinal tract; it is argued that they may prime the immune system against infection.

Peltonen et al. (2000) investigated the ability of six probiotic bacteria to bind a common food carcinogen, aflatoxin B₁(afB₁). *Lactobacillus* strains and one *Bifidobacterium* strain were used as probiotic bacteria in their study. The strains were

incubated in vitro with afB1 and the toxin residue in the supernatant was measured using high-performance liquid chromatography. The aflatoxin-binding capacity of the strains was found to range from 5.8 to 31.3% of the initial afB1 concentrations. The results further support the observation that a number of probiotic bacteria are able to bind specific dietary contaminants. It was reported that these results may explain some of the antimutagenic and anticarcinogenic effects of probiotic microorganisms.

Probiotics and Helicobacter pylori

There is substantial evidence that probiotics modulate *Helicobacter pylori* colonization of the gastric mucosa. In this case, interaction between probiotics and *H. pylori*, the importance of lactic acid production by probiotics and their capacity to release bacteriocins or secrete antibiotics are considered.

Coronary Heart Disease

Probiotic supplementation can affect plasma cholesterol concentrations and consequently the incidence of coronary heart disease. The changes of total or LDL (low density lipoprotein) cholesterol levels in plasma can be determined in response to dietary intervention. Schaafsma et al. (1998) found that daily feeding of 125 ml test probiotic milk significantly lowered serum LDL cholesterol levels and total serum cholesterol. Potentially, a probiotic may:

- Interfere with cholesterol absorption from the gut
- Directly assimilate cholesterol
- Produce metabolites that affect the systemic levels of blood lipids

Digestive Aid

It is thought that probiotics help the digestion of food materials. This would be directly related to their viability and ability to colonise effectively.

Nutritional Effects

The nutritional content of fermented milk is not significantly different from that of the raw milk from which it is made (Anon, 1997). The fermentation process may also increase protein availability by the proteolytic action of the starter bacteria.

Immune Stimulation

One of the most interesting aspects of probiotic supplementation is directed towards the immune response. In a human trial, 24 subjects were fed 450 g of yoghurt per day for 4 months, and showed significant increase in the production of c-interferon (Halpern et al., 1991). In animal models, probiotics have been shown to stimulate the production of antibodies (local and systemic), enhance the activity of macrophages, increase c-interferon levels and increase the concentration of natural killer cells.

2.5. Mechanisms of Probiotic Activity

The exact manner in which probiotics may achieve their effects is still uncertain. However, a number of mechanisms can be considered.

Biochemical Effects

One mechanism is based on the production of bacteriocins. Bacteriocin producing organisms may inhibit other microorganisms by helping of these substances. This inhibition was noticed as non-pH related effect. For example, *B. bifidum* was found to excrete a bacteriocin which affected *Listeria*, *Enterococcus*, *Bacillus*, *Lactobacillus*, *Leuconstoc* and *Pediococcus* (Anand et al., 1984). Other bacterial species known to produce bacteriocins, include lactobacilli and lactococci (Talarico and Dobrogosz, 1989).

Short chain fatty acids (SCFA) are also produced in varying quantities as metabolic end products by probiotic bacteria, and it is thought that these may induce an antagonistic effect against other organisms. A lowering of the gut pH may act directly to inhibit the growth of ha

Competition for Nutrients

Certain bacterial species have exact nutritional requirements and it is likely that one population utilizes nutrients at the expense of other species. This competitive interaction may be fortified through probiotic use.

Immune Effects

The potential of the immune response to control the growth of micro-organisms in the gut is an important consideration. Further work may establish how stimulation of the systemic components of the immune system, through non-pathogenic means, can help regulate the gut microflora. Immune modulation effects can be evaluated in two cases as related to adhesion and non related to adhesion. In the first case, the adhesive strains cause to increase in the phagocytosis of infective organisms. In the second case, immune-stimulating activity has been attributed to bacterial cell envelope constituents (Fooks et al., 1999; Ouwehand et al., 1999)

Colonisation

One possible mechanism for the action of probiotics is their ability to adhere to the intestinal mucosa. In this case, they can resist peristalsis and occupy a niche at the expense of harmful organisms.

CHAPTER 3

NATURAL ZEOLITES

The usage of the natural zeolite of the clinoptilolite rich minerals in the biomedical applications were increased in the recent years. One of the important point behind this approach is that it has good stability in its transit through the gastrointestinal tract and it is harmless to the human body. Natural zeolite of clinoptilolite mineral has been reported to be nutritionally inert adsorbent and non-toxic to animals (Papaioannou et al., 2002; Rivera et al., 1998; Rivera et al., 2000; Rivera et al., 2003). In order to explain and clarify the reasons of the some beneficial health effects, the literature information on the description, structure and applications of the zeolites were presented in this chapter.

Zeolites are a group of naturally occurring framework aluminosilicates with high adsorption and cation exchange capacities and hydration-dehydration properties. About fifty different species of this mineral group have been identified, but only eight zeolite minerals make up the major part of volcano sedimentary deposits: analcime, chabazite, clinoptilolite-heulandite, erionite, ferrierite, laumontite, mordenite and phillipsite. The structure of each of these minerals is different but they all have large open 'channels' in the crystal structure that provide a large void space for the adsorption and exchange of cations. The internal surface area of these channels can reach as much as several hundred square meters per gram of zeolite, making zeolites extremely effective ion exchangers and adsorbents (Mumpton, 1984).

Some zeolitic crystal structures can be synthesized by hydrothermal reaction in a uniform, phase-pure state. The raw materials of zeolites are silica and alumina. More than 150 types of zeolite have been synthesized and are designated by a letter or group of letters (Type A, Type X, Type Y, Type ZSM, etc.) (Yang, 2003).

Zeolites are crystalline, hydrated aluminosilicates of alkaline or alkaline earth metals, especially, sodium, potassium, calcium, magnesium, strontium and barium. Structurally, zeolite is the "framework" aluminosilicate which is based on an infinitely extending three dimensional network of AlO_4 and SiO_4 tetrahedra linked to each other by sharing all of the oxygens. This framework contains channels and interconnected

voids which are occupied by the cation and water molecules. The cations are quite mobile and can usually be exchanged, to varying degrees, by other cations. These cations play a very important role in determining the adsorption and gas-separation properties of zeolites. These properties depend heavily on the size, charge density, and distribution of cations in the porous structure.

3.1. Structure of the Zeolites

Zeolite structure consists of two types of building units namely, primary and secondary. The primary building unit of the zeolite framework is the tetrahedron in which the center is occupied by a silicon or aluminum atom with four oxygen atoms at the corners as shown in Figure 3.1. Each oxygen atom is shared between two tetrahedra. Substitution of Si^{+4} by Al^{+3} defines negative charge of framework, compensated by monovalent or divalent cations located together with water molecules in the channels. Cations in the channels can be substituted easily and therefore they are termed exchange or extra framework cation while Si and Al, which are not exchanged under ordinary conditions, are called tetrahedral (T) or framework cations (Tsisthivilli et al., 1992).

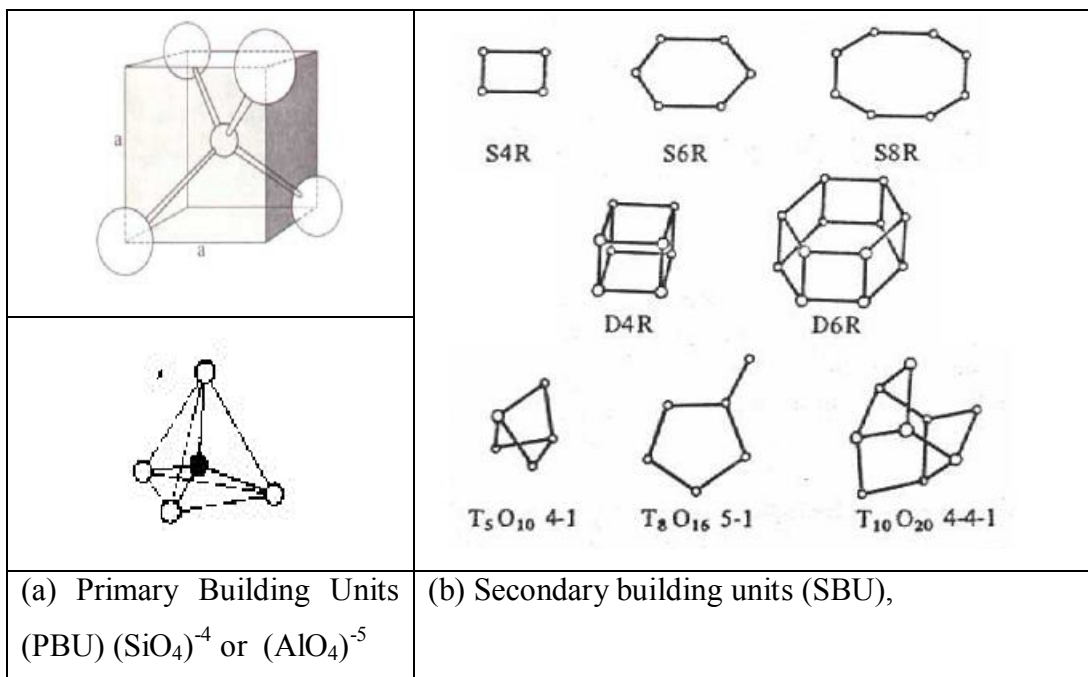


Figure 3.1. Primary and secondary building units of zeolite structure (Source: Breck, 1974; Tsitsishvili et al., 1992)

Zeolite structure also contains secondary building units (SBU), which are formed by the linking of the primary building tetrahedral. They consist of double and single rings of tetrahedra, forming the three dimensional structure of the zeolite. In the SBU Si-Al distribution is neglected, only the positions of the tetrahedral silicons or aluminums are shown. Oxygen atoms lie near the connecting the solid lines.

Clinoptilolite is a member of the Heulandite group natural zeolite so it has HEU topology, whose secondary building unit can be described by 4-4-1 type (Breck, 1974). The the structure of clinoptilolite consists of a three dimensional system of three types channels, A (10-member ring) and B (8-member ring) ring) are parallel to each other while C channel (8-member ring) intersects both the A and B channels as shown in Figure 3.2. Channel characteristics and cation sites of clinoptilolites are presented in Table 3.1.

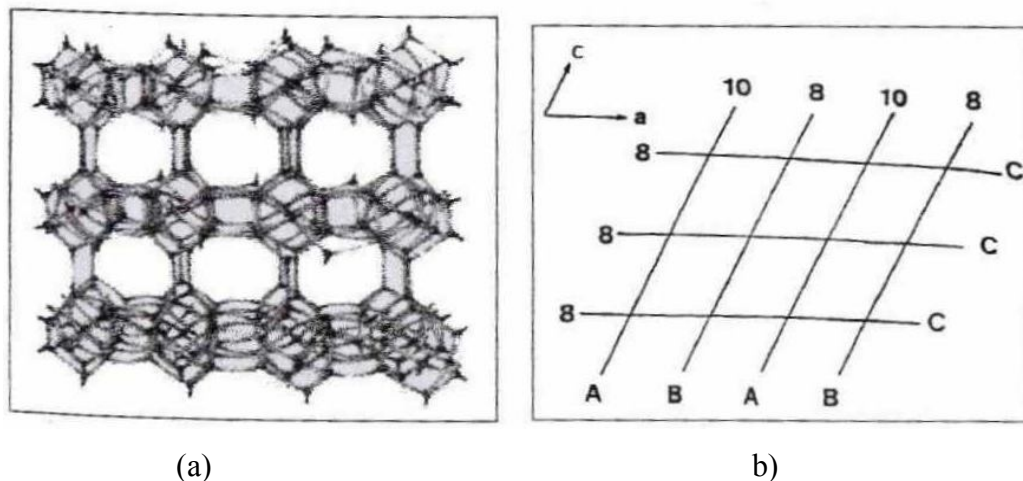


Figure 3.2. (a) Model framework for structure of clinoptilolite. (b) Orientation of clinoptilolite structure of clinoptilolite (Source: Ackley et al., 1991)

Table 3.1. Channel Characteristics and Cation Sites in Clinoptilolite
(Source: Ackley and Yang, 1991a, b)

Channel	Tetrahedral ring size/channel axis	Cation site	Major cations	Approximate channel dimensions, nm×nm
A	10/c	M(1)	Na, Ca	0.72×0.44
B	8/c	M(2)	Ca, Na	0.47×0.41
C	8/a	M(3)	K	0.55×0.40
A	10/c	M(4)	Mg	0.72×0.44

3.2. Properties of Zeolites

Commercial applications of natural zeolites make use of one or more of several physical or chemical properties. Main applications were presented below,

They have an ability to act as catalysts in the chemical reactions that place within the internal cavities. The cations would be expected to affect the catalytic properties.

Natural zeolites have ion exchange property. The exchange of ions is a chemical reaction between two phases and necessarily stoichiometric and each ion removed from the solution is replaced by an equivalent amount of ion exchanger of the same sign by conserving electro neutrality. Removal of ammonia and removal of cesium and strontium are the examples of the ion exchange applications.

Another important property is adsorption and separation. The most fundamental consideration regarding the adsorption of chemical species by zeolites is molecular sieving. Species with a kinetic diameter which makes them too large to pass through a zeolite pore are effectively “sieved”. This “sieve” effect can be utilized to produce sharp separations of molecules by size and shape. They also adsorb molecules with permanent

dipole moment with selectivity not found in other adsorbents (Breck, 1974). In the Table 3.2 properties of some commercial adsorbents were presented.

Most of the separation processes are based on differences in adsorption equilibrium and in adsorption/desorption kinetics or the micropore diffusivities. Molecular sieving is a process in which one of the components is allowed to enter the micropores while the others can not enter. If the micropores are sufficiently small so that the diffusivity is controlled by repulsive forces. Therefore, there may be large differences in diffusivity between the components. Size of the micropores should be comparable with the molecular diameter of the sorbate for efficient kinetic selectivity, the choice of adsorbents is limited to zeolites and carbon molecular sieves for separation of light gases with molecular diameters of few Angstroms. The adsorbents can be modified (pore size of the adsorbent can be increased or decreased) suitably in order to control the kinetic selectivity.

Table 3.2. Properties of Commercial Adsorbents
(Source: Sing, 1989)

Adsorbent	Porosity	Polarity	Adsorption Capacity
Activated aluminas	micro-meso	strong	moderate
Activated clays	variable	strong	moderate
Silica beads	meso-macro	moderate	high
Silica gels	micro-meso	moderate	moderate
Silicalite	micro	very weak	low
Zeolites	micro (well-defined)	very strong	moderate
Activated carbons	micro-meso-macro	weak	high
Molecular sieve carbons	micro (slit shaped, narrow pore size distribution)	weak	low
Polymers/ resins	variable	variable	moderate

All commercial adsorbents have high specific surface areas, which are generally located within well developed pore structures. Therefore, it is useful to classify pores according to their sizes. According to the IUPAC classification pores are grouped as;

- micropores have widths up to ~ 2 nm, ($d < 20\text{\AA}$)
- mesopores have widths in the range 2 – 50 nm, ($20\text{\AA} < d < 500\text{\AA}$)
- macropores have widths greater than ~ 50 nm. ($500\text{\AA} > d$)

3.3. Natural Zeolites and Clinoptilolite-Rich Natural Zeolite

Clinoptilolite is the most abundant of the natural zeolites (Mumpton et al., 1976), but composition and purity vary widely among the deposits found throughout the world. It belongs to the heulandite group, with a three dimensional framework of silicon and aluminum tetrahedral.

The theoretical composition of clinoptilolite is $(K_2, Na_2, Ca)_3[Al_6Si_{30}O_{72}] \cdot 24H_2O$, it can also contain some Mg^{2+} and Fe^{2+} ions. Main properties are tabulated (Table 3.3). The content of non-tetrahedral cations (K^+ , Na^+ , Ca^{2+} and Mg^{2+}) as well as Si/Al ratio can change depending on the mineral (Breck, 1974). The total pore volume based on $cm^3 H_2O/cm^3$ crystal was reported as 34 % (Barrer, 1978). Clinoptilolite crystals belong to monoclinic C2/m group with the following unit cell parameters: $a=17.62 \text{\AA}$, $b=17.91 \text{\AA}$, $c=7.39 \text{\AA}$ and $\beta=116.40^\circ$ (Gottardi and Galli, 1985).

The adsorption characteristics of zeolites are dependent upon their chemical and structural properties. The cation type, size, charge density, location and the extent to which it is exposed to the adsorbate molecules as well as the Si/Al ratio have a strong effect upon both adsorption capacity and selectivity. The Si/Al ratio is between 4.25-5.25 for clinoptilolite and 2.7-4 for heulandite. Heulandite transforms into two phases at about 230°C and becomes non-crystalline at about 350°C . Clinoptilolite keeps its crystal structure up to about 700°C . (Tsitsishvili et al., 1992).

Table 3.3. Summary of clinoptilolite characteristic properties
(Source: Breck, 1974)

Structure group	7
Chemical Composition	$(\text{Na}_2\text{K}_2\text{O}) \cdot \text{Al}_2\text{O}_3 \cdot 10\text{SiO}_2 \cdot 8\text{H}_2\text{O}$
Typical Unit Cell contents	$\text{Na}_6[(\text{AlO}_2)_6(\text{SiO}_2)_{30}] \cdot 24\text{H}_2\text{O}$
Variations	Ca, K, Mg also present; Na, K >> Ca Si/Al, 4.25 to 5.25
Crystallographic Data	
Symmetry	Monoclinic Density: 2.16 g/cc
Space Group	I 2/m Unit cell volume: 2100 Å ³
Unit Cell Constants	a= 7.41 Å, b=17.89 Å, c= 15.85 Å β=91° 29'
Structural Properties	
Framework	Possibly related to heulandite but not determined
Void volume	0.34 cc/cc Framework Density: 1.71 g/cc
Dehydrated-Effect of Dehydration	Very stable-in air to 700 °C
Largest Molecule Adsorbed	O ₂
Kinetic Diameter, σ, Å	3.5

3.4. Natural Zeolites in Health Studies

An important particular structural property of zeolites relative when compared other aluminosilicate materials and other crystalline materials in general, is the existence of channels and/or cavities linked by channels. One of the characteristics that distinguishes zeolites from other porous materials is their variety of pore sizes and shapes. Zeolites are widely used in modern technology as selective adsorbents, molecular sieves, and particularly as catalysts. It is obvious that the ion sieving and other remarkable properties of zeolites will be utilized in the near future for the environmental and health care industries (Figure 3.3.) The reasons for this are as follows (Pavelic and Hadzija, 2003)

- (a) Zeolites have known biological properties along with long-term chemical and biological stability.
- (b) They reversibly bind small molecules such as oxygen and nitric oxide.
- (c) They possess size and shape selectivities.
- (d) They offer the possibility of metalloenzyme mimicry.
- (e) They have immunomodulatory activity.

Since many biochemical processes are closely related to some zeolite properties (ion exchange, adsorption, and catalysis), it can be expected that natural and synthetic zeolites may lead to significant advances in biology, medicine, and in the pharmaceutical industry.

3.4.1. Effect on Aflatoxicosis

Clinoptilolite incorporated into the diet can reduce the deleterious effects of aflatoxin. There are several animal studies on using of the natural zeolites in animal feeding . Some animal health studies indicated that zeolite adding to the feed can reduce the risk of aflatoxicosis. Clinoptilolite incorporated into the diet at 1.5% and 2.5% was evaluated for ability to reduce the deleterious effects of 2.5 mg total aflatoxin on broiler chickens (Oğuz et al., 2000). When compared with the controls, aflatoxin treatment



Figure3.3.Biochemical effects of zeolites
(Source:Aurbach et al., 2003)

significantly reduced serum total protein, albumin, inorganic phosphorus, uric acid, total cholesterol, and the hematocrit, red blood cell count, mean corpuscular volume, hemoglobin, thrombocyte count, and monocyte count, while increasing the white blood cell and neutrophil counts. The addition of clinoptilolite to the aflatoxin diet reduced the adverse effects of aflatoxin and should be helpful in solving the aflatoxicosis problem in poultry (Oğuz et al., 2000).

Ortatatlı et al., 2005 evaluate the pathological changes in broilers fed a diet containing low-levels of aflatoxin , and clinoptilolite until 42 days of age. The addition of clinoptilolite to the 100 ppb aflatoxin containing diet significantly decreased the number of affected broilers and/or the severity of lesions in the livers.

Clinoptilolite incorporated into the diet at 50 g/kg reduces the deleterious effects of aflatoxin in growing Japanese quail chicks from 10 to 45 days of age. While aflatoxin decreased food consumption and body weight gain from the third week onward, addition of clinoptilolite significantly reduced the negative aflatoxin effects on food consumption ratio (Miazzo et al., 2000).

An another important case related to using of zeolites in animal feeding is whether zeolites influence vitamin and microelement adsorption. Neither amino acids (tryptophan and phenylalanine) nor vitamins (A, D, E) are adsorbed by clinoptilolite. Natural zeolites have a low efficiency for binding vitamin B6 in vitro. This process is dependent on crystallinity and the mineralogical composition of the zeolitic samples. On the other hand, vitamin B6 is tightly bound to the clay mineral bentonite. Cu, Zn, Co, and Mn are bound less tightly to zeolite than to bentonite. These data suggest that the bentonite material would reduce micronutrient availability more than zeolite (Tomasevic et al., 2000).

3.4.2. Removal of Heavy Metals and Organopoisoning

Heavy metals released in wastewater are one of the major due to their cumulative effects along the food chain. The natural zeolites clinoptilolite, phillipsite, and chabazite are particularly useful in selectively eliminating ammonia and heavy metals such as Cd^{2+} , Pb^{2+} , Zn^{2+} , Cu^{2+} , and, partially, Cr^{3+} . Generally, clinoptilolite is stable in an acidic environment and shows high selectivity for many heavy metals. Erdoğın Cansever and Ülkü (2011) reported ammonium adsorption properties of the

clinoptilolite rich mineral from Gördes region of Turkey recently. They suggested that clinoptilolite rich mineral is a promising material for ammonium removal in wastewater treatment.

3.4.3. Antimicrobial Effects

Metal-exchanged zeolites have been proposed in the last decade for controlled release of agents against microbial pollution. For example, Silver exchange clinoptilolite was suggested as antimicrobial material by Top and Ülkü (2004). They reported the antibacterial activity of Ag clinoptilolite against *Proteus* spp. and *Pseudomonas aeruginosa* comparable to commercial antibiotics. Recently, bactericidal properties of nitric oxide releasing natural zeolite were found also (Narin et al., 2011).

Antimicrobial properties of natural and synthetic zeolites conditioned in some cation forms tested in a variety of applications. An antifungal material, Ag-zeolite (Zeonic), was combined with a commercial tissue conditioner as a successful agent against *Candida albicans* growth and/or acid production (Pavelic and Hadzija, 2003). The inhibitory effects of these materials on fungal growth were decreased by the presence of a saliva coat, particularly with zeolite specimens and special tissue conditioner. Test specimens containing 2–5% Zeonic showed a significantly greater effect on the delay in rapid decline of pH as compared with the other specimens examined. These results suggest that zeolite-combined tissue conditioner would be a potential aid in denture plaque control. A silver zeolite mouth rinse was prepared by suspending zeolite powder into phosphate-buffered saline at a concentration of 3% (w/w). A double-blind crossover clinical study confirmed that silver zeolite significantly reduced plaque formation compared to the placebo.

3.4.4. Effects on Gastrointestinal Disorders

The low resorption rate from the gastrointestinal tract, weaker clinical signs of intoxication, and longer time span for the onset of specific therapy are factors that create conditions for inclusion of natural zeolite in the arsenal of rational prevention and therapy of organophosphate poisoning. Observations were made first in animal nutrition. Ten percent of clinoptilolite or mordenite as dietary supplements for swine

and poultry showed that animals generally grew faster, and the number and severity of intestinal diseases were reduced. Thus, some drug studies were developed due to the positive effects on gastrointestinal disorder due to the antacid activity. These were mentioned in the drug studies.

3.4.5. Immunological Consequences

It is known that there is a relation between autoimmune diseases and some alumina silicates. For example, silicon breast implants have been implicated in occurrence of autoimmune and other diseases. Asbestos and fibrous zeolites have been implicated in pathogenesis of mesothelioma, lung fibrosis, and some autoimmune disorders. Although there exist an autoimmune diseases after exposure to silicate materials, it was proposed that silicate materials can also act as super antigen. This case can be evaluated in immunomodulatory effect and immunization. In the case of the immunomodulatory effect, Pavelic et al. (2002) reported that of clinoptilolite has provoked the accumulation macrophages in the peritoneum. In their study, the number of peritoneal macrophages after exposed to clinoptilolite was 7 times higher than in control mice. The concentration of O_2^- was 10 times higher in macrophages of treated mice than in controls. Since O_2^- release was calculated for 10^6 cells, the increased release was not the result of increased number of macrophages, but represents truly increased activity.

Additionally, Korkina et al. (2006) found that natural clinoptilolite exhibits a high hemolytic activity and cytotoxicity. The ability of macrophages to induce phagocytosis was decreased. Modification of the clinoptilolite surface by ammonia ions led to a decrease in its cytotoxic properties. Ethanol, mannitol, and sodium azide had no effect, whereas catalase reduced the ability of clinoptilolite to damage the membranes of macrophages and red cells.

3.4.6. Effects on Tumor Growth

Finely ground clinoptilolite has been proposed as a new adjuvant in anticancer therapy (Pavelic et al., 2001). Such treatment of mice and dogs suffering from a variety of tumor types led to improvement in the overall health status, a prolonged life span,

and a decrease in tumor size. Local application of clinoptilolite to skin cancers of dogs effectively reduced tumor formation and growth. In vitro tissue culture studies showed that finely ground clinoptilolite inhibits protein kinase B . The effects on tumor growth was studied in mainly two area which are cell signalling and apoptosis and proliferation of tumor cell lines in vitro. Studies performed in tissue culture in vitro indicate that natural clinoptilolite treatment affects proliferation and survival of several cancer cell lines of human origin (Pavelic et al., 2001). Addition of clinoptilolite inhibited cell proliferation in a concentration dependent manner, in part due to induction of inhibitors of cycline-dependent kinases, inhibition of B/Akt expression, and induction of programmed cell death.

Zarkovic et al. (2003) studied on treatment of cancer bearing mice and dogs with micronized zeolite clinoptilolite. They show that this treatment leads improvement the overall health status, prolongation of life span, and decrease in tumor sizes.

3.4.7. Toxicology of Clinoptilolite

In human medicine, zeolites have been used as antidiarrheal remedies, for the external treatment of skin wounds and athlete's foot, and in kidney dialyses for the removal of ammonia ions from body fluids. There were not many data showing the systemic effects of zeolites on physiological systems of the body. The beneficial effects of zeolites on hematopoiesis, and various disease states, including tumours, have been observed. No toxic effects were observed in toxicology study of clinoptilolite. The physical status of examined animals showed no evidence of any harmful reaction during the studies (Pavelic and Hadzija, 2003).

Clinoptilolite is well suited for these applications because of its large pore space, high resistance to extreme temperatures, and chemically neutral framework. There are a few toxicology studies of clinoptilolite obtained from different locations. The conclusion from all of them is that natural clinoptilolite is not toxic and can be used in human as well as in veterinary medicine. Preclinical toxicology of clinoptilolite from Vranje, southern Serbia, was studied by setting the "limit" test. This refers to administering high doses of clinoptilolite (2 - 200 and 2 -500 mg/mouse per day orally by gavage) for 6, 14, and 30 days. This limit test, an "up-and-down" test on mice was performed, with daily doses ranging from 60 to 4000 mg/per mouse. Again, no toxicity

was observed. Classical acute, subacute, and chronic toxicity studies on mice and rats of both sexes were performed. The duration of the study was as follows: acute, 1 month; subacute, up to 3 months; chronic toxicity, up to 6 months. Animals were monitored for phenotypic changes, changes in behavior and survival, changes in body weight, amount of food and water consumed, changes in hematological parameters.

Martin-Kleiner et al. (2001) compared the effects of two preparations of clinoptilolite differing in particle size on serum chemistry and hematopoiesis in mice. One preparation was a powder obtained from tribomechanical treatment (MTCp) of the clinoptilolite and another was normally ground. Young adult mice were supplied with food containing 12.5%, 25%, or 50% clinoptilolite powder. Control animals received the same food, ad libitum, without the clinoptilolite. Clinoptilolite ingestion was well tolerated, as judged by comparable body masses of treated and control animals. A 20% increase of the potassium level was detected in mice receiving the zeolite-rich diet, without other changes in serum chemistry.

3.4.8. Drug Studies

Due to the some beneficial health properties and desirable functional characteristics natural zeolites have many applications in the development of the new drugs. Rodriques-Fuantez et al. (1997) reported that pharmacological and clinical studies that natural clinoptilolite from the Tasajeras deposit in Cuba does not cause any biological damage in humans. In 1997, a new antidiarrheic drug for humans was introduced based on the physical and chemical properties of a purified natural clinoptilolite. A series of physical, chemical, technological, pharmacological, microbiological, and clinical studies was successfully conducted to meet the requirements of the Cuban Drug Quality Agency (Rodriguez-Fuentes et al., 1997). The structural stability of natural clinoptilolite during its transit through the gastrointestinal tract as compared to synthetic zeolites, the use of purified natural clinoptilolite as a gastric alcalinizant, and the use of antacids containing sodium carbonate all suggested that a study of a Na₂CO₃-clinoptilolite (combination product formed via hydrothermal transformation) as an improved antacid was warranted. Rivera et al. (1998) showed that Na₂CO₃-clinoptilolite has more than twice of the neutralization capacity of clinoptilolite. They suggest that a 400 mg dose of such hydrothermally transformed

zeolite would be able to increase the stomach pH to the value expected of an antacid treatment. In addition, UV spectroscopy demonstrated that the zeolite did not affect the concentration and stability of the enzyme pepsin in synthetic gastric juice.

Lam et al. (1998) performed a theoretical study of the physical adsorption of aspirin on natural clinoptilolite. Because the aspirin molecule is larger than the dimensions of the zeolite channels, only interaction with the external surface of zeolite is possible. The aspirin molecule was oriented to the cavities in three principal directions: 8-ring window model, 10-ring window model, and surface model. Their results support the possibility of the physical adsorption of aspirin by clinoptilolite. The best results have been obtained for a pure silicon structure, followed by a structure with one hydrogen cation and then a structure with one sodium cation. At the same time, the presence of more aluminum atoms and compensating cations in the structures did not significantly alter the results. The aspirin molecule might therefore be adsorbed in gastrointestinal juices in a stronger fashion to an acid zeolite than to a sodium zeolite .

Based on these observations the gastric antacid Neutacid has been registered. As a nutraceutical, it consists mostly of the naturally occurring zeolite clinoptilolite, along with vitamins and minerals having antioxidative properties. It also possibly reduces the gastrointestinal toxic burden by affecting the anaerobic fermenting processes after digestion of food and by removing harmful metabolites after medical treatment of cancer and/or liver and kidney failure (Pavelic and Hadzija, 2003).

One of potentially many exciting pharmacological applications of such zeolites and mesoporous silicates is the encapsulation of different ions and molecules with delayed-release properties. Many proteins (enzymes) can indeed be encapsulated, and the enzymes when released often show almost full activity. Zeolites are also used as support matrices for enzymes and antibodies. Glucose oxidase has been fixed onto zeolite 4A and zeolite X. Coenzymes have been stabilized on 4A. Thermal stability of trypsin adsorbed onto zeolite 4A is highly enhanced.

Farias et al. (2003) studied on physicochemical interaction between natural zeolite and two drugs, metronidazole and sulfamethoxazole, which cause considerable gastric side effects. By considering the biological properties of the purified natural clinoptilolite, they proposed some possible usages in order to solve the side effects of these two drugs. They suggested the possibility of parallel administration of these products.

A clinoptilolite-rich rock was evaluated as inorganic Zn^{2+} releasing carrier for antibiotic erythromycin (Cerri et al., 2004). In the use of the topical treatment of acne, a diffused skin pathology, it is expected to give the efficacy of zinc-erythromycin combination against resistant *Propionibacterium* strains. The simultaneous release of zinc and erythromycin were evaluated in phosphate buffer. Eighty-two percent of the loaded antibiotic was released after 30 min. Zinc exchange is substantially unaffected by the contemporary drug release. Then, in-vitro characterization and preliminary formulation studies were conducted for the same subject (Bonferoni et al., 2007).

In another drug study, a potential application of purified natural clinoptilolite has been explored (Rivera and Farias, 2005). Three kinds of surfactants have been employed for the obtainment of different surfactant/natural zeolite composites.

In other study, the possible use of clinoptilolite-rich mineral as a novel carrier for the active constituents present in Ginkgo biloba leaf extract solutions was investigated (Göktaş et al., 2008). In the experiments, the decrease in antioxidant activity was found to be related in the phenolic constituent adsorption on zeolite and the use of clinoptilolite as a novel drug carrier for the flavonoid aglycone constituents were suggested.

Recently (Farias et al., 2009), K- and Li-enriched forms of natural zeolites have been prepared and the release properties have been examined for the biomedical applications. Potassium and lithium ions are commonly employed in the treatment of different pathologies and their findings have been proposed to be for the drug studies to overcome the side effects of the lithium and potassium salts.

3.4.9. Other Health Related Cases

Zeolite and Reproduction

Clinoptilolite has been given to the mice as a powder mixed with standard food at the ratio of 25% clinoptilolite. The treatment was continued during the pre-pregnancy and during the lactation period. Special consideration was given to the teratological influence of zeolite on organogenesis (from 6 to 16 days of pregnancy). The pre-pregnancy period in mice treated with clinoptilolite was shorter than in control (nontreated) mice. The number of pups per litter (both before and after birth) was increased in clinoptilolite-treated mice. In addition, the average body weight of pups

was lower (on average 100 mg per pup). In conclusion, the clinoptilolite equalized (regulated) and shortened the pre-pregnancy period. The number of pups per litter was increased in clinoptilolite-treated mice. Decreased birth weight may have been a consequence of increased number of pups per litter. Regarding other parameters, including teratogenesis, clinoptilolite-treated mice were not different from control mice and did not show negative results, which suggests no attributable toxicity of clinoptilolite on reproduction (Pavelic and Hadzija, 2003).

External Applications

Zeolites can protect polymers from ultraviolet degradation therefore it provides wide spectrum of external application of zeolites in cosmetics and dermatology. Zeolite powder has been found to be effective in the treatment of athlete's foot and to reduce the healing time of wounds and surgical incisions. In Cuba, it is a common practice to dust the cuts of horses and cows with clinoptilolite to hasten the healing process (Pavelic and Hadzija, 2003).

Radioprotection

Many studies have showed the ability of several natural zeolites to take up certain radionuclides (e.g., ^{90}Sr , ^{137}Cs , ^{60}Co , ^{45}Ca , and ^{51}Cr). For instance, mordenite has effectively decontaminated soils contaminated with ^{137}Cs and ^{90}Sr (Valcke et al., 1997). In another case, clinoptilolite shows a significant protective effect reducing radiocesium-137 accumulation in male broiler chickens exposed to alimentary contamination. The reduction of radiocesium in meat ranged between 60% and 70% and in edible organs it was greater than 50%. Clinoptilolite supplementation in food eliminated ^{137}Cs deposition in some organs and tissues. Akyuz, 1996 showed that clinoptilolite from Cankiri-Corum Basin is an excellent sorber for both cesium and strontium ions therefore it can be used for the treatment of radioactive wastewater and other decontamination purposes. Similar properties of clinoptilolite from other deposits are known as well.

Effects on Diabetes Mellitus

Zeolites have potential use in the treatment of diabetes. Although the natural, finely ground clinoptilolite did not significantly decrease the blood glucose levels in the

animals, there have been some indications that zeolite did in fact sorb a small amount of the glucose. The hydrothermal transformation of natural, purified clinoptilolite using FeSO_4 has been shown to cause selectivity for glucose adsorption (Conception-Rosabal et al.,1997)

CHAPTER 4

AFLATOXINS

4.1. Structure

The human diet contains a wide variety of natural carcinogens. Aflatoxins (AFs), a group of potent mycotoxins with mutagenic, carcinogenic, teratogenic, hepatotoxic and immunosuppressive properties, are of particular importance because of their adverse effects on animal and human health (Lewis et al., 2005). Contamination of feed with *Aspergillus flavus* was first discovered after an outbreak of sudden death among several hundred thousand ducklings and turkeys in the year 1960 and was later named “Turkey X Disease” (Blount, 1961). This finding led to the isolation of a fluorescent compound referred to as aflatoxin as an abbreviation of “*Aspergillus flavus* toxin” (Nesbit et al., 1962). The chemical structures of the six major dietary aflatoxins are shown in Figure 4.1. and main characteristics of afB1 is tabulated (Table 4.1).

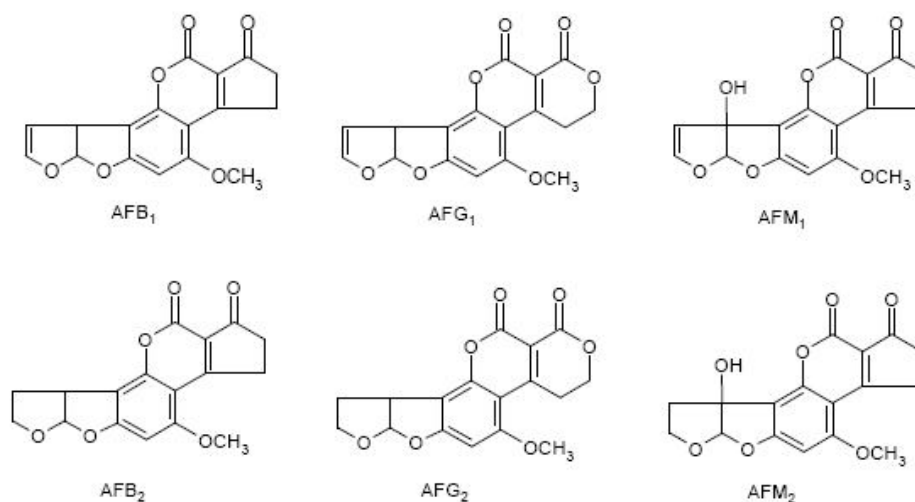
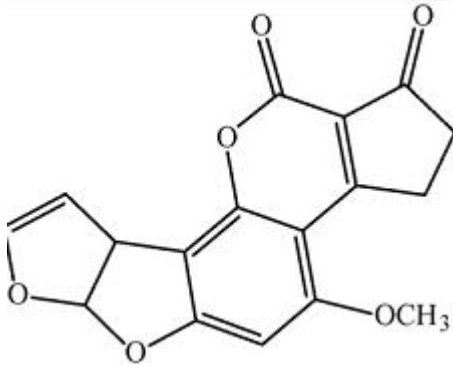


Figure 4.1. Chemical structures of major dietary aflatoxins namely aflatoxin B1, G1 and M1 with the double bonds in 8-9 positions and aflatoxins B2, G2 and M2 without the double

Table 4.1. Some chemical and structural properties of Aflatoxin B1
(Source: Dakovic et al., 2008; Colella, 2007 ; Grant and Phillips, 1998)

Name	Aflatoxin B1
Structural formula2007;	
Molecular formula	C ₁₇ H ₁₂ O ₆
Molecular weight (g/mol)	312.3
Solubility in water (mg/L)	10-30
Solubility in other solvents	Methanol, chloroform, dimethyl sulfoxide
Dipole moment	9.5
Size (Horizontal and vertical cross sectional area)	52.8 Å ² and 88.3 Å ²
Kinetic diameter range	5.18 Å to 6.50 Å

Chemically, aflatoxins are a group of difuranocoumarin derivatives that show fluorescence under ultraviolet light. According to the color of the fluorescence the aflatoxins are grouped into aflatoxin B1 and B2 (AFB1, AFB2) for blue, and G1 and G2 (AFG1, AFG2) for green, where subscripts refer to the chromatographic mobility. Aflatoxin M1 and M2 (AFM1, AFM2), known as milk aflatoxins, are metabolites of AFB1 and AFB2 (Carnaghan et al., 1963).

AFB1 is the most toxic and most prevalent compound, followed by G1, B2 and G2 with decreasing toxicity (Busby, 1984). AFM1 is frequently detected in dairy products, and its toxicity is comparable to AFB1 (Busby, 1984). Aflatoxins can be produced by the four toxic species of *Aspergillus*: *A. flavus*, *A. flavus ssp. parasiticus*, *A. nomius* and *A. pseudotamarii* (Pitt, 2000) as secondary metabolites. Daily human aflatoxin exposure varies between countries and was estimated between 4184 ng/kg body weight in various African countries, 122027 ng/kg body weight in Southern China

and 753 ng/kg body weight in Thailand, as compared to <3 ng/kg body weight in the USA (Williams et al., 2004).

Maximum legal concentrations of total aflatoxins in foodstuffs are set in many countries. The legal limits may vary from one country to another, depending on the degree of development and economic consideration. The Scientific Commission of the European Community have regulated the maximum allowable level of 2 µg/kg AFB1 and 4 µg/kg total aflatoxins for nuts, peanuts, cereals and other products processed for direct intake while, for nuts and dried fruit to be subjected to sorting or other physical treatment, before human consumption or use as human ingredient in foodstuffs, the limit stands at 5 µg/kg for AFB1 and 10 µg/kg for total aflatoxins (Commission of the European Communities, 2001). In the US, the FDA has set a maximum admissible level of 20 µg/kg for total aflatoxins in all foods for human consumption (Creppy, 2002). In Turkey, Turkish legal limits for AFB1 and total aflatoxins are 5 and 10 µg/kg respectively (Turk Gıda Kodeksi Teblig , 2002).

aFB1, the most toxic aflatoxin, is of particular interest because it is a frequent contaminant of many food products and one of the most potent naturally occurring mutagens and carcinogens known. Concerns related to the negative health impacts of aflatoxins have led to the investigation of strategies to prevent their formation in foods, as well as, to eliminate, inactivate or reduce the bioavailability of these toxins in contaminated products. Techniques to eliminate, inactivate or reduce the bioavailability of aflatoxins include physical, chemical, and biological methods.

4.2. Toxicity and Carcinogenicity of Aflatoxins

The toxic exposure can occur through the oral route and inhalation. Mainly, exposure occurs orally because aFB1 is a common food contaminant. The other case can be valid for people that work in the areas of contaminated grain dust. Following ingestion, aFB1 is efficiently absorbed in the intestinal tract.

Toxicity of aflatoxins can be evaluated in two cases as acute toxicity and chronic toxicity. Acute toxicity generally has a rapid onset and an obvious toxic response, while chronic toxicity is characterized by low-dose exposure over a long time period, resulted in cancers and other generally irreversible effects. Chronic toxicity studies have also been conducted with lower levels of aflatoxin exposures.

Effects on Humans

An outbreak of aflatoxicosis in Kenya has resulted in 125 deaths among 317 cases of poisoning (CDC, 2004). The case fatality rate was 39%, caused by levels of aFB1 in homegrown maize reaching up to 8 mg/kg maize. Several previous outbreaks of aflatoxicosis have occurred in Africa and India, mostly in adults with poor nutritional status and maize as staple food. The clinical picture indicated acute toxic liver injury manifested as jaundice with a mortality rate of 10-60% (Peraica et al., 1999). From these findings it can be concluded that the acute lethal dose for adult humans is in the order of 10-20 mg (Pitt, 2000). In humans, numerous studies have linked the incidence of primary hepatocellular carcinoma with the intake of aflatoxins, leading to the classification of aFB1 as class 1 human carcinogen by the IARC (IARC, 1993). Areas of high incidence of liver cancer such as China, Taiwan and subSaharan Africa, also have the highest prevalence for aflatoxin exposure and hepatitis B virus, leading to the theory that these two hepatocarcinogens act synergistically (Kew, 2003).

Besides the carcinogenic effects, aflatoxins are also implicated with immunomodulatory effects and the occurrence of infectious disease as well as with growth faltering effects in children (Williams et al., 2004). Epidemiological studies show geographical similarities in the occurrence of aflatoxins in food and kwashiorkor (Peraica et al., 1999).

Another effect on humans occurs by consuming the contaminated animal products. Milk carries a metabolite of aFB1 known as afM1. This chemical is highly regulated because infants and young children may consume large quantities of milk, and the young of all species are more susceptible to the effects of aflatoxins.

Effects on Animals

Toxic and especially carcinogenic effects of aflatoxins have been reported in several different animals, but susceptibility to these toxins varies greatly with sex, age, species and strain within a species (Busby, 1984). Experimentally verified LD₅₀ values (lethal dose for 50% of animals) for rats for example, vary between 0.75 and 17.9 mg/kg body weight between animals of different age, sex or strain (Busby, 1984). Numerous animal studies have shown that the liver is the main target organ and therefore the main symptoms of aflatoxin exposure in domestic and laboratory animals are hepatic injuries (Busby, 1984).

One of the major effects is a general reduction in weight gain for a variety of production animals, including pigs, cattle and poultry. Also, milk production in dairy animals can be decreased in the presence of aflatoxin- contaminated food (CAST, 1989)

CHAPTER 5

ADSORPTION PHENOMENA AND ADSORPTION OF AFLATOXINS

5.1. Introduction to Adsorption

Adsorption is a physical and/or chemical process in which compounds are accumulated at the interface of solid – liquid or solid-gas mixtures. Solid material on which the solutes of interest adhere is called “adsorbent”. Adsorbent must possess certain engineering properties depending on the applications such as large surface area, porous structure, rigidity, mechanical stability etc. Most common adsorbents are activated carbon, silica, zeolites and polymers. Also there are composite adsorbents. The material in fluid phase which is capable of being adsorbed is called “adsorbate” and the material adsorbed on to solid surface is called as “adsorbent”. This accumulation provides separation of the components from the fluid phase to solid phase. Affinity of the solute towards solid plays a critical role in adsorption. Main driving forces may be due to the electrostatic, chemical or van der Waals attractions. According to these interaction mechanisms adsorption process is classified into two groups as physical adsorption (physisorption) and chemical adsorption (chemisorption) based on the intermolecular forces involved and the comparison is given in Table 5.1.

Table 5.1. Comparison of physisorption and chemisorption.
(Source: Ruthven, 1984)

Physical adsorption	Chemisorption
Nonspecific	Highly specific
van der Waals, no electron transfer, although polarization of adsorbate may occur.	Electron transfer and sharing leading to bond formation between adsorbate and surface.
Monolayer or multilayer	Monolayer only
Only significant at relatively low temperatures	Possible over a wide range of temperatures
No dissociation of adsorbed species	May involve dissociation
Rapid, nonactivated, reversible	Activated, may be slow and irreversible, so desorption can be difficult hence high temperatures or modification of pH and eluent concentrations are required.
Low heat of adsorption (1.0 to 1.5 times latent heat of evaporation)	High heat of adsorption (>1.5 times latent heat of evaporation)

5.1.1. Physical Adsorption

Physical adsorption is relatively non-specific, the bonds are much weaker, and hence the process is reversible. Bonds formed in physical adsorption are held by columbic (or electrostatic) forces or hydrophobic attractions. The columbic forces originate in the ionic atoms and polar groups on the surface. The physical interactions among molecules, based on electrostatic forces, include dipole-dipole interactions, dispersion interactions and hydrogen bonding. When there is a net separation of positive and negative charges within a molecule, it is said to have a dipole moment. When two dipoles are near each other, the attraction between these molecules is called *dipole dipole interaction*. Hydrogen bonding is a special case of dipole-dipole interaction in which the hydrogen atom in a molecule has a partial positive charge and attracts an atom on another molecule, which has a partial negative charge. When two neutral molecules, which have no permanent dipoles, approach each other, a weak polarization is induced because of quantum mechanical interactions between their distributions of charge. This weak attraction is known as the dispersion interaction or the London-van der Waals force. Nonpolar compounds are adsorbed more strongly to nonpolar adsorbents. This is known as hydrophobic attraction. Longer hydrocarbon chain is more

nonpolar, so, degree of this type of adsorption increases with increasing molecular length (Yang, 1999).

5.1.2. Chemical Adsorption

The attraction between adsorbent and adsorbate is more powerful in chemisorption. Covalent or electrostatic chemical bonds with shorter bond length and higher bond energy occur between atoms. Chemisorption involves electron transfer and is essentially two-dimensional chemical reaction. The bond between adsorbate and surface is specific to particular sites or functional groups on the surface of the adsorbent.

5.2. Adsorption Equilibria

When the adsorbent and the adsorbate are in contact, adsorption takes place and after a sufficiently long time, the adsorbent and the adsorbate reach equilibrium. Adsorption equilibrium is experimentally determined. The data are used to construct a correlation namely adsorption isotherms. Adsorption isotherms are the representation of adsorbed amount as a function of pressure or concentration at constant temperature (Ülkü and Mobedi, 1991). Measurement of adsorption isotherm is an important step in the characterization of the interaction between the adsorbent and adsorbate.

The expression of adsorption equilibria for this study involves the uptake of aflB1 as adsorbate onto clinoptilolite rich PNZ. The basic factors affecting adsorption equilibrium are; the nature of the adsorbent, the nature of adsorbate, temperature and the concentration of adsorbate.

5.3. Adsorption Isotherm Models

Adsorption isotherms describe the equilibrium conditions for an adsorbate onto surface of an adsorbent. In general, the amount of material adsorbed is some complex function of the concentration therefore several models are proposed to describe the adsorption isotherms such as Langmuir, Freundlich, Redlich-Peterson and Temkin,

BET, Dubinin-Radushkevich isotherm model equations. However, most of the isotherms are described by the Langmuir, Freundlich adsorption isotherm models. These models describe the equilibrium characteristics of the adsorption. Each isotherm model has specific assumptions. In order to validity of the model, the assumptions for which the model should be taken into account.

5.3.1. Langmuir Model

Langmuir adsorption isotherm assumes that adsorption occurs on a homogenous adsorbent surface. The surface is made up of identical sites that are available equally and energetically equivalent with each sites carrying equal numbers of molecules. There is no interaction between adsorbate molecules. The langmuir equation can be used to describe adsorption behaviour of monomolecular layer.

The Langmuir isotherm is expressed as in Equation (5.1).where K:adsorption equilibrium constant and q_m : maximum adsorption capacity with fairly rapid attainment of a well-defined plateau and high affinity to a solid.

$$q_e = \frac{K \cdot q_m \cdot C_e}{1 + K \cdot C_e} \quad (5.1)$$

When it linearized, q_e approaches the the saturation value and a plot of the $1/q_e$ vs $1/C_e$ gives intercept of $1/q_m$ and the slope K/q_m

One of the characteristics of the Langmuir isotherm is given by separation factor R_L . The value of R_L give information about type of isotherm. R_L can be defined as follow .

$$R_L = \frac{1}{(1 + K C_0)} \quad (5.2)$$

Depending on the value of R_L , the characteristics of adsorption isotherm can be determined as follows;

$R_L=0$, the isotherm is irreversible;

$0 < R_L < 1$, the isotherm is favorable;

$R_L=1$, isotherm is linear

$R_L>1$, isotherm is unfavorable.

5.3.2. Freundlich Model

The Freundlich Adsorption Isotherm accounts the variety of the energy of adsorption on real surfaces. It can be used to describe both monolayer and multimolecular layer adsorption behaviour. It is expressed as below and where, where the constant K_f is a measure of adsorption capacity and n is a measure of affinity.

$$q_e = K_f \cdot C_e^{1/n} \quad (5.3)$$

A linearized form of Freundlich Equation can be written as;

$$\ln q_e = \ln K_f + n \ln C_e \quad (5.4)$$

K_f and n values can be calculated from the intercept and the slope of the linear regression line from the plot of $\ln q_e$ vs $\ln C_e$.

5.4. Factors Affecting the Adsorption

Many parameters affect the adsorption and adsorption isotherms like nature of the adsorbent and adsorbate, pH, temperature, nature of the solvent, nature of support, ionic strength, particle size, presence of extraneous ions, and solid/liquid ratio.

The nature of the adsorbate and adsorbent; Adsorption of solute is inversely proportional to its solubility in the solvent. Size of the solute is also important. If the rate of the adsorption is controlled by intraparticle diffusion, reaction generally will precede more rapidly within a given class of a compound with the smaller the adsorbate molecule. The physicochemical nature of the adsorbent have effects on both rate and capacity of adsorption. Specific surface area, pore size distribution of the micropores are the important features. Additionally, surface polarity is another important property.

Surface polarity corresponds to affinity with polar substances such as water therefore polar adsorbents are called “hydrophilic” and zeolites are included in.

pH effect; The pH of the medium strongly affects the adsorption in aqueous solutions. Hydrogen and hydroxide ions are adsorbed quite strongly where other ions are influenced by the pH of the solution. It directly affects the surface charge of the adsorbent. Within the varying pH values surface charge of the molecules are changed. This affects the electrostatic interactions. Because at the isoelectric point (pI) of the molecules net charge is zero.

Temperature; Temperature can decrease or increase the adsorption capacity of adsorbents. If the adsorbed amount increases with the increasing temperature, then the process is endothermic. On the other hand, if the adsorption decreases with the increasing temperature, then the process is said to be exothermic and the heat of adsorption is negative.

Solid/Liquid Ratio; The adsorption efficiency can increase or decrease with increasing solid/liquid ratio. This is due to the availability of the surface area of the adsorbent during the adsorption.

Initial concentration of adsorbate; Initial concentration of adsorbate affects the adsorption. In the lower initial adsorbate concentration lower driving force occurs between the adsorbent and solution.

Particle size; Decreasing the particle size leads to increase in the surface area. Thus, more active sites occur for the adsorption.

5.5. Adsorption Mechanism and Kinetics

Determination of adsorption mechanism is very important for design purposes. The adsorption process is described by four consecutive steps. In the first step, the solute is transported from the bulk solution to the external layer of the adsorbent. Step 2 involves diffusion of solute across the external film surrounding the particle. The third step is composed of pore diffusion and surface diffusion. Pore diffusion is the diffusion of solute in the pores and surface diffusion following surface reaction occurs along the adsorbent surface. In the step 4, solute is sorbed on the sorbent surface with surface reaction due to the physical or chemical interaction. In well agitated vessels, bulk diffusion is very rapid. External film diffusion occurs by molecular diffusion due to the

concentration difference between in the bulk fluid and the surface of the adsorbent. This case is generally limited in early stages because of rapid decrease of the driving force. Next, macropore mass transfer due to diffusion in the pores together with diffusion along the adsorbent surface can be considered. Finally, micropore diffusion occurs. If the micropore resistance is dominant, uptake rate is independent of the particle size. Therefore, effect of the particle size can show whether micropore resistance or macropore resistance is the dominant one.

Generally, more than one mechanism is effective in the adsorption. This phenomena is very complicated and the approaches were developed based on the simplification by identifying the rate controlling resistances. In order to identify the rate controlling mechanisms, different parameters should be analyzed in the kinetic experiments. The effects of the several experimental parameters (initial adsorbate concentration, pH, agitation speed and particle size and etc.) should be tested in order to identify the controlling mechanisms. For example, the experiments in different agitation speeds can provide information whether the external film diffusion is the controlling one or not. With the increase in the agitation speed, it is expected that diffusion rate of adsorbate from the bulk to the liquid boundary layer surrounding to the adsorbent becomes higher and the external mass transfer coefficients become higher also. Additionally, the external film diffusion can be effected by changing the particle size. Increase in the particle size results in decrease in the adsorbent surface area. If the external mass transfer is the controlling one, it is expected that increase in the particle size leads decrease in the uptake rate. In lower particle sizes, rapid initial uptake can be observed and equilibrium can be achieved in a shorter time. Furthermore, increasing the particle size causes higher intraparticle diffusion resistances and uptake rates become smaller. In the case of intraparticle control by macropore diffusion, adsorption rate is dependent to the particle size and there exists a concentration gradient through the particle whereas for micropore diffusion controlling system the rate of adsorption is not dependent on the particle size.

It is important to differentiate the diffusion and reaction controlled process. It is known that diffusion controlled systems are less temperature dependent. In the case of reaction controlled systems, adsorption is more dependent on the temperature. Therefore the results of temperature effect on adsorption provide information about the adsorption mechanism. The magnitude of the activation energy (E_a) indicates whether adsorption process is chemisorption or physical sorption. In the physical sorption, equilibrium

between adsorbate and adsorbent is rapid and reversible. The energy requirements are small due to the weak forces. In the chemisorption, sorption energy is usually greater than 25-30 kJ/mol.

The model equations and derivations are discussed in the following parts and the applications of these models were checked by comparing the model equations and the experimental data in the chapter 7.

5.6. Adsorption Kinetic Models

5.6.1. Adsorption Reaction Models

First Order Rate Model (Lagergren's model)

Lagergren presented first order rate equation to describe the kinetic process of liquid-solid phase adsorption in 1898. It is believed to be the earliest model describing the adsorption rate with respect to the adsorption capacity. This model is considered to include all steps in the adsorption process such as external diffusion, pore diffusion and binding to active sites (Chang et al., 2006).

The kinetic rate equation described below, where;

q_e : the adsorption capacity at equilibrium (mg/g),

q_t : the adsorption capacities at time t , (mg/g)

t : time (min),

k_{p1} (min^{-1}): the rate constant.

$$\frac{dq_t}{dt} = k_{p1}(q_e - q_t) \quad (5.5)$$

For the boundary conditions,

$t=0, q_t=0$

$t=t, q_t= q_t$

After integrating the equation becomes as follow;

$$\log(q_e - q_t) = \log(q_e) - \frac{k_{p1}}{2.303} t \quad (5.6)$$

$\log(q_e - q_t)$ versus t diagram is plotted and k_{p1} can be calculated from the slope.

Pseudo-second Order Rate Model (Ho's second order model)

Second order rate kinetic expressions were used in the adsorption studies in several ways (Sobkowsk and Cherwinski, 1974; Rithie, 1977; Blanchard et al., 1984 ; Ho, 1995). In order to distinguish the kinetics equation based on the concentration of a solution from the adsorption capacity of solids, this second-order rate equation has been called a pseudo-second-order rate equation. Ho's second order equation has been also called as pseudo-second-order rate equation (Ho, 2006)

In 1995, Ho described a kinetic process of the adsorption of divalent metal ions onto peat (Ho and McKay, 1998b), in which the chemical bonding among divalent metal ions and polar functional groups on peat, such as aldehydes, ketones, acids, and phenolics are responsible for the cation-exchange capacity of the peat. The main assumptions were the adsorption may be second-order, and the rate limiting step may be chemical adsorption involving valent forces through sharing or the exchange of electrons between the peat and divalent metal ions. In addition, the adsorption follows the Langmuir equation.

When the rate of adsorption is a pseudo-second order mechanism, the kinetic rate equation is presented as below;

$$\frac{dq_t}{dt} = k_{p2}(q_e - q_t)^2 \quad (5.7)$$

For the boundary conditions,

$$t=0, q_t=0$$

$$t=t, q_t= q_t$$

After integrating the equation becomes as follow;

$$\frac{1}{q_e - q_t} = \frac{1}{q_e} + k_{p2}t \quad (5.8)$$

$$\frac{t}{qt} = \frac{1}{k_{p2}q_e^2} + \frac{1}{q_e}t \quad (5.9)$$

q_e : the adsorption capacity at equilibrium (mg/g),

q_t : the adsorption capacities at time t , (mg/g)

t : time (min),

k_{p2} : the rate constant of Pseudo-second order rate model (g/mg.min).

The (t/q_t) versus t diagram is plotted and k_{p2} is calculated from the slope and q_e is calculated from the intercept.

The evaluation of rate constant k_{p2} is reported as; if the adsorption is chemically rate controlled, the slope will be independent of particle diameter and will depend only on the concentration of the adsorbate in solution and the temperature (Ho and McKay, 1998).

Elovich Reaction Rate Model

A kinetic equation of chemisorption was established by Zeldowitsch (1934) and was used to describe the rate of adsorption of carbon monoxide on manganese dioxide that decreases exponentially with an increase in the amount of gas adsorbed (Ho, 2006), which is the so-called Elovich equation as follows

The model equation is expressed below where

$$\frac{dq_t}{dt} = \alpha \exp(-\beta q_t) \quad (5.10)$$

α : the initial adsorption rate (mg/g.min)

β : the desorption constant(g/mg)

The Elovich equation is simplified with the assumption $\alpha\beta t \gg 1$ and the constants are calculated from the slope and the intercept of the plot with the axis q_t against $\ln(t)$.

5.6.2. Adsorption Diffusion Models

In the typical liquid/solid adsorption system, adsorption diffusion models involve bulk diffusion, film diffusion, intraparticle diffusion and surface reaction (mass action), For physical adsorption mass action is a rapid process and can be neglected for kinetic study.

5.6.2.1. External Film Diffusion

If the adsorbent particle is nonporous or diffusion within the particle is very rapid, than adsorption is observed on the outer surface of the particle. Diffusion takes place through the laminar film surrounding the external surface of the particle. The adsorbate concentration at the particle surface is in equilibrium with the fluid phase concentration (Karger and Ruthven 1992; Ülkü, 1991). Mass transport rate through the external laminar film can be expressed with rate law,

$$\frac{d\bar{q}}{dt} = k_f a (C - C^*) = \frac{3k_f a}{R_p} (C - C^*) \quad (5.11)$$

Where \bar{q} is the average solute concentration in the adsorbent, k_f is the film mass transfer coefficient, a is the specific surface area for the spherical adsorbent particle ($a = \frac{3}{R_p}$), R_p is the radius of the particle, C is the uniform concentration in the bulk solution, C^* is the equilibrium concentration.

At low concentrations, the relationship is linear and it is expressed by Henry's law $q^* = KC$.

$$\frac{d\bar{q}}{dt} = \frac{3k_f a}{R_p} (q^* - \bar{q}) \quad (5.12)$$

By applying the following boundary conditions,

$$t < 0, \quad C = q = 0$$

$$t > 0, \quad C = C_\infty = q_\infty / K$$

Equation 5.12 can be integrated by using the \bar{q} in the following equation and boundary conditions above. Therefore, Equation 5.13 can be obtained.

$$\bar{q} = \frac{3}{R^3} \int_0^R q r^2 dr \quad (5.13)$$

Equation 5.12 is rearranged and Equation 5.14 is obtained.

$$\frac{\bar{q}}{q_{\infty}} = 1 - \exp\left[\frac{3k_f t}{KR_p}\right] \quad (5.14)$$

$$\ln\left(1 - \frac{\bar{q}}{q_{\infty}}\right) = -R't \quad R' = \frac{3k_f}{R_p K} \quad (5.15)$$

R_p is the particle radius K is the constant of linear equilibrium ($q=KC$) and k_f is the film mass transfer coefficient. When the film diffusion or surface resistance is the rate limiting step, the plot of $\ln(1-q/q_{\infty})$ versus t should be a straight line and the slope is $-R'$. Actually the same relationship proposed by Boyd et al. (1947) as follow;

$$q = q_{\infty} [1 - \exp(-Rt)] \quad (5.16)$$

$$R = \frac{3D_e^1}{r_0 \Delta r_0 k'} \quad (5.17)$$

Where R (min^{-1}) is liquid film diffusion constant, D_e^1 (cm^2/min) is effective liquid film diffusion coefficient, r_0 (cm) is radius of adsorbent beads, Δr_0 (cm) is the thickness of liquid film, and k' is equilibrium constant of adsorption.

If the negligible intraparticle resistance is unrealistic, the analogous situation of external film control exist.

$$\frac{\bar{q}}{q_{\infty}} = 1 - \exp\left[\frac{3k_s t}{R_p}\right] \quad k_s = \frac{D_s}{\delta} \quad (5.18)$$

Mathew and Weber (1977) proposed an expression by using rate law fundamental equation with helping the following conversion (Equation 5.19). The concentration decay of adsorbate concentration in the solution for the initial period of adsorption can be used for the calculation of the external mass transfer coefficient.

$$V \frac{dC}{dt} = -w \frac{dq}{dt} \quad (5.19)$$

$$\ln \frac{C_t}{C_0} = -k_f St \quad (5.20)$$

In the expression, the surface area for mass transfer is defined as:

$$S = \frac{6m/V}{d_p \rho_p (1 - \varepsilon_p)} \quad (5.21)$$

where m is the mass of adsorbent, V is the volume of solution, d_p is the particle diameter, ρ_p is particle density and ε_p is particle porosity.

Dimensionless numbers can also be used to determine the experimental film mass transfer coefficients. Correlations given for Sherwood (*Sh*) number which characterizes the film mass transfer coefficients, can be used for this purpose.

$$Sh = \frac{2Rp k_f}{D_{AB}} = f(Sc, Re) \quad (5.22)$$

5.6.2.2. Particle Diffusion

Macropore Diffusion

There are several mechanisms taking place in macropore diffusion. The fundamentals are; molecular diffusion, Knudsen flow, surface diffusion and Poiseuille flow (Ülkü, 1991). In liquid systems, molecular diffusion is almost always dominant. Molecular diffusion takes place especially in large pores and at higher pressures. The effective pore diffusivity under molecular diffusion control is given below

$$\varepsilon_p D_p = \frac{\varepsilon_p D_m}{\tau} \quad (5.23)$$

Where, ε_p ; porosity of particle, D_p ; pore diffusivity, D_m ; molecular diffusivity and τ ; tortuosity factor.

In the case of the small pores and at low pressures, collision of diffusing molecules with the pore walls is more dominant compared to the collision within the

each other. This case can be expressed by Knudsen diffusion and Knudsen diffusivity for a straight cylindrical pore can be expressed below,

$$D_k = 9700 \bar{r} \frac{T^{0.5}}{M} \quad (5.24)$$

Where D_k is the Knudsen diffusivity (cm^2/s), \bar{r} is the average pore diameter, T is the temperature and M is the molecular weight.

Overall diffusivity can be considered where both Knudsen and molecular diffusivity are effective (Equation 5.25).

$$\frac{1}{\varepsilon_p D_p} = \frac{\tau}{\varepsilon_p} \left(\frac{1}{D_k} + \frac{1}{D_m} \right) \quad (5.25)$$

If micropore diffusion is rapid in the system, the concentration gradient within microparticles is uniform but there will be a concentration gradient through macroparticles. Hence macropore resistance is dominant. The expression is derived with the assumption of the local equilibrium reached between the adsorbed phase and fluid phase (Ruthven, 1984; Ülkü, 1991). The pore diffusivity is assumed to be independent of concentration:

$$(1 - \varepsilon_p) \frac{\partial q}{\partial t} + \varepsilon_p \frac{\partial c}{\partial t} = \varepsilon_p D_p \left[\frac{\partial^2 C}{\partial R^2} + \frac{2}{R} \frac{\partial C}{\partial R} \right] \quad (5.26)$$

Macropore diffusion in linear equilibrium ($q^* = KC^*$) is written as;

$$\frac{\partial C}{\partial t} = \frac{\varepsilon_p D_p}{\varepsilon_p + (1 - \varepsilon_p)K} \left[\frac{\partial^2 C}{\partial R^2} + \frac{2}{R} \frac{\partial C}{\partial R} \right] \quad (5.27)$$

Uptake curve equation can be written by using following boundary conditions.

$$C(R,0) = C_0,$$

$$q(R,0)=q_0=KC_0;$$

$$C(R_p,t)=C_0$$

$$q(R_p,t)=q_\infty=KC_0$$

$$\left. \frac{\partial C}{\partial R} \right|_{R=0} = \left. \frac{\partial q}{\partial R} \right|_{R=0} = 0$$

$$\frac{q_t}{q_\infty} = 1 - \frac{6}{\pi^2} \sum_{n=1}^{\infty} \frac{1}{n^2} \exp\left(\frac{-n^2 \pi^2 t D_p \varepsilon_p}{R_p^2 (\varepsilon_p + K - K \varepsilon_p)}\right) \quad (5.28)$$

Which is the same relationship proposed by Boyd et al. (1947) based on the solution of Barrer (1941).

$$F = \frac{q_t}{q_\infty} = 1 - \frac{6}{\pi^2} \sum_{n=1}^{\infty} \frac{1}{n^2} \exp\left(\frac{-n^2 \pi^2 t D^i}{r_0^2}\right) \quad (5.29)$$

In the equation 5.28 $\frac{D_p \varepsilon_p}{R_p^2 (\varepsilon_p + K - K \varepsilon_p)}$ is the time constant for the macropore diffusion and D_{eff} can be described as below.

$$D_{\text{eff}} = \frac{D_p \varepsilon_p}{(\varepsilon_p + K - K \varepsilon_p)} \quad (5.30)$$

Boyd et al. (1947), proposed a equation for pore diffusion based on the solution of Barrer (1941) and they expressed following equation;

$$F(t) = \frac{q_t}{q_\infty} = 1 - \frac{6}{\pi^2} \sum_{n=1}^{\infty} \frac{1}{n^2} \exp(-n^2 B t) \quad (5.31)$$

$$B = \frac{\pi^2 D_i}{r^2} \quad (5.32)$$

The value of B_t is can be calculated by using Reichenberg Table (Reichenberg, 1952) or using following expressions as given below;

$$F(t) < 0.85, B_t = \left(\sqrt{\pi} - \sqrt{\pi - \left(\frac{\pi^2 F(t)}{3} \right)} \right)^2 \quad (5.33)$$

$$F(t) > 0.85, B_t = 0.4977 - \ln(1 - F(t)) \quad (5.34)$$

The value of B_t is calculated for each F value and B_t versus time plot is drawn. Those plots are called Boyd plots and provide idea for controlling mechanisms (Malash and El-Khaiary, 2010; Jian Zhang et al., 2010; Yang et al., 2011)

- if the plot is linear and passes through the origin then intraparticle-diffusion controls the rate of mass transfer.
 - If the plot is nonlinear or linear but does not pass through the origin, then it is concluded that film-diffusion or chemical reaction control the adsorption rate
- Malash and El-Khaiary (2010) imply that using single formula (Equation 5.34) which is valid at $F(t) > 0.85$ is used in various studies and this causes some incorrect results.

Micropore Diffusion

When the system is isothermal and only micropore diffusion resistance exists, the diffusion equation for a spherical particle is:

$$\frac{\partial q}{\partial t} = \frac{1}{r^2} \frac{\partial}{\partial r} \left[r^2 D_c \frac{\partial q}{\partial r} \right] \quad (5.35)$$

For the following boundary conditions ,

$$\left. \begin{array}{l} t < 0, C=C_0, q =q_0 \text{ (r and t , independent)} \\ t \geq, C=C_\infty, q(r_c, t) = q_\infty \\ t \rightarrow \infty, C=C_\infty, q(r, t) \rightarrow q_\infty \end{array} \right\} \frac{\partial q}{\partial r} \Big|_{r=0} = 0 \quad \text{for all t.}$$

Crank proposed the following equation, which is the same equation with 5.28 and 5.29 where D_c is the intracrystalline diffusivity is replaced by D_{eff} . The approach based on the idea that if the spherical particle is initially free of solute, and the concentration of solute at the surface remains constant, external film resistance can be neglected according to the constant surface concentration.

$$\frac{q_t}{q_\infty} = 1 - \frac{6}{\pi^2} \sum_{n=1}^{\infty} \left(\frac{1}{n^2} \right) \exp\left(\frac{-n^2 \pi^2 D_c t}{r_c^2} \right) \quad (5.36)$$

Also, the equation 5.36 can be expressed in equivalent form (Equation 5.37)

$$\frac{q_t}{q_\infty} = 6 \left(\frac{D_c t}{r_c^2} \right)^{0.5} \left[\frac{1}{\sqrt{\pi}} + 2 \sum_{n=1}^{\infty} i \operatorname{erfc} \left(\frac{nr_c}{\sqrt{D_c t}} \right) \right] - 3 \frac{D_c t}{r_c^2} \quad (5.37)$$

$$\frac{q_t}{q_\infty} = 1 - \frac{6}{\pi^2} \exp\left(\frac{\pi^2 D_c t}{r_c^2} \right) \quad (5.38)$$

In the short time region ($\frac{q_t}{q_\infty} < 0.3$), the equation 5.38 can be simplified by neglecting the higher order terms and Equation 5.39 can be obtained. The system is assumed isothermal, infinite volume and diffusivity is assumed constant which occurs if concentration change is small (Karger and Ruthven 1992; Ülkü, 1991).

$$\frac{q_t}{q_\infty} = \frac{6}{\sqrt{\pi}} \left(\frac{D_c t}{r_p^2} \right)^{1/2} \quad (5.39)$$

In the long time region ($\frac{q_t}{q_\infty} > 0.7$), Equation 5.40 can be written as,

$$1 - \frac{q_t}{q_\infty} \cong \frac{6}{\pi^2} \exp\left(\frac{-\pi^2 D_c t}{r_c^2} \right) \quad (5.40)$$

Equation 5.39 can be rearranged into equation 5.41 and this expression is known as Weber-Morris Model Equation as presented in equation 5.41.

$$q_t = \frac{6}{\sqrt{\pi}} q_\infty \left(\frac{D_e t}{r_p^2} \right)^{1/2} \quad (5.41)$$

$$q_t = k_d t^{0.5} \quad (5.42)$$

Therefore, Intraparticle rate constant (k_d) in Weber-Morris equation can be written as,

$$k_d = \frac{6D_i^{0.5} q_\infty}{\sqrt{\pi} r_p} \quad (5.43)$$

The Weber Morris model equation provides information on the rate controlling mechanisms. The practical way is plotting the q_t vs $t^{0.5}$ graph and if the straight line passes through the origin, intraparticle diffusion is the rate limiting step. Otherwise, other mechanisms can contribute for controlling.

Besides the rate equations, dimensionless numbers can provide information to determine the rate control mechanisms. Biot number is used to make a comparison between the internal mass transfer resistance and external mass transfer.

$$Bi = \frac{k_f r}{3\epsilon D_p} = \frac{k_f r}{D_e} = \frac{Sh}{6} \frac{D_m}{\epsilon_p D_p} \quad (5.44)$$

Where, k_f is the external mass transfer coefficient (m/s), r is the radius of particle (m), ϵ is the porosity of particle D_p is the pore diffusivity (m^2/s), D_e is the effective diffusivity (m^2/s), D_m is the molecular diffusivity (m^2/s).

External mass transfer and internal mass transfer mechanisms can be discriminated by considering the limitations about Bi number. The criterion for negligible external mass transfer resistance is given as $Bi > 20$ (Ruthven, 1984). If the rate of mass transfer in the external film increases as compared to the intraparticle mass

transfer rate, Bi increases. For Biot number $\ll 1$, the adsorption rate is external mass transfer resistance controlled. While for $Bi \gg 100$, pore diffusion is predominant (Maiti et al., 2009).

5.7. Thermodynamic Properties

In the design of adsorption systems, thermodynamic properties are critical to estimate the performance and predict the mechanism of the adsorption. These parameters include directly measurable properties (like temperature, equilibrium constant), and properties which cannot be measured directly such as activation energy (E_a), activation parameters, Gibbs' free energy enthalpy, entropy change and heat of adsorption. In the adsorption studies, both energy and entropy factors must be considered in order to determine which processes will occur spontaneously.

Gibbs Free Energy (ΔG°), Enthalpy (ΔH°), and Entropy (ΔS°) Change

The Gibbs free energy change ΔG° (kJ/mol), is the fundamental criterion of spontaneity and defined by the Gibbs–Helmholtz equation:

$$\Delta G^\circ = -RT \ln K \quad (5.45)$$

Therefore in the Equation 5.44 ; K is the Langmuir constant, R is the universal gas constant, 8.314×10^{-3} (kJ/mol.K), T is the absolute temperature (K).

In the Van't Hoff equation, the equilibrium constant is expressed in terms of enthalpy ΔH° (kJ/mol), and entropy ΔS° (kJ/mol), changes.

$$\ln K_{LF} = \frac{\Delta S^\circ}{R} - \frac{\Delta H^\circ}{RT} = -\frac{\Delta G^\circ}{RT} \quad (5.46)$$

Enthalpy (ΔH°) and entropy (ΔS°) change can be obtained by plotting the experimental data $1/T$ versus $\ln K$. Entropy and enthalpy changes can be calculated from slope and intercept values respectively. The magnitude and sign of enthalpy change give information on the types of adsorption (physical or chemical) and nature of

adsorption (exothermic or endothermic process). Entropy change (ΔS°) provides information on randomness at solid /liquid interface.

Activation Energy

The activation energy of adsorption can be calculated by Arrhenius relationship:

$$\ln K = \ln A - \frac{E_a}{RT} \quad (5.47)$$

Where K is the rate constant, A the Arrhenius constant which is a temperature independent factor, E_a the activation energy (kJ/mol), R the gas constant ($8.314 \cdot 10^{-3}$ kJ/mol K) and T is the temperature in Kelvin (K)

The rate constants for the 2nd order model or intraparticle diffusion model can be used to estimate the activation energies. The magnitude of the activation energy (E_a) gives an idea about the type of sorption processes.

In physical sorption, equilibrium between the adsorbent surface and the adsorbate is usually rapidly attained and easily reversible, in which the energy requirements are small, because the forces involved in physical adsorption are weak. Chemical sorption is specific and much stronger forces are involved. In chemical sorption the adsorbed molecules are held on the surface by chemical bonds. In this case, the sorption energy is usually greater than 25-30 kJ/mol. However, diffusion sorption processes have lower energies.

Table 5.2. Recent thermodynamic studies for different adsorbent-adsorbate pairs

Adsorbent adsorbate pair	Thermodynamic criteria and evaluation of results	Calculation method	Reference																			
Arsenic(V)-dolomite	<table border="1"> <tr> <th colspan="2">T(K), ΔG° (kJ/mol)</th> </tr> <tr> <td>T=293</td> <td>80.57</td> </tr> <tr> <td>T=318</td> <td>87.75</td> </tr> <tr> <td>T=338</td> <td>93.50</td> </tr> <tr> <td>T=353</td> <td>97.81</td> </tr> <tr> <th colspan="2">ΔH° kJ/mol)</th> </tr> <tr> <td colspan="2">-3.67</td> </tr> <tr> <th colspan="2">ΔS° (kJ/mol)</th> </tr> <tr> <td colspan="2">-287.35</td> </tr> </table>	T(K), ΔG° (kJ/mol)		T=293	80.57	T=318	87.75	T=338	93.50	T=353	97.81	ΔH° kJ/mol)		-3.67		ΔS° (kJ/mol)		-287.35		<ul style="list-style-type: none"> • Positive ΔG°, sorption was not spontaneous, and may be chemisorption • Negative ΔS° decreased randomness at the solid liquid interface during sorption • Negative ΔH°, exothermic 	$\ln \frac{K_{2ads}}{T} = \left[\ln \left(\frac{k_B}{h_p} \right) + \frac{\Delta S^\circ}{R} \right] - \frac{\Delta H^\circ}{R} \left(\frac{1}{T} \right)$ <p> k_B, Boltzmann constant, (1.3807×10^{-23} J/K) h_p, Planck constant (6.6261×10^{-34} J s), R, the ideal gas constant ($8.314 \text{ J g}^{-1} \text{ K}^{-1}$), K_{2ads}, pseudo-second-order constant (k2) </p> $\ln K_{2ads} = \ln(K_0) - \frac{E}{R} \left(\frac{1}{T} \right)$	Salameh et al., 2010
T(K), ΔG° (kJ/mol)																						
T=293	80.57																					
T=318	87.75																					
T=338	93.50																					
T=353	97.81																					
ΔH° kJ/mol)																						
-3.67																						
ΔS° (kJ/mol)																						
-287.35																						
Methylene blue-natural zeolite	<table border="1"> <tr> <th colspan="2">T(K), ΔG° (kJ/mol)</th> </tr> <tr> <td>T=298</td> <td>-9.60</td> </tr> <tr> <td>T=318</td> <td>-11.3</td> </tr> <tr> <td>T=333</td> <td>-12.2</td> </tr> <tr> <th colspan="2">ΔH° kJ/mol)</th> </tr> <tr> <td colspan="2">12.9</td> </tr> <tr> <th colspan="2">ΔS° (kJ/mol K)</th> </tr> <tr> <td colspan="2">-0.0758</td> </tr> </table>	T(K), ΔG° (kJ/mol)		T=298	-9.60	T=318	-11.3	T=333	-12.2	ΔH° kJ/mol)		12.9		ΔS° (kJ/mol K)		-0.0758		<p>Negative ΔG°, spontaneous adsorption with a high preference of MB onto zeolite. The negative value of ΔG° decreases with an increase in temperature, indicating that the spontaneous nature of adsorption were inversely proportional to the temperature and higher temperature favored.</p> <p>Positive ΔH°, endothermic nature Positive ΔS°, increased randomness at the solid-solute</p>	$K'_c = \frac{c_{ad,e}}{c_e}$ $\Delta G^\circ = \Delta H^\circ - T\Delta S^\circ$ $\Delta G^\circ = -RT \ln K'_c$	Han et al., 2009		
T(K), ΔG° (kJ/mol)																						
T=298	-9.60																					
T=318	-11.3																					
T=333	-12.2																					
ΔH° kJ/mol)																						
12.9																						
ΔS° (kJ/mol K)																						
-0.0758																						

(cont. on next page)

Table 5.2.(Cont.)

Adsorbent adsorbate pair	Thermodynamic Criteria and evaluation of results		Calculation method	Reference																					
Aminobenzoic acid- different polymeric adsorbents	<table border="1"> <tr> <th colspan="2">T(K), ΔG° (kJ/mol)</th> </tr> <tr> <td>T=283</td> <td>-6.19</td> </tr> <tr> <td>T=298</td> <td>-6.52</td> </tr> <tr> <td>T=313</td> <td>-6.53</td> </tr> <tr> <th colspan="2">ΔH° (kJ/mol)</th> </tr> <tr> <td colspan="2">-23.14</td> </tr> <tr> <th colspan="2">ΔS° (kJ/mol)</th> </tr> <tr> <td>T=283</td> <td>-59.89</td> </tr> <tr> <td>T=298</td> <td>-55.77</td> </tr> <tr> <td>T=313</td> <td>-53.07</td> </tr> </table>		T(K), ΔG° (kJ/mol)		T=283	-6.19	T=298	-6.52	T=313	-6.53	ΔH° (kJ/mol)		-23.14		ΔS° (kJ/mol)		T=283	-59.89	T=298	-55.77	T=313	-53.07	<p>Negative ΔG°, sorption was spontaneous Negative ΔS°, more ordered arrangement of solute molecules is shaped on the surface of the adsorbent (indicative of an enthalpy-driven adsorption.) the absolute values of enthalpy changes are in the 10–30 kJ/mol range , the integrated adsorption mechanism involving the π–π interaction, the Van derWaals force and hydrogen-bonding interaction and indicates physical adsorption</p>	$\lg(1/C_e) = \lg(K_0) + \left(\frac{-\Delta H^\circ}{2.303RT} \right)$ $\Delta G^\circ = -nRT$ $\Delta S^\circ = \frac{\Delta H^\circ - \Delta G^\circ}{T}$ n, Freundlich const	Wang et al., 2007
T(K), ΔG° (kJ/mol)																									
T=283	-6.19																								
T=298	-6.52																								
T=313	-6.53																								
ΔH° (kJ/mol)																									
-23.14																									
ΔS° (kJ/mol)																									
T=283	-59.89																								
T=298	-55.77																								
T=313	-53.07																								
Remazol Black B (diazo) Dye-activated lignite	<p>Negative ΔH°, exothermic. Negative ΔG°, a spontaneous adsorption process. The small entropy value may indicate that the dye adsorption is accompanied by dehydration, which liberates water molecules, thus increasing the overall entropy change and compensating for the loss of freedom caused by the dye adsorption</p>		$\ln K_L = \frac{\Delta S^\circ}{R} - \frac{\Delta H^\circ}{RT} = - \frac{\Delta G^\circ}{RT}$ $\ln K_L = (\Delta S^\circ/R) - (\Delta H^\circ/RT) = - \Delta G^\circ$	Petrolekas and Maggenakis, 2007																					
Aflatoxin B1-HSCA clay	<p>Enthalpy was near or above -40 kJ/ mol. ΔG° was negative (-29 kJ/mol), and so the adsorption was spontaneous.</p>	<p>enthalpy of <20 kJ/mol (physisorption), enthalpy >20 kJ/mol (chemisorption).</p>	$K_d = \frac{q}{(Q_{\max} - q)C_w}$ $\Delta G^\circ = -RT \ln K_d$ $\Delta H^\circ_{ads} = - \frac{R \ln \left(\frac{K_{d2}}{K_{d1}} \right)}{\frac{1}{T_2} - \frac{1}{T_1}}$	Grant and Phillips, 1998																					

5.8. Adsorption of Aflatoxins by Minerals

In the chapter 4, aflatoxins are described and mentioned in detail. Although it is known that the one of the reason behind the beneficial properties of the clay minerals in health studies is found to be related with the property of the clay minerals to remove toxin materials, there has not been a detailed adsorption study until this time. Factors for adsorbent's efficiency to adsorb mycotoxins are shown in the following list.

- Adsorption features /selectivity
- Hydrophobicity
- Surface electric charge
- Polarity of mycotoxins

Zeolite and bentonite minerals in non-organic form adsorb more polar mycotoxins such as aflatoxins whereas less polar and non-polar mycotoxins are hardly adsorbed or not adsorbed at all. Negative surface charge of adsorbents facilitates adsorption of mycotoxins requires partial correction of the mineral surface charge and surface hydrophobicity (Dakovic et al., 2005). The kinetic diameters of aflatoxins range from 5.18 Å to 6.50 Å. Given the dimensions of these molecules, they can not normally enter the channels of clinoptilolite crystals as mentioned in Chapter 3. Cation composition, and therefore the extent of surface hydration, was proved to be effective in adsorption of mycotoxins, especially those of less polarity such as ochratoxins and zearalenone, whereas it was less effective in the adsorption of more polar ones like aflatoxins. The adsorption capacity of clinoptilolite for mycotoxins, which is of the order of some hundred µg/g, was demonstrated to be a function of various parameters including temperature pH, concentration and presence of interfering species in the solution as well as the nature of the adsorbent. Also the specific properties of the adsorbate, such as polarity, solubility, size, shape and capacity played a significant role in the adsorption process. Dakovic et al. (2000) reported that adsorption kinetics turned out to be very rapid in the first minutes of reaction, at which most of the adsorption capacity was exhausted, then it slowed down noticeably to reach an asymptot. Soption kinetics of aflatoxins B1 on clinoptilolite was proved to be, in the early stages, a first order reaction (Dakovic at al., 2000).

The studies on the adsorption of aflatoxins on different minerals including clays, zeolites, and the results obtained are summarized in Table 5.3.

Table 5.3. Studies on adsorption of AfB1 by several clay minerals

Clay	Aflatoxin	pH	Temperature (°C)	Adsorption amount	Solid /liquid ratio	Reference
Smectite Clays	afB1	from 7.1 to 9.6	25 °C	from 0.06 to 0.68 (mol/kg)	$\frac{0.1}{100}$	Arvide et al., 2008
Organozeolite and unmodified zeolitic tuff	afB1	pH 3, pH 7, pH 9	Room temperature	adsorption index pH3, 95% pH7, 87% pH9, 87%	$\frac{0.4}{100}, \frac{0.2}{100},$ $\frac{0.1}{100}, \frac{0.08}{100},$ $\frac{0.04}{100}$	Dakovic et al., 2005
Clinoptilolite	afB1	3.8	25 °C	1.8 µg/mg	$\frac{1}{100}$	Tomasevic-Canavic et al., 2001

5.9. Adsorption of Aflatoxins by Probiotic Lactic Acid Bacteria

Fermentation of food has been used as a method of preservation for centuries, and it is known that LAB reduces mold growth and aflatoxin production. Inhibition of aflatoxin biosynthesis is due to lactic acid or lactic acid metabolites, which are heat stable and low molecular weight compounds. Furthermore, systemic beneficial effects of probiotics, as discussed in the previous section, will also play a role in reducing the adverse effect of aflatoxins in animals and humans. This case is also evaluated in development of the strategies to prevent aflatoxin toxicity. Actually, the strategies to prevent the presence of aflatoxins in foods include some physical, chemical, and biological methods to eliminate, inactivate or reduce the bio-availability of these mycotoxins in contaminated products. It is known that lactic acid bacteria (LAB) and some yeast, *Saccharomyces cerevisiae*, are capable to bind aflatoxins in liquid media to

cell wall components, polysaccharides and peptidoglycans (Haskard et al, 2001;Lahtinen et al., 2004)

During the last decade, aflatoxin binding of lactic acid bacteria has been extensively studied (El Nezami et al., 1998; Haskard et al., 2001; Peltonen et al., 2000; Peltonen et al., 2001;Lahtinen et al., 2004; Hernandez-Mendoza et al.,2009; Hamidi et al., 2012). Several bacterial strains, of food or human origin, have been tested for their ability to bind aflatoxins and other mycotoxins to their surface and some of these studies tabulated (Table 5.4). Actually, several factors can affect the afB1 adsorption property such as species and strain type, initial afB1 concentration, organism concentration and etc. A number of different strains of lactic acid bacteria and bifidobacteria have been tested for AFB1 removal from buffered aqueous solution *in vitro* .But, only one initial afB1 concentration (5 µg/ml)was used in most of the these studies. It is known that initial afB1 concentration is effective on removal percentage. Therefore, this point should be taken account in evaluation also. ElNezami et al (1998) found that Gram-positive bacteria (five strains of *Lactobacillus* and one *Propionibacterium*) were more efficient in removing aflatoxin from liquid medium than Gram-negative *E. coli*. Among the five strains of *Lactobacillus*, *L. rhamnosus* strain GG (GG) and strain LC705 (LC705), found to be most efficient binders for aflatoxin B1(80% removing approximately).They reported that binding occurs within first few minutes of incubation, which implies that it is a very rapid process. These two strains were later confirmed as most efficient AFB1 binders among nine stains of *Lactobacillus* (Haskard et al., 2001). Peltonen and coworkers (Peltonen et al., 2001) also studied a range of *Lactobacilli* and *Bifidobacteria* and found remarkable differences in AFB1 binding abilities, even in strains very closely related. The removal was influenced by both temperature and bacterial concentration. Different minimum concentrations have been reported such as 5×10^9 CFU/ml of either *L. acidophilus* or *B. longum* to remove only 13% of the AFB1 within one hour (Bolognani et al., 1997) or 2×10^9 CFU/ml of *Lactobacilli* and *Propionibacterium* to remove 50% of free AFB1 but higher binding occurred at 10^{10} CFU/ml (ElNezami et al., 1998a). When the bacteria are subjected to various chemical and physical treatments, their ability to remove AFB1 can be increased significantly. Autoclaved cells of *L. casei* remove significantly more AFB1 from phosphate buffered saline (PBS) compared to viable bacteria (Thyagaraja and Hosono, 1994). Heat treatment (boiling for 1 hour) and acid treatment also significantly enhanced AFB1 binding (ElNezami et al., 1998a, b). Peltonen and coworkers compared

the binding ability of various strains of viable and heat treated *Bifidobacteria* and found that the viable bacteria bound 4-56% while heat-treated bacteria bound 12-82% of the AFB1 (Peltonen et al., 2001). In contrast, Lankaputra and coworkers found that viable bacteria bound more dietary mutagens compared to heat treated bacteria (Lankaputhra and Shah, 1998).

In order to clarify the *in vitro* aflatoxin B1 removal by lactic acid bacteria and *S. cerevisiae*, a mathematical model has been proposed (Bueno et al., 2006). This model suggests the attachment of Aflatoxin B1 molecules to the surface of the organism and takes two process into consideration; Binding (adsorption) and release (desorption) of aflatoxin to and from the binding site on the surface of the organisms (Bueno et al., 2006 ; Lee et al., 2003). This model allows to estimate the number of aflatoxin B1 binding sites (M), the system equilibrium constant (K_{eq}) and the effectiveness.

In another *in vitro* study the binding ability of GG, LC705 and PJS for AFB1 was tested *ex vivo* in the intestinal lumen of chicks (ElNezami et al., 2000a). Authors report that GG removed 54%, LC705 removed 44% and PJS removed 36% of the AFB1 from the soluble fraction of the luminal fluid within one minute. These results imply that bacterial AFB1 binding appears under physiological conditions in the animal and that this could be used to reduce the bioavailability of aflatoxin in the organism.

Table 5.4. Some of the studies on binding of Aflatoxins by Lactic Acid Bacteria

Organism	Tested Aflatoxin concentration, solution type, pH, Temperature (°C), time (1 h)	Adsorption	Main results	Reference
<i>L. rhamnosus</i> GG, LLb. <i>L. rhamnosus</i> LC-705, <i>Propionibacterim freudenreicii</i> subsp. <i>shermanii</i> JS	afB1, 0.0017 - 13.3 µg/ml PBS 7.3, 37 °C, 1 h	specific rate 1.5-5 µg/10 ¹⁰ cells/h	Higher adsorption affinities and lower desorption constants for heat killed lactobacilli that viable counterparts	Lee et al., 2003
<i>L. fermentum</i> subsp. <i>cellobiosus</i> , <i>L. acidophilus</i> , <i>Saccharomyces cerevisiae</i>	5 µg/ml, PBS 7.3, 37 °C, 1 h	7.2 % to 42.8 (%afB1 bound)	Binding is rapid process(no more than 1 min) Binding is reversible Binding is bacteria and toxin concentration dependent Similar results were obtained for heat killed and viable organism	Bueno et al., 2007
<i>L. paracasei</i> F19 <i>B. lactis</i> Bp 12 <i>L. crispatus</i> M247 <i>L. crispatus</i> MU5 <i>L. salivarius</i> LM2 - 118 <i>L. johnsonii</i> LJ-1	5 µg/ml, PBS 7.3, 37 °C, 1 h	5.8 to 31.3%. (%afB1 bound)	Results may explain some of the antimutagenic and anticarcinogenic effects of probiotic micro-organisms	Peltonen et al., 2000

CHAPTER 6

MATERIALS AND METHODS

6.1. Materials

6.1.1. Chemicals

The chemicals used in the study were listed in Appendix A.

6.1.2. Investigated Probiotic Sources

In this study, 3 different sources (Human milk, boza and fermented cabbage) were used to investigate probiotic potential. The samples were microbiologically analyzed by means of the lactobacilli loads. One of the human milk was kindly provided by healthy volunteer mother of 2 months baby and the milk was transferred into sterile falcon tubes after sampling and it was transferred into laboratory and kept at the refrigerator conditions (4 °C) to avoid the contamination and analyzed within the 24 h. Two kinds of boza were used. They were wheat fermented and corn fermented boza samples. All the food samples were prepared by conventional home style fermentation techniques without adding any commercial starter culture. Natural flora is involved in the fermentation process.

6.1.3. Reference Strains

Following reference lactobacilli reference stains provided by National Center for Agricultural Utilization Research were used in the microbiological experiments as controls.

1. *Lactobacillus casei* subsp. *casei* NRRL-B 1922
2. *Lactobacillus plantarum* NRRL-B 4496

6.1.4. Reference Minerals and Natural Zeolite Samples

Clinoptilolite rich reference mineral and Rhyolite type mineral were used in the experiments as controls.

In the purification study, the clinoptilolite reference with >95 clinoptilolite content obtained from Mineral Research, Clarkson, New York was supplied kindly by F. Mumpton in powder (27031, Castle Creek, Idaho) and it is referred as Idaho in the thesis and used in the purification and characterization studies.

Rhyolite type reference mineral (JR-3) from Japanese Reference Rock Standards (JRRS) were supplied by Geological Survey of Japan. Due to the certified chemical composition it was used in elemental analysis as a control.

As parent mineral, clinoptilolite rich mineral from the Grdes region, which were prepared and characterized by Narin (Narin,2009), were used in the study after purification.

6.2. Methods

6.2.1. Isolation and Characterization of Organism

6.2.1.1. Isolation of Lactobacilli Strains from Different Sources

Different lactic acid bacteria sources (human milk, 2 wheat fermented and 1 corn fermented boza, and 2 fermented cabbage) were used as potential probiotic sources. For the isolation procedure, 10 g of the samples were homogenized in 90 ml of 0.1 % (g/g) pepton /water solution and this homogenate was considered as 10⁻¹ dilution. Then, serial dilutions were prepared aseptically by transferring 1ml of the homogenate into 9 ml of the 0.1 % (g/g) pepton /water solution. This serial dilution procedure was continued until obtaining the 10⁻⁸ dilution. For the lactobacilli load analyses, 1 ml aliquot of the 10⁻⁵, 10⁻⁶, 10⁻⁷, 10⁻⁸ dilutions were plated with MRS (Man Rogosa Sharpe) agar by using double layer pour plate technique and they were incubated for 48 h at 37 °C in MRS agar (pH5.6) plates. After incubation, plates that have colonies between 30-300 were used for counting. The results were expressed as colony forming

units (CFU) per ml. This counts provided general idea for microbial load and lactobacilli capacities of the samples.

6.2.1.2. Purification and Preliminary Identification

For the purification, one of the colonies was streaked several times and colony morphologies (color, shape and size) were examined visually until obtaining pure cultures. The isolates were coded according to the sources.

6.2.1.3. Catalase Test

Catalase is an enzyme produced by many organisms. This enzyme breaks down hydrogen peroxide into water and oxygen and gas bubbles were observed.



Lactobacilli organisms were catalase negative. The lack of catalase is a significant diagnostic characteristic. Overnight cultures of the isolates were grown on MRS agar plates at 37 °C and catalase status were determined by dropping 3%(v/v) hydrogen peroxide solution on to colonies. The isolates demonstrating catalase positive property was eliminated at this stage.

Then, each strain was tested for the catalase reaction. Catalase negative isolates were chosen. The isolates were Gram stained and cell appearances were observed under the light microscopy. Gram positive and bacilli shape stains which belong to Lactobacilli genus and these isolates were chosen. The isolates which have heterogeneous cell morphologies were eliminated.

6.2.1.4. Microscopic Examination of the Cell Morphology

Simple staining technique was applied to observe the cell morphologies under the light microscope. This technique consists of following steps.

1. Transferring a loop full culture onto microscope slide.
2. Drying aseptically.
3. Heat fixation (exposing to flame 2-3 times for 1-2 sec)
4. Staining with methylene blue for 1-2 min.
5. Washing under the tap water.
6. Drying by blotting onto cotton towels and keeping at laboratory conditions until microscopic observations.

After staining, the cell shapes and arrangements were examined under the light microscope. The yeast cells and cocci shaped cells were differentiated from bacilli shaped cells. The isolates having rod shape cell morphology were used for progressive studies. Others were eliminated.

6.2.1.5. Gram Status

The Gram status of the isolates was determined by Gram staining technique. Lactobacilli organisms were Gram positive and the blue-purple color indicates the Gram positive property. Overnight cultures were transferred into 1.5 ml of the sterile eppendorf tubes. Cells were centrifuged for 5 min at 5000 rpm and concentrated by removing most of the supernatant above and resuspended in remaining phase. Then, Gram staining procedure was applied as follows,

1. Transferring approximately 10 μ L of the cell suspension onto microscope slide.
2. Drying near the flame.
2. Heat fixation (exposing to flame 2-3 times for 1-2 sec)
3. Primary staining with crystal violet for 1 min.
4. Washing excess stain under the tap water.
5. Applying of Gram's Iodine mordant for 1 min.
6. Washing excess mordant under the tap water.
7. Applying acetone or alcohol (95%) decolorizing agent for 6 sec.
8. Counter staining with safranin for 30 sec.
9. Washing excess stain under the top water
10. Drying by blotting onto cotton towels and keeping at laboratory conditions until microscopic observations.

6.2.1.6. Long Term Preservation of the Isolates

The isolates indicating catalase negative property and rod shaped cell morphology were preserved in MRS broth medium with 20%(v/v) glycerol as frozen stocks at -80 °C. Basically, 0.5 ml of the overnight cultures were mixed with 0.5 ml of the MRS broth medium with 20%(v/v) glycerol in cryotubes and stored at -80 °C refrigerator.

6.2.1.7. Gas Production from Glucose

This test provided the homofermentative or heterofermentative status of the isolates. 80 µL of the overnight cultures were inoculated into citrate lacking MRS broths with inverted durham tubes (Appendix B.1) After incubation at 37 °C, gas accumulation in durham tubes was indicator of the evidence for CO₂ production from glucose.

6.2.1.8. Growth at Different Temperatures

80 µL of the overnight cultures were transferred into the tubes containing 5 ml of the test media (Appendix B.2). After, inoculation incubation was carried out at 15 °C and 45 °C for 7 days. Cell growth was detected by change the color of the culture from purple to yellow.

6.2.1.9. Growth at Different Salt Concentrations

80 µL of the overnight cultures were transferred into the tubes which contained 5 ml of the NaCl test media (Appendix B.3). Isolates were tested for growth at 6.5% NaCl concentration. They were incubated at 37 ° for 7 days. Cells growth was detected by changing the color of the culture from purple to yellow.

6.2.1.10. Arginine Hydrolysis

80 µL of the overnight cultures were transferred into the tubes containing 5 ml of the arginine test media (Appendix B.4). They were incubated at 37 °C for 5 days. After the incubation, ammonia production was detected by using Nessler reagent. 50 µL of the culture broth were pipetted into each well of the 96 well plates and 50 µL of the Nessler reagent was added. Immediate orange color formation indicates the ammonia production.

6.2.1.11. Species Level Identification

Species level characterization was performed on the basis of their sugar fermentation profiles. All the reactions were performed by using 96-well microtitre plates. Three different sugars were used. For each test, strains were inoculated in 5 ml MRS broth (50ml/L), and were then incubated at 37 °C for 24 h to obtain overnight cultures. Next, cultures were centrifuged at 10 000 rpm for 10 min. Pelleted cells were washed and resuspended in MRS (without glucose) containing bromocresol purple as the pH indicator. 40µl of filter sterilized (0.22µm, Millipore) 10% sugar solutions were pipetted into each well. On to the sugar solutions, 160 µl of suspended cells were added. Thus, 2% final sugar concentration was obtained. Duplicate reactions were prepared for each of the sugar fermentations experiment. After 24 h incubation at 37°C, the absorbances were read at 690 nm (Ins). Glucose fermentation was used for positive control, and samples without sugar were used for negative control.

6.2.2. Tests for Probiotic Criteria

6.2.2.1. Acid Tolerance

The pre-selected isolates were grown in their specific broths at 37 °C for 24 h. The cells were harvested by centrifugation, separated and suspended in sterile phosphate-buffered saline (PBS pH 7.3) prepared dissolving NaCl (9 g/l), Na₂HPO₄x2H₂O (9 g/l), and KH₂PO₄ (1.5 g/l) in distilled water. The concentrations of

the suspensions were 6–8 log CFU/ml. 30 µl aliquot of each bacterial suspension was inoculated into serial sterile microtiter plate wells with 270µl of PBS at pH values of 2.5 and 5 adjusted using HCl. The pH 5 was used as a control. The microtiter plates were incubated at 37°C and the Viable count (VC) were counted on their specific media after exposure for 4 h. Strains with a VC no lower than 2 logcfu/ml with respect to the control were considered to be acid resistant.

6.2.2.2. Bile Salts Tolerance

The isolates were grown in their specific broths at 37 °C for 24 h. 30µl aliquot of incubated broth was inoculated in the wells of sterile microtiter plates with 270µl of sterile MRS broth. For each strain, the following experiments were performed in triplicate: MRS broth was used at pH values of 5 and 7 prepared with and without 0.3% (w/v) oxgall. The inoculated microtiter plates were incubated at 37°C. The VC of control (no bile) and test cultures (0.3% oxgall) was monitored at 0, 1, 2, 4 and 8 h.

6.2.2.3. Pancreatic Enzyme Tolerance

The isolates were grown in their specific broths at 37°C for 24 h; 30µl aliquots of incubated broth were inoculated into the wells of microtiter plates with 270 µl of the test medium (150 mM NaHCO₃ and 1.9 mg/ml pancreatin (Sigma); pH 8). The cultures were shaken for 3 h at 37°C. Survival of the strains was examined by plating onto their specific media after 0 and 3 h.

6.2.2.4. Susceptibility to Antibiotics

The susceptibility to antibiotics were tested for each strain. The isolates were grown in their specific broths at 37°C for 24 h. 0.5ml of the overnight cultures were mixed with 19.5 ml of the MRS agar and plated. After solidification, antibiotic discs (Oxoid) were placed onto MRS agar plates and the plates were incubated 48 h at 37°C. h in anerojars. After incubation diameters of the inhibition zones were recorded.

6.2.3. Characterization of Bacterial Surface

6.2.3.1. Hydrophobicity

The hydrophobicity of organisms was characterized using the microbial adhesion to hydrocarbons (MATH) test, according to the method of Rosenberg et al. (1980). The cells were washed twice with PBS, pH 7.3 and resuspended in the same buffer to an absorbance ($\lambda = 600$ nm) of about 0.25 ± 0.03 in order to standardize the number of bacteria (10^7 to 10^8 CFU/ mL). After addition of an equal volume of p-xylene or n-hexadecane, the two-phase system was thoroughly mixed by vortexing for 1 min. The aqueous phase was removed after an 1 h incubation at room temperature and its absorbance at 600 nm was measured.

Affinity to hydrocarbons (hydrophobicity) was reported as the adhesion percentage according to the formula:

$$\frac{A_0 - A}{A_0} \times 100 \quad (6.2)$$

where A_0 and A are the absorbance before and after extraction with organic solvents, respectively. Hydrophobicity was calculated from three replicates as the percent decrease in the absorbance of the original bacterial suspension due to partitioning of cells into the hydrocarbon layer.

6.2.3.2. Surface Charge

The net surface charge of organisms was measured (Zetasizer 3000 HAS, Malvern Instruments). The cells were suspended in 1 mM KNO_3 , and after pH adjustment with dilute HNO_3 or NaOH , the suspension was diluted to a final concentration of about 10^8 cells/mL. The pH range studied was from 2 to 12. Each analysis was made in triplicate.

6.2.4. Preparation of Natural Zeolites for Health Studies

This section included the preparation of zeolite with high clinoptilolite content and characterization of the purified material.

6.2.4.1. Purification Steps of Natural Zeolites

75-150 μm of clinoptilite rich mineral which was prepared by Narin (Narin, 2010) was used to obtain purified natural mineral with a high clinoptilolite content. The separations were done as reported in (Narin, 2010). Separation processes is based on the friability and density properties of clinoptilolite relative the other constituents (Hardness is 7 for quartz and 3.5-4 for clinoptilolite in Mohs scale)

In the purification, serial grinding and sedimentation operations were done. Initially particle size was decreased and uniform particle size was obtained. Then, the purification and separation was achieved by applying Stoke's law in several sedimentation processes. These steps were presented below in detail. The fractions were separated for different settling times. After the settling time, the suspended portion was removed using a peristaltic pump and the remaining sediment was kept in a static oven at 65 °C for 24 hours.

1. 50 g of clinoptilite rich natural mineral (75 μm wet sieved) was weighted and 500 ml of deionized water was added . This mixture was stirred in ultrasonic bath for 30 min.
2. The mixture was sedimented for 15 min. Then, settled particles were separated and dried at 65 °C for 24 h.
3. Settled fraction was ground (Grinding 1) by ball mill(30 ball, 300 rpm, 2 min left, 2 min right).
4. 500 ml of deionized water was added to ground particles and the mixture was stirred in ultrasonic bath for 30 min.
5. The steps from 2 to 4 were repeated in three times until to achieve Grinding 4. Ground particles were analysed by particle size analyzer (Mastersizer 2000) and ground particles (1-20 μm) were obtained and several settling experiments were conducted in the following parts.

6. 500 ml of deionized water was added into ground particles and the mixture was stirred in ultrasonic bath for 30 min.
7. Settling was performed in graduated cylinder for 3.9 min and suspended portion was removed using a peristaltic pump and the remaining sediment was kept in a static oven at 65 °C for 24 hours. This fraction was called as heavy part.
8. Suspended portion was settled in graduated cylinder for 3 h 48 min and suspended portion was removed using a peristaltic pump and the remaining sediment was kept in a static oven at 65 °C for 24 hours. This fraction was called as clinrich part.
9. Suspended portion was settled in graduated cylinder for 94 h 53 min and suspended portion was removed using a peristaltic pump and the remaining sediment was kept in a static oven at 65 °C for 24 hours. This fraction was called as clinrich B pa
10. In the end, removed parts were collected in a one container and it was called as retry part.

After separation and collection of all fractions, they were analyzed by XRD technique and clinrich part was chosen and purity of the this fraction was calculated.

6.2.4.2. Preparation of Homogenized Representative PNZ

Clinrich parts were separated and mixed together in one container then all samples were separated into eppendorph tubes as 0.5 g by using the representative sample maintaining technique; quartering. All of the experiments were performed by using these representative samples.

6.2.5. Characterization of Purified Natural Zeolites (PNZ)

After obtaining the homogenized representative PNZ, following techniques were used to characterize the samples.

6.2.5.1. Topographic and Microstructural Examination; SEM

The crystalline morphology of clinoptilolite samples was investigated by using the Scanning Electron Microscopy (Philips, XL30). This technique allows to monitor the crystalline structure of zeolitic rocks.

6.2.5. 2. Particle Size Distribution Measurement

The particle size distribution of the samples were determined by the laser beam scattering technique using a Malvern Mastersizer 2000 particle size analyzer (Malvern Instruments Ltd., Worcestershire, UK). The zeolites were mixed with a viscosity specific fluid (0.05 % calgon solution) then they were put into ultrasonic bed for 15 minutes and small particles which agglomerate on the big particles were disaggregated. Obscurations in the range of 10–20% were used during the measurements.

6.2.5.3. Mineralogy and Crystallinity of the Samples

The purity and crystallinity of the purified zeolites were determined by powder X-ray Diffraction techniques (Philips X-Pert Pro) using CuK α radiation in the range of 2 tetha: 2°-40°. Qualitative analyze was performed by using search-match method and quantitative analyses performed by using reference minerals. The clinoptilolite references with >90 % clinoptilolite content (# 27031, Castle Creek, Idaho and # 27023, Hector, California) were obtained from Mineral Research, Clarkson, New York.

The quantitative analysis method including the application of multiple analytical XRD lines proposed by Nakamura et al. was employed (Nakamura et al., 1992). This method is based on the ratio of the summation of intensities of the seven characteristic peaks belong to clinoptilolite in the 2 θ range of 9.82°–19.02° (2 θ = 9.82°, 11.15°, 13.07°, 14.89°, 16.91°, 17.28°, and 19.02°) for the sample to the summation of characteristic peaks of the reference mineral. The calibration curves were constructed by plotting the sum of the diffraction intensities of these lines against the mass fractions of the standard materials in the calibrating mixtures.

6.2.5.4. Thermal Analysis

Differential Scanning Analysis (DSC), Thermogravimetric Analysis (TGA) and Differential Thermal Analysis give information about the dehydration properties of zeolites. Thermogravimetric analyses of the zeolites were performed using TGA (Shimadzu TGA-51, Shimadzu). The samples were heated in a dry N₂ stream up to 1000 °C at a heating rate of 10 °C/min and water content of clinoptilolite rich mineral was examined.

6.2.5.6. Pore Volume and Surface Area Analysis

Pore volume and Surface area of the zeolite samples were determined using volumetric adsorption device (Micromeritics ASAP 2010 M) with nitrogen at 77 K. The samples were dried in oven at 200°C for 3 hours prior to degassing and degas conditions were performed at 350°C for 24 hours under vacuum (10⁻⁵ mbar). Adsorption data were collected in the relative pressure range P/P₀ of 0.05 to 0.2.

6.2.5.7. Infrared Spectroscopy

The zeolite samples were characterized using transmission Fourier transform infrared (FTIR) Spectroscopy. The samples were prepared using the standard potassium bromide (KBr) pellet method (sample/KBr:1/200 by weight). The sample-KBr mixtures were ground together in an alumina agate and pelletized under 4 tons/cm² pressure for 1 minute by a hydraulic press. The infrared spectra were recorded in the region of 400–4000 cm⁻¹ at room temperature after 256 scans at 2 cm⁻¹ resolution using a spectrometer (FTIR-8400S, Shimadzu). For all the spectra, the baseline correction and normalization (with respect to the most intense band) were done.

6.2.5.8. Zeta-potential Measurements

The zeta potential of zeolite samples was measured by a zeta potential measurement instrument (Zetasizer 3000 HAS, Malvern Instruments). The zeta

potential measurements were carried out as a function of pH of the phosphate buffer saline solution (PBS). pH was adjusted to 3, 4, 6, 8 and 10 using NaOH and HCL. The acidic pH value (pH 3.0) represented the simulated the gastric environment and pH 7.3-8 represented the simulated intestinal environment. The average of ten measurements was taken to represent the measured potential.

6.2.5.9. Analysis of Major Elements by Inductively Coupled Plasma Atomic Emission Spectroscopy (ICP-AES)

Zeolite samples were digested and analysed by ICP-AES (Varian ICP 96). For this procedure, 0.1 g of sample was mixed with 1 g lithium tetraborate and fused at 1000 °C for 1 hour .After cooling, samples were removed from the container with the aid of the nitric acid solution and mixture volume was adjusted to 250 ml. The samples were dissolved in HNO₃ solution adjusting the 2.5 %(v/v) acid concentration for the final solution. The samples were acidified and diluted for the detection range of the instrument. Multielement standard solutions, silicon standard solutions and blank solution were prepared. 0.5 ppm, 1 ppm, 5 ppm , 10 ppm and 20 ppm of multielement standard solution with 2.5 %(v/v) HNO₃ were prepared and silicon standards ; 10 ppm, 20 ppm and 30 ppm were prepared with the same acid content. Calibration curves for each element was obtained by using the standard solutions and the element composition of each sample was determined.

6.2.5.10. Minor and Trace Element Analysis by Inductively Coupled Plasma Mass Spectroscopy(ICP-MS)

The microwave digestion method modified by Hassan et al. (2007) was applied to determine minor and trace elements. For this work, the certified reference mineral (Rhyolite JR-3, Japanese Rock Standard) was also used in the experiments. The microwave-assisted digestion systems used in the study is the Model CEM MARS 5 (CEM Corporation. Matthews. NC). The microwave parameters are listed in Table 6.1

First, 30 mg of the samples were digested with 3 mL HNO₃ or 3 mL of HNO₃/HCl mixture in the Teflon vessels. Reagent blanks were also prepared with

concentrated HNO₃ acid or HNO₃/HCl mixture in the proportions shown in Table 6.1. The vessels were capped and placed in the microwave system and digested using the parameters listed in Table 6.1. At the end of the program, the vessels were cooled to room temperature in a fume hood and the pressure inside the vessels slowly released. After cooling the digested samples were transferred to 50 mL graduated polypropylene centrifuge tubes. Then, they washed three times with DDW (Double deionized water) to a volume of 50 mL and centrifuged for 20 min at 2500 rpm to remove any remaining undissolved solid particles that might block the nebulizer. A 1 mL sample of the digest was then diluted to 50 mL with DDW. Element standards and blank was prepared by using 1%(v/v) HNO₃.

Table 6.1. Operating parameters and digestion reagents for microwave digestion system

Parameters	MARS 5 Microwave
Power (W)	0-1.200
No of vessels	14
Vessel volume (mL)	120
Micro-vessels volume(mL)	7.0
Sensors control	P and T
Ramp time (min)	5.5
Hold time (min)	10
Hold temperature (°C)	175
Mass (mg)	30
HNO ₃ digestion solution	3mL concentrated HNO ₃
HNO ₃ /HCl digestion mixture	3 mL of 5.6% HNO ₃ and 16.7% HCL (v/v)

6.2.6. Aflatoxin B1(afB1) Adsorption Experiments

afB1 adsorption experiments were conducted in 3 main groups. Uptake rate data were collected by measuring the afB1 concentration in solution against time.

1. afB1 Adsorption kinetic and parametric experiments by using PNZ as an adsorbent alone (Table 6.2).
2. afB1 Adsorption experiments by using probiotic lactobacilli strain as an adsorbent alone (Table 6.3).
3. afB1 Adsorption experiments within the presence of both PNZ and probiotic lactobacilli together (Table 6.4).

AfB1 Adsorption Experiments by using PNZ alone

Adsorption studies were performed in batch mode by using 50 ml of schott bottles in a temperature controlled water bath at constant temperature and agitation speeds. All working solutions of varying concentrations were obtained by diluting the stock solution of afB1 (25 ppm) with PBS PH 7.3. Different experimental parameters were tested for the adsorption study (Table 6.2). Samples were taken against time and they were centrifuged (10000 rpm 10 min) to separate the solid part. The afB1 concentrations in the samples were analyzed by using the HPLC-FLD (High Performance Liquid Chromatography -Fluorescence Detection).The operating conditions were given in Appendix C.

Experimental studies were conducted for investigating the adsorption study at different initial concentrations (0.25 ppm, 0.5 ppm, 0.75 ppm, 1 ppm and 2ppm). Three different adsorbent amounts as 12.5 mg, 25 mg PNZ and 100 mg PNZ were tested to see the effect on the adsorption. Additionally, pH effect was investigated. The adsorption experiments were continued with the experiments at different temperatures (15 °C, 25 °C and 37 °C) and agitation speeds (50 rpm, 130 rpm and 200 rpm) in order to see the effects on adsorption. To see the effect of particles size, the parent mineral was crushed to different sizes and used in the experiments. The results provided kinetic data for uptake curves and adsorption isotherms. Controls without PNZ were included in all of the experiments.

Table 6.2. Experimental conditions of the various kinetic adsorption experiments for the removal of afB1 at constant volume of toxin solution (10 ml)

Parameter	Initial afB1 Concentraion (ppm)	Mass of adsorbent (mg)	pH	Agitation speed	Temperature (C°)	Particle size
Initial afB1 conc. (ppm)	0.25, 0.5, 0.75, 1	2.5	7.3	130	37	8 µm (PNZ)
Mass of adsorbent (mg)	0.25	12.5, 25 and 100	3.0	130	37	8 µm (PNZ)
pH	0.25	25	3.0, 5.0 and 7.3	130	37	8 µm (PNZ)
Agitation speed	0.25	25	7.3	50, 130, 200	37	8 µm (PNZ)
Temp. (C°)	0.25	25	7.3	130	15, 25, 37	8 µm (PNZ)
Particle size	0.25	25	7.3	130	37	Extra small, small, coarse

AfB1 Adsorption Experiments by using Probiotic Lactobacilli Alone

Overnight culture of probiotic strain was grown in MRS broth (pH 5.6) at 37 °C by using the -80 glycerol stock of the isolates. Then, 100 µl of the overnight culture inoculated into 10 ml of the MRS broth (pH 5.6) and incubated for 24 h at 37°C°. After incubation, the viable cell count was performed in order to check the cell number. For each experiment, the same procedure was repeated to set the viable cell number to 10⁹. This 10ml of the cell suspension in the MRS broth was centrifuged at 8000 rpm for 10 min and supernatant was removed. Then, the cells were washed with PBS 7.3. After the centrifugation, the cells were resuspended in 9 ml of the PBS at pH 7.3.

Adsorption studies were performed in batch mode by using 50 ml of schott bottles in the temperature controlled water bath at constant temperature and agitation speeds. AfB1 desirable dilutions were obtained by diluting the stock solution of afB1 (25 ppm) with PBS PH 7.3. 1ml of the afB1 dilution was added to 10 ml of the cell suspension. Different experimental parameters were tested for the adsorption study (Table 6.3). Samples were taken during the equilibrium period and they were centrifuged (10000 rpm, 10 min) to separate the solid part. The afB1 concentrations in the samples were analyzed by using the HPLC-FLD

Table 6.3. Experimental conditions of the various kinetic adsorption experiments for the removal of afB1 by probiotic lactobacilli alone at constant volume of toxin solution (10 ml)

Parameter	Strain Type	Initial afB1 conc (ppm)	Amount of organism,	Agitation speed	Temp (C°)	pH
Strain Type	LP1, LP2, LP3, and reference strains	0.25	10^{10}	130	37	7.3
Initial afB1 conc(ppm)	LP2	0.25, 0.17, 0.06	10^{10}	130	37	7.3
Amount of organism	LP2	0.25	2×10^{10} to 10^4	130	37	7.3
Agitation speed	LP2	0.25	10^{10}	50,130, 200	37	7.3
Temp (C°)	LP2	0.25	10^{10}	130	37	15,25,37
pH	LP2	0.25	10^{10}	130	37	3, 5.0,7.3

AfB1 Adsorption Experiments by using PNZ and Probiotic Lactobacilli

The cell suspension with varying afB1 concentrations were prepared as mentioned above. Then, PNZ were added and kinetic studies were conducted for various experimental parameters presented in Table 6.4.

Table 6.4. Experimental conditions of the various kinetic adsorption experiments for the removal of afB1 at constant volume of toxin solution (10 ml)

Parameter	Initial afB1 Concentration (ppm)	Mass of adsorbent (mg)	pH	Temperature (C°)
Initial afB1 concentration (ppm)	0.25, 0.17, 0.06	25 mg 10^{10} cell	7.3	37
Mass of adsorbent (mg)	0.25	25 mg 10^{10} cell	7.3	37
pH	0.25	25 mg 10^{10} cell	3, 5.0 and 7.3	37
Temperature(C°)	0.25	25 mg 10^{10} cell	7.3	15,25,37

6.2.7.1. Aflatoxin Standards and HPLC Quantification

The afB1 standard substance (25 ppm) prepared in 100 % acetonitrile solution was purchased from the Biopharm and stored at -20 °C. afB1 in various samples were quantified by using Agilent 1100 Series HPLC system equipped with a G1312A fluorescence detector, G1322a model degasser, G1316 model column oven and G1328 manual injection unit. The column was a C18 Hypersil ODS, 5 µm particle size, 250 mm × 4.6 mm. The operating conditions were given in Appendix B . The retention time for AFB1 was around 11 min (Appendix C). Dilutions were prepared by using PBS pH 7.3 solution and calibration curve was obtained (Appendix D) to quantify the concentration of afB1 in the experiments.

CHAPTER 7

RESULTS AND DISCUSSION

7.1. Isolation and Characterization of the Probiotic Candidates

7.1.1. Isolation of Lactobacilli

A few type of probiotic strains were used in various commercial products. In order to investigate new potential probiotic sources, different sources were used and the preliminary results were tabulated (Table 7.1) Viable cell counts were expressed as CFU (Colony forming unit/ml) and these numbers indicated the microbial load of the sources. Human milk has the lowest CFU value as expected among the sources. Fermented sources have lower pH values when they are compared with human milk. The human milk has approximately neutral pH (pH 7.13) and CFU numbers represents the natural microflora. Decrease in pH values indicates the acid production due to the fermentation. Higher CFU/ml's were observed for sources with lower pH values. Although MRS agar (pH5.6) medium is used to indicate lactobacilli potential of the sources, other organisms can also grow. Heterogen colony morphologies observed for Boza samples supported this case. Some of colonies were simple stained and examined under microscope and they were identified as yeast cells.

Table 7.1. Summarized isolation data for lactobacilli organism

Source	pH	CFU/ml	Colony Morphologies
Human Milk	7.13	$1.4 * 10^4$	Small colonies, white yellowish color, different sizes
Boza 1 (fermented by using corn)	4.19	$8.4 * 10^6$	Heterogen colony morphologies from small to very big colonies, white and yellowish color
Boza 2 (fermented by using wheat)	3.71	$1.71 * 10^8$	
Boza 3 (fermented by using wheat)	3.59	$2.06 * 10^8$	
Pickled cabbage	4.34	$1.6 * 10^5$	Similar colony morphology, middle size, white yellowish color

7.1.2. Purification and Preliminary Identification

After isolation of the colonies, subsequent transfers were performed into MRS broths and isolates which indicates good growth properties were streaked several times until reaching the pure colony morphologies. After catalase test and Gram staining Lactic Acid Bacteria were identified as given below (Table 7.2). Rod shaped isolates were called “bacilli” and with catalase negative property, they were identified as lactobacilli and selected others were eliminated. In the result of preliminary identification study 110 purified isolates were identified as lactobacilli on the basis of genus level and stored at -80 °C refrigerator for long term storage.

It was found that it was difficult to study with human milk due to the difficulty of maintaining viable organisms in MRS broth. This may be related to kinds of the organism. These isolates could not be lactic acid bacteria for this reason they could not grow at pH 5.6 in MRS broth. Most of the isolates from human milk were catalase positive for this reason they were eliminated. The eliminated pure cultures of human milk were also stored at -80°C for possible future uses. The human milk was found not to be a good source for lactobacilli genus. Preliminary identification results indicated that other fermented food sources (Boza and fermented cabbage) have high potential for lactobacillus genus. Most of the purified isolates showed catalase negative property and most of the catalase negative isolates were rod shaped.

Table 7.2. Summarized elimination, purification data

Source	Purified isolates by Streaking	Catalase test		Cell Morphologies		Gram Status
		Negative	Positive	Bacilli	Cocci	
Human Milk	22	8	14	1	7	Gram Positive
Boza 1	45	40	5	35	5	
Boza 2	55	52	3	31	21	
Boza 3	35	30	5	25	5	
Pickled cabbage	30	30	0	28	2	
				110		

The cell morphology was examined under the light microscope by using Gram staining technique. In the Gram staining technique, the cells having Gram positive property remains in blue color. This case is related with the cell wall structure of the organisms. The cell wall of Gram negative bacteria has a greater complexity than the Gram positive bacteria. Gram negative bacteria include additional outer membrane, which is composed of lipopolysaccharide and proteins, when compared with the gram positive ones. The images demonstrated that the rod shaped Gram positive cells could

be obtained in the pure culture form (Figure 7.1). Also Scanning Electron Microscopy images were obtained (Figure 7.2). Gram staining and examination under light microscope provides confirmation of purity and identification of cell morphology.

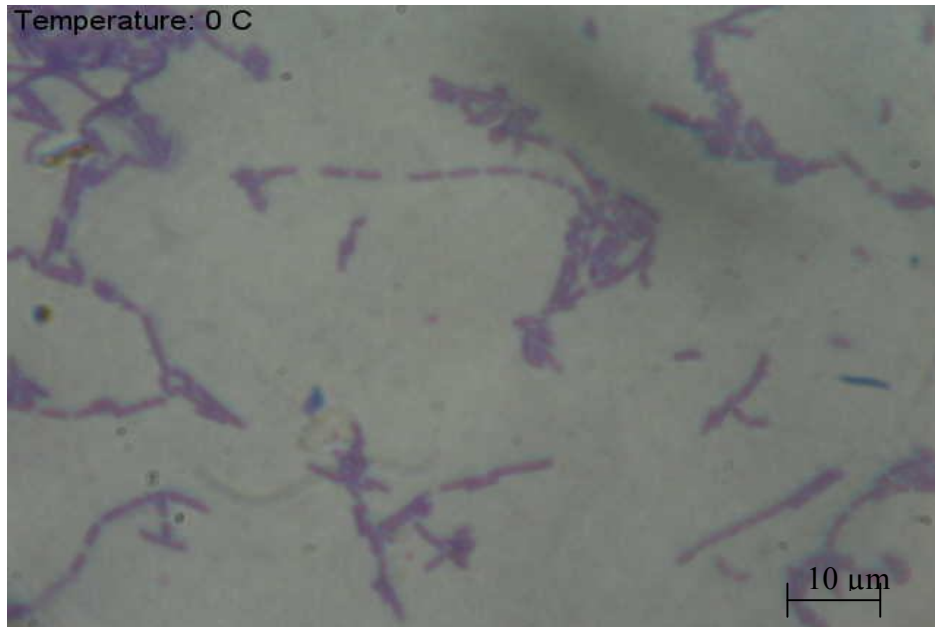


Figure 7.1. Representative optical microscopy picture of the isolated *Lactobacillus* strains.

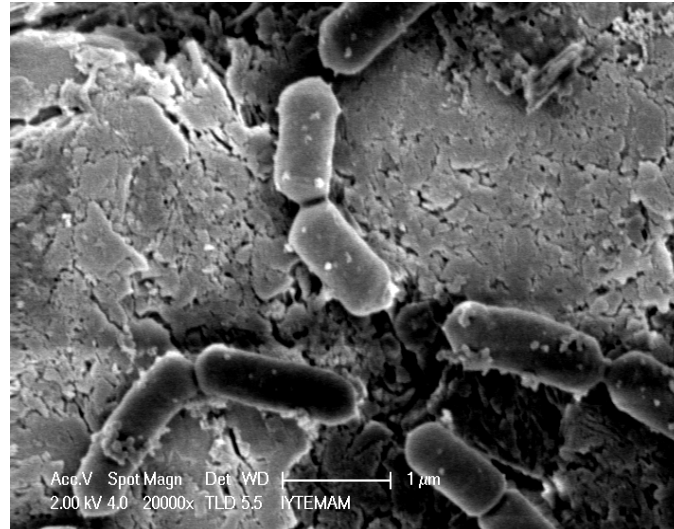


Figure 7.2. Representative Scanning Electron Microscopy picture of the isolated *Lactobacillus* strains.

These selected isolates were further analyzed in the simulated gastric conditions. The isolates indicating resistance to gastric acidity were chosen and identification studies on species level were performed for those strains. For the species level identification, three carbohydrates, namely arabinose, sucrose and lactose were used. It is known that organisms can be differentiated by their abilities to ferment the different kinds of carbohydrates.

7.1.3. Identification at Species Level

These isolates were further analyzed in the simulated gastric conditions. The isolates that have resistance to stomach conditions were selected and identified at species level. In Table 7.3, the letter of B stands for strains isolated from Boza and the letter of L stands for strains isolated from fermented cabbage.

Table 7.3. Physiochemical and biochemical identification results

No	Code	6.5% NaCl	15 °C	45 °C	Acid and gas from glucose	NH ₃ from arginine	Lactose	Sucrose	Arabinose
1	B1	-	+	+	-	-	+	+	-
2	B3	-	+	-	+	-	+	+	-
3	B9	-	+	-	+	-	+	+	-
4	B11	+	+	-	+	-	+	+	-
5	B22	+	+	-	-	-	+	+	+
6	B28	+	+	-	-	+	+	+	+
7	B32	+	+	-	-	+	+	+	+
8	L3	+	+	-	-	-	+	+	-
9	L4	+	+	-	-	-	+	+	-
10	L5	+	+	-	-	-	+	+	-
11	L7	+	+	-	-	-	+	+	+
12	L10	+	+	-	-	-	+	+	+
13	L15	+	+	-	-	-	+	+	+
14	L22	+	+	-	-	-	+	+	+
15	L23	+	+	-	-	-	+	+	+

7.1.4. Probiotic Properties

Resistance to Low pH

Resistance to acidic pH values is one of the major selection criteria for probiotics. For this aim, isolated strains were screened for their resistance to acidic environment that simulated the gastric passage. The time that takes during the digestion in the stomach is 3 hours. Thus, all the isolates were detected whether they were resistant to pH 3.0 during the 3 hours. After the 3 hour, viable cell count were performed and the 10^9 to 10^8 CFU were defined as resistant and 10^4 - 10^8 CFU were defined as slightly resistant and lower than the 10^4 were defined as non resistant. Table 7.4. shows that 15 of the 110 isolates were found to be resistant to pH 3.0 and all of these isolates were lactobacilli.

Table 7.4. The results of the resistance of the isolates the pH

	Number of strains	source	genus
resistant	15	Boza 2, Boza 1 and pickled gabbage	Lactobacilli
Slightly resistant	20	Boza 3, Boza 2, Boza 1 and pickled gabbage	Lactobacilli
non resistant	75	Boza 3, Boza 2, Boza 1 and pickled gabbage Human milk	Streptecocci, Lactobacilli.

Panceratic Enzyme and Bile Salt Tolerance

All lactobacilli stains were screened for pancreatic enzyme and bile salt tolerance and the results were tabulated below.

Table 7.5. Screening results for Pancreatic enzyme and bile salt tolerance

Source	Number of Strains	Pancreatic enzyme tolerance	Bile salt tolerance
		Positive	Positive
Boza 1	45	30	40
Boza 2	55	25	35
Boza 3	35	18	27
Pickled cabbage	30	22	20

The strains that have acid resistance, pancreatic enzyme and bile tolerance property were identified. Physicochemical and biochemical tests indicated that three of the isolates were identified as *Lactobacillus plantarum* by including the other sugars to differentiate at species level.

Antibiotic Sensivity Analysis

Inhibition zones were measured and representantive picture is given in Figure 7.3 other results are drawn in Figure 7.4.

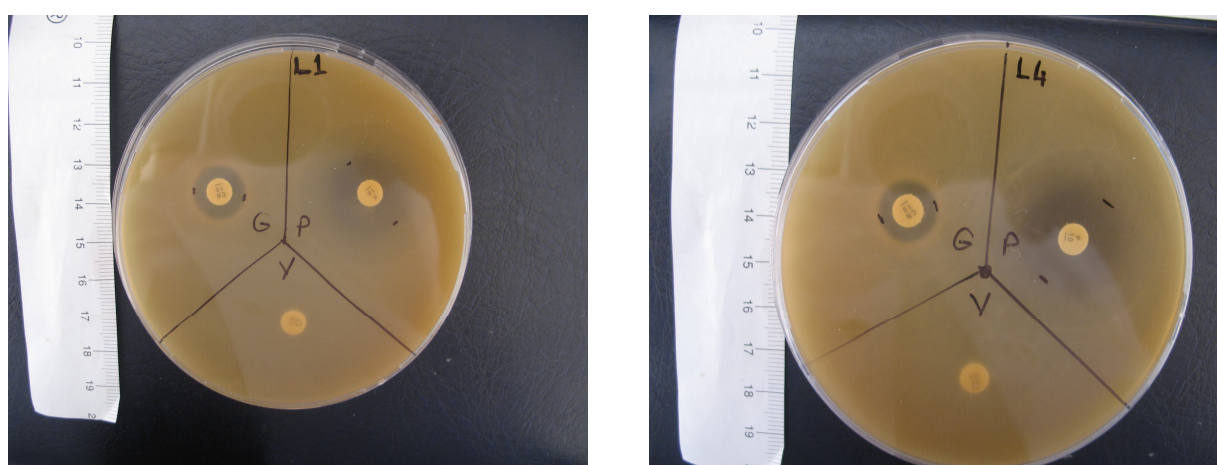


Figure 7.3. Antibiotic sensitivities of the two Isolated strains(L1 and L4) of *Lb plantarum* which resistant to gastric environment and bile salts

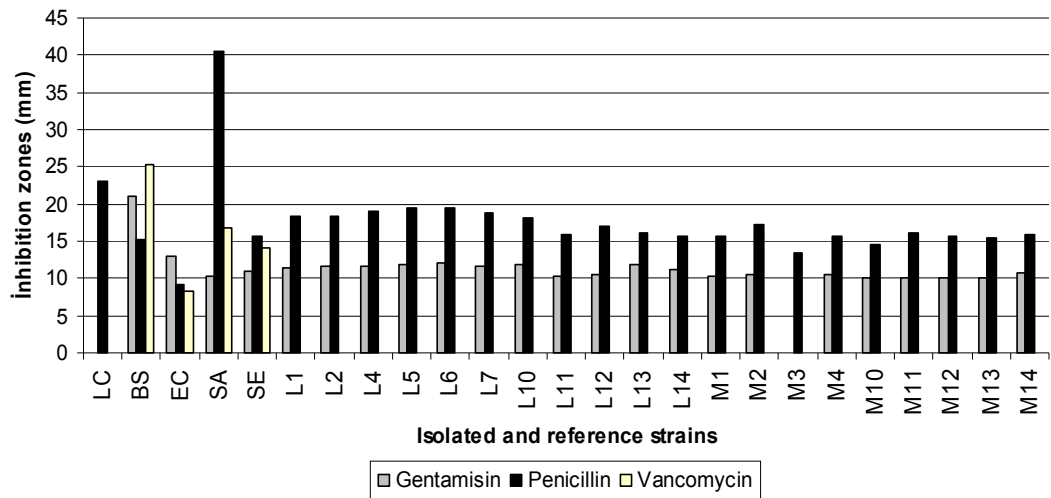


Figure 7.4. Antibiotic sensitivities of the isolates and some reference strains

7.1.5. Characterization of Bacterial surface

Surface Charge of the Lactobacillus plantarum Strain

Figure 7.5 indicated the change of the zeta potential of the isolated *Lactobacillus* strain as a function of pH. Surface charge measurements of *L. plantarum* were performed in PBS solution. Increase in pH value of PBS solution results in increase in negative charge on the cell surface. In the pH range of 2 to 10, it was found that the surface charge remains in negative. The pH values of 2.0 and 3.0 simulate the gastric environment.

Zeta potentials of the *lactobacillus* surfaces were reported in many studies to identify the cell surfaces (Millsap et al., 1996 ; Reid et al., 1999; Zammaretti and Ubbink, 2003). Millsap et al. (1996) reported that all the lactobacilli strains indicated negative surface property at pH 7 (10mM PBS) and negative charge increased by increasing the pH. They reported that surface property is a strain specific property. In the same study, two different strains of *L. fermentum* show different cell surface charge property. Although surface charge of , *L. fermentum* ATCC 14931 was -37.7 mV, *L. fermentum* 854 has -6.1 mV of surface charge at pH 7.0.

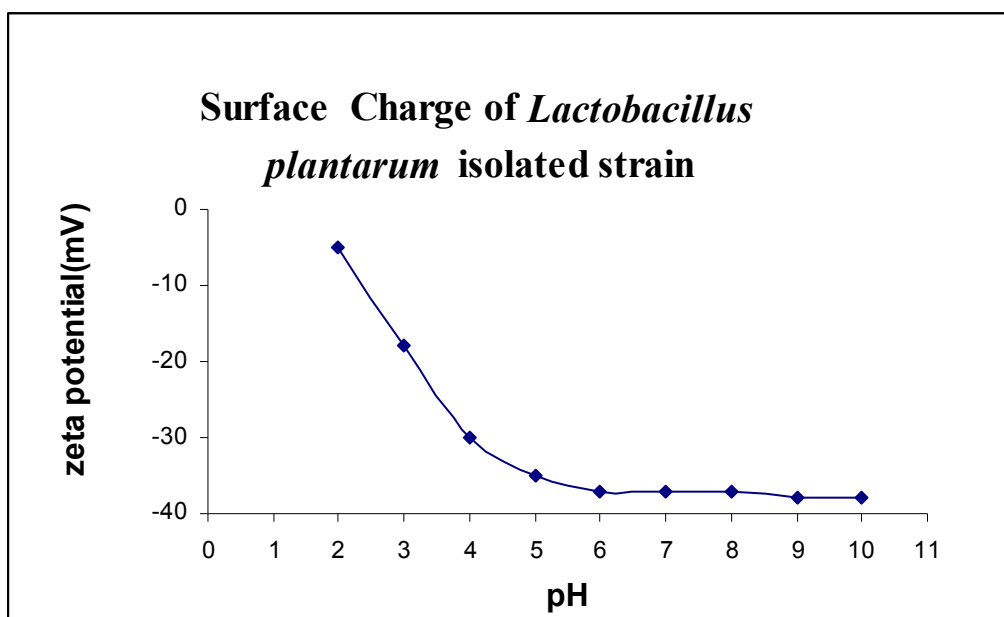


Figure 7.5. The variation of the zeta potential of isolated *lactobacillus* strain in the different pH values of PBS solution

Hydrophobicity of the Lactobacillus plantarum Strains

All tested strains indicated higher percentage of hydrophobicity for xylene (Table 7.6). *Lactobacilli* were classified in three groups depending on their hydrophobic property: low (0–35%), moderate (36–70%), and high (71–100%). The results showed that tested strains have low and moderate hydrophobic character.

Table 7.6. Adhesion properties to hydrocarbons

Strain	Hydrophobicity (%)	
	Hexadecane	Xylene
<i>L. plantarum</i> S1 (L1)	32	45
<i>L. plantarum</i> S2(L4)	23	32
<i>L. plantarum</i> S3(L9)	17	22

7.2. Purification and Characterization of Clinoptilolite Rich Mineral

7.2.1. Purification of the Natural Zeolite

After purification procedure different parts were analyzed and characterized. After SEM imaging, XRD and ICP analyzing clinrich part was selected as PNZ. For further characterization, both of the PNZ and reference mineral of IDAHO were used together.

The qualitative results of the XRD analysis indicated that different impurities are observed in the samples (Table 7.7). The starting zeolite powder contained predominantly clinoptilolite, and feldspars, quartz, biotite as mineral impurities. In order to get qualitative data, the intensities from the The X-Ray powder diffractograms were used.

Table 7.7. Qualitative Analysis Results by Search-Match

S1 (Clinrich)	S2 (Clinrich B)	S3 (Heavy)	S4 (Retry)	S5 (Before purification)	S6 (Before purification)
Clinoptilolite	Clinoptilolite	Clinoptilolite	Clinoptilolite	Clinoptilolite	Clinoptilolite
Orthoclase	Orthoclase	Albite high	Sanidine	Microcline	Orthoclase
Quartz	Muscovit	Quartz low	Cristobalite low	Muscovit	Albite high
Sanidine	Anorthoclase	Orthoclase	Mica	Anorthoclase	Anorthoclase
Muscovit		Biotite 2 M1		Quartz	Quartz
Quartz low				Quartz alpha,syn	Mica(Cr bearing)

The X-Ray powder diffractograms of the reference minerals were indicated in Figure 7.6 and Figure 7.7. The characteristic peaks of the clinoptilolite (pointed as “C” letter) were expressed in these diffractograms. In the purification study, different fractions were obtained and purified part with different fractions were analysed by

XRD and patterns were obtained and presented in Figure 7.8. for comparison. The purity of clinoptilolite samples was determined according to the Nakamura et al., (1992). In this method, the diffraction intensity was calculated by the sum of seven intensities of the (9.82), (11.15), (13.07), (14.89), (16.91), (17.28), and (19.02) 2 theta values, which are characteristic peaks for clinoptilolite. The calibration curve (Appendix D) prepared by Narin, 2009 was used in the quantitative analyses. The equation for the calibration curve was obtained by using the Nakamura's method (Equation. 7.1) and it was used to calculate the clinoptilolite content.

In the equation, CC stands for the clinoptilolite content and clinoptilolite content of the Clinrich sample was calculated as 98% and this part was collected and mixed in one batch. This high clinoptilolite content of natural zeolite with a high purity was recommended for the health related studies and it was used for all the characterization studies and the adsorption experiments.

$$SumI = I_{9.82} + I_{11.15} + I_{13.07} + I_{14.89} + I_{16.91} + I_{17.28} + I_{19.02} = 8307.2 \times CC \quad (7.1)$$

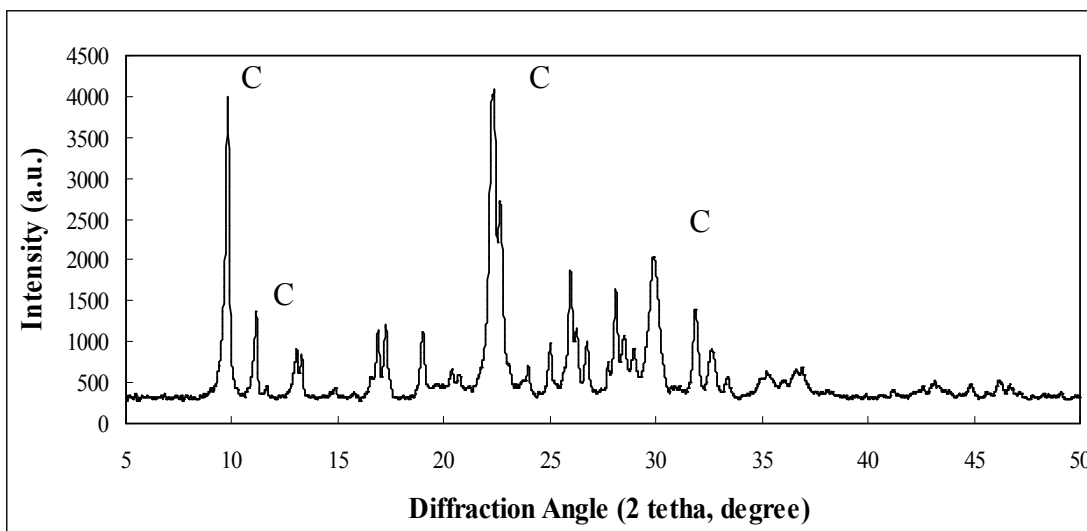


Figure 7.6. XRD diagram of Mineral Reference of Idaho.

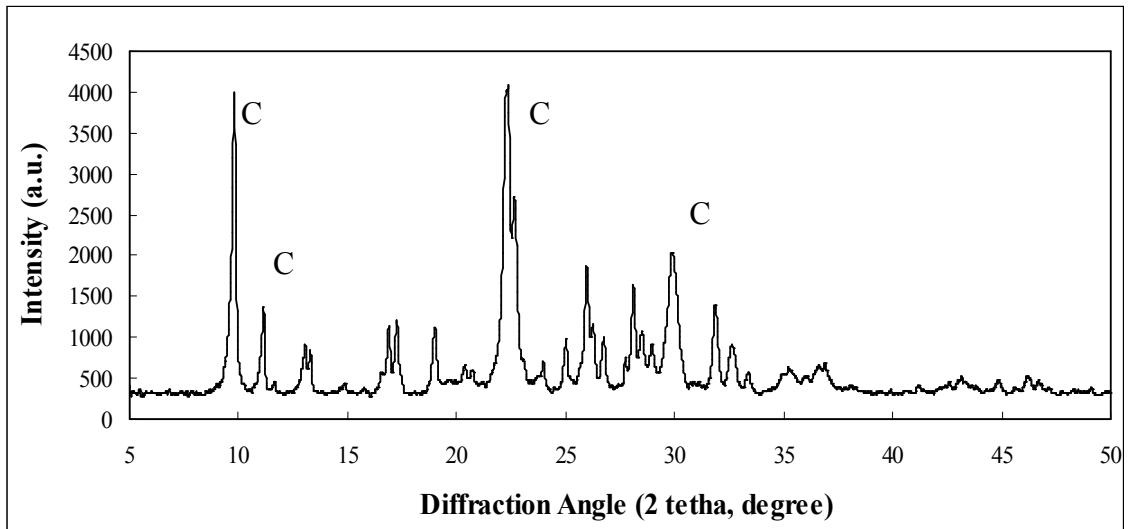


Figure 7.7. XRD diagram of Mineral Reference of California.

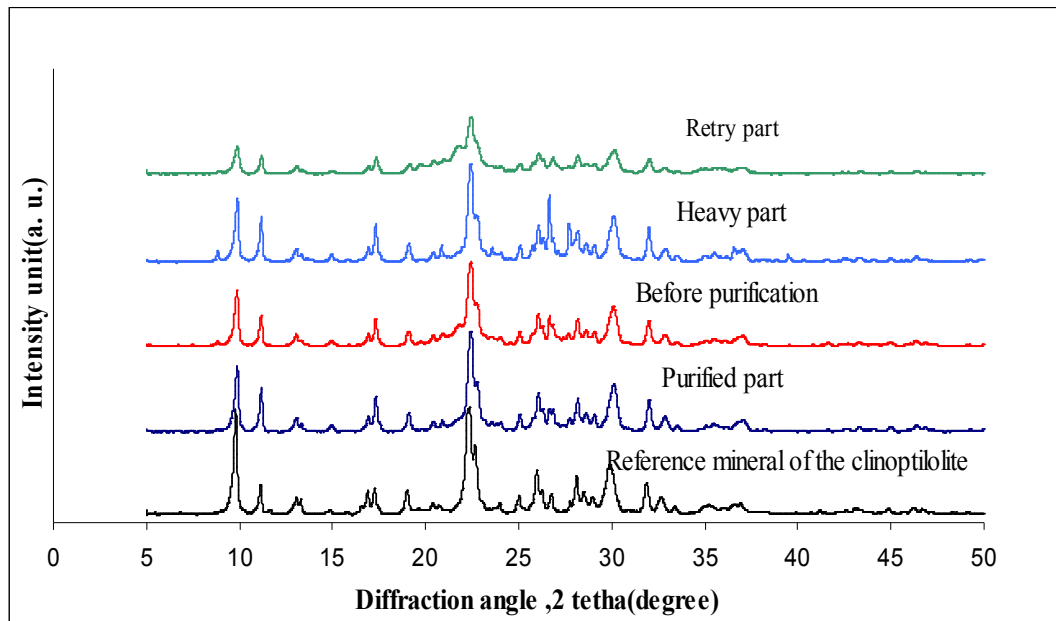


Figure 7.8. X-ray powder diffractograms of the reference clinoptilolite mineral (Idaho) and the different fractions in the purification study.

The qualitative mineralogical analysis revealed that starting material contained predominantly clinoptilolite (JCPDS 25-1349) as well as quartz (JCPDS 83-2465) ($2\theta=20.9^\circ$, 21.9° , 26.7°), feldspars (microcline JCPDS 83-1604, sanidine JCPDS 86-0683) ($2\theta=27.1^\circ$, 27.7°) and biotite (JCPDS 76-0885) ($2\theta=8.9^\circ$). The quantitative analyses results for different fractions were presented (Table 7.8).

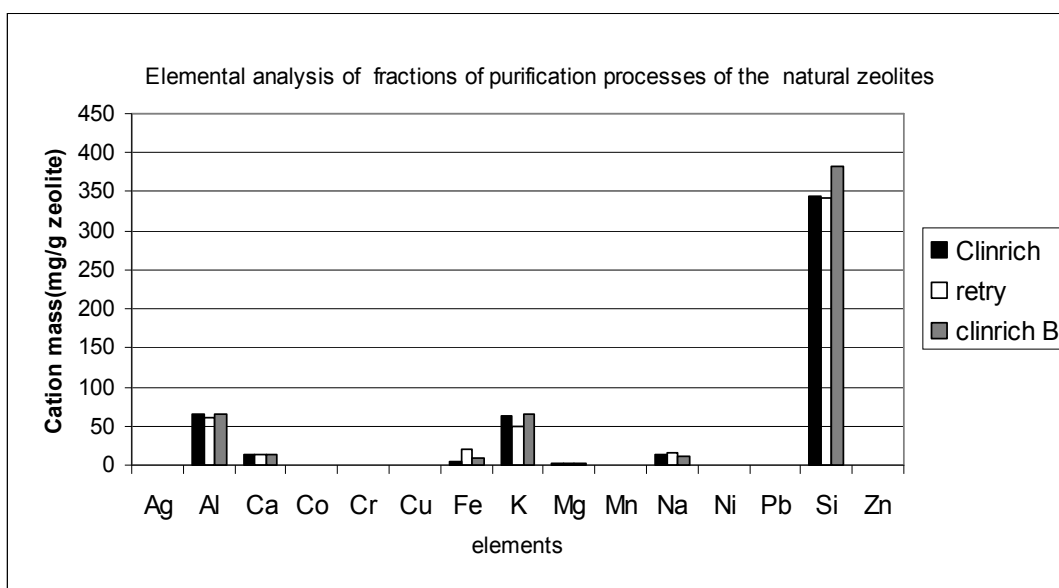


Figure 7.9. Elemental analysis results of different fractions during purification

In the elemental analysis of the different fractions, aluminium silicon amount was high. In the retry part, cation mass of Fe was extremely higher than the other clinrich parts. No significant changes were observed in the concentration of other cations.

Table 7.8. Purity determination of the different phases during purification study.

Method applied	Clinoptilolite content, CC (% weight)			
	<75 μm	Heavy	ClinRich	ClinRich-B
Nakamura's method	66	70	98	90

7.2.2. SEM Examination Results

The crystalline morphologies of the samples were investigated by using the Scanning Electron Microscopy (Philips, XL30). Clinoptilolite possesses the regular plate like structure. The morphology of sample before purification shows the characteristic clinoptilolite crystal structure (Figure 7.10.). It is clear that there are abundant the typical hexagonal crystal structure of the clinoptilolite before the purification procedure.

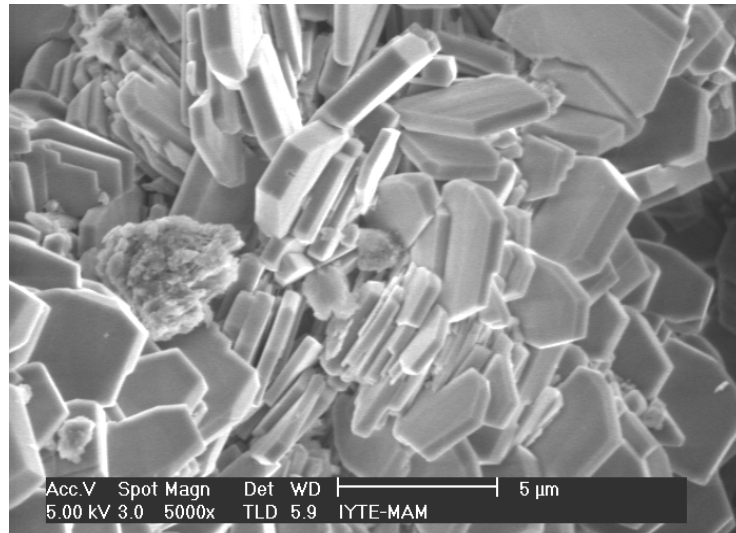
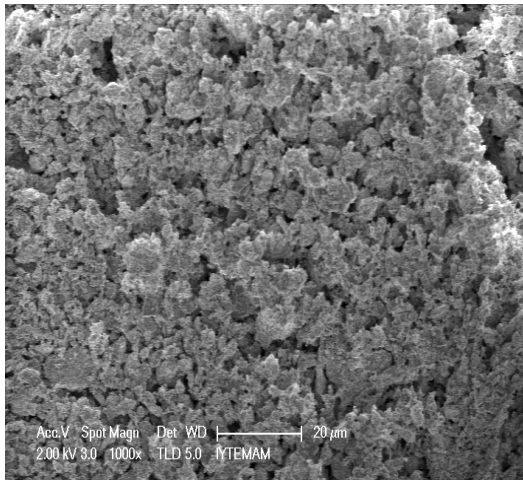
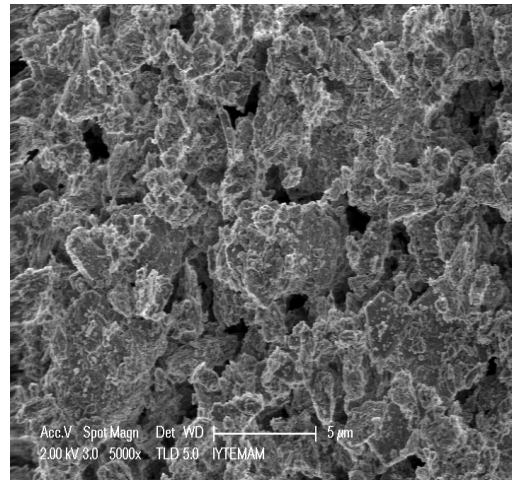


Figure 7.10. Scanning electron micrographs of clinoptilolite rich natural zeolite before purification.

However, after purification procedure, it was difficult to see this structure (Figure 7.12) The SEM images for reference mineral and PNZ were examined and representative pictures were presented for two different magnifications(Figure 7.11 and Figure 7.12). It was observed that reference mineral has smaller particles than PNZ. It was very difficult to see characteristic hexagonal crystalline structure for both samples. In the grinding processes crystal structure were disappeared due to their breaking down into smaller sizes. Only a few crystalline structures were observed for PNZ. (Figure 7.12)

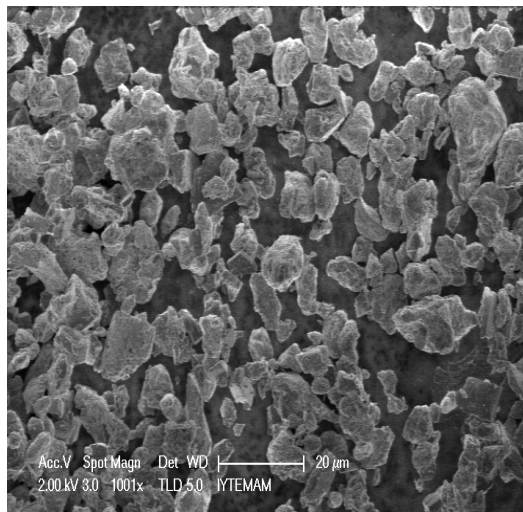


a)

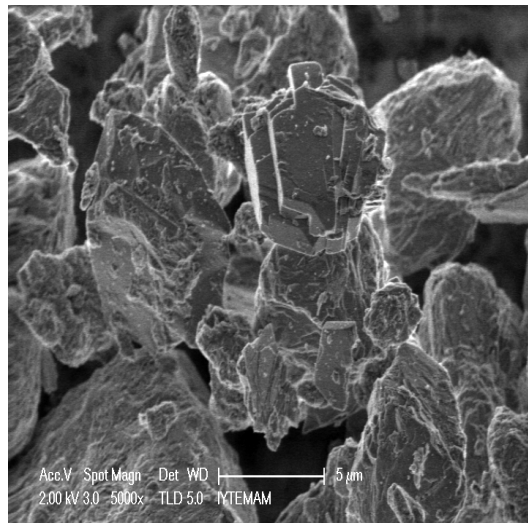


b)

Figure 7.11. Scanning electron micrographs of reference mineral of clinoptilolite-rich natural zeolite. (a) Magnification: 1000x (b) Magnification: 5000x



a)



b)

Figure 7.12. Scanning electron micrographs of purified local type clinoptilolite-rich natural zeolite.(PNZ); (a) Magnification: 1001x (b) Magnification: 5000x.

7.2.3. Particle Size Distribution

Three measurements were done for the PNZ and the reference mineral of Idaho. The weighted means and averages with standard deviations were expressed in Table 7.9. In the Figure 7.13. particle size distribution for the one measurement can be seen.

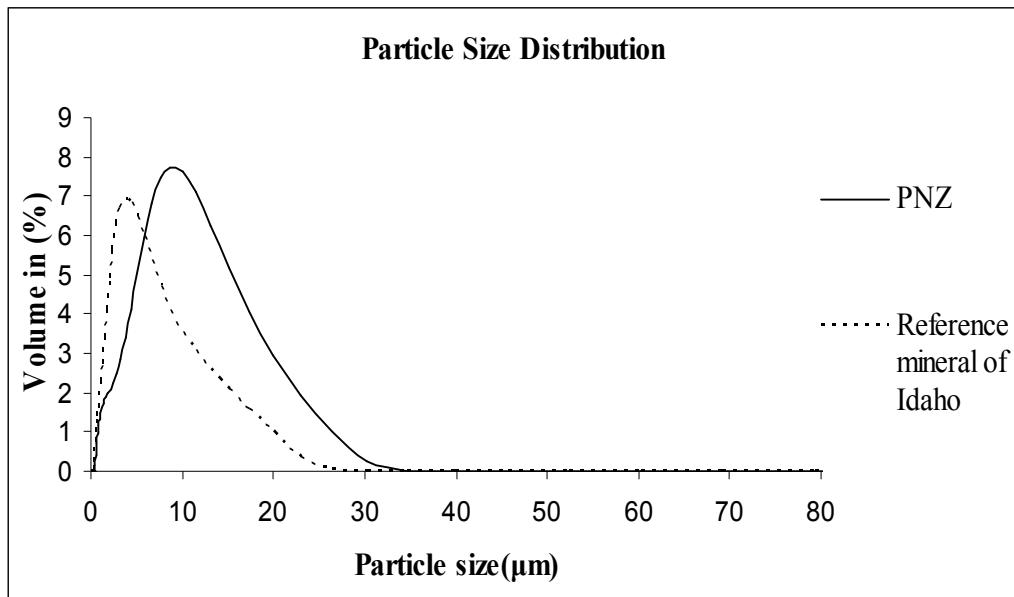


Figure 7.13. Particle size distributions of purified local type clinoptilolite-rich natural zeolite.(PNZ) and reference mineral of Idaho

Table 7.9. Particle size analysis results of reference mineral and PNZ

Sample	Volume weighted mean (µm)			
	Measurement 1	Measurement 2	Measurement 3	Average (±s.d.)
Reference mineral	5.556	5.419	5.649	5.541 (±0.116)
PNZ	7.743	7.701	7.638	7.694 (±0.053)

7.2.4. IR Absorption Results

FTIR spectra are useful in obtaining crucial information about the structure of zeolite minerals. The spectra are given in Figure 7.14. The bands can be characterized as follows (Breck, 1974).

1. Bands due to the Si–O–Si and Si–O–Al vibrations, in the regions 1200–950/cm and 420–500/cm. In the first region (1200–950/cm) the strongest vibration band appears. It is found in all zeolites due to the internal tetrahedron vibrations, and is assigned to a T–O stretching mode. In the second region (420–500/cm) there is the next strongest band that is assigned to a T–O bending mode.
2. Bands due to presence of zeolite water. The three typical bands observed are the broad band, characteristic of hydrogen-bonded OH to oxygen ions at about 3440/cm, at 3619/cm, and the usual bending vibration of water at 1640/cm.
3. Bands due to pseudo-lattice vibrations found in the region 500–800/cm. These are insensitive to the nature of the channel cations, as well as to the Si/Al ratio.

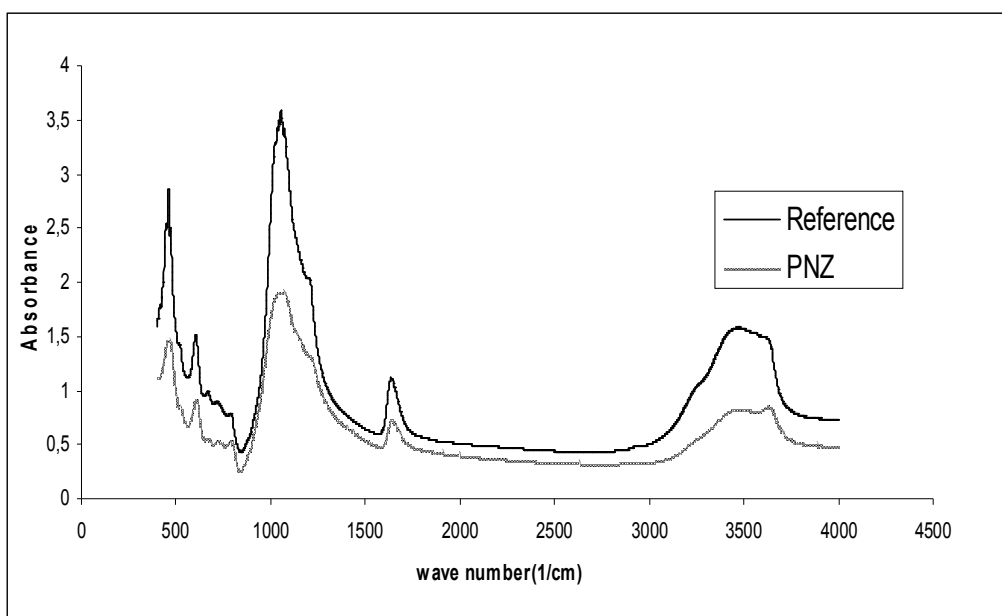


Figure 7.14. Infrared spectra of the reference and purified local type minerals

7.2.5. Surface Area Analysis Results

Samples were also analyzed by ASAP 2010 M for sorption properties using N₂ gas at 77.6 K. In the result of the analyses, N₂ adsorption and desorption isotherms of reference mineral of Idaho and local type mineral were determined (Figure 7.15) and these results were used to determine the surface area and pore properties of the samples (Table 7.10). As seen in Table 7.10 surface areas of reference mineral were found to be a bit higher than PNZ. In the surface analyses, BET model is used for comparative purposes.

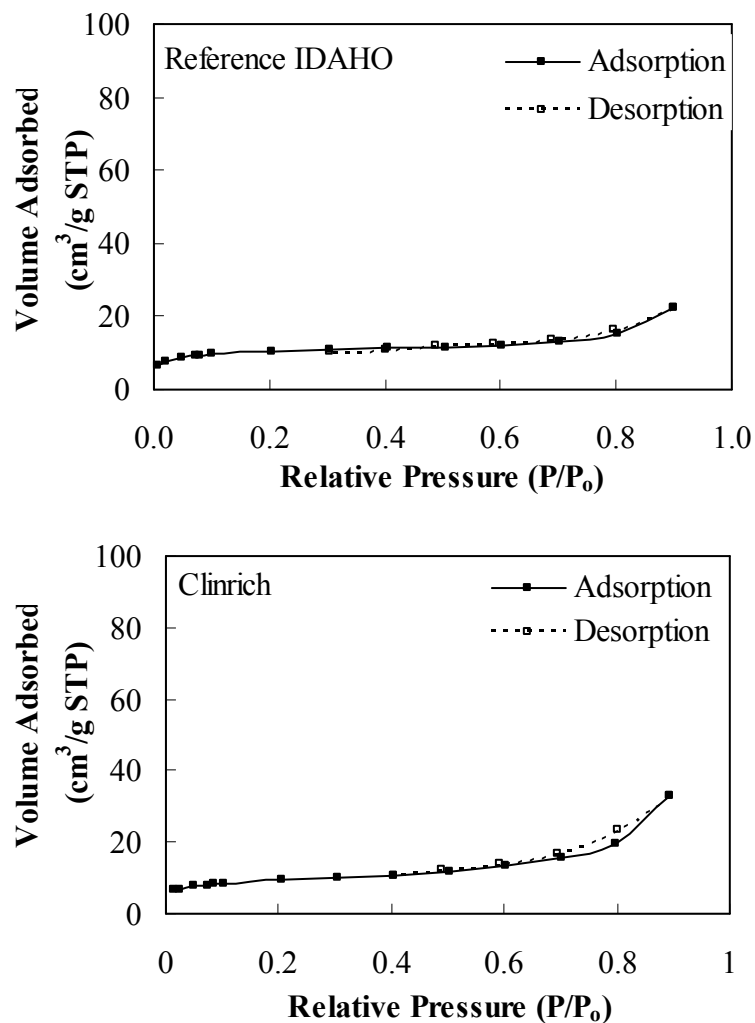


Figure 7.15. N₂ adsorption and desorption isotherms of reference mineral of Idaho and local type mineral (-196 °C).

Table 7.10. Analysis results of ASAP 2010

Property	Refence mineral of IDAHO	Clinrich
Area		
BET Surface Area (m ² /g)	33.07	30.78
Langmuir Surface Area(m ² /g)	48.76	44.68
Micropore Area (m ² /g)	13.93	10.39
Volume		
Micropore Volume (m ³ /g)	0.025	0.047
Pore size		
Average Pore Diameter , 4 V/A by BET, (Å)	41.813	65.98
Horvarth-Kawazoe (HK) Method		
Max Pore Volume(m ³ /g)	0.015	0.013
Median Pore Diameter (Å)	9.66	11.0003

Pore size distributions of the samples are given in Figure 7.16. Results showed that mineral samples have a mesoporous structure. Distributions of pore sizes were high approximately in the range of 20-120 Å. Both of the minerals exhibited bimodal mesopore size distribution at around 30 Å and 70 Å. The mesopore volume in the microporous solids is attributed to the pores between the crystals (intercrystalline pores). Micropore region could not be obtained due to the characteristics of the instrument and adsorptive gase (N₂) used

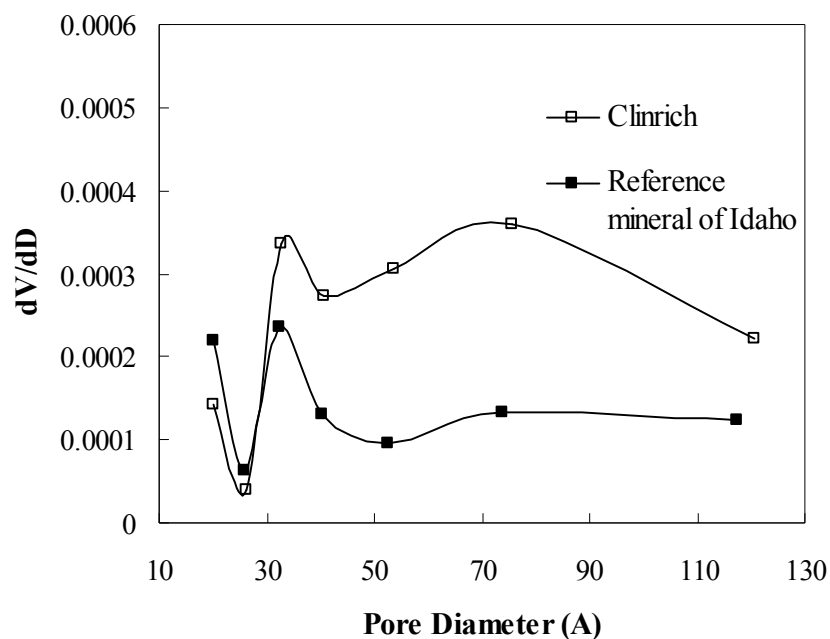


Figure 7.16. Pore size distribution of the purified local type clinoptilolite-rich natural zeolite (PNZ) and reference mineral of Idaho

7.2.6. Thermal Gravimetric Analysis (TGA)

In the TGA method, the percent weight losses of the natural zeolite samples as a function of temperature were examined. The results provided information about the dehydration properties of zeolites. Continuous curves indicated that the dehydration is reversible and the structure did not destroyed by heating. Results of the thermal gravimetric analyzes were given in Figure 7.17. Identification and quantification of water was performed and water content was categorized into three classes. They are known as external water, loosely bound water and tightly bound water. The external water was released up to 85 °C, and loosely bound water was rapidly lost up to 285 °C. The clinoptilolite started to loose the tightly bound water after 285 °C.

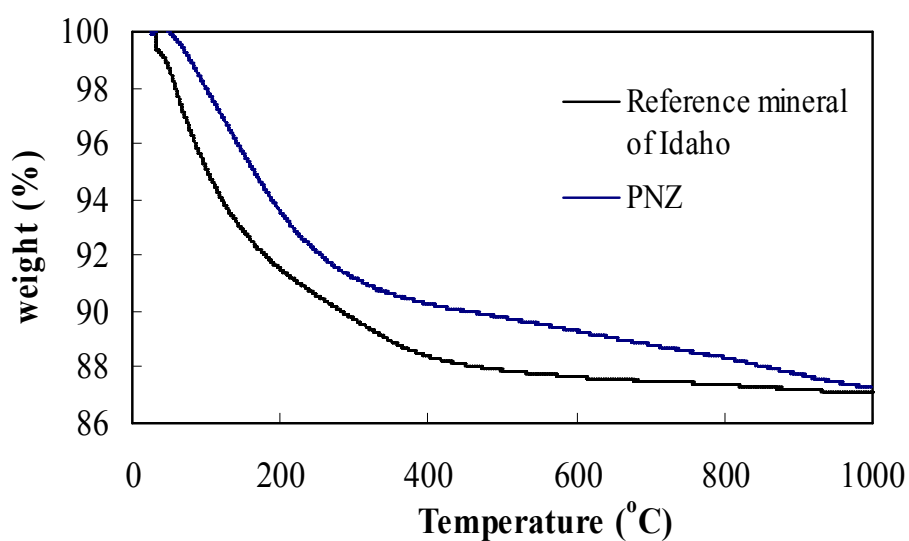


Figure 7.17. TGA curves of PNZ and reference mineral of Idaho.

The weight losses indicating water content were in the 12.99 and 12.71%. Reference mineral and our PNZ indicated similar dehydration properties (Figure 7.17 and Table 7.11).

Table 7.11. Percent weight losses that indicate the various water contents

Sample	Weight loss (%)				Integrated weight loss (%)
	External Water	Loosely Bound Water	Tightly Bound Water		
	(<85°C)	(85°C - 285°C)	(285°C-500°C)	(>500°C)	
Reference mineral	3.91	5.35	2.92	0.81	12.99
PNZ	1.33	6.17	2.70	2.51	12.71

7.2.7. Elemental Analysis of Clinoptilolite rich PNZ

Elemental analysis of the material is important for the characterization of the zeolite samples in order to explain, understand and evaluate the results of the adsorption experiments and interaction studies. Moreover, the elemental analysis has importance for the health related approaches. Therefore elemental analyses were examined in two sections as major element analysis and minor and trace element analysis, respectively.

7.2.7.1. Major Element Analysis

The major elemental analysis was determined with ICP-AES analysis after alkali (lithium tetraborate) fusion by direct calibration method. Three samples were weighed and digested then analysed. The average values as expressed in percentages with standard deviations were reported (Table 7.10). The major element amounts for reference mineral were in good agreement with the certified values and it was confirmed that the digestion method and analyses conditions could be suggested for major element analyses of the natural zeolite.

Elemental analysis of the adsorbent provides useful information in the adsorption processes. Zeolitic material can be described and classified by using the results of the major element analysis. Si/Al ratio is one of the useful criteria for describing the adsorbent material. The Si/Al ratio was significant for the classification of the zeolitic material as Heulandite-Clinoptilolite rich. According to the Si/Al, the material can be classified as (Tsitsishvili et al., 1992).

1. High-silica heulandite(3.5-4)
2. Low-silica clinoptilolite(4.0-4.5)
3. High-silica clinoptilolite (4.5-5.5)

ICP/AES results indicated that the Si/Al ratio was 5.2 ($\text{SiO}_2/\text{Al}_2\text{O}_3$; 5.89) which indicated that samples were high silica clinoptilolite (Table 7.12).

The Si/Al ratio can be related with the thermal stability and hydrophobicity of natural zeolites. Higher Si/Al character ratio indicates more hydrophobic and this property is very important for adsorption studies in aqueous solutions.

TCEC (Theoretical cation exchange capacity) can be used for the some explanations related to the adsorption experiment results. Moreover, TCEC was calculated from the summation of the exchangeable cations (Na^+ , K^+ , Ca^{2+} and Mg^{2+}) and determined as 2.08 meq/g.

The results also indicated that our samples can be identified as potassium rich clinoptilolite.

Table 7.12. Major elements in oxide form for Clinoptilolite rich PNZ and Reference mineral

Major Components in oxide form	PNZ	Reference mineral of Rhyolite	
	(w/w)%	(w/w)%	Certified (w/w)%
SiO₂	74.73(±1.31)	77.69 (±1.51)	72.76
Al₂O₃	12.703(±0.99)	12.45 (±0.81)	11.9
Fe₂O₃	0.730(±0.14)	5.508(±0.92)	4.72
K₂O	7.783(±0.95)	5.845(±0.81)	4.29
Na₂O	2.004(±0.05)	6.524(±0.65)	4.69
CaO	1.760(±0.09)	0.059(±0.08)	0.093
MgO	0.287(±0.07)	0.045(±0.03)	0.05

7.2.7.2. Minor and Trace Element Analysis

Minor and trace element analysis were performed for health related considerations. In the case of ingestion of minerals by human, it is recommended to determine whole chemical composition of mineral. Considering that the elements reported are present as solute, it could be expected that they are all immediately available to the organism. For this, useful reference represented by the admissible daily dose established for drinking waters (CEE regulation no. 80/778) was suggested (Tateo et al.,2001).The limits for drinking water take into account toxicological consideration, safety factors and a daily uptake of 2 L /person . Further considerations is based on the classification of elements developed by the National Academy of Sciences (Tateo et

al.,2001). The latter ones can provide the link between inorganic geochemistry and man's health

- Essential macronutrients (100 mg/day or more are needed):

Ca, Cl, Mg, P, K, Na, S;

- Essential micronutrients (no more than a few mg/day are needed):

Cr, Co, Cu, F, I, Fe, Mn, Mo, Se, Zn;

- Micronutrients which are likely to be essential:

Ni, Si, Sn, V;

- Trace contaminants: Al, As, Cd, Pb, and Hg.

The concentration of essential elements could be evaluated in terms of deficiency /toxicity (excess), whereas for non-essential elements, a threshold could be established (WHO, 1996).

Table 7.13. Guide-value and maximum admissible concentration of selected elements in drinking waters(CEE no. 80/778) and calculated maximum daily dose in water (considering an uptake of 2L/day/person)

Element	Guide Value (mg/L)	Maximum admissible concentration (mg/L)	Equivalent maximum daily dose(mg/day)
Ca	100	-	-
Mg	30	50	100
K	10	-	-
Al	0.05	0.20	0.4
Fe	0.05	0.20	0.4
Mn	0.02	0.05	0.1
Ni	-	0.05	0.1

Table 7.14. Minor and trace element concentrations determined by microwave assisted ICP-MS technique using two different acid digestions.

Elements	Microwave digestion (HNO₃+HCl) (µg /g)	Microwave digestion (HNO₃) (µg /g)	Microwave digestion (HNO₃+HCl) (µg /g)	Microwave digestion (HNO₃) (µg /g)
	Reference-JR-3		PNZ	
Li	84.17(±3.2)	33.68	23.71(±2.2)	11.27
Cr	12.83(±1.1)	5.40	22.64(±1.5)	8.62
Mn	405.56(±12.2)	232.30	140.47(±9.5)	103.69
Co	7.33(±0.8)	2.99	17.70(±1.3)	11.43
Ni	46.12(±3.1)	26.64	106.90(±9.6)	30.05
Cu	56.81(±5.1)	32.21	57.51(±5.9)	58.79
Zn	181.82(±15.2)	134.94	49.70(±9.3)	75.17
Cd	10.02(±0.9)	2.08	8.16(±0.9)	2.62
Ba	250.00(±20.3)	109.64	569.70(±15.7)	270.34
Pb	87.38(±8.2)	49.78	33.26(±2.3)	67.61
As	2.86(±0.7)	n.d.	11.93(±1.5)	n.d.
Hg	3.12(±0.5)	n.d.	3.73(±0.4)	n.d.

Two different digestions were applied for the reference mineral and PNZ by using microwave assisted technique. The results were converted into µg/g for each element. Most of the minor elements and trace elements were tabulated (Table 7.14.). Using of this acid mixture combined with microwave assisted technique provided better recoveries of the minor and trace elements for both reference mineral and PNZ and this digestion procedure was suggested for minor element analysis. It is known that some of these elements have distinct importance in terms of the toxicological point. These are Cd, Pb, As and Hg. For this reason they are evaluated in the toxicological limits determined by the international criteria.

Estimated exposures/intakes of arsenic, cadmium, mercury, and lead were assessed with respect to safe/tolerable exposure levels described by various national and public health organizations. The FAO/WHO recommended a The Provisional Tolerable

Weekly Intake (PTWI)for (FAO/WHO, 1993) and PTWI of the these elements are presented (Table 7.15). One gram of clinoptilolite contains 33.26 µg lead. 8.16 µg cadmium. 3.08 µg mercury and of 11.93 µg arsenic. The PTWI's greater respectively than the quantities consumed in 7 grams (one week's recommended intake) as consumed by a 60 kg individual assuming 100% solubilization of these metals in the stomach. In fact, only a small proportion of each of these elements is likely to be solubilised. The estimated intakes of As, Pb, Cd, and Hg for the PNZ do not exceed the toxicological reference values established by the FAO/WHO.

Table 7.15. Estimated toxic elements and safe/tolerable exposure levels

Toxic elements	µg/g zeo	PWTI (µg/kg body)	PWTI for 60 kg body weight	µg element/week
Pb	33.26	25	1500	232.3
Cd	8.16	7	420	57.1
Hg	3.08	5	300	21.5
As	11.93	15	900	83.5

7.2.8. Surface Charge Measurements of the PNZ

Figure 7.18. indicated the change of the zeta potential of the PNZ as a function of pH. The zeta potential of the PNZ was changed by the solution acidity. When the solution pH was increased, the negativity of the mineral surface increased. In the pH range of 3 to 10, it was found that the surface charge remained in negative. The pH3.0 also represented the gastric pH value and at this pH surface charge is -14 mV and intestinal pH was represented by pH 7.3 and zeta potential is -26 mV.

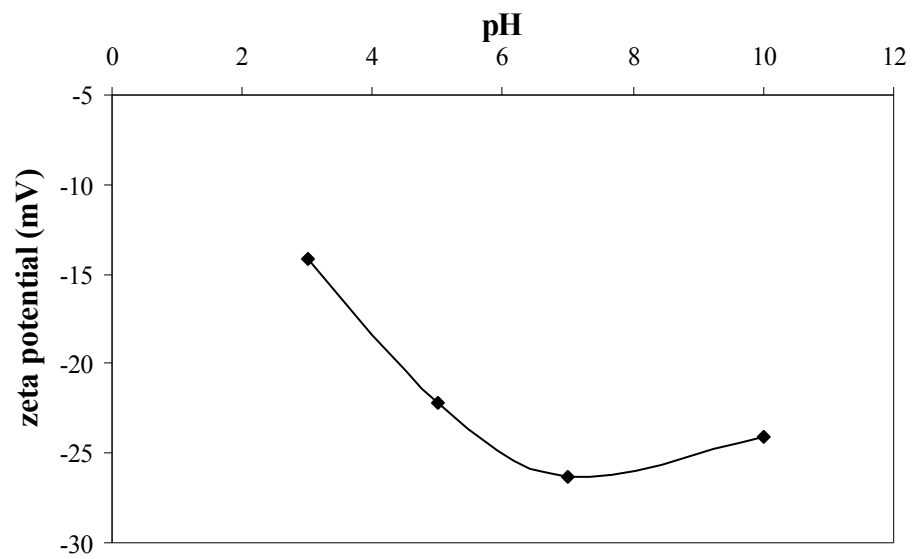


Figure 7.18. Variations in the zeta potential of PNZ (2.5 mg/ml) at different solution pH values (potassium phosphate buffer).

7.3. The Results of the Adsorption Experiments

afB1 adsorption experiments results were evaluated in three sections; adsorption behavior of the clinoptilolite rich mineral, probiotic *lactobacillus* organism and their combination were investigated and discussed.

7.3.1. Adsorption Experiments by Clinoptilolite Rich Mineral

AfB1 adsorption characteristics of the clinoptilolite rich mineral were determined by evaluating the data of uptake rate measurements. Adsorption isotherms were constructed and adsorption mechanism was discussed by applying several models.

7.3.1.1. Adsorption Equilibrium and Adsorption Isotherms

From the uptake rate measurements, the equilibrium time period was determined as 120 min. Adsorption isotherms were given in Figure 7. 19. and 7.23. Uptake curves were also presented for the isotherms (Figure 7.20, 7.21, 7.22 and Figure 7.24,7.25)

As seen in the Figure 7.19 and 7.23, afB1 adsorption equilibrium data is well represented by Henry's law for low concentrations as expected and for the high concentrations a tendency for the formation of a plateau was observed. Results showed that equilibrium adsorbed amounts were decreased with the increasing temperature. This result means that afB1 adsorption by PNZ is favored in the lower temperatures and this indicates exothermic nature of the adsorption process. This is also confirmed by negative enthalpy change in the thermodynamic analysis as given Table 7.19.

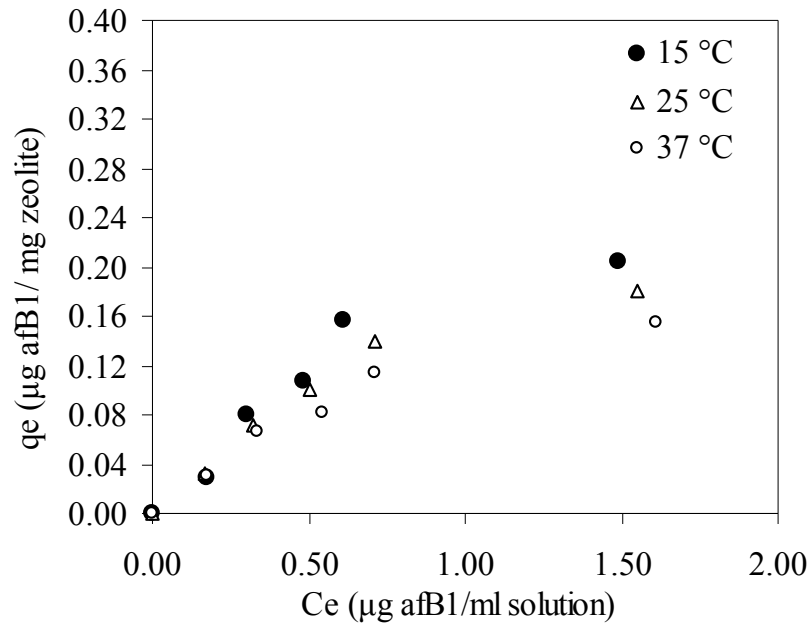


Figure 7.19. Effect of temperature on adsorption isotherms. (T: 15 °C, 25 °C and 37 °C. agitation speed: 130 rpm, S/L:25mg/10 ml, working solution: PBS pH 7.3, particle size: 8 µm).

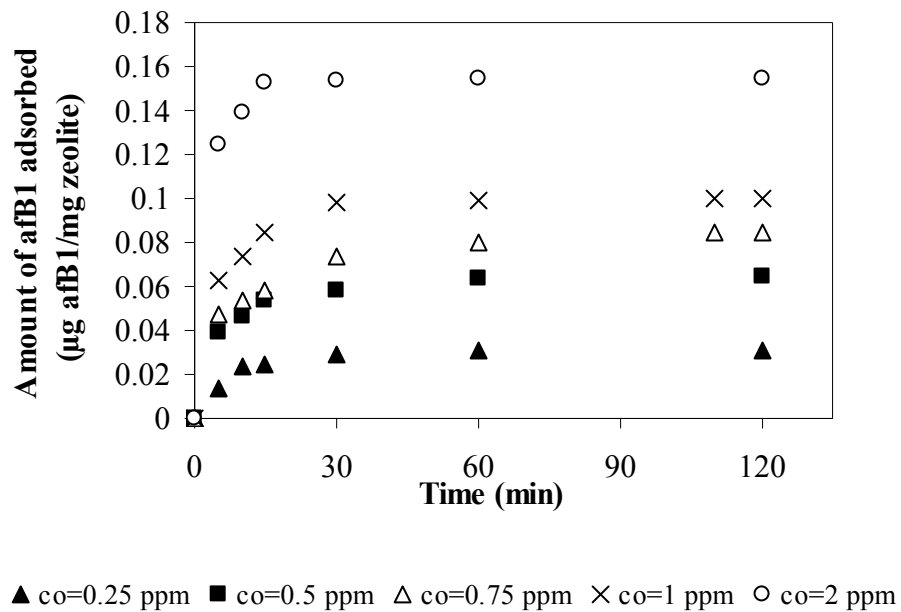


Figure 7.20. Uptake curves at 37 °C (agitation speed: 130 rpm, S/L:25mg/10 ml, working solution: PBS pH 7.3, particle size: 8 µm).

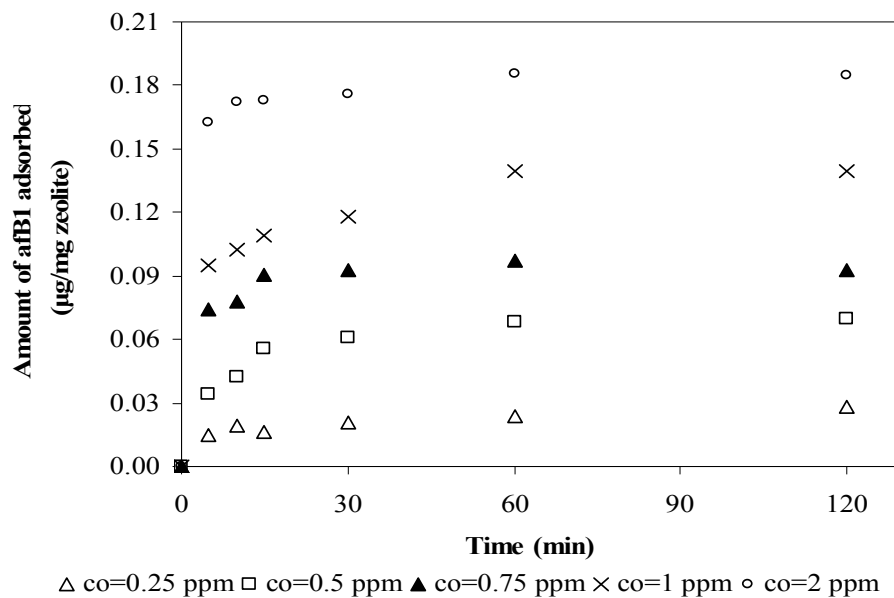


Figure 7.21. Uptake curves at 25 °C.(agitation speed: 130 rpm, S/L:25mg/10 ml, working solution: PBS pH 7.3, particle size: 8 µm).

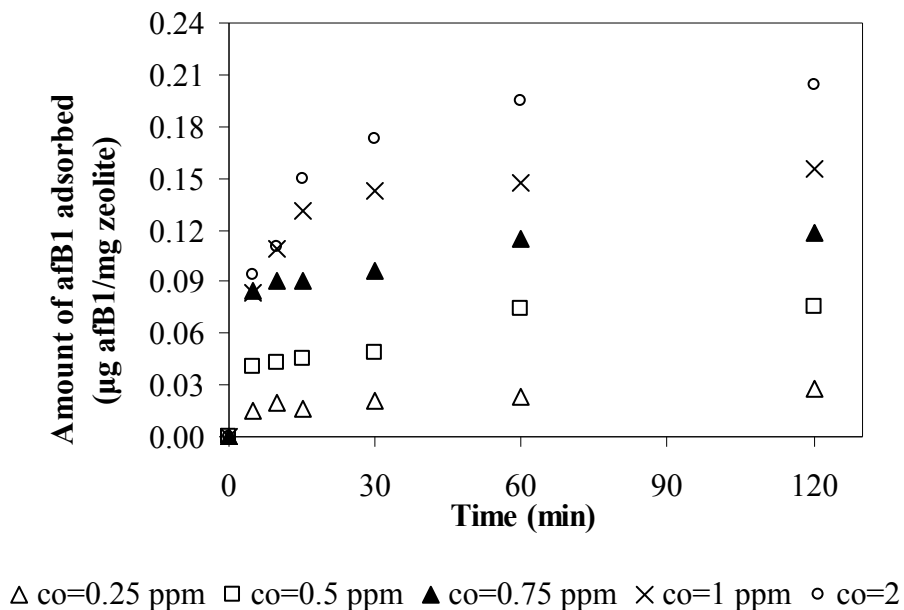


Figure 7.22. Uptake curves at 15 °C.(agitation speed: 130 rpm, S/L:25mg/10 ml, working solution: PBS pH 7.3, particle size: 8 µm).

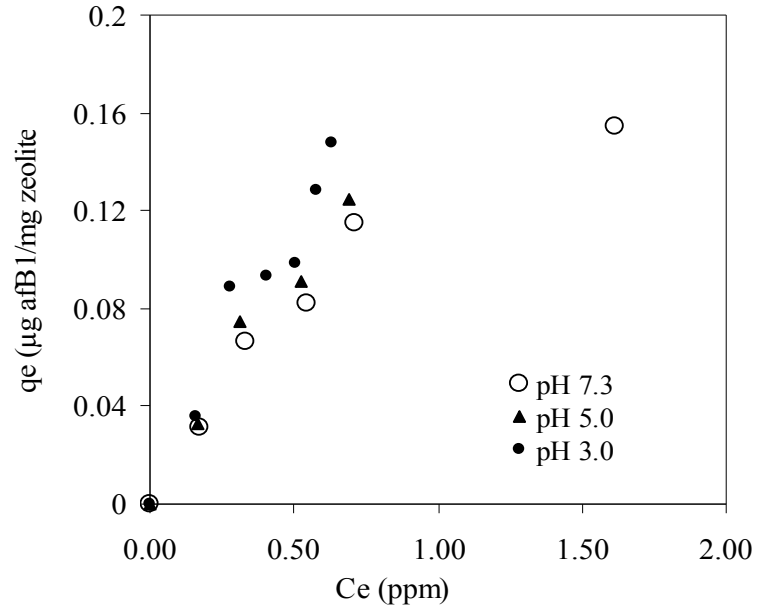


Figure 7.23. Effect of pH on adsorption isotherms. (T:37 °C, ω = agitation speed: 130 rpm, S/L:25mg/10 ml, working solution: PBS, particle size: 8 μm).

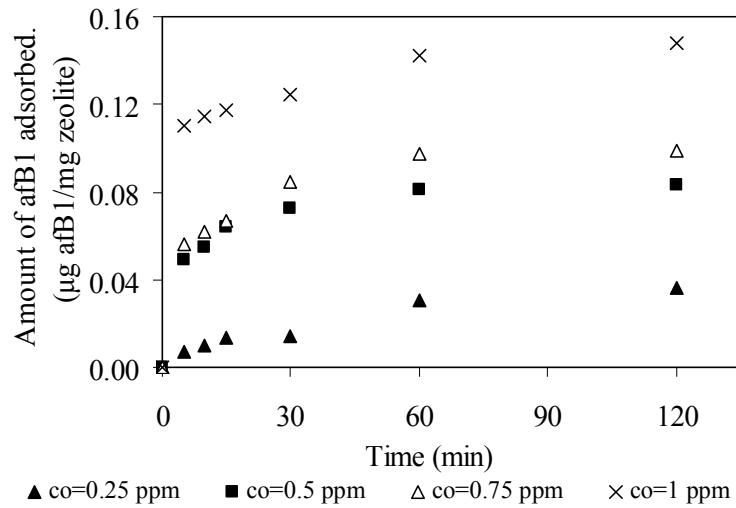


Figure 7.24. Uptake curves for pH 3.0. (T: 37 °C, agitation speed: 130 rpm, S/L:25mg/10 ml, working solution: PBS, particle size: 8 μm).

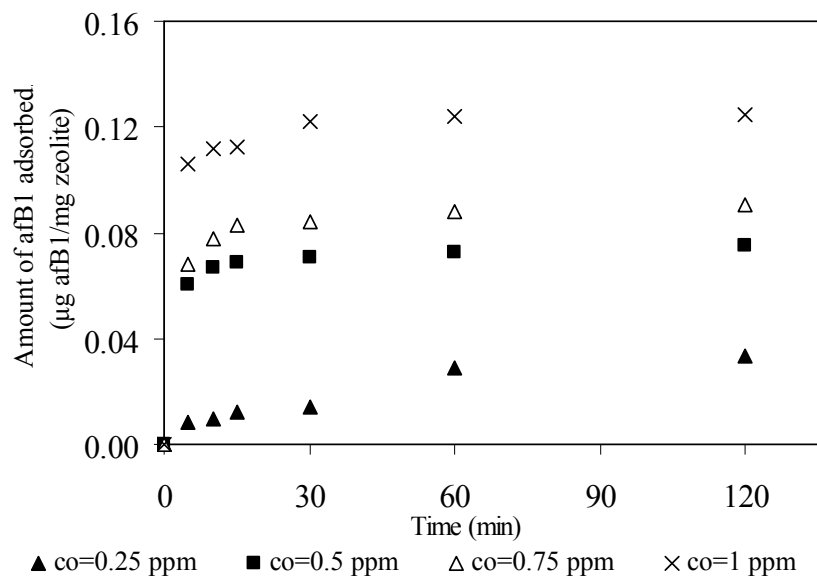


Figure 7.25. Uptake curves for pH 5.0. (T: 37 °C, agitation speed: 130 rpm, S/L: 25mg/10 ml, working solution: PBS, particle size: 8 µm).

Effect of pH on adsorption isotherms is given in the Figure 7.23; for pH 3.0 and pH 5.0 only low concentration experiments had been performed. Increase in the amounts adsorbed with the decrease in the pH values was observed.

In the Table 7.16, applied adsorption isotherm models and the solution strategies in the estimation of isotherm constants are presented. Calculation results and correlation coefficients for model equation fittings are presented in Table 7.17. It is known that in the case of Langmuir isotherm, there exist several linearization types which affect the results as it was also discussed and nonlinear regression was suggested by El-Khaiaryl M. N. and Malash. G. F (2011). Therefore, applied linearization type is also given in the comparison of the results.

Table 7.16. Applied adsorption isotherm models and the determination of their constants

Adsorption isotherm model	Solution strategy	Solution
Langmuir $q_e = \frac{K_L \cdot C_e}{1 + a_L \cdot C_e}$	Linearization $\frac{C_e}{q_e} = \frac{1}{K_L} + \frac{a_L C_e}{K_L q^m}$	Plot C_e and $\frac{C_e}{q_e}$ Intercept; $\frac{1}{K_L}$ Slope; $\frac{a_L}{K_L}$
Freundlich $q_e = K_F C_e^{(1/n)}$	Linearization $\ln q_e = \ln K_F + \frac{1}{n} \ln C_e$	Intercept; $\ln K_F$ Slope; $\frac{1}{n}$
Langmuir-Freundlich (Sip's) $q_e = \frac{K_{LF} C_e^{n_{LF}}}{1 + a_{LF} C_e^{n_{LF}}}$	Non linear regression analysis	solver tool of the excel program was used.
Henry's Law $q_e = K_H C_e$	Applied for low concentration region	Plot c_e and q_e . and slope ; K_H

In the equations, q_e is the adsorbed afB1 concentration at equilibrium ($\mu\text{g}/\text{mg}$), C_e is the equilibrium afB1 concentration in the solution ($\mu\text{g}/\text{mL}$), and K_L (mL/mg) and a_L ($\text{mL}/\mu\text{g}$) are the Langmuir constants. K_L/a_L gives the maximum adsorption capacity (monolayer saturation capacity) ($\mu\text{g}/\text{mg}$), a_L indicates the affinity of the binding sites (a distribution coefficient, affinity parameter). For the Freundlich model, where K_F ($\mu\text{g}/\text{mg} (\text{mL}/\mu\text{g})^{1/n}$) and n_F (dimensionless) are the Freundlich's constants indicating adsorption affinity and adsorbent surface heterogeneity, respectively. Higher values of K_F indicate greater affinity between the adsorbate and the adsorbent. More heterogeneous adsorbent surface yields higher values of $1/n_F$. In the Sips isotherm model, n_{LF} characterizes heterogeneity of the adsorbent surface. For $n = 1$, the Langmuir-Freundlich model reduces to the Langmuir equation. The larger n_{LF} the higher the degree of heterogeneity of the adsorbent surface.

Table 7.17. Comparison of applied adsorption isotherm models

Models						
Langmuir	Temperature	K_L (mL/mg)	a_L (mL/ μ g)		SSE	R^2
	37 °C	0.233	0.853		0.00022	0.93
	25 °C	0.258	0.723		0.0005	0.83
	15 °C	0.299	0.911		0.0021	0.90
Freundlich		K_F $\frac{\mu\text{g}}{\text{mg}} \left(\frac{\text{mL}}{\mu\text{g}} \right)^{1/n_F}$	n_F		SSE	R^2
	37 °C	0.126	1.410		0.00084	0.94
	25 °C	0.155	1.284		0.0021	0.93
	15 °C	0.147	1.532		0.0035	0.82
Langmuir-Freundlich (Sips)		K_{LF} $\left(\frac{\mu\text{g}}{\text{mg}} \left(\frac{\text{mL}}{\mu\text{g}} \right)^{1/n_{LF}} \right)$	n_{LF}	a_{LF} $\left(\frac{\mu\text{g}}{\text{mL}} \right)^{1/n}$	SSE	R^2
	37 °C	0.355	1.263	1.738	0.0002	0.98
	25 °C	0.671	1.630	3.218	0.00007	0.99
	15 °C	1.126	1.964	5.039	0.00034	0.95

Calculated isotherm constants for the models applied are given in Table 7.17 and representative comparative diagram for the models is given Figure 7.26, 7.27 and 7.28 . The validity of the adsorption equilibrium models was determined by comparing the sum of the squares of the differences between the experiment and the calculated data (SSE) for each model. Experimental data was best represented by Sips isotherm model with the lowest SSE error values as also seen in the Figures (7.26, 7.27 and 7.28.) The calculated maximum afB1 adsorption capacity of PNZ at 37 ° was found to be 0.21 μ g afB1/mg PNZ by using the Sips isotherm model equations and this value is a bit higher than observed value (0.16 μ g afB1/mg PNZ).

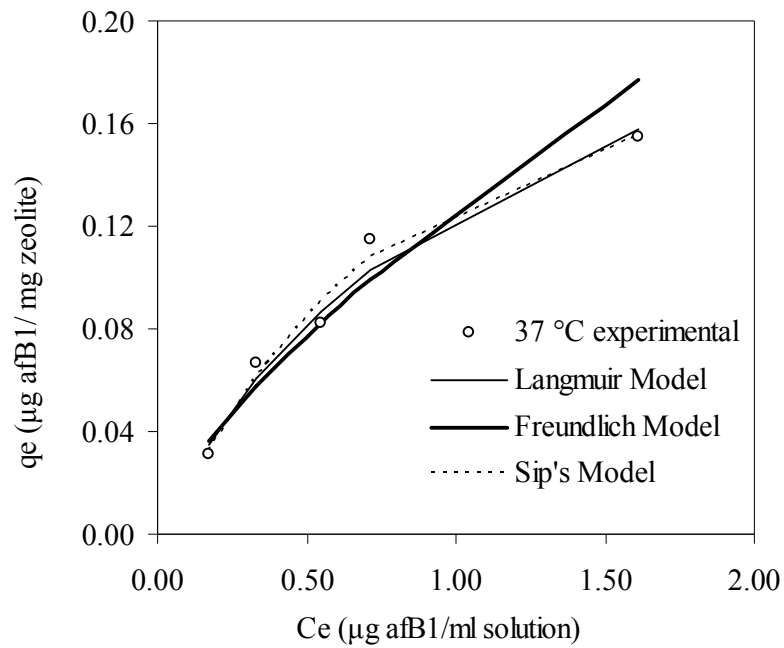


Figure 7.26. Experimental isotherm data and isotherm models for afB1 adsorption by PNZ (T:37°C, agitation speed: 130 rpm, S/L:25mg/10 ml, working solution: PBS pH 7.3, particle size: 8 µm)

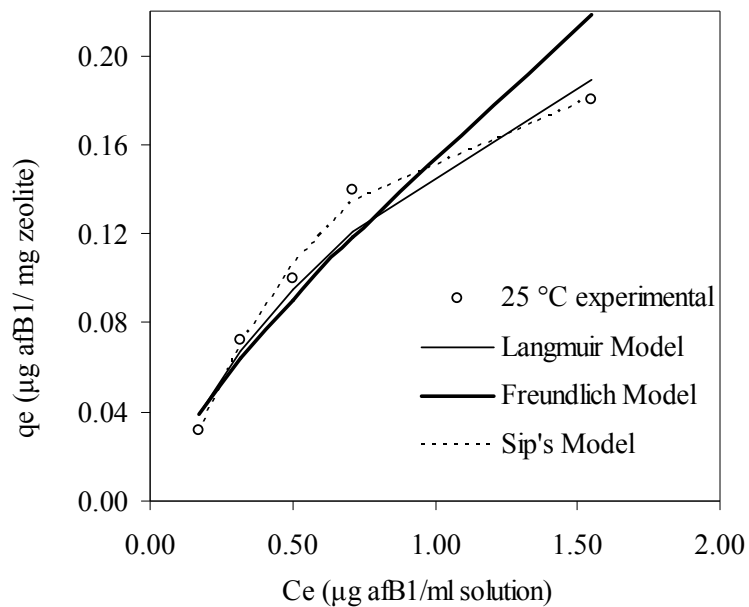


Figure 7.27. Experimental isotherm data and isotherm models for afB1 adsorption by PNZ (T:25 °C, agitation speed: 130 rpm, S/L:25mg/10 ml, working solution: PBS pH 7.3, particle size: 8 µm)

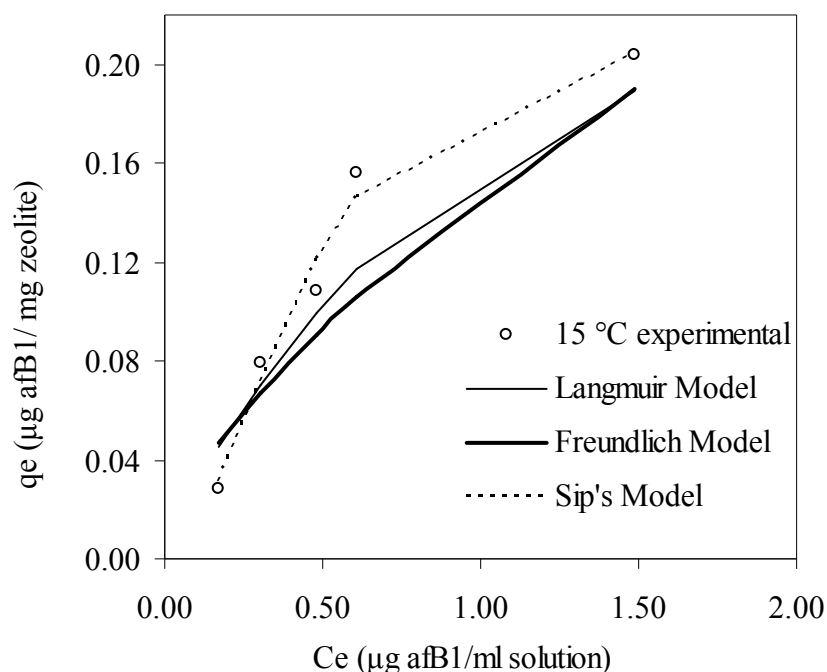


Figure 7.28. Experimental isotherm data and isotherm models for afB1 adsorption by PNZ (T:15 °C. agitation speed: 130 rpm. S/L:25mg/10 ml, working solution: PBS pH 7.3, particle size: 8 µm)

Table 7.18. Henry's modeling of adsorption isotherm for different pH's

pH	Henry's Law Constant	SSE	R ²
pH 3.0	0.230	0.001	0.93
pH 5.0	0.186	0.0003	0.97
pH 7.3	0.163	0.0002	0.97

Adsorption equilibrium isotherm data for different pH s were compared by Henry's law modeling and it is clear from the Table 7.18 equilibrium constant was highest for pH 3.0 and validity of Henry's law is also confirmed by the low SSE values in the low concentration range (0.25-1 ppm afB1)

In the literature, there exists limited number of studies for the removal of afB1 by zeolites (Tomasevic et al., 2001; Dakovic et al., 2005; Thieu1 and Pettersson, 2008). There is not adsorption equilibrium isotherm modeling study for clinoptilolite rich natural mineral.

By considering the experimental conditions (temperature, pH, type of working solution, ,agitation speed) comparison can be made only by Tomasevic et al. (2001). Adsorption amount can be calculated from published data as 0.18 μg afB1/mg clinoptilolite. This clinoptilolite mineral was identified as Ca-rich clinoptilolite mineral. Adsorption experiments were conducted at 37 °C and pH 3.8 (aqueous electrolyte having a composition similar to that of gastric juices of animals). Although any adsorption isotherm modeling study was not presented in this paper, calculated adsorbed amount (0.18 μg afB1/mg clinoptilolite) indicated similarity with our results.

7.3.1.2. Effects of Experimental Parameters on Adsorption

The discussions of the effect of experimental parameters (initial afB1 concentration, adsorbent dose, temperature, pH, particle size and agitation speed) on the adsorption kinetics were presented in the following section.

7.3.1.2.1. Analysis of Experimental Uptake Curves

Effect of Initial afB1 Concentration

The effect of initial concentration on uptake curve is given Figure 7.29. The initial uptake rate was high at the beginning of the adsorption since there were many available unoccupied sites in the adsorbent. Later, uptake rate gradually slowed down since the adsorbent active sites had been continuously occupied and fewer available sites were involved in the adsorption. At equilibrium, the uptake rate approached to zero. Results of the uptake values for afB1 adsorption at different initial concentrations showed that adsorption equilibrium was reached after 60-120 min depending up the initial adsorbate concentration. Increase in initial concentrations results in increase in the adsorption rates. The equilibrium adsorbed amounts increased from 0.011 to 0.155 $\mu\text{g}/\text{mg}$ with the increase in the initial afB1 concentrations from 0.1875 to 2 ppm.

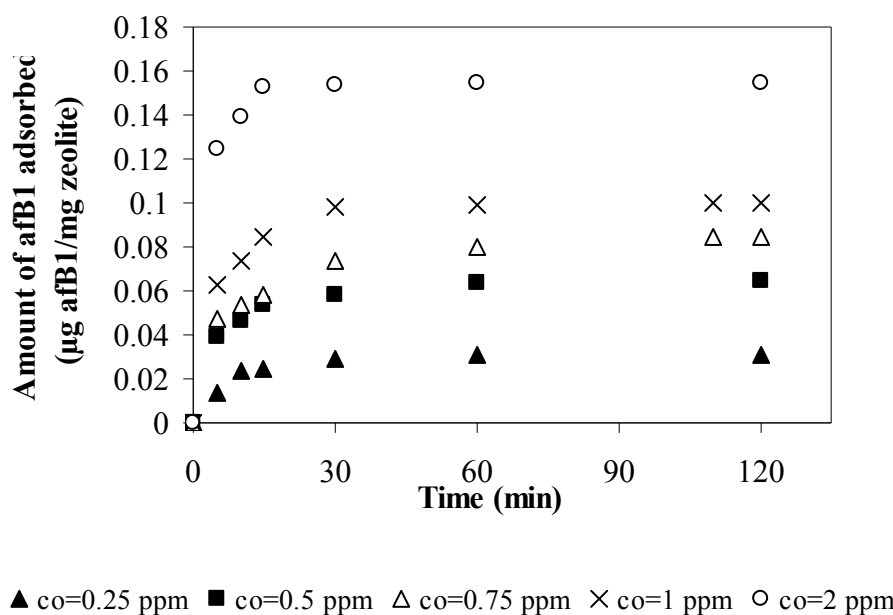


Figure 7.29. Effect of initial adsorbate concentration on adsorption kinetics of afB1 by PNZ (T:37 °C, agitation speed: 130 rpm, S/L:25mg/10 ml, working solution: PBS pH 7.3, particle size: 8 µm).

Effect of Adsorbent Dose (Solid/Liquid Ratio)

Changing the solid-liquid ratio affected the adsorbed amount of afB1. Three different adsorbent amounts (12.5 mg, 25 mg and 100 mg of PNZ) were tested to see the effect of solid/liquid ratio. The results given in Figure 7.30 and 7.31 showed a decrease in the amount of afB1 adsorbed per mg PNZ (µg afB1/mg) with increase in zeolite amount. On the other hand, the total amount adsorbed increased with increase in zeolite amount. In order to reach max adsorption capacity, solid liquid ratio of 12.5 mg PNZ: 10 ml PBS solution was found to be sufficient.

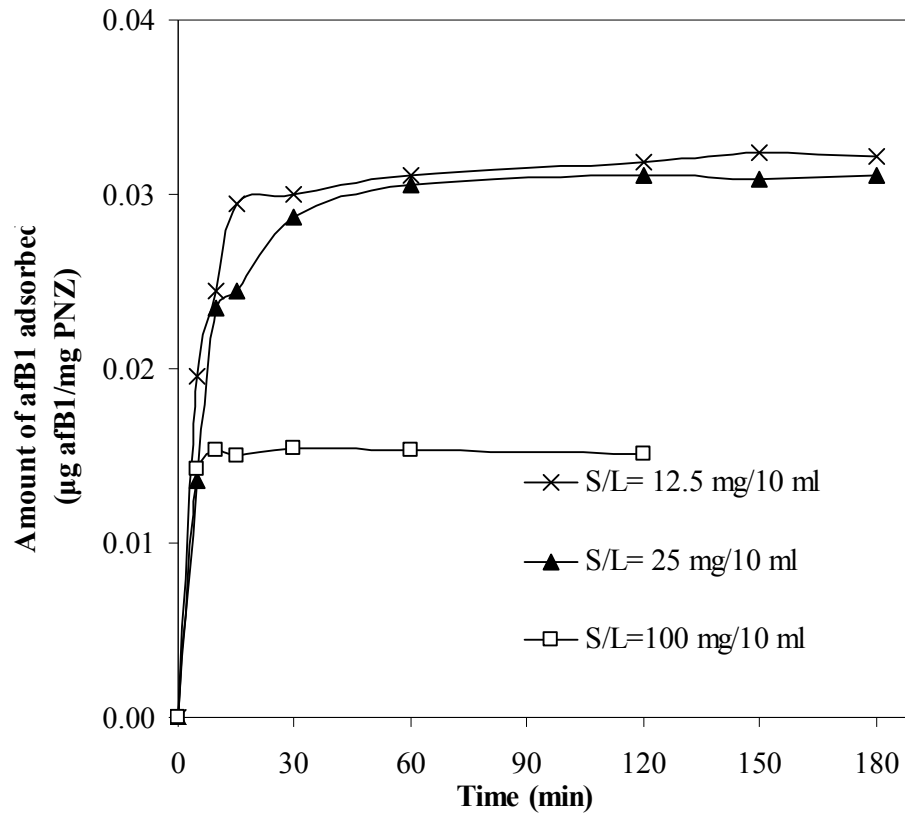


Figure 7.30. Effect of solid liquid ratio on adsorption kinetics of afB1 by PNZ (T:37°C, $c_0=0.25$ ppm afB1, agitation speed: 130 rpm, S/L:12.5-100 mg/10 ml, working solution: PBS pH 7.3, particle size: 8 μm)

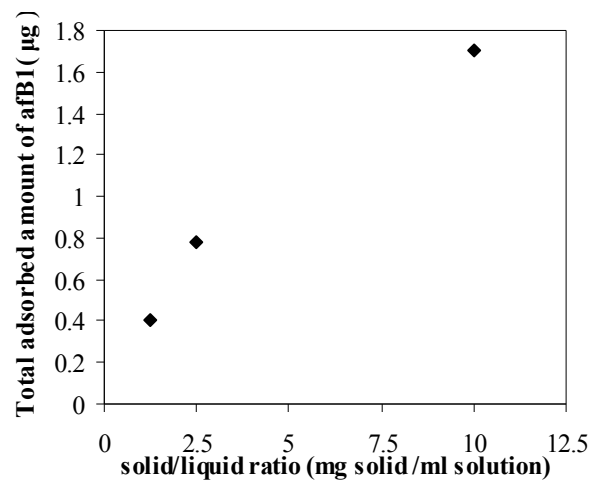
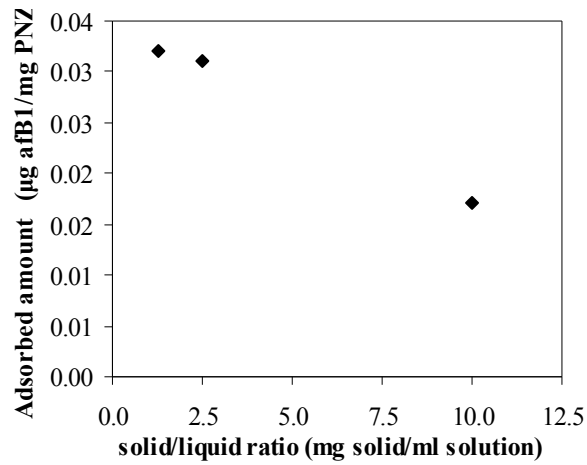


Figure 7.31 Effect of solid liquid ratio on adsorbed amount at equilibrium and on the total adsorbed amount of afB1 (T:37°C, $c_0=0.25$ ppm afB1, agitation speed: 130 rpm, S/L:12.5-100mg/10 ml, working solution: PBS pH 7.3, particle size: 8 µm)

Effect of Particle Size

The change in the particle size affected the adsorbed amount of afB1. Clinoptilolite rich mineral (75-150 μm) was ground serially and three different particle sizes (course and small and extra small) were obtained. Figure 7.32 illustrated the effects of particle size on the afB1 adsorption. The results indicated that the amount of afB1 adsorbed at equilibrium was increased when the particle size was decreased. Total surface area of clinoptilolite rich mineral is composed of external and internal surface areas which cover pores and channels. When the particle size of the mineral is reduced, only the external surface area increases. Internal surface area does not change with changing particle size, except the clogged pores. After critical particle size, decrease in particle size did not effect the uptake curve.

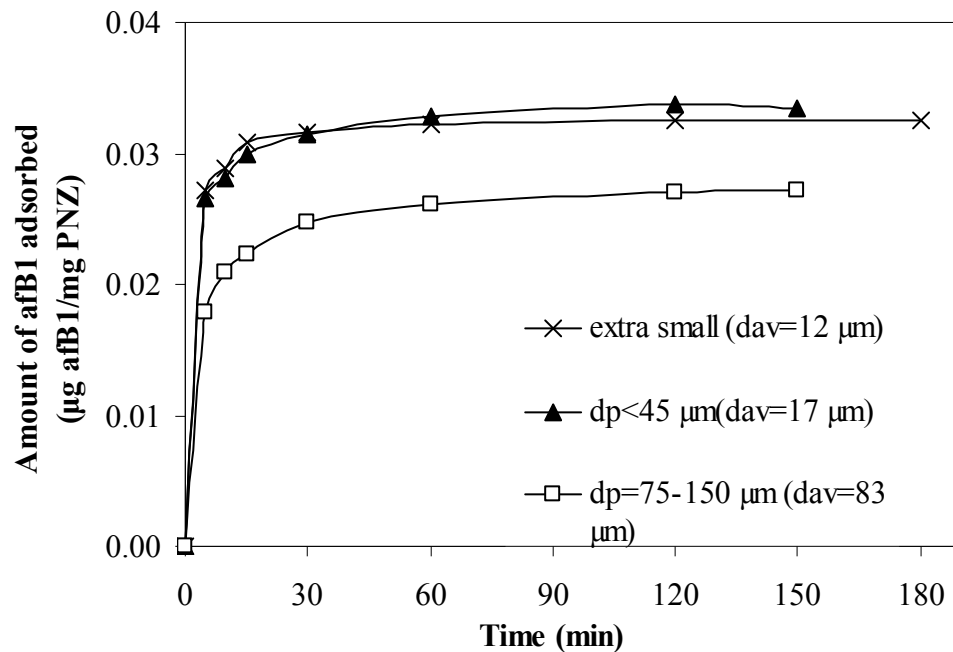


Figure7.32. Effect of particle size on adsorption kinetics of afB1 by PNZ (T:37°C, $c_0=0.25$ ppm afB1, agitation speed: 130 rpm, S/L:25 mg/10 ml, working solution: PBS pH 7.3)

Effect of Agitation Speed

Experiments were conducted for three different agitation speeds (50 rpm, 130 rpm and 200 rpm) and results are presented (Figure 7.33). Agitation speed is important for the distribution of the molecules in the solution and it affects the film thickness of the liquid layer surrounding the PNZ. By increasing the agitation speed, the thickness of the boundary layer decreases and thus the external mass transfer resistance becomes smaller. For agitation speed of 50 rpm, equilibrium could not be achieved even up to 360 min and it is expected that equilibrium will be reached in a longer time. Results showed that the adsorption rate increased with the increase in the agitation speed up to a critical value; after which the effect of external film resistance seems to have minor degree of effect.

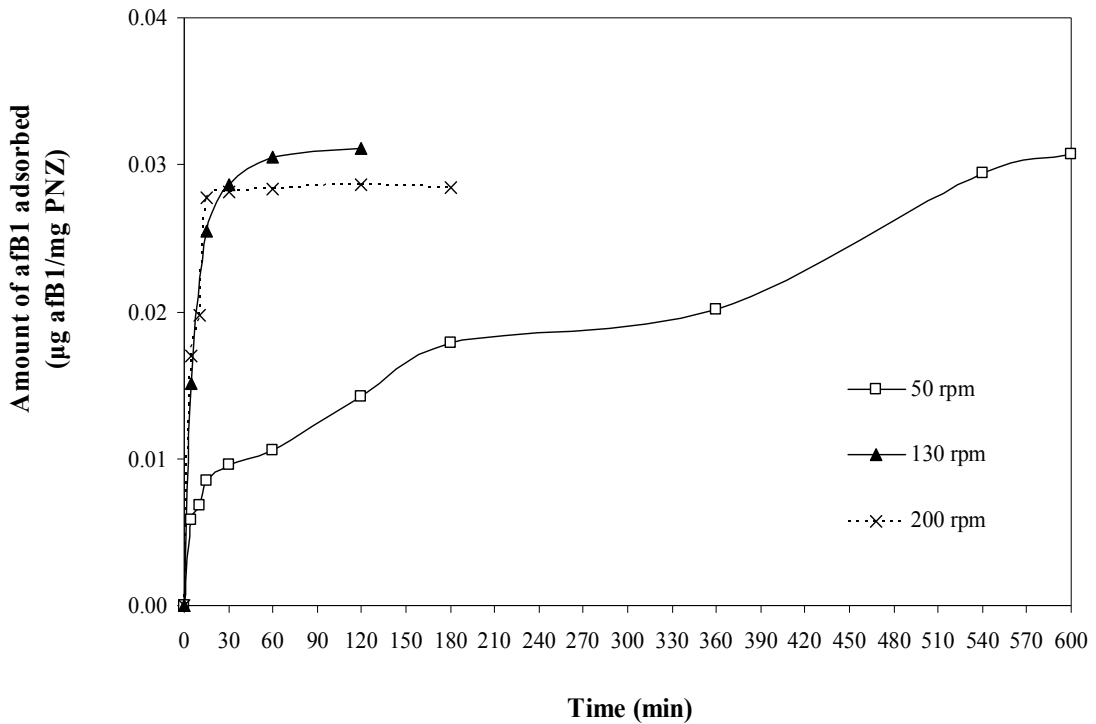


Figure 7.33. Effect of agitation speed on adsorption kinetics of afB1 by PNZ. (T:37°C, $c_0= 0.25$ ppm afB1, S/L:25 mg/10 ml, working solution: PBS pH 7.3, particle size: 8 µm)

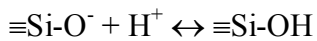
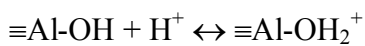
Effect of Solution pH

Three different pH values (pH 3.0, pH 5.0 and pH 7.3) were studied to see their effects on adsorption kinetics (Figure 7.34). pH 3.0 simulates the gastric environment and pH 5.0 and pH 7.3 simulates the fasted and fed intestinal system. Results showed that adsorption kinetics were affected with the pH of the solution. Decrease in the pH resulted in higher amounts of afB1 adsorbed.

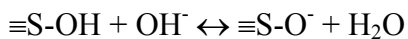
In order to analyze this result, surface charge of the zeolite should be considered. Zeta potential measurements of zeolite in solutions with different pH values were performed and results showed that zeolite was net negatively charged (Figure 7.20). The negativity increased with increase in the solution pH value.

Since afB1 is nonionizable, slight increase in the equilibrium adsorption capacity of the zeolite for afB1 at the lower solution pH can be explained by the change of the zeolite surface with the pH. Dakovic et al. (2005) have reported similar results for pH effect on afB1 adsorption by natural zeolite mineral. With increasing pH, OH ions in the solution might bind to the adsorption sites on the zeolite surface thereby might prevent interactions of the afB1 with the adsorption sites.

In acidic and neutral pH range, the neutral and negative surface hydroxyl groups are protonated:



In the basic pH range, OH⁻ ions may react with clinoptilolite surface and caused the surface to be deprotonated:



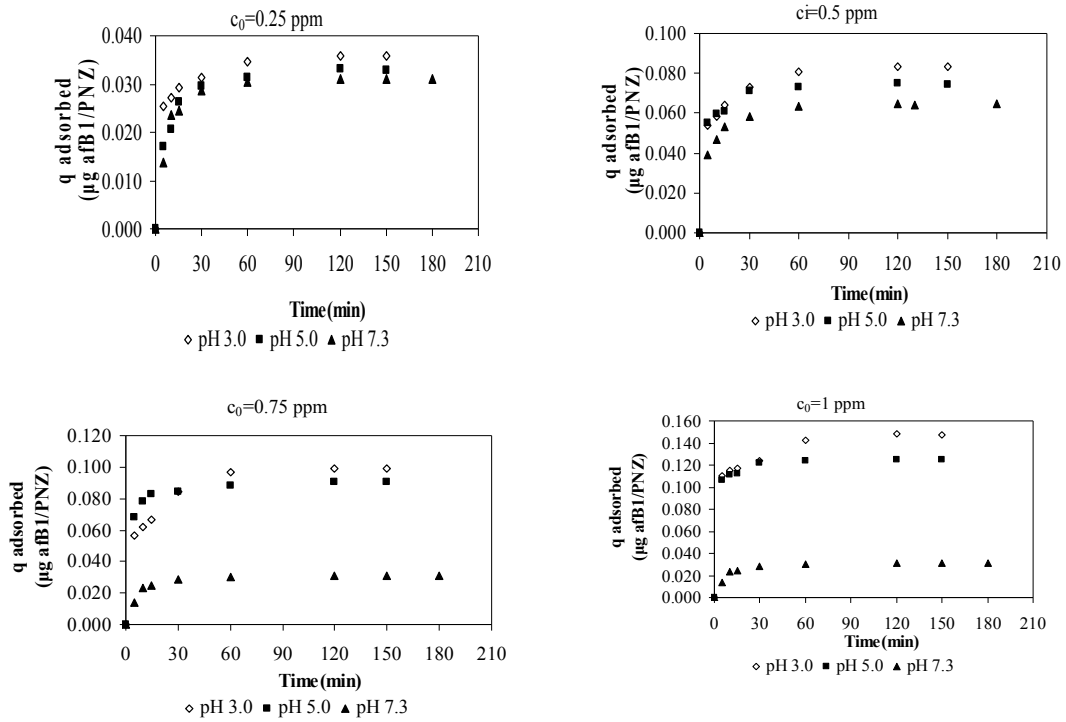


Figure 7.34. Effect of solution pH on adsorption kinetics of afB1 by PNZ (T:37°C, $c_0 = 0.25$ ppm afB1, agitation speed: 130 rpm, S/L:25 mg/10 ml, working solution: PBS pH 7.3, particle size: 8 μm)

Effect of Temperature

Three different temperatures (15°C, 25°C and 37°C) were tested to see the effect of temperature on the adsorption equilibrium. The result of temperature effect is shown in Figure 7.35. The results indicated that the amount of afB1 adsorbed at equilibrium was decreased when the temperature was increased from 15°C to 37°C. This case was more obvious for higher initial afB1 concentrations.

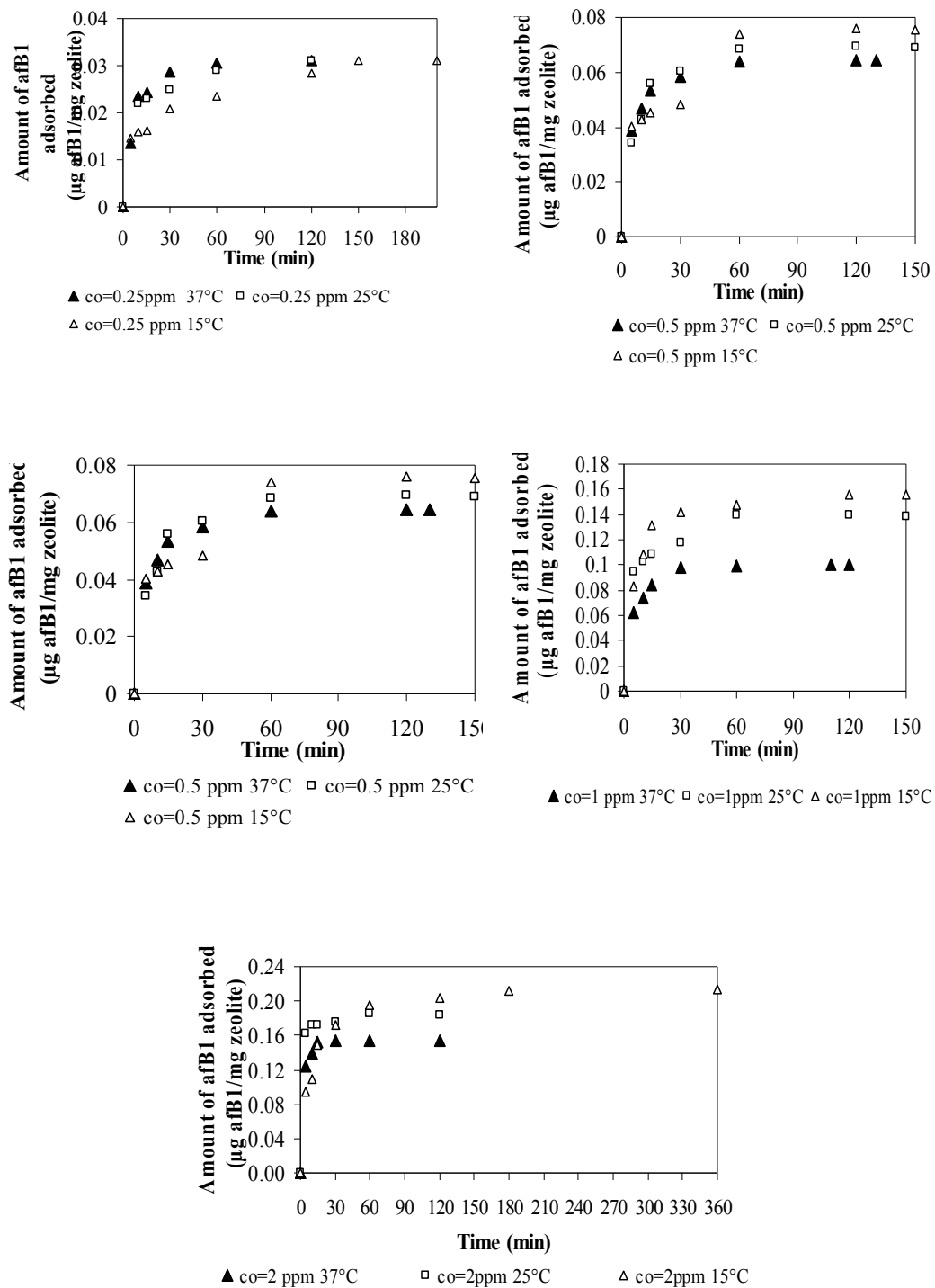


Figure 7.35. Effect of temperature on adsorption kinetics of afB1 by PNZ (T:15°C-37°C, c₀= 0.25 ppm afB1, agitation speed: 130 rpm, S/L:25 mg/10 ml, working solution: PBS pH 7.3, particle size: 8 µm)

7.3.1.3. Thermodynamic Parameters

Thermodynamic parameters such as Gibbs free energy (ΔG°), enthalpy (ΔH°) and entropy (ΔS°) change can be calculated in the following equation:

$$\ln K_{LF} = \frac{\Delta S^\circ}{R} - \frac{\Delta H^\circ}{RT} = -\frac{\Delta G^\circ}{RT} \quad (5.46)$$

where K_{LF} is the Langmuir-Freundlich isotherm parameter. ΔS° is the entropy change, ΔH° is the enthalpy of adsorption and ΔG° is the Gibbs standard free energy change of adsorption. The free energy change, ΔG° (J mol^{-1}) of adsorption is given by:

$$\Delta G^\circ = -RT \ln K \quad (5.45)$$

Langmuir-Freundlich (Sips) isotherm has superiority to represent the adsorption equilibrium therefore K_{LF} was used to determine thermodynamic parameters. In the equation; K is the isotherm constant (mL/mg). In another way, initial linear region (Henry's) was used to determine the isotherm constant. The enthalpy and entropy change are calculated from the slope and intercept of the van't Hoff plot ($\ln K_{LF}$ versus $1/T$) As seen in the Figure 7.36. Slope is $-\Delta H^\circ/R$ and intercept is $\Delta S^\circ/R$. Calculated thermodynamic parameters are given in Table 7.19. The values of ΔG° were negative indicating that the adsorption was feasible and spontaneous in nature. The negative value of entropy (ΔS°) showed the decreased randomness at the solid-liquid interface during the adsorption. The adsorption of compounds to a surface can be categorized as either physisorption or chemisorption on the basis of the enthalpy change of adsorption (ΔH°) and of the change in Gibbs free energy (ΔG°). Physisorption involves weak associations which include van der Waals, dipole-dipole, induced dipole and hydrogen bonding with enthalpy change of < 20 kJ/mol. Chemisorption implies a chemical reaction or sharing of electrons between the adsorbent and the adsorbate with enthalpy change of > 20 kJ/mol (Gu et al., 1994).

It has been reported that ΔG° values up to -20 kJ/mol are consistent with physical sorption while ΔG° values more negative than -40 kJ/mol indicates the chemical sorption (Horsfall et al., 2004).

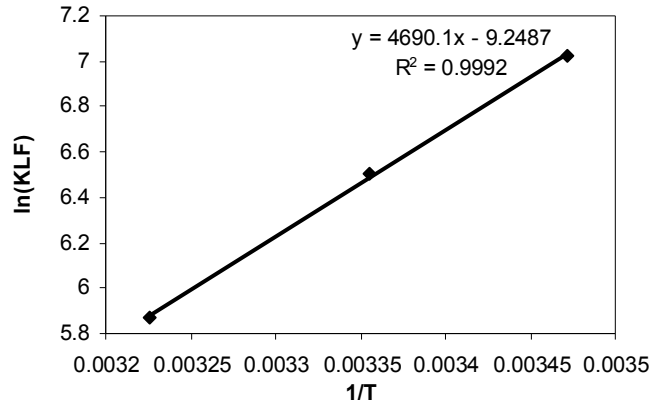


Figure 7.36. Change of the Langmuir-Freundlich (Sips) isotherm parameter (K_{LF}) with the adsorption temperature (T: 15 °C, 25 °C and 37 °C, agitation speed: 130 rpm, S/L:25mg/10 ml, working solution: PBS pH 7.3, particle size: 8 μ m)

Table 7.19. Thermodynamic parameter for afB1 adsorption on PNZ

T [K]	ΔG° (kJ/mol)	ΔH° (kJ/mol)	ΔS° (kJ/molK)	Ea(k ₂) (kJ/mol)	Ea(k _d) (kJ/mol)
288	-16.82	-38.99	-0.08	23.36	26.78.
298	-16.13				
310	-15.13				

The activation energy of afB1 adsorption by PNZ can be calculated by Arrhenius relationship:

$$\ln K = \ln A - \frac{E_a}{RT} \quad (5.47)$$

where K is the rate constant, A the Arrhenius constant which is a temperature independent factor, E_a the activation energy (kJ/mol), R the gas constant (8.314 J/mol K) and T is the temperature in Kelvin (K).

The rate constants for the 2nd order model (k_2) or intraparticle diffusion model (k_d) can be used to estimate the activation energies (Al-Ghouti et al., 2005). The values of activation energy (E_a) were determined and the results are given (Table 7.19). The magnitude of activation energy gives an idea about the type of sorption which is mainly physical or chemical. Low activation energies (5–40 kJ/mol) are characteristics for physical sorption, while higher activation energies (40–800 kJ/mol) are characteristic for chemical sorption. The activation energy values were found as 23.36 and 26.78 kJ/mol.

Consequently, calculated ΔG° , ΔH° and activation energies indicated physical adsorption.

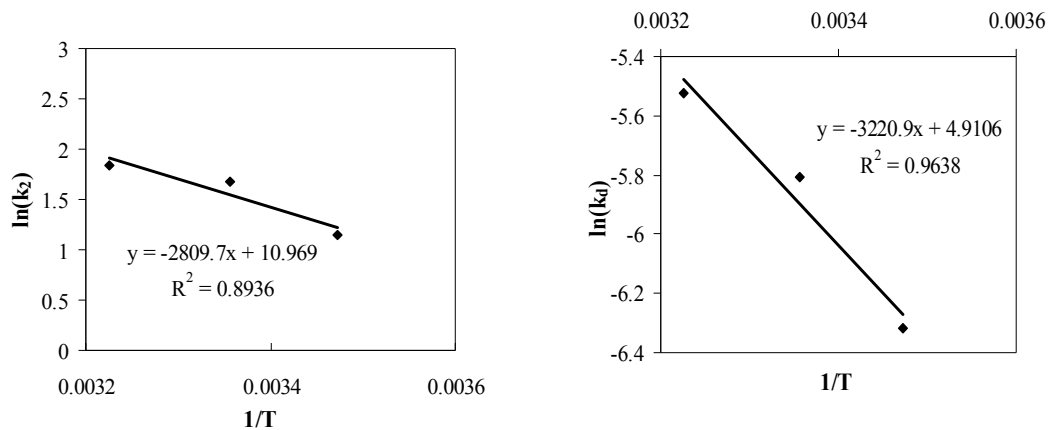


Figure 7.37. Arrhenius plot ($\ln k_2$ vs $1/T$ and $\ln k_d$ vs $1/T$) Experiment conditions: T: 15 °C, 25 °C, 37 °C, $c_i = 0.25$ ppm afB1, agitation speed: 130 rpm, S/L: 25 mg/10 ml, working solution: PBS pH 7.3, particle size: 8 μm .

7.3.1.4. Adsorption Mechanism and Modelling of Kinetic Data

Considering the relatively small dimensions of afB1 molecule (ranging from 5.18 Å to 6.5 Å), afB1 can enter even the micropores of the PNZ and it can be expected that adsorption reaction can take place not only on the external surface. Therefore, experimental adsorption rate data for afB1 adsorption by PNZ were interpreted with diffusional models (external mass transfer models, intra particle diffusion models) as well as reaction kinetic models (pseudo first-order, pseudo second-order kinetic models). For physical adsorption, usually mass action is rapid and can be neglected for

the kinetic study. Generally, the rate of adsorption is limited by external mass transfer for a system with poor mixing, low adsorbate concentration, high affinity to adsorbent and small particles.

In order to decide which step is the rate limiting step, effects of the experimental parameters such as agitation speed, particle size, initial concentration, pH and temperature were discussed. Mathew-Weber diffusion model, Boyd diffusional model and Weber-Morris diffusion model were used in the analysis.

7.3.1.4.1. Analyzing the Adsorption Kinetic Data by Diffusional Models

In all the simplified models which are given below, the assumptions are;

- (a) Isothermal system.
- (b) Perfect mixing.
- (c) Spherical adsorbent particles.
- (d) Diffusion only in radial direction.
- (e) Linear equilibrium relationship.
- (f) Constant diffusivity.

External Fluid Film or Surface Resistance Control

To analyze the external mass transfer, two different model approaches were used (Mathew-Weber model and Boyd Model). Both of these model solutions are based on the solution of main mass transfer rate equation (Equation 5.11). One of the main differences is the definition of specific area. In the Mathew-Weber model, specific area is defined in terms of mass of the sphere whereas in the Boyd model which is the classical solution of rate equation, specific area is defined in terms of volume of the sphere (Mathew and Weber ,1976; Boyd et al,1947)

External fluid film mass transfer control can be analysed by using the solution of classical mass transfer rate equation (Equation 5.11). For dilute solute concentrations, if diffusion within the particle is very rapid or if adsorbent is nonporous, external film mass transfer can be analysed using following equations which are also proposed by

Boyd et al. (1947). External mass transfer coefficient can be calculated using equation given below,

$$\frac{\bar{q}}{q_{\infty}} = 1 - \exp\left[-\frac{3k_f t}{KR_p}\right] \quad (5.14)$$

$$\ln\left(1 - \frac{\bar{q}}{q_{\infty}}\right) = -R' t \quad R' = \frac{3k_f}{R_p K} \quad (5.15)$$

Where R (min^{-1}) is the liquid film diffusion constant. R_p is the particle radius. K is the constant of linear equilibrium ($q=KC$) and k_f is the film mass transfer coefficient. The slope of the $\ln(1-q/q_e)$ versus time diagram is used in determination of external mass coefficient.

If the negligible intraparticle resistance is unrealistic, the analogous situation of external film control situation exists. Mass transfer into the particle can be controlled by skin resistance at the solid surface and leads to mathematically similar with Equation 5.14.

$$\frac{\bar{q}}{q_{\infty}} = 1 - \exp\left[-\frac{3k_s t}{R_p}\right] \quad k_s = \frac{D_s}{\delta} \quad (5.18)$$

Slopes of $\ln\left(1 - \frac{\bar{q}}{q_{\infty}}\right)$ versus time graphs are used to calculate the skin resistance mass transfer coefficients and included in Table 7.20.

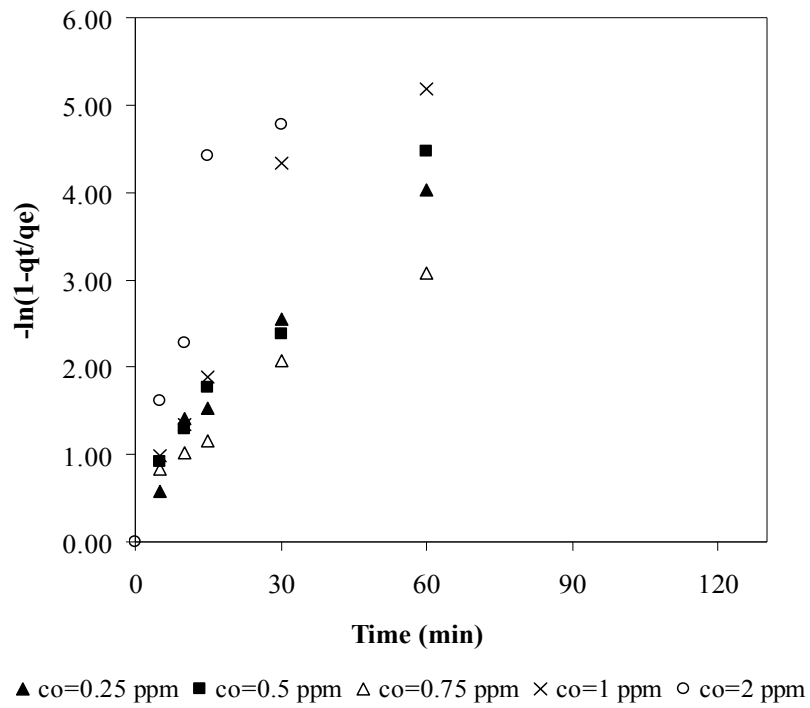
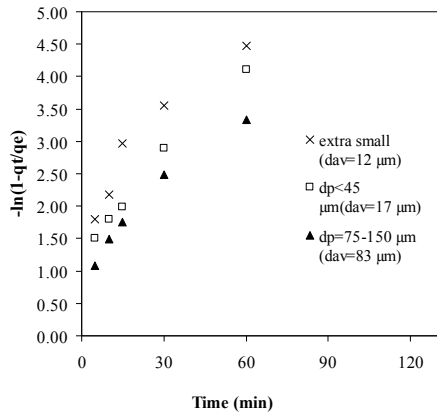


Figure 7.38. Analysing of kinetic data by Boyd model for different initial concentrations (exp conditions : $c_i=0.25-2$ ppm afB1, 25 mg PNZ 10ml of the PBS pH 7.3 (S/L=1/400), 130 rpm, 37 °C, particle size 8 μ m)

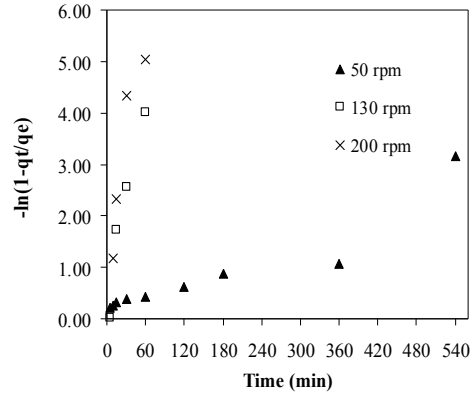
Table 7.20. Analysing the External Film Mass Transfer and Skin resistance

Temperature (T)		Slope, R'(min ⁻¹)	k _s (m/s)*10 ⁷	k _f (m/s)*10 ⁷	R ²	SSE
ci=0.25ppm afB1 m=25 mg v= 10ml (PBS pH 7.3) A.S.=130 rpm. P.S.=8µm	T1(15 °C)	0.0192	0.004	0.661	0.96	0.088
	T2(25 °C)	0.0543	0.012	1.870	0.97	0.032
	T3(37 °C)	0.0587	0.013	2.022	0.97	0.199
Particle size (P.S.)		Slope, R'(min ⁻¹)	k _s (m/s)*10 ⁷	k _f (m/s)*10 ⁷	R ²	SSE
ci=0.25ppm afB1 m=25 mg v= 10ml (PBS pH 7.3) A.S.=130 rpm. T=37 °C	P.S1 (extra small)	0.0462	0.010	1.591	0.91	0.401
	P.S2 (small)	0.0474	0.011	1.633	0.99	0.0327
	P.S2 (big)	0.0394	0.009	1.357	0.97	0.1038
Agitation speed (A.S.)		Slope, R'(min ⁻¹)	k _s (m/s)*10 ⁷	k _f (m/s)*10 ⁷	R ²	SSE
ci=0.25ppm afB1 m=25 mg v= 10ml (PBS pH 7.3) P.S.=8µm T=37 °C	AS1(50 rpm)	0.0046	0.001	0.158	0.87	0.451
	AS2 (130 rpm)	0.0587	0.013	2.022	0.97	0.199
	AS3(200 rpm)	0.0774	0.017	2.666	0.86	1.967
pH		Slope, R'(min ⁻¹)	k _s (m/s)*10 ⁷	k _f (m/s)*10 ⁷	R ²	SSE
ci=0.25ppm afB1 m=25 mg A.S.=130 rpm. P.S.=8µm T=37 °C	pH 3.0.	0.0342	0.008	1.178	0.96	0.037
	pH 5.0	0.0402	0.009	1.385	0.94	0.214
	pH7.3	0.0587	0.013	2.022	0.97	0.199
Initial Concentration (c ₀)		Slope, R'(min ⁻¹)	k _s (m/s)*10 ⁷	k _f (m/s)*10 ⁷	R ²	SSE
m=25 mg v= 10ml (PBS pH 7.3) A.S.=130 rpm. P.S.=8µm	0.25	0.0587	0.013	2.022	0.97	0.199
	0.5	0.0627	0.014	2.160	0.99	0.058
	0.75	0.0638	0.014	2.198	0.99	0.165
	1	0.0767	0.017	2.642	0.86	1.646
	2	0.0854	0.019	2.942	0.85	2.453

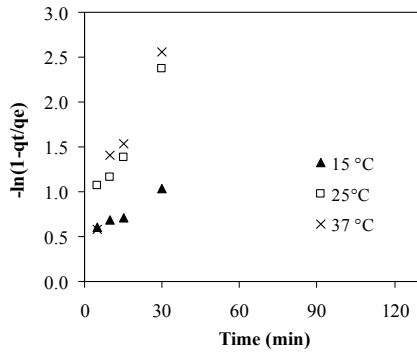
If film diffusion or surface skin resistance is controlling the adsorption processes. $\ln\left(1 - \frac{\bar{q}}{q_{\infty}}\right)$ vs time should result in straight lines that pass through origin (Boyd et al., 1947; Ruthven, 1984). Therefore, the effectiveness of the external mass transfer or surface skin mass transfer can be evaluated by comparing external mass transfer coefficients and analyzing the $\ln(1-q/q_e)$ versus time profile for different experimental parameters. Figure 7.38 and 7.39 demonstrate the effect of different experimental parameters on external mass transfer plot of Boyd model. As it seen from all figures, deviations from expected straight lines indicate that external mass transfer is not rate limiting and intra particle diffusion should also be considered. Additionally, expected straight lines do not pass through the origin. This also indicates that film diffusion is not the limiting step of the overall adsorption process. As it seen from Figure 7.38, logarithmic data are found be more deviated from expected straight lines at higher concentrations and linearity is decreased in higher concentrations as seen from R^2 values in the Table 7.21.



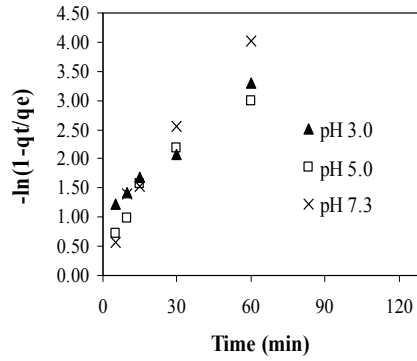
(a) $c_i=0.25$ mg PNZ 10ml of the PBS pH 7.3 (S/L=1/400), 130 rpm, 37 °C



(b) $c_i=0.25$ ppm, 25 mg PNZ 10ml of the PBS pH 7.3 (S/L=1/400), 37 °C, particle size 8 μ m



(c) $c_i=0.25$ ppm, 25 mg PNZ 10ml of the PBS pH 7.3 (S/L=1/400), 130 rpm, particle size 8 μ m



(d) $c_i=0.25-1$ ppm, 25 mg PNZ 10ml of the PBS, (S/L=1/400), 130 rpm, 37 °C, particle size 8 μ m

Figure 7.39. Analysing of kinetic data by Boyd model for different experimental parameters (a) Particle size (b) agitation speed (c) temperature and (d) pH

External Mass Transfer Coefficient (k_f) was also determined by Mathew-Weber Model (Mathew and Weber, 1976) and the model equations are given below (Equation 5.20). One of the assumptions of this model is that only external film diffusion was dominant during the initial sorption period and controlled the sorption rate and surface concentration is negligible.

$$\ln \frac{C_t}{C_0} = -k_f St \quad (5.20)$$

The surface area for mass transfer is defined as:

$$S = \frac{6m/V}{d_p \rho_p (1 - \varepsilon_p)} \quad (5.21)$$

where m is the mass of adsorbent, V is the volume of solution, d_p is the particle diameter, ρ_p is particle density and ε_p is particle porosity.

From the slope of the linear part of the $\ln C_t/C_0$ versus t diagram (first 15 min), the external mass transfer coefficients (k_f) were calculated. Representative diagram for calculation is given (Figure 7.40).

For the same amount of the adsorbent, higher concentration decay rate is observed for the lower initial aflB1 concentration as seen in Figure 7.40.

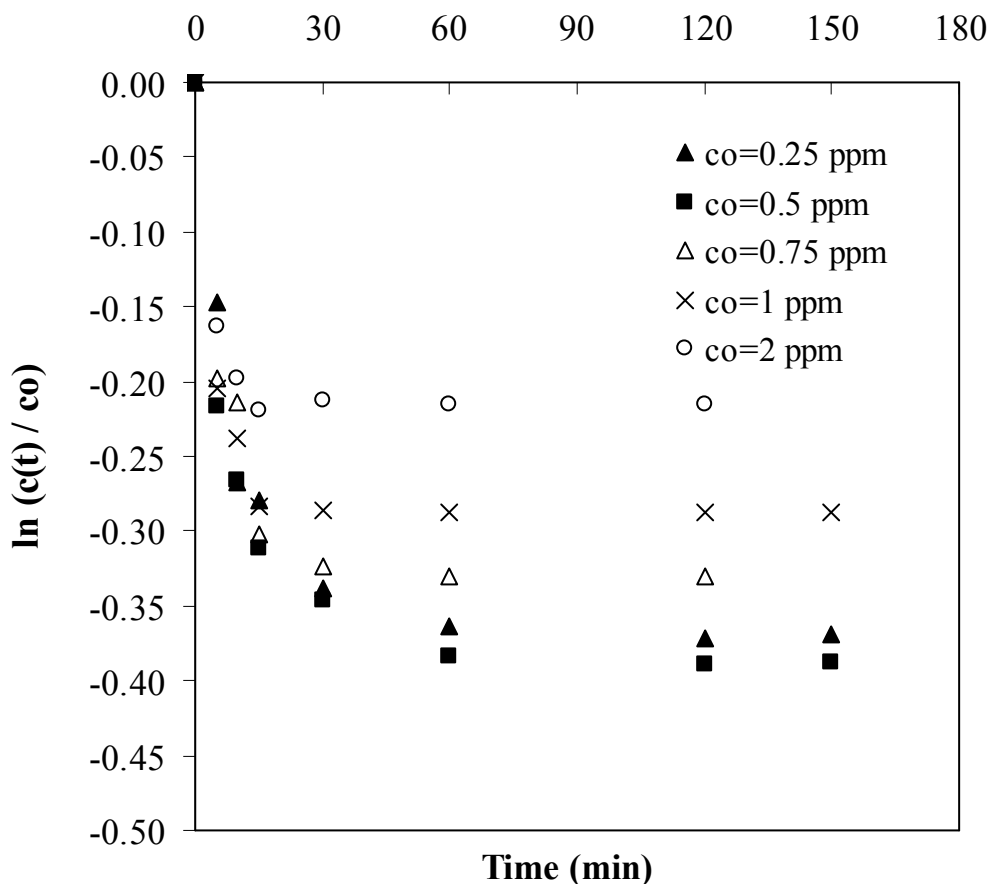
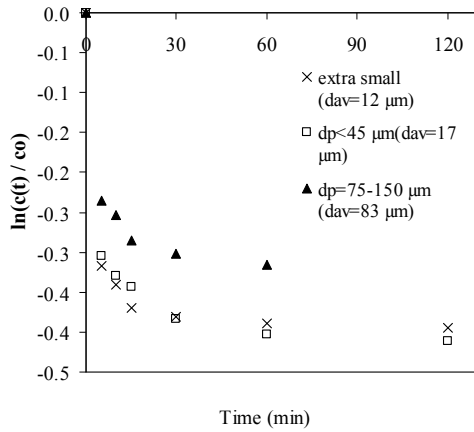
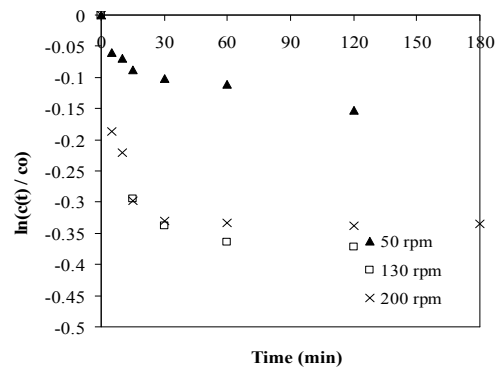


Figure 7.40. Mathew Weber Plot for different afB1 initial concentrations (exp conditions : $c_i=0.25-2$ ppm afB1 ,25 mg PNZ 10ml of the PBS pH 7.3 (S/L=1/400, 130 rpm, 37 °C, particle size 8 μ m)

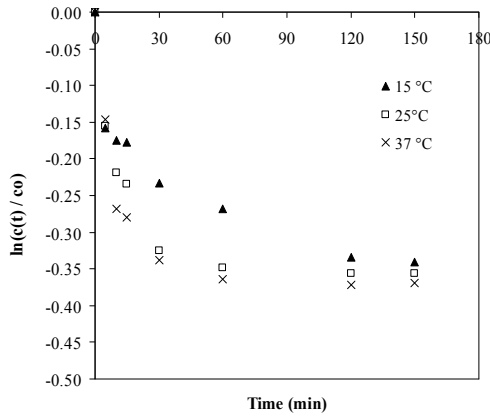
When the effect of other parameters on Mathew Weber plot is examined, it is seen that the extra small ($d_{av}=12\mu$ m) and small particles ($d_{av}=17\mu$ m) indicates similar profile and they show higher concentration decay than the big particles ($d_{av}=83\mu$ m). As seen from the concentration decay curve for the different agitation speeds (Figure 7.41), although for the 130 and 200 rpm, the curves almost coincide and reach equilibrium in 120 minutes, for 50 rpm equilibrium could not be attained even in 120 min. Lower concentration decay data are observed for lower temperatures. Decrease in pH resulted in higher concentration decay data



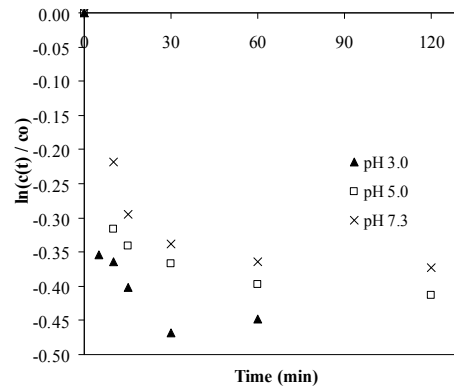
(a) $c_i=0.25$, 25 mg PNZ 10ml of the PBS pH 7.3 (S/L=1/400), 130 rpm, 37 °C



(b) $c_i=0.25$ ppm, 25 mg PNZ 10ml of the PBS pH 7.3, (S/L=1/400), 37 °C, particle size 8 μm



(c) $c_i=0.25$ ppm, 25 mg PNZ 10ml of the PBS pH 7.3 (S/L=1/400), 130 rpm, particle size 8 μm



(d) $c_i=0.25-1$ ppm, 25 mg PNZ, 10ml of the PBS (S/L=1/400), 130 rpm, 37 °C, particle size 8 μm.

Figure 7.41. Mathew weber plot for different experimental parameters (a) Particle size. (b) agitation speed. (c) temperature and (d) pH

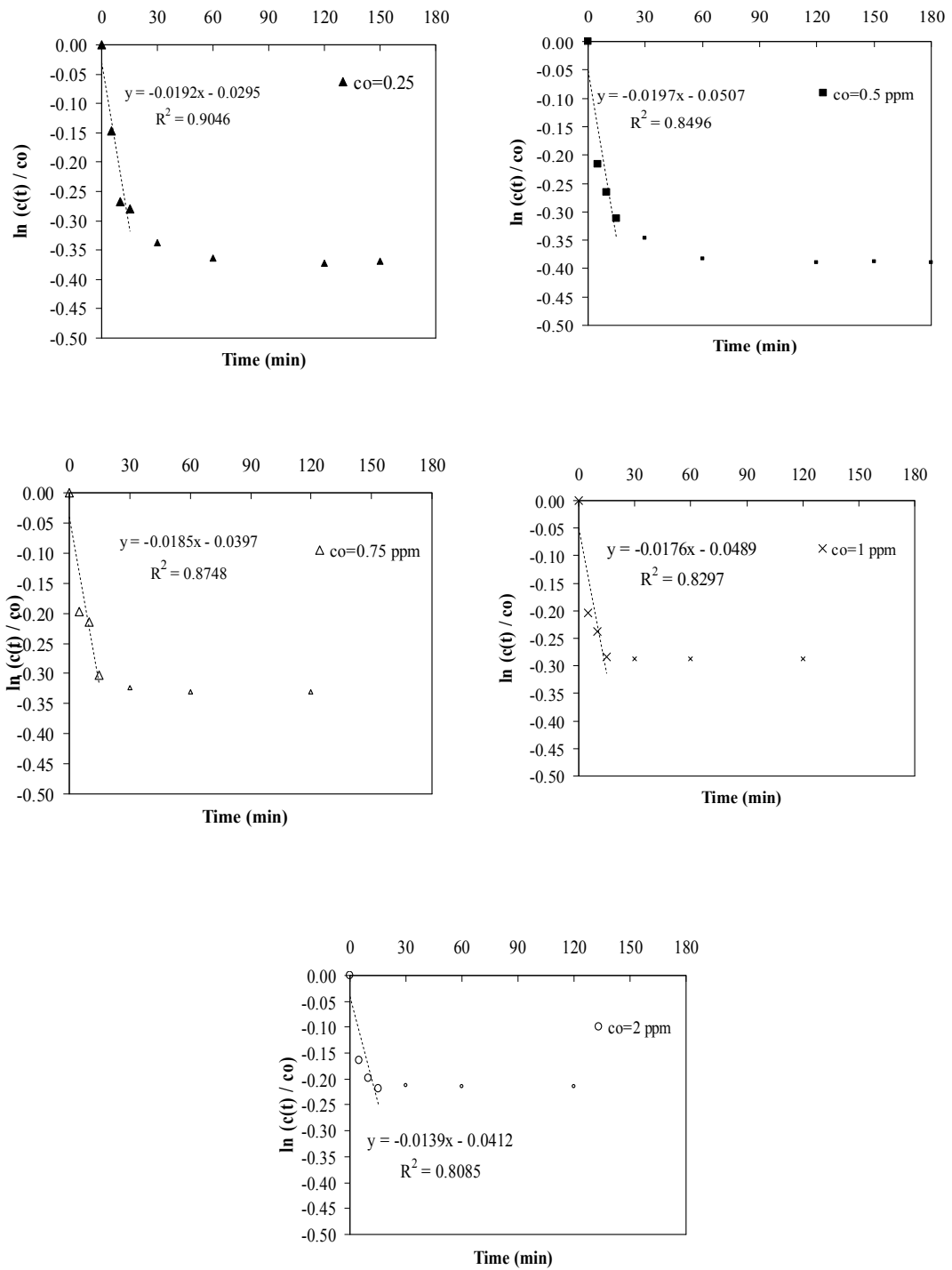


Figure 7.42. Analyzing external mass transfer coefficient by Mathew-Weber plot for different initial afB1 concentrations ($c_i=0.25-2$ ppm, 25 mg PNZ 10ml of the PBS pH 7.3, (S/L=1/400), 130 rpm, 37 °C, particle size 8 μ m)

External mass transfer coefficient throughout the study was determined using the Equation 5.20 and tabulated for all the experimental conditions (Table 7.21). The results indicated that the change in external mass transfer coefficient is irregular with increasing temperature and initial afB1 concentrations. Similar behaviour was reported by several investigators for different adsorbent adsorbate pairs (Chang et al., 2006; Sağ and Aktay, 2006). The results indicated that the external mass transfer coefficient increased with increasing agitation speed whereas decreased with decreasing particle size. The effect of particle size can be explained in terms of momentum, since under well agitated conditions larger particles have a higher momentum and therefore thinner boundary layers occur. Similar results were also reported by Sağ and Aktay (2000), Quada et al. (2007), El-Gouti et al. (2009), El Quada et al. (2007). Increasing agitation speed caused to decrease in the thickness of the boundary layer resistance surrounding the particle and thus external mass transfer resistance decreased with increasing agitation speed. After critical agitation speed, no significant effect on external mass transfer resistance was observed.

Table 7.21. Analyzing the External Film Mass Transfer by Mathew-Weber Model.

Temperature (T)		Slope($-k_f S$)	$k_f(\text{m/s}) \times 10^7$	R^2	SSE
ci=0.25pp m afB1 m=25 mg v= 10ml (PBS pH 7.3) A.S.=130 rpm. P.S.=8μm	T1(15 °C)	-0.015	2.165	0.83	0.014
	T2(25 °C)	-0.0153	1.893	0.85	0.016
	T3(37 °C)	-0.019	2.351	0.91	0.004
Particle size(P.S.)		Slope($-k_f S$)	$k_f(\text{m/s}) \times 10^7$	R^2	SSE
ci=0.25pp m afB1 m=25 mg v= 10ml (PBS pH 7.3) A.S.=130 rpm. T=37 °C	P.S1 (extra small. 12 μ m)	-0.023	4.268	0.72	0.017
	P.S2 (small. 17 μ m)	-0.021	5.521	0.73	0.016
	P.S3 (big.83 μ m)	-0.017	21.822	0.75	0.009
Agitation speed(A.S.)		Slope($-k_f S$)	$k_f(\text{m/s}) \times 10^7$	R^2	SSE
ci=0.25pp m afB1 m=25 mg v= 10ml (PBS pH 7.3) P.S.=8μm T=37 °C	AS1(50 rpm)	-0.006	0.742	0.97	0.00015
	AS2(130 rpm)	-0.019	2.351	0.91	0.004
	AS3(200 rpm)	-0.018	2.227	0.98	0.00012
pH		Slope($-k_f S$)	$k_f(\text{m/s}) \times 10^7$	R^2	SSE
ci=0.25pp m afB1 m=25 mg A.S.=130 rpm. P.S.=8μm T=37 °C	pH 3.0.	-0.023	2.846	0.76	0.015
	pH 5.0	-0.0231	2.858	0.91	0.005
	pH7.3	-0.019	2.351	0.91	0.004
Initial Concentration(c_0)		Slope($-k_f S$)	$k_f(\text{m/s}) \times 10^7$	R^2	SSE
m=25 mg v= 10ml (PBS pH 7.3) A.S.=130 rpm. P.S.=8μm	0.25	-0.019	2.351	0.91	0.004
	0.5	-0.02	2.474	0.85	0.018
	0.75	-0.018	2.227	0.88	0.005
	1	-0.018	2.227	0.83	0.006
	2	-0.014	1.732	0.81	0.010

Intraparticle Diffusion Control

Due to the porosity of range adsorbent and dimensions of the afB1 molecule intraparticle diffusion even in the micropores in the crystals was expected. Diffusion in the pores were analysed by using Weber Morris model and Boyd pore diffusion solution model. Both of the solutions are based on the solution of diffusion in the adsorbent particle (Equation 5.31 and 5.42). Weber Morris model equation is;

$$q_t = k_d t^{1/2} \quad (5.42)$$

This model assumed that external mass transfer resistance in the aqueous solution is negligible, the direction of diffusion was radial and the concentration did not change with angular position and the intraparticle diffusivity was constant. (Weber and Morris, 1963). Considering the intraparticle mass transfer, fractional uptake versus square roots of time curves were analysed and intra particle rate constants (k_d) were calculated (Figure 7.43, Figure 7.44 and 7.45). It is known that intercepts of Weber Morris plot diagrams can be related to external mass transfer resistance or surface skin resistance. Segmentation of plot is recommended to interpret the results. Recent critics (El-Khaiary and Malash, 2011) indicated that there are several incorrect applications of Weber Morris model. They suggested Piecewise linear regression segmentation of the Weber Morris plot and also suggested that linear regressions should not include the equilibrium points

In the Figure 7.43 intra particle diffusion plot for different initial concentrations were presented. When the data were analysed as whole, linear regression lines do not pass through origin and results in increasing intercepts by increasing initial concentrations. On the other hand, segmented intra particle plot (Figure 7.45) results in smaller intercept values.

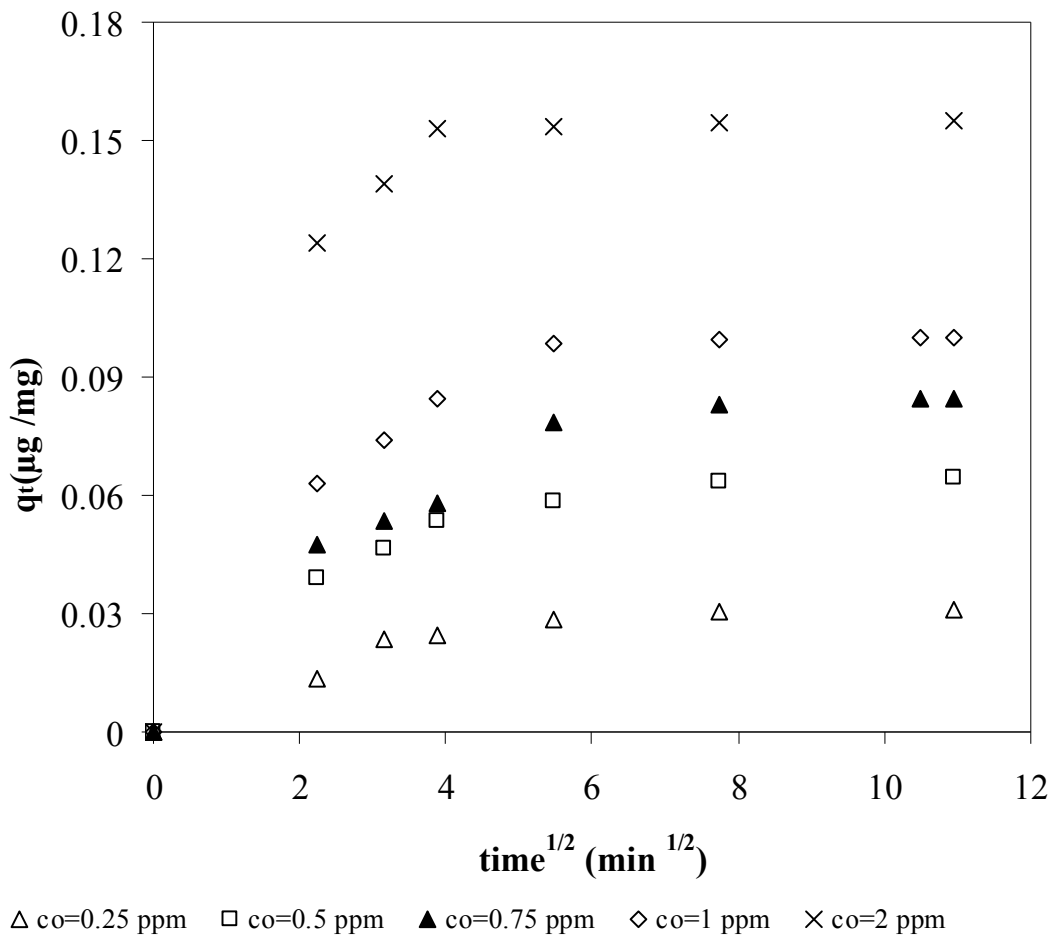
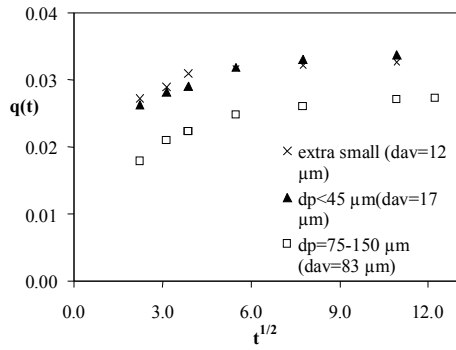
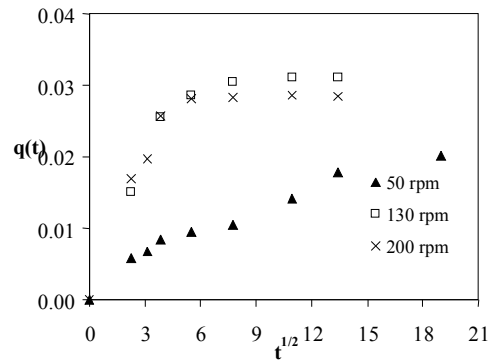


Figure 7.43. Weber Morris Plot for different initial concentrations (exp conditions : $c_0=0.25-1$ ppm afB1 ,25 mg PNZ, 10ml of the PBS pH 7.3, (S/L=1/400),130 rpm,37 °C)

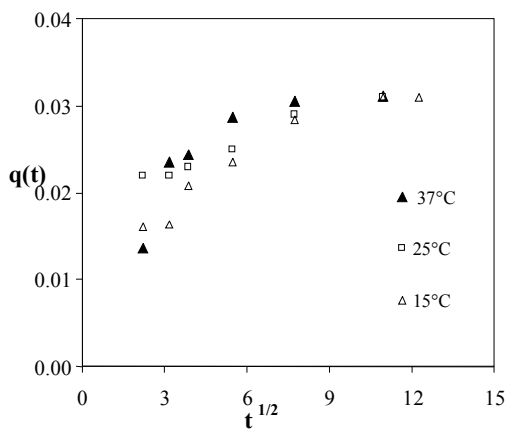
As seen Figure 7.43 above, expected linear portions can be attributed to intraparticle diffusion and final plateau can be considered as equilibrium.. In the Weber Morris model,, solution of mass transfer in the adsorbent particle (Equation 5.39 and 5.40) is more convenient for short times therefore it was suggested that initial region of uptake curve should be used for the analysis and calculation of intraparticle diffusion constants (k_d).



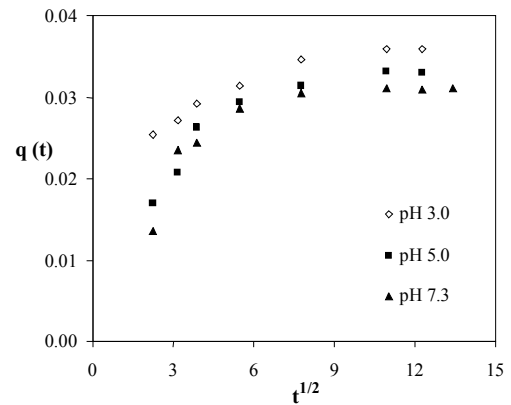
(a) $c_i=0.25, 25$ mg PNZ 10ml of the PBS
pH 7.3 (S/L=1/400), 130 rpm, 37 °C)



(b) $c_i=0.25$ ppm, 25 mg PNZ 10ml of the PBS
pH 7.3 (S/L=1/400), 37 °C. particle size 8 μm)



(c) $c_i=0.25$ ppm, 25 mg PNZ 10ml of the PBS
pH 7.3 (S/L=1/400), 130 rpm, particle size
8 μm



(d) $c_i=0.25-1$ ppm, 25 mg PNZ 10ml of the PBS
(S/L=1/400), 130 rpm, 37 °C, particle size 8 μm

Figure 7.44. Weber Morris plot for different experimental parameters a) Particle size
b) agitation speed c) temperature and d) pH

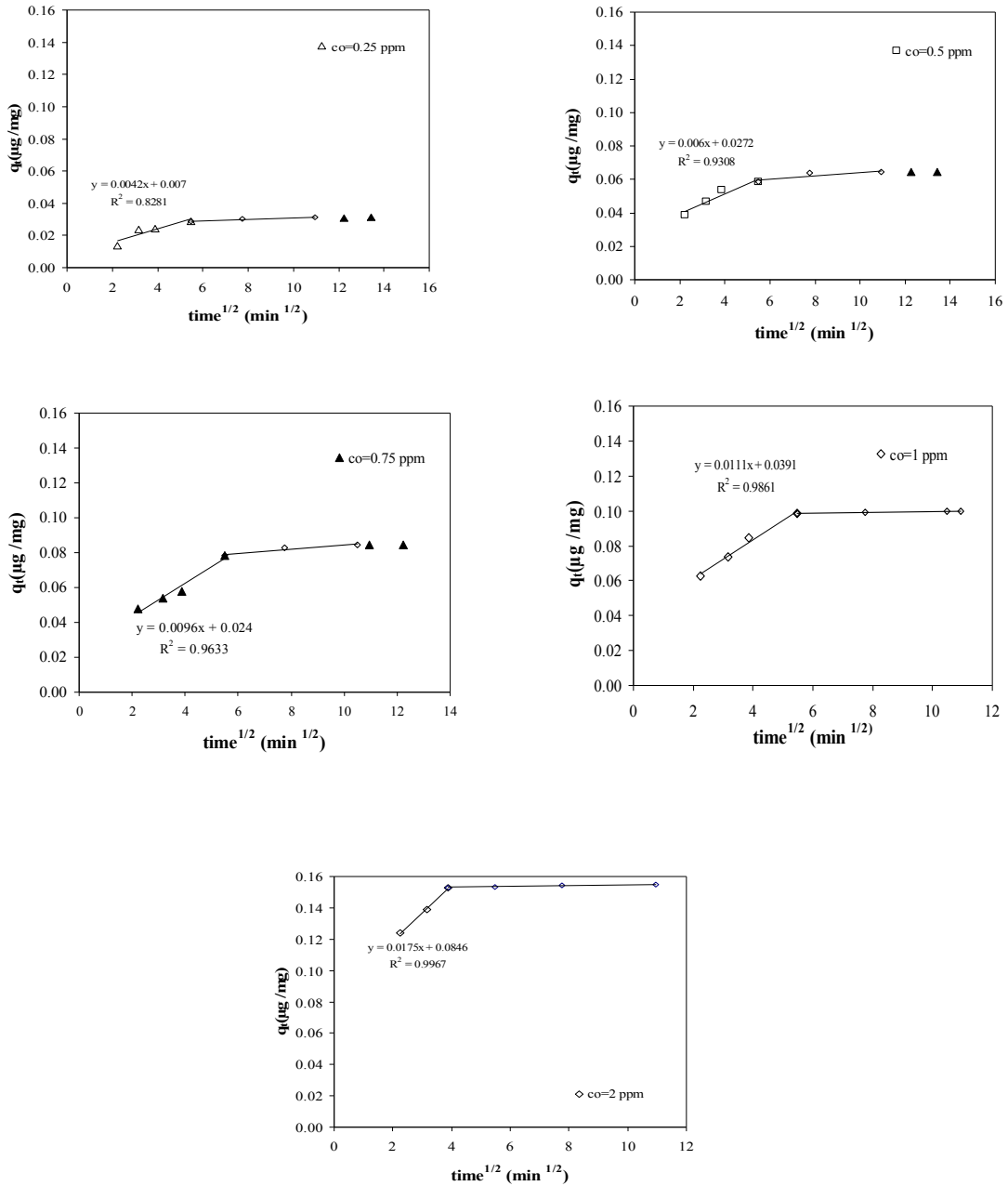


Figure 7.45. Analyzing diffusion constant by Weber Morris plot for different initial afB1 (exp conditions : ci=0.25-1 ppm ,25 mg PNZ 10ml of the PBS pH 7.3 (S/L=1/400), 130 rpm,37 °C)

Table 7.22. Analysing the kinetic data by Weber-Morris Model

Temperature(T)		$k_{d1}(\mu\text{g}/\text{mg min}^{0.5})$	$kd_2(\mu\text{g}/\text{mg min}^{0.5})$	R^2	SSE
ci=0.25ppm afB1 m=25 mg v= 10ml (PBS pH 7.3) A.S.=130 rpm. P.S.=8μm	T1(15 °C)	0.002	0.0003	0.97	0.000013
	T2(25 °C)	0.003	0.0003	0.95	0.000014
	T3(37 °C)	0.004	0.00023	0.83	0.000021
Particle size(P.S)		$k_{d1}(\mu\text{g}/\text{mg min}^{0.5})$	$kd_2(\mu\text{g}/\text{mg min}^{0.5})$	R^2	SSE
ci=0.25ppm afB1 m=25 mg v= 10ml (PBS pH 7.3) A.S.=130 rpm. T=37 °C	P.S1(extra small)	0.0014	0.0001	0.88	0.000001
	P.S3(small)	0.0017	0.0003	1.00	0.000000
	P.S3(big)	0.0027	0.0009	0.95	0.000004
Agitation speed(A.S.)		$k_{d1}(\mu\text{g}/\text{mg min}^{0.5})$	$kd_2(\mu\text{g}/\text{mg min}^{0.5})$	R^2	SSE
ci=0.25ppm afB1 m=25 mg v= 10ml (PBS pH 7.3) P.S.=8μm T=37 °C	AS1(50 rpm)	0.0021	0.00003	0.91	0.00013
	AS2(130 rpm)	0.004	0.00023	0.83	0.000021
	AS3(200 rpm)	0.0045	0.00023	0.87	0.00017
pH		$k_{d1}(\mu\text{g}/\text{mg min}^{0.5})$	$kd_2(\mu\text{g}/\text{mg min}^{0.5})$	R^2	SSE
ci=0.25ppm afB1 m=25 mg A.S.=130 rpm. P.S.=8μm T=37 °C	pH 3.0.	0.00038	0.00023	0.91	0.00013
	pH 5.0	0.0022	0.00022	0.89	0.00015
	pH7.3	0.004	0.00023	0.83	0.000021
Initial Concentration (c_0)		$k_{d1}(\mu\text{g}/\text{mg min}^{0.5})$	$kd_2(\mu\text{g}/\text{mg min}^{0.5})$	R^2	SSE
m=25 mg v= 10ml (PBS pH 7.3) A.S.=130 rpm. P.S.=8μm	0.25	0.004	0.00023	0.83	0.000021
	0.5	0.006	0.0011	0.93	0.000015
	0.75	0.010	0.0021	0.96	0.000020
	1	0.011	0.0003	0.99	0.000010
	2	0.018	0.0003	1.00	0.000001

When the Table 7.22 is examined, it is noticed that intra particle diffusion rate constant (k_d) increases slightly with increasing agitation speed, temperature and particle size. After the critic agitation speed, there is no significant effect of agitation speed on intra particle diffusion parameter.

It is known that when the particle size increased, time and pathway required to diffuse interior parts of the zeolite would also be increased. Therefore, it leads higher intraparticle diffusion resistance thus k_d values can be lower. Ho and Mckay (1998); Sağ and Aktay (2000); Sze and McKay (2010) were also reported similar results. The effect of particle size on intraparticle model coefficient can be used for the analyzing predominant rate limiting step (Al Ghouti et al., 2009; Poots and Mckay, 1976) and Figure 7.46 given below shows there is a linear relationship between intra particle rate constant and square root of the particle diameter therefore intra particle diffusion might be predominant rate controlling for afB1 adsorption by PNZ. Changing the pH shows no significant effect again. In the case of initial concentration increasing the initial concentration leads tendency to increase coefficient. Actually, increase of afB1 concentration results in increase in the diffusion rate due to the higher driving forces of diffusion. This behaviour was also reported by several investigators for different adsorbent adsorbate pairs (Walker et al., 2003; Chu et al., 2004; Allen et al., 2005; Quada et al., 2007)

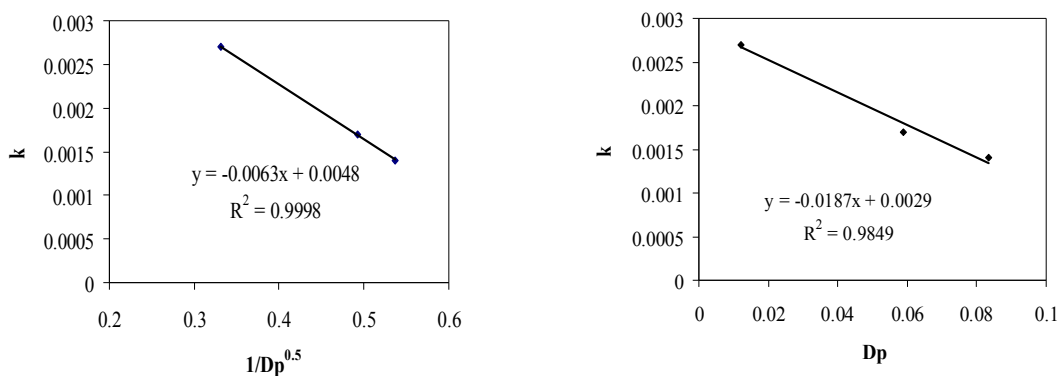


Figure 7.46. Relationship of intra particle rate constant with square root of particle diameter.

Diffusion in the pores was further analysed by kinetic expression given by Boyd et al. (1947). Diffusion in adsorbent particle was solved by using solution of diffusion equation which is based on the solution of Fick's law made by Barrer (1941). By using

this approach, it can be possible to identify whether film diffusion or intraparticle diffusion controls the rate of adsorption process.

$$F(t) = \frac{q_t}{q_\infty} = 1 - \frac{6}{\pi^2} \sum_{n=1}^{\infty} \frac{1}{n^2} \exp(-n^2 Bt) \quad (5.31)$$

$$B = \frac{\pi^2 D_i}{r^2} \quad (5.32)$$

Where D_i is the effective diffusion coefficient (m^2/s) and Bt values can be obtained for each observed value of F , using Reichenberg's table .(Reichenberg, 1952) If the plot of Bt versus t is a straight line passing through the origin, then the rate-limiting step in the adsorption process is the intra-particle diffusion and vice versa.

When kinetic data analysed by using single formula (Equation 5.34) which is valid for $F > 0.85$ to calculate the Bt values, the lines do not pass through the origin (Figure 7.47), and this application causes some incorrect analyses. As seen from the figure given below, F values for the first two experimental data are below 0.85 and it is recommended to use Equation 5.33 or use Reichenberg table for whole data. In several studies, the results were concluded that intra particle is not rate limiting and external mass transfer was found to be rate limiting by using this incorrect calculation and only this differentiation. (Nghah and Hanfiah, 2008; El Kad et al., 2011). The recent article criticizes this incorrect application of Boyd Model by showing the original article of Boyd et al. (1947). Therefore, the analysis are made by considering this critic in this work. The effective diffusion coefficient D_i (m^2/s) can be calculated by the obtained B values and the radius of the adsorbent particle r (m) using the equation 5.32.

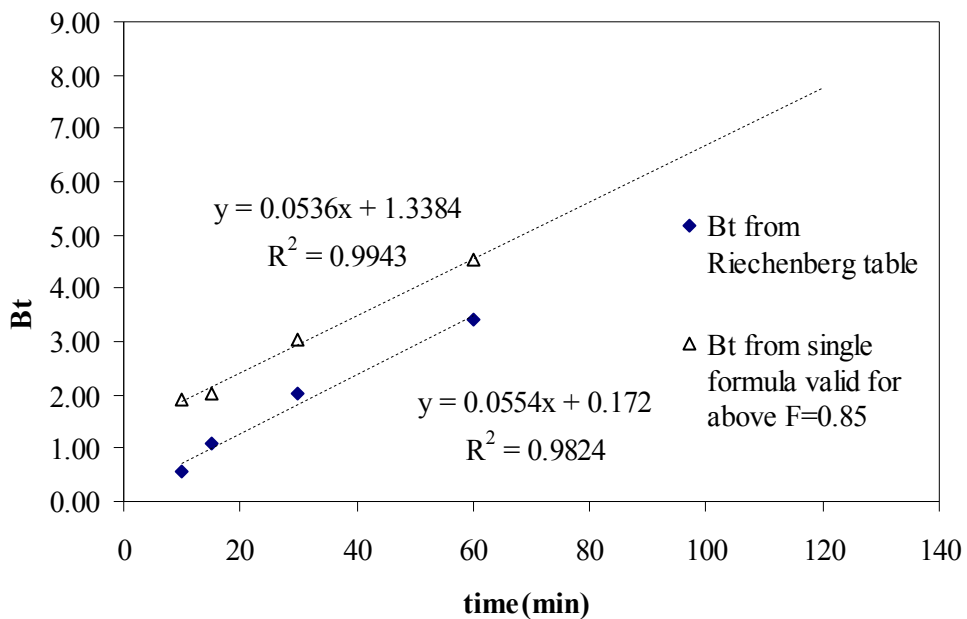


Figure. 7.47. Representative comparison of Boyd (exp conditions : $c_i=0.25$ ppm afB1, 25 mg PNZ 10ml of the PBS pH 7.3 (S/L=1/400), 130 rpm, 37 °C, particle size $8\mu m$)

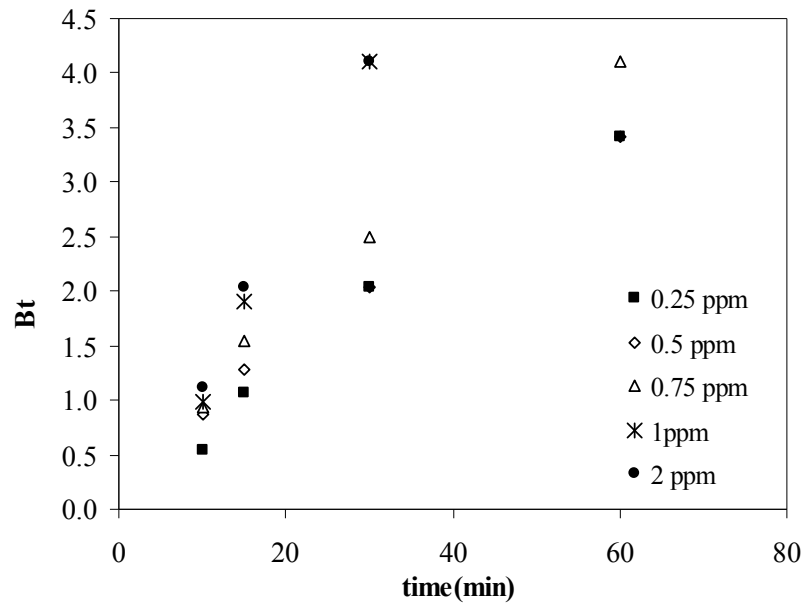
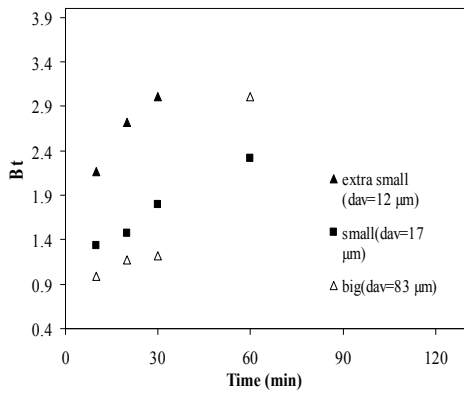


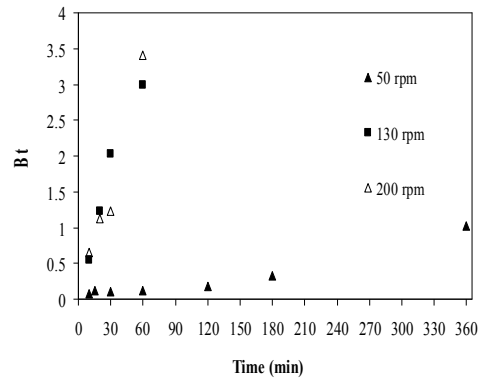
Figure 7.48. Boyd plot for different initial afB1 concentrations (exp conditions : $c_i=0.25-2$ ppm afB1 ,25 mg PNZ, 10ml of the PBS pH 7.3 (S/L=1/400),130 rpm,37 °C, particle size 8 μ m)

The plots of Bt versus time (t) at different afB1 concentrations are shown in Fig.7.48 and the values of B can be obtained from the slopes of the plots. It is observed that expected straight lines do not pass through the origin and pore diffusion is not likely to be rate limiting alone. The intercepts and deviations from expected linear curves show that external mass transfer or surface resistance is also effective on overall adsorption process kinetics.

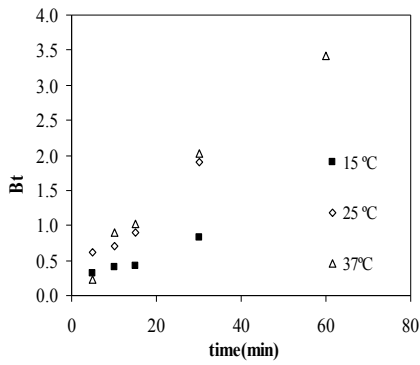
Agitation speeds of 130 and 200 rpm experiments result in similar Boyd profile; on the other hand, 50 rpm results in lower Bt values. Higher Bt values are observed in higher temperatures and increase in temperature results in increase in diffusivities.



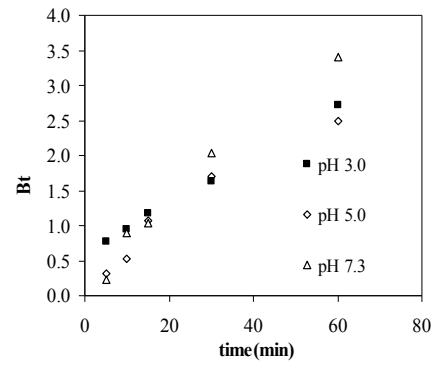
(a) $c_i=0.25, 25$ mg PNZ 10ml of the PBS pH 7.3 (S/L=1/400), 130 rpm, 37 °C



(b) $c_i=0.25$ ppm, 25 mg PNZ 10ml of the PBS pH 7.3 (S/L=1/400), 50, 130 and 200 rpm, 37 °C, particle size $8 \mu m$



(c) $c_i=0.25$ ppm, 25 mg PNZ 10ml of the PBS pH 7.3 (S/L=1/400), 130 rpm, 15, 25, 37 °C, particle size $8 \mu m$



(d) $c_i=0.25-1$ ppm, 25 mg PNZ 10ml of the PBS pH 3.0-5.0 and 7.4 (S/L=1/400), 130 rpm, 37 °C, particle size $8 \mu m$

Figure 7.49. Boyd plot for different experimental parameters a) Particle size b) agitation speed c) temperature and d) pH)

Table 7.23. Analysing the kinetic data by Boyd Model

Temperature		Slope	$D \times 10^{15}(\text{m}^2/\text{s})$	R^2	SSE	Bi
ci=0.25ppm afB1 m=25 mg v= 10ml (PBS pH 7.3) A.S.=130 rpm. P.S.=8μm	T1(15 °C)	0.0358	3.952	0.91	0.00013	954
	T2(25 °C)	0.0456	4.99	0.95	0.00014	737
	T3(37 °C)	0.0554	5.99	0.98	0.00011	591
Particle size		Slope	$D \times 10^{15}(\text{m}^2/\text{s})$	R^2	SSE	
ci=0.25ppm afB1 m=25 mg v= 10ml (PBS pH 7.3) A.S.=130 rpm. T=37 °C	P.S 1(extra small)	0.455	3.899	0.95	0.00014	792
	P.S3(small)	0.421	5.475	0.96	0.00015	774
	P.S3(big)	0.453	10.524	0.95	0.00014	605
Agitation speed		Slope	$D \times 10^{15}(\text{m}^2/\text{s})$	R^2	SSE	
ci=0.25ppm afB1 m=25 mg v= 10ml (PBS pH 7.3) P.S.=8μm T=37 °C	AS1(50 rpm)	0.0048	0.227	0.95	0.00014	89
	AS2(130 rpm)	0.0554	5.99	0.98	0.00011	591
	AS3(200 rpm)	0.0558	6.031	0.96	0.00015	658
pH		Slope	$D \times 10^{15}(\text{m}^2/\text{s})$	R^2	SSE	
ci=0.25ppm afB1 m=25 mg A.S.=130 rpm. P.S.=8μm T=37 °C	pH 3.0.	0.0591	6.02	0.96	0.00015	585
	pH 5.0	0.0575	6.01	0.95	0.00014	473
	pH7.3	0.0554	5.99	0.98	0.00011	591
Initial Concentration		Slope	$D \times 10^{15}(\text{m}^2/\text{s})$	R^2	SSE	
m=25 mg v= 10ml (PBS pH 7.3) A.S.=130 rpm. P.S.=8μm	0.25	0.0554	1.50	0.98	0.00011	591
	0.5	0.0495	1.34	0.99	0.00009	690
	0.75	0.061	1.65	0.99	0.00009	543
	1	0.147	3.97	0.99	0.00009	559
	2	0.154	4.16	0.99	0.00009	543

The Biot number (Bi) of the system is defined as $Bi = k_f r / D_{eff}$. Biot number is an important parameter to quantify the film diffusion contribution in the total mass transfer mechanism. Biot number represents the ratio of the rate of transport across the liquid

layer to the rate of diffusion into the the particle. For $Bi \ll 1$, the adsorption rate is external mass transfer resistance controlled. While for $Bi \gg 100$, particle diffusion is the predominant mass transfer controlling mechanism.

$Bi \gg 100$ this indicates the particle diffusion is the predominant mechanism. Calculated Biot numbers are presented in Table 7.23 for different experimental parameters and Biot number is below 100 for only 50 rpm agitation speed .

As it seen experimental data can be represented by both intraparticle model and external film or surface skin mass transfer model except 50 rpm. This indicates existence of surface resistance rather than external film resistance for 130-200 rpm which are actually represented by similar relationships (Equation 5.14 and Equation 5.18) and Henry's law region skin resistance coefficient can be expressed given below;

$$k_s = \frac{k_f}{K} \quad (7.1)$$

In the result of analyzing diffusional models, it was found that both film diffusion and intra particle diffusion is effective on adsorption depending on the experimental conditions. The afB1 adsorption by PNZ was very rapid process and it is difficult to identify the stages that external mass transfer is rate limiting alone.

7.3.1.4.2. Analyzing the Adsorption Kinetic Data by Reaction Models

Analyzing the Adsorption Kinetic data by Reaction Kinetic Models

Pseudo first order and Pseudo Second order kinetic models were applied to kinetic data of afB1 adsorption. Following equation is used to determine 1st order reaction rate constants:

$$\log(q_e - q_t) = \log(q_e) - \frac{k_{p1}}{2.303} t \quad (5.6)$$

$\log(q_e - q_t)$ vs t plot was used to determine k_1 where k_1 can be calculated from the slope of the plot (Figure 7.50)

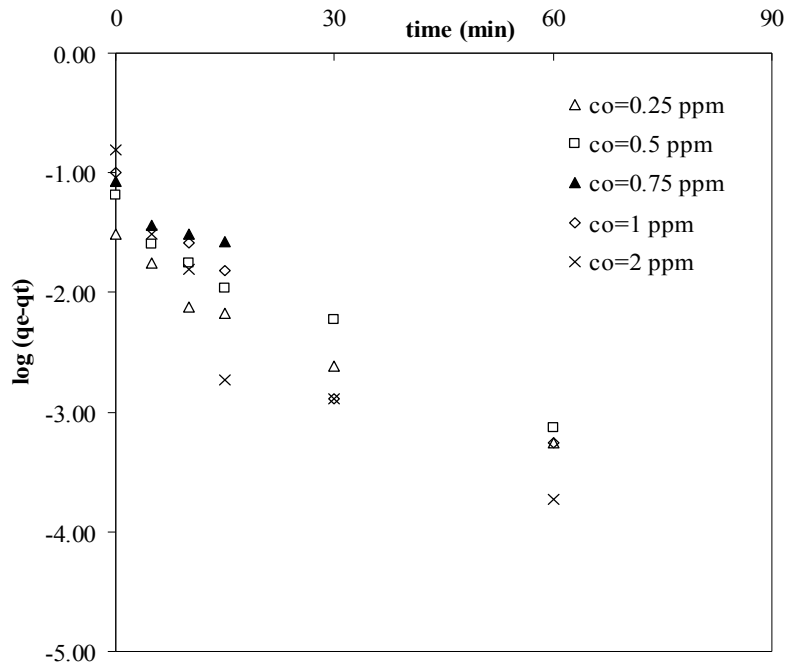


Figure 7.50. First order Kinetic plot for the adsorption of afB1 by zeolite (C₀ 0.25- 1.0 ppm, 37°C. 130 rpm, S/L: 25 mg/10 ml, pH 7.3, particle size: 8-10 μm)

Representative plot for first order kinetic model was presented in Figure 7.50. Other parameters were also analyzed by this model and listed in Table 7.24.

Table 7.24. Kinetic data analysis using first order model

Temperature		Slope	k_1 (min ⁻¹)	intercept	q_e ($\mu\text{g}/\text{mg}$)	R^2
ci=0.25ppm afB1 m=25 mg v= 10ml (PBS pH 7.3) A.S.=130 rpm. P.S.=8μm	T1(15 °C)	-0.008	0.018	-1.689	0.185	0.93
	T2(25 °C)	-0.036	0.083	-1.589	-1.589	0.92
	T3(37 °C)	-0.028	0.064	-1.686	0.185	0.96
Particle size		Slope	k_1 (min ⁻¹)	intercept	q_e ($\mu\text{g}/\text{mg}$)	R^2
ci=0.25ppm afB1 m=25 mg v= 10ml (PBS pH 7.3) A.S.=130 rpm. T=37 °C	P.S 1(extra small)	-0.062	0.142	-4.688	0.009	0.77
	P.S3(small)	-0.091	0.210	-3.805	0.022	0.89
	P.S3(big)	-0.126	0.291	-3.884	0.021	0.91
Agitation speed		Slope	k_1 (min ⁻¹)	intercept	q_e ($\mu\text{g}/\text{mg}$)	R^2
ci=0.25ppm afB1 m=25 mg v= 10ml (PBS pH 7.3) P.S.=8μm T=37 °C	A.S1(50 rpm)	-0.001	0.003	-1.615	0.199	0.87
	A.S2(130 rpm)	-0.028	0.064	-1.686	0.185	0.96
	A.S3(200 rpm)	-0.059	0.136	-1.579	0.206	0.97
pH		Slope	k_1 (min ⁻¹)	intercept	q_e ($\mu\text{g}/\text{mg}$)	R^2
ci=0.25ppm afB1 m=25 mg A.S.=130 rpm. P.S.=8μm T=37 °C	pH 3.0.	-0.02	0.046	-1.691	0.184	0.90
	pH 5.0	-0.038	0.088	-1.594	0.203	0.96
	pH7.3	-0.028	0.064	-1.686	0.185	0.96
Initial Concentration		Slope	k_1 (min ⁻¹)	intercept	q_e ($\mu\text{g}/\text{mg}$)	R^2
m=25 mg v= 10ml (PBS pH 7.3) A.S.=130 rpm. P.S.=8μm	0.25	-0.028	0.064	-1.686	0.185	0.96
	0.5	-0.030	0.068	-1.383	0.251	0.97
	0.75	-0.032	0.073	-1.162	0.313	0.83
	1	-0.038	0.087	-1.239	0.290	0.89
	2	-0.044	0.101	-1.368	0.255	0.84

The effects of experimental parameters on 1st order reaction rate constant are tabulated (Table 7.24). The results indicated that changing experimental parameters (temperature and pH) resulted in irregular change in reaction rate constants and theoretical equilibrium adsorbed amounts. Differently, increase in initial afB1

concentration, agitation speed and particle size results in increase in reaction rate constants.

Following equation is used to determine 2nd order reaction rate constant where. k_{p2} is the rate constant of pseudo second-order adsorption ($\mu\text{g}/\text{mg min}$).

$$\frac{1}{q_e - q_t} = \frac{1}{q_e} + k_{p2}t \quad (5.8.)$$

$$\frac{t}{qt} = \frac{1}{k_{p2}q_e^2} + \frac{1}{q_e}t \quad (5.9.)$$

The plot of (t/q_t) against t of equation should give a linear relationship from which q_e and k_{p2} can be determined from the slope and intercept of the plot, respectively. The results for pseudo second order model were tabulated (Table 7.25)

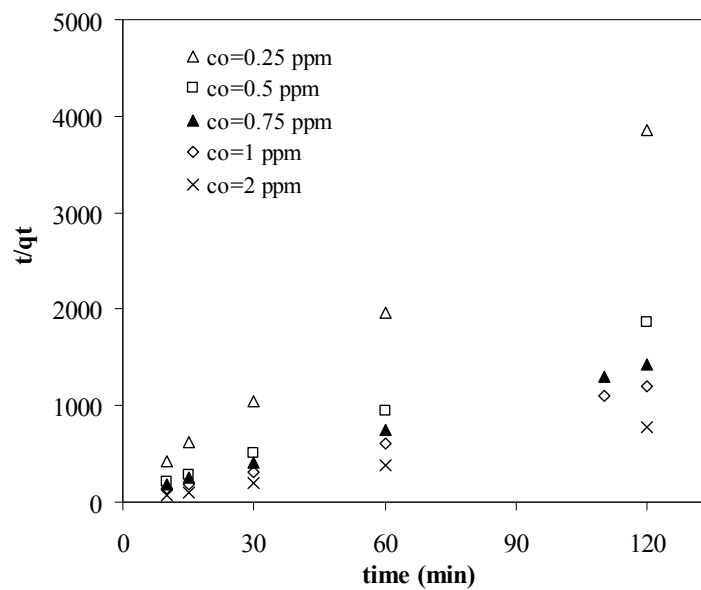


Figure 7.51. Pseudo second order kinetic plot for the adsorption of afB1 onto zeolite (C_0 : 0.25- 1.0 ppm, 37°C, 130 rpm, S/L:25 mg/10 ml, pH7.3. particle size:8-10 μm)

Table 7.25. Analyzing the kinetic data by Pseudo Second order Model

Temperature		Slope	k_2 (mg/ μ gmin)	intercept	qe(μ g/mg)	R ²
ci=0.25ppm afB1 m=25 mg v= 10ml (PBS pH 7.3) A.S.=130 rpm. P.S.=8 μ m	T1(15 C)	33.26	3.129	353.5	0.030	0.989
	T2(25 C)	31.59	5.359	186.2	0.032	0.998
	T3(37 C)	30.74	6.300	150	0.033	0.999
Particle size		Slope	k_2 (mg/ μ gmin)	intercept	qe(μ g/mg)	R ²
ci=0.25ppm afB1 m=25 mg v= 10ml (PBS pH 7.3) A.S.=130 rpm. T=37 °C	P.S1 (extra small)	30.56	38.16	24.48	0.03	0.999
	P.S2 (small)	29.36	17.91	48.14	0.03	0.994
	P.S3(big)	75.95	65.75	87.73	0.01	0.995
Agitation speed		Slope	k_2 (mg/ μ gmin)	intercept	qe(μ g/mg)	R ²
ci=0.25ppm afB1 m=25 mg v= 10ml (PBS pH 7.3) P.S.=8 μ m T=37 °C	AS1(50rpm)	46.90	1.382	1591..50	0.02	0.978
	AS2(130rpm)	30.74	6.300	150	0.033	0.999
	AS3(200rpm)	34.44	29.347	40.41	0.033	0.994
pH		Slope	k_2 (mg/ μ gmin)	intercept	qe(μ g/mg)	R ²
ci=0.25ppm afB1 m=25 mg A.S.=130 rpm. P.S.=8 μ m T=37 °C	pH 3.0.	26.91.	0.403	116.96	0.037	0.900
	pH 5.0	29.594	10.455	83.767	0.034	0.960
	pH7.3	30.74	6.300	150	0.033	0.999
Initial Concentration		Slope	k_2 (mg/ μ gmin)	intercept	qe(μ g/mg)	R ²
m=25 mg v= 10ml (PBS pH 7.3) A.S.=130 rpm. P.S.=8 μ m	0.25	30.74	6.300	150	0.033	0.999
	0.5	14.56	3.859	67.27	0.067	0.999
	0.75	10.01	1.555	92.21	0.089	0.999
	1	8.5673	1.234	44.79	0.106	0.999
	2	5.2532	1.193	35.23	0.21	0.999

When first order reaction model of the kinetic data is compared to pseudo second order kinetic model, higher correlation coefficients are obtained for pseudo second order kinetic model and the experimental kinetic data is well represented. As seen in the Table 7.25, the rate coefficient of the pseudo –second order kinetic model increased by increasing agitation speed and decreased by increasing the initial afB1 concentration. Quada et al. (2007); Sulak et al. (2007); Al-Ghouti et al. (2009); Han et al. (2010) also reported that increasing initial concentration results in decrease in pseudo second order rate constant. Increasing agitation speed results in increase in rate constant. This situation can be explained by a decrease in the resistance to adsorption attributed to the hydrodynamic boundary between adsorbent particle and afB1 molecule. The surface area includes internal and external surface areas. Decrease in particle size leads in increase in external area especially. In addition, clogged pores are opened. Increasing agitation speed decreases the film resistance to mass transfer surrounding the adsorbent particle and increases the mobility of the system. The pH and temperature effect on the rate coefficient was found to be irregular

IR Spectrum of PNZ after Adsorption

In order to clarify the mechanism, IR spectrum was examined after adsorption and compared. In the spectra, there could not be observed any band shift and extra peaks for the PNZ. This evidence can also support the physical sorption mechanism.

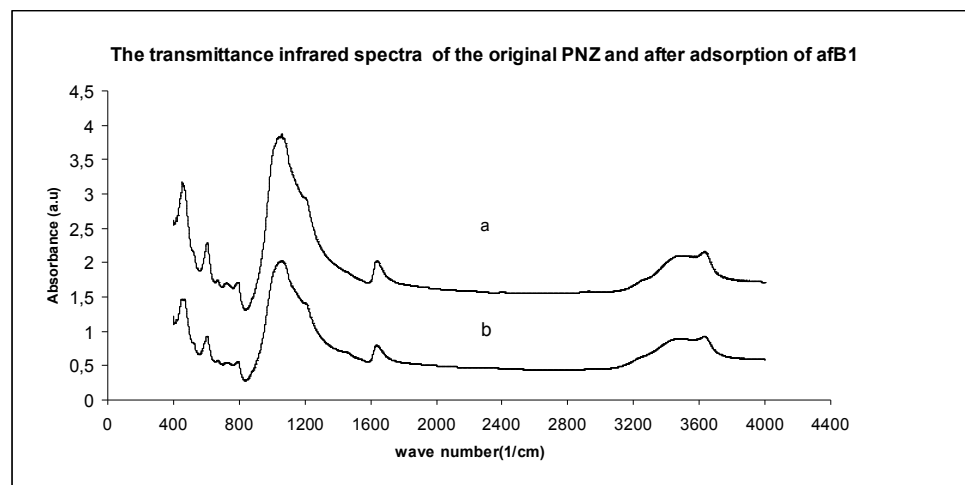


Figure 7.52. Transmittance infrared spectra of the PNZ. (a) After adsorption afB1 (b) Original clinoptilolite rich PNZ

7.3.2. Adsorption Experiments by Probiotic Bacteria

AfB1 adsorption experiments were conducted by using lactobacilli organisms for different parameters also. As a first consideration, different strains were tested and strain that posses highest afB1 removal was chosen.

7.3.2.1. Adsorption Equilibrium and Adsorption Isotherms

Equilibrium experiments were conducted for 3 different temperatures (15 °C, 25 °C and 37 °C) and uptake curves were given below. It was seen that adsorption was favorable at higher temperatures this result can be explained by the endothermic nature of the adsorption.

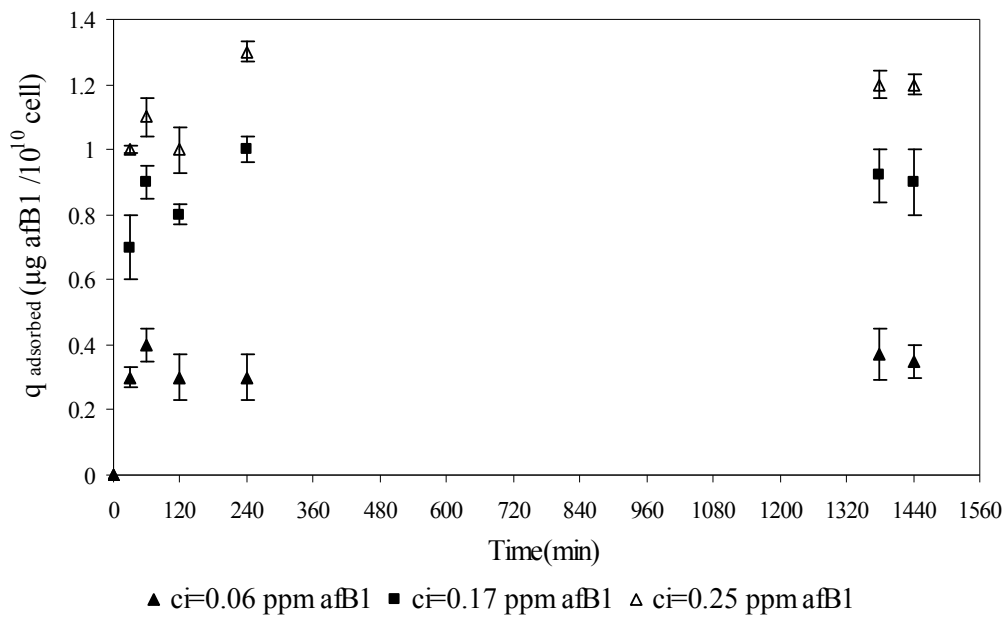


Figure 7.53. Uptake curves of afB1 adsorption by *L. plantarum* S2 (Ci:0.06-0.25 ppm, 37°C, 130 rpm, S/L: 10¹⁰ cell/10 ml, pH 7.3)

After obtaining equilibrium data, adsorption isotherm was constructed as given below (Figure 7.54).

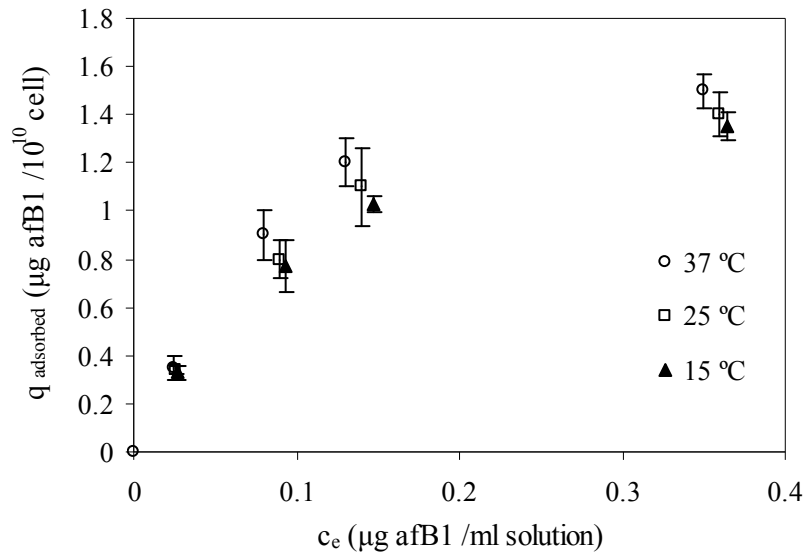


Figure 7.54. Adsorption isotherms of afB1 by *L. plantarum* S2 (C_i :0.06-0.5 ppm,37°C. 130 rpm, S/L: 10^{10} cell /10 ml, pH7.3)

Adsorption Equilibrium data was fitted to isotherm model equations than results are given (Table 7.26.) It was seen that isotherm data is better represented by Langmuir model equation. This model assumes homogenous adsorbent surfaces and monolayer adsorption and this assumption was in consistent with adsorption system.

As it seen Table 7.26 below, decrease in temperature results in decrease in Langmuir isotherm constant and affinity parameter this indicates adsorption is favored in higher temperatures.

Table 7.26. Comparison of applied adsorption isotherm models

Models					
Langmuir	Temperature	K_L (mL/unit g)	a_L (mL/ μ g)	SSE	R^2
	37 °C	19.802	10.160	0.011	0.99
	25 °C	16.694	9.047	0.006	0.99
	15 °C	15.152	8.435	0.002	0.99
Freundlich		K_F $\frac{\mu\text{g}}{\text{Unitg}} \left(\frac{\text{mL}}{\mu\text{g}} \right)^{1/n_F}$	n_F	SSE	R^2
	37 °C	3.195	1.785	0.0007	0.96
	25 °C	2.809	1.808	0.0003	0.97
	15 °C	2.644	1.808	0.0003	0.97

7.3.2.2. Parametric Study of afB1 Adsorption by *L. plantarum* S2

Effect of parameters (strain type of probiotic lactobacilli organism, viability state of bacteria, bacteria concentration, solution pH and temperature, initial afB1 concentration and agitation speed) on afB1 adsorption by *L. plantarum* S2 were analysed and the results were presented in the following section.

Effect of Viability of Bacteria on afB1 Adsorption

As seen in Figure 7.55 viable and non viable (dead cells obtained by autoclaving) indicate similar afB1 removal behaviour and this observation supported the idea that afB1 decrease in solution is not due to metabolic conversion or degradation.

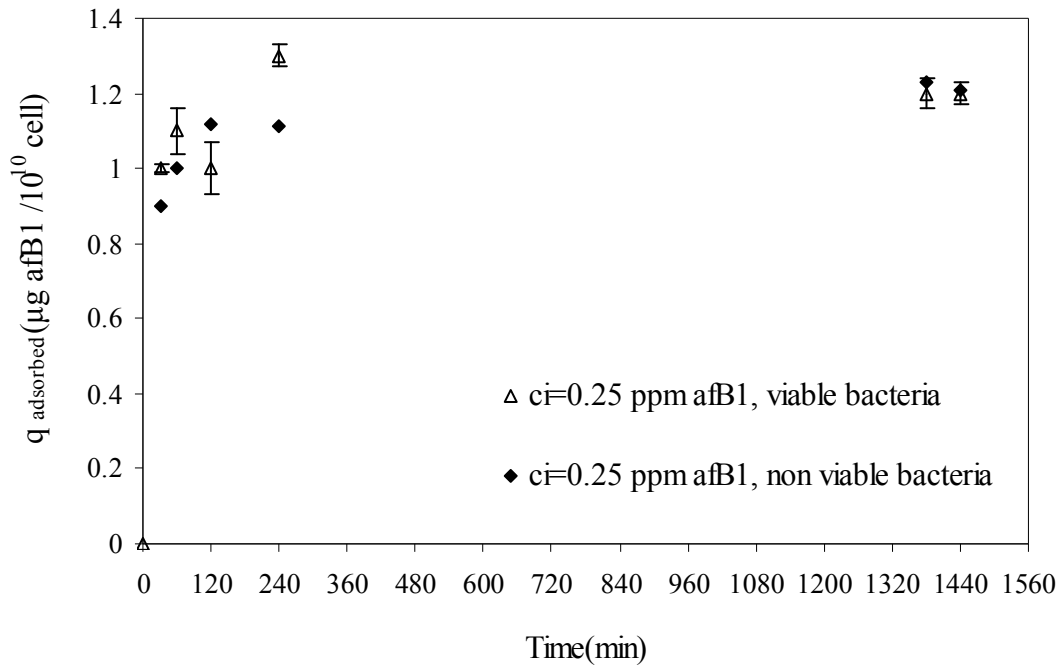


Figure 7.55. Effect of viability of bacteria on uptake curves of afB1 adsorption by *L. plantarum* S2 (C_i :0.25 ppm, 37°C, 130 rpm, S/L: 10^{10} cell/10 ml, pH 7.3)

Effect of Strain Type on AfB1 Adsorption

Comparison of different strains shows that *L. plantarum* S2 is the best one among the strains studied (toxin removal 45%). The afB1 binding property changes in the species and also in the strains of the Lactobacilli species. This result was supported by several authors also (Table 7.27). Although there has been performed several study on afB1 adsorption by bacteria, there has not been done any equilibrium or isotherm study.

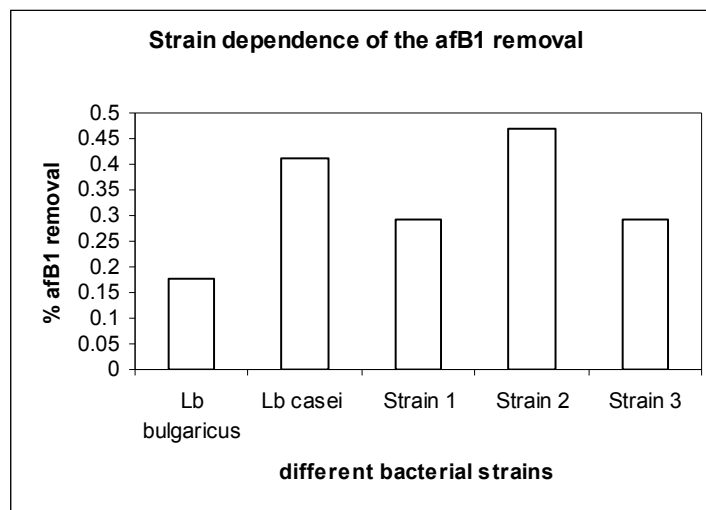


Figure 7.56. Effect of bacteria type on afB1 removal (C_i:0.25 ppm, 37°C, 130 rpm, S/L:10¹⁰ cell/10 ml, pH7.3)

Table 7.27. Some of the studies on binding of Aflatoxins by Lactic Acid Bacteria

Organism	Tested Aflatoxin conc. solution . pH. Temperature (°C). time (1 h)	Adsorption	Reference
<i>L. fermentum</i> subsp. <i>cellobiosus</i> . <i>L. acidophilus</i> . <i>Saccharomyces cerevisiae</i>	5 µg/ml. PBS 7.3, 37 °C, 1 h	7.2 % to 42.8 (%afB1 bound)	Bueno et al.. 2007
<i>L. rhamnosus</i> GG. LLb. <i>L. rhamnosus</i> LC-705. <i>Propionibacterim freudenreicii</i> subsp. <i>shermanii</i> JS	afB1. 0.0017 -13.3 µg/ml PBS 7.3, 37 °C, 1 h	specific rate 1.5-5 µg/10 ¹⁰ cells/h	Lee et al.. 2003
<i>L. paracasei</i> F19 <i>B. lactis</i> Bp 12 <i>L. crispatus</i> M247 <i>L. crispatus</i> MU5 <i>L. salivarius</i> LM2 - 118 <i>L. johnsonii</i> LJ-1	5 µg/ml. PBS 7.3, 37 °C, 1 h	5.8 to 31.3%. (%afB1 bound)	Peltonen et al.. 2000

Effect of initial afB1 concentration on AfB1 Adsorption

With increase in the initial afB1 concentration, increase in adsorbed amount was observed as expected.(Figure 7.53).

Effect of Lactobacillus plantarum (Adsorbent) Amount on afB1 Adsorption

Different cell amounts (2×10^{10} , 1×10^{10} , 0.5×10^{10} , 0.1×10^{10} , 10^5 , 10^4) were tested in order to see the effect adsorbent amount on afB1 adsorption. As seen Figure 7.58, detectable afB1 adsorption could be observed after over than 0.1×10^{10} . Increase in total afB1 adsorbed was observed within increase in bacteria amount, but adsorbed amount per unit bacteria decreases after a critic bacteria concentration

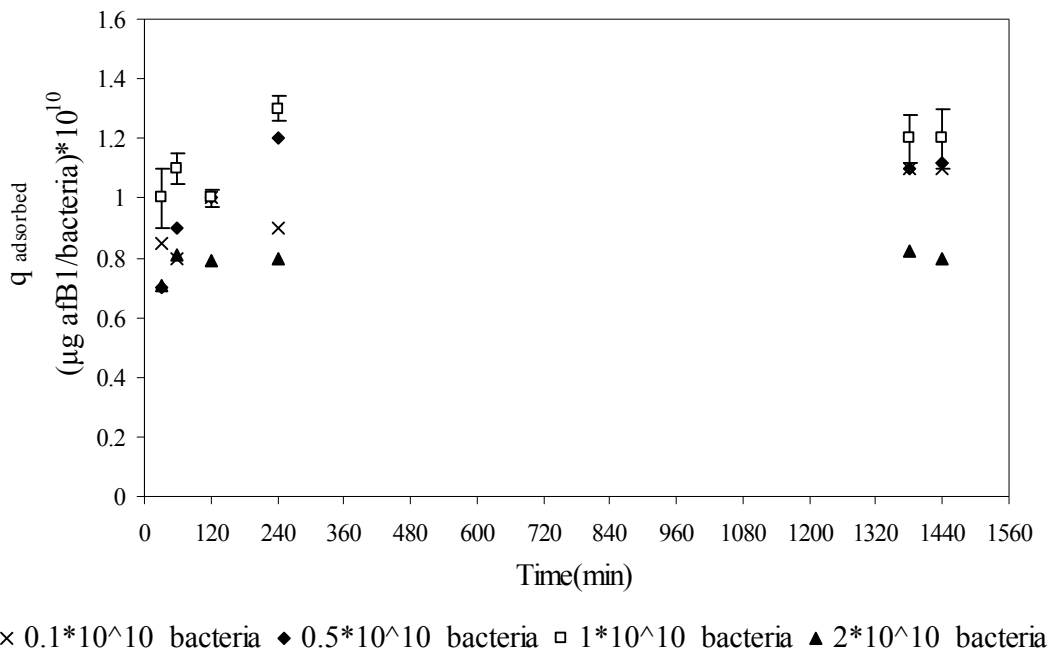


Figure 7.57. Effect of organism amount on uptake curves (10 ml PBS pH 7.3,130 rpm agitation speed , 37 °C, ci=0.25 ppm).

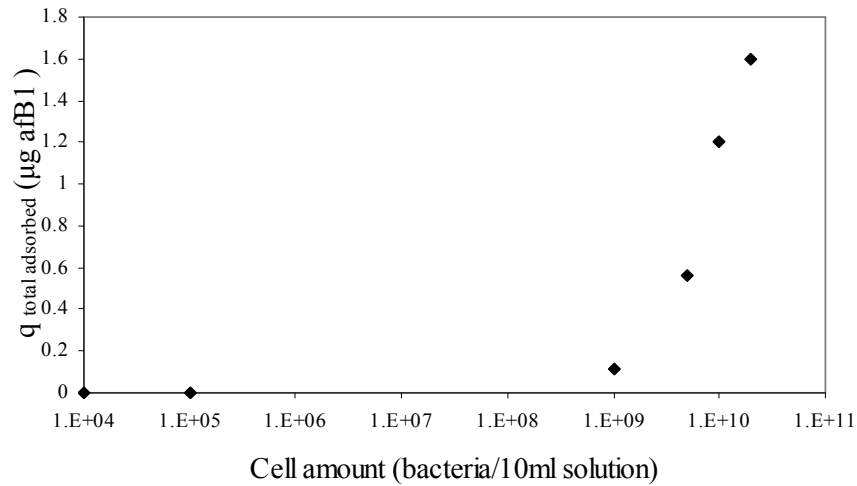


Figure 7.58. Effect of bacteria amount on total afB1 adsorbed amount (10 ml PBS pH 7.3,130 rpm agitation speed , 37 °C, ci=0.25 ppm).

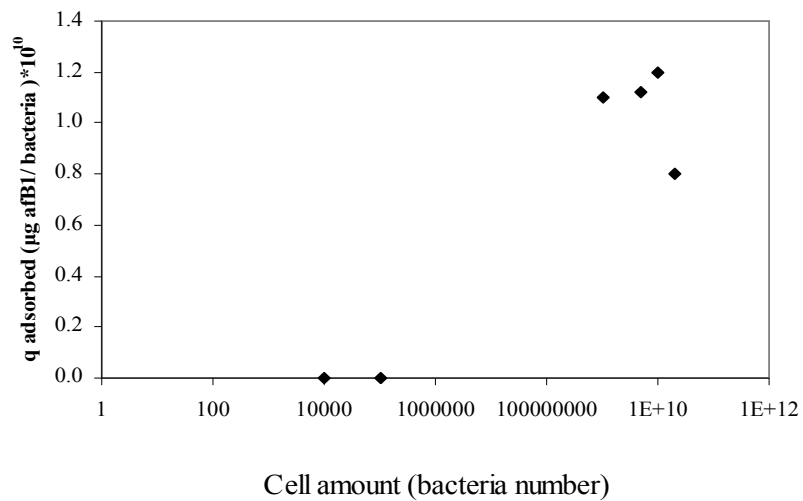


Figure 7.59. Effect of bacteria amount on afB1 adsorbed per bacteria (10 ml PBS pH 7.3,130 rpm agitation speed , 37 °C, ci=0.25 ppm).

Effect of Agitation Speed

Increase or decrease in agitation speed did not cause significant effect on afB1 adsorption similar behavior was observed.

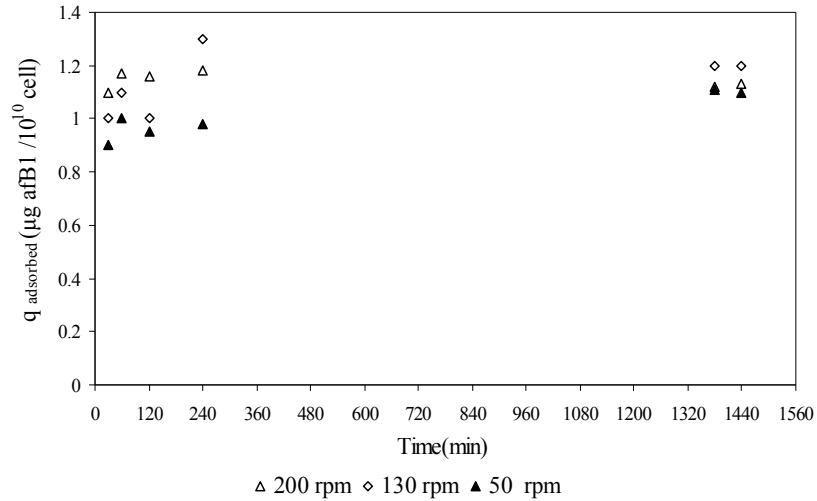


Figure 7.60. Effect of agitation speed on afB1 adsorbed per bacteria (10 ml PBS pH 7.3 , 37 °C, ci=0.25 ppm).

Effect of Solution pH

Decrease in solution pH resulted in increase in adsorbed amounts. It is known that decrease in solution pH results in decrease in negativity of the bacteria surface (Figure 7.61). The bacterial surface is all negative experimented pH ranges.

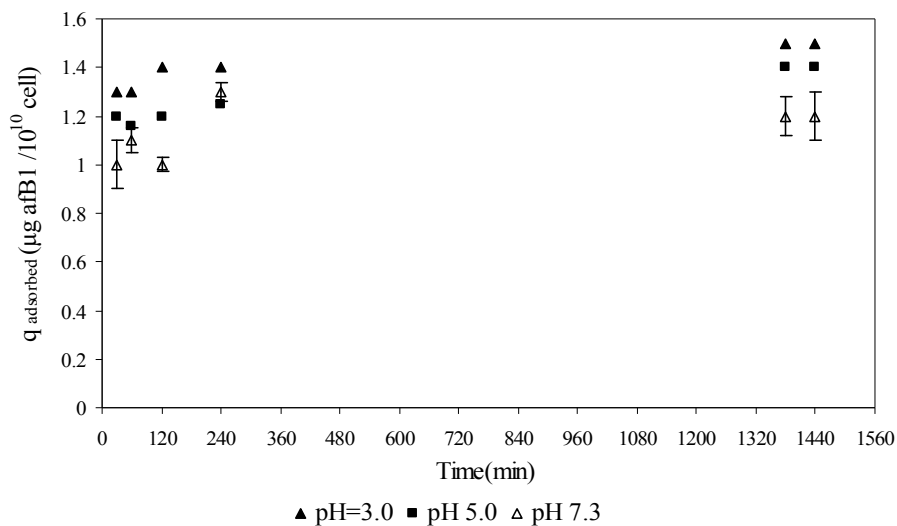


Figure 7.61. Effect of pH on uptake curves (10 ml PBS pH 7.3,130 rpm agitation speed , 37 °C, ci=0.25 ppm).

Effect of Temperature

Effect of temperature on adsorption equilibrium are given below (Figure 7.62) also uptake curves were presented in Figure .7.63. Slight increase in adsorbed amounts was observed increase in temperature.

The effect of temperature on isotherm coefficients were used to determine Gibbs free energy (ΔG°), enthalpy (ΔH°) and entropy (ΔS°) change.

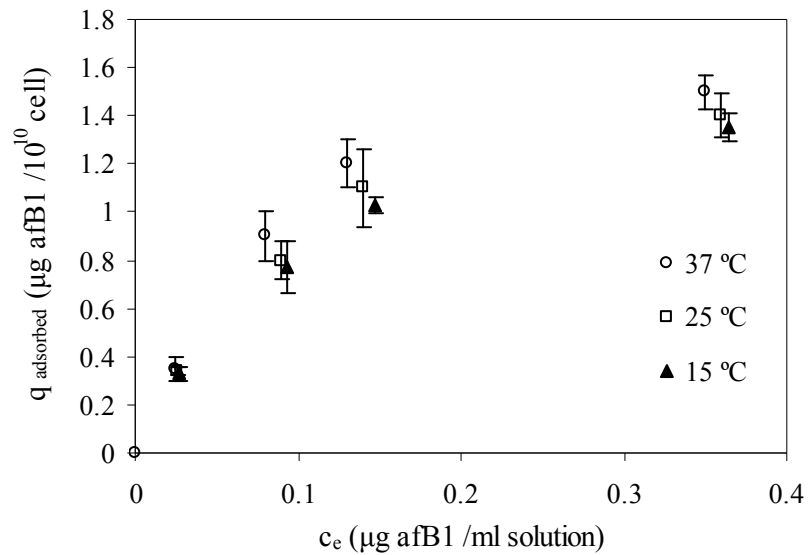


Figure 7.62. Effect of temperature on adsorption isotherms (10 ml PBS pH 7.3,130 rpm agitation speed , 37 °C, $c_i=0.25$ ppm).

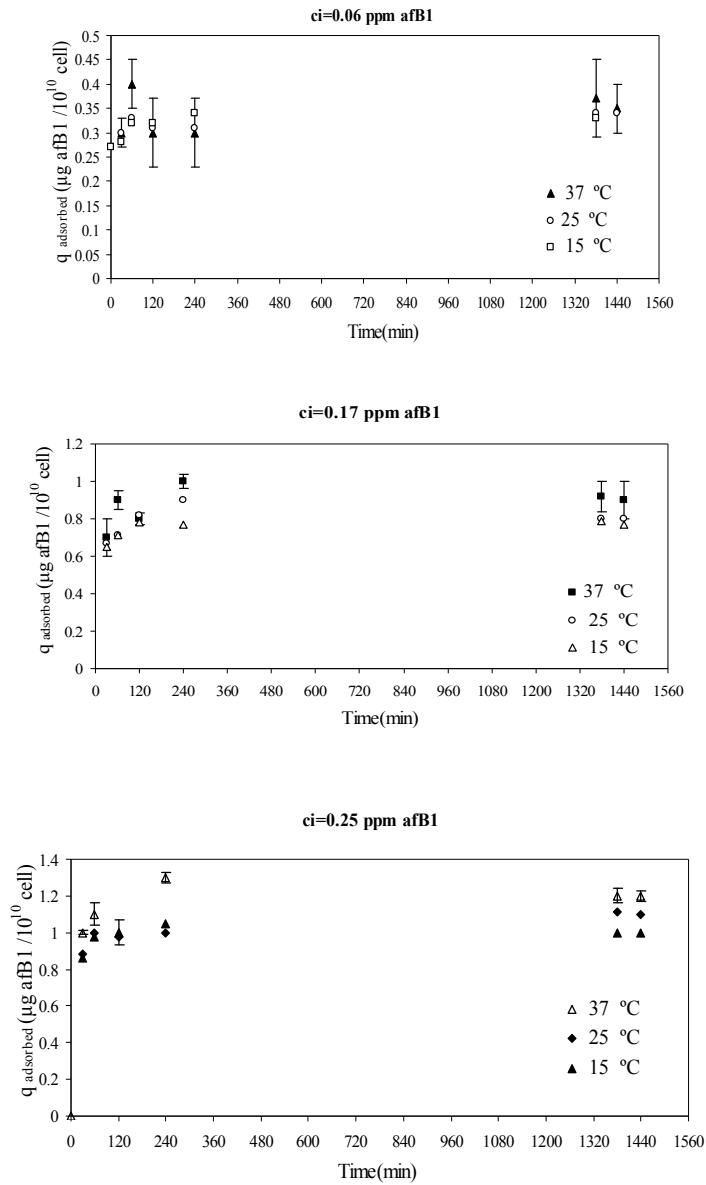


Figure 7.63. Effect of temperature on uptake curves (10 ml PBS pH 7.3,130 rpm agitation speed , $C_0=0.25$ ppm).

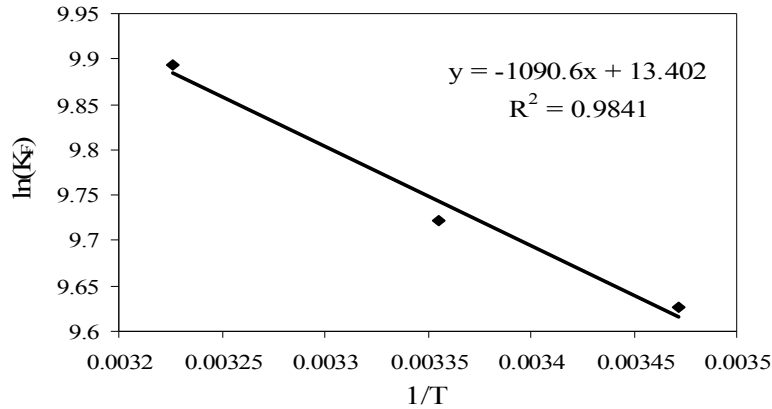


Figure 7.64. Van't Hoff's plot for afB1 adsorption by bacteria.

Langmuir isotherm has superiority to represent the adsorption equilibrium therefore K_L was used to determine thermodynamic parameters

$$\ln K_L = \frac{\Delta S^\circ}{R} - \frac{\Delta H^\circ}{RT} = -\frac{\Delta G^\circ}{RT} \quad (5.46)$$

The enthalpy and entropy change are calculated from the slope and intercept of the van't Hoff plot ($\ln K_L$ versus $1/T$) As seen in the Figure 7.64. Slope is $-\Delta H^\circ/R$ and intercept is $\Delta S^\circ/R$. Gibbs free energy is also calculated as below.

$$\Delta G^\circ = -RT \ln K \quad (5.45)$$

Calculated thermodynamic parameters are given in Table 7.28. The values of ΔG° were negative indicating that the adsorption was feasible and spontaneous in nature. The positive value of entropy (ΔS°) showed the increased randomness at the solid-liquid interface during the adsorption. The adsorption of compounds to a surface can be categorized as either physisorption or chemisorption on the basis of the enthalpy of adsorption (ΔH°) and of the change in Gibbs free energy (ΔG°). Physisorption involves weak associations which include van der Waals, dipole-dipole, induced dipole and hydrogen bonding with enthalpy of < 20 kJ/mol. Chemisorption implies a chemical reaction or sharing of electrons between the adsorbent and the adsorbate with > 20 kJ/mol (Gu et al., 1994).

It has been reported that ΔG° values up to -20 kJ/mol are consistent with physical sorption while ΔG° values more negative than -40 kJ/mol indicates the chemical sorption (Horsfall et al., 2004). Therefore, thermodynamic parameters showed that afB1 adsorption by *Lactobacillus plantarum* was physical adsorption

Table 7.28. Thermodynamic parameters for afB1 adsorption on *L. plantarum* S2

T [K]	ΔG° (kJ/mol)	ΔH° (kJ/mol)	ΔS° (kJ/molK)
288	-23.69	7.97	0.11
298	-24.93		
310	-26.11		

7.3.3. Adsorption Experiments by PNZ and *L plantarum* S2(together)

When the bacteria and PNZ were used together for the same experimental conditions the results indicated that more afB1 adsorbed than they were alone (Figure 7.65). In order to explain the reason for this, effect of PNZ on viability of organisms were checked. The presence of PNZ has no positive effect on the viable number of the organism (Table 7.29 and Table 7.30). This additional afB1 removal property can be beneficial for possible new biomedical applications.

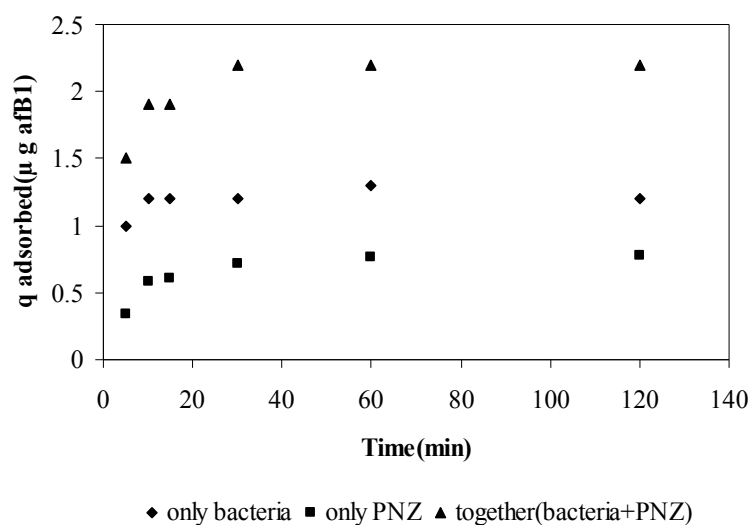


Figure 7.65. Effect of presence of PNZ with probiotic bacteria together on adsorbed amounts (25 mg PNZ+ 10^{10} cell/10 ml PBS pH 7.3,130 rpm agitation speed ,37 °C, $c_0=0.25$ ppm).

Experimental Results on Lactobacilli Zeolite Interaction

The effect of the clinoptilolite rich mineral on viability of the Lactobacilli organism was presented for two different zeolite amount (Table 7.29 and Table 7.30). The experiments were planned to investigate any interaction on zeolite and lactobacilli organism. The experiments were conducted in the PBS pH7.3 and the cells were added into the solution. During the time periods given below, no significant organisms dead was observed therefore no bactericidal property of PNZ was determined. There is not significant change in viable bacteria number compared with control.

Table 7.29. Viable organism numbers during time Exp 1 g NZ / 9ml cell suspension in PBS pH 7.3. 25-106 μ m NZ

Dilution number	Samples	
0 h (Time)	Control (cell suspension in PBS without PNZ)	Zeolite (cell suspension in PBS with PNZ)
-7	153 153x10 ⁷ CFU/ml	73 73x10 ⁷ CFU/ml
-8	14	4
-9	2	2
3 h	Control	Zeolite
-7	>300	>300
-8	26	16
-9	7	3
6h	Control	Zeolite
-7	113 113x10 ⁷ CFU/ml	173 173x10 ⁷ CFU/ml
-8	19	23
-9	2	0

Table 7.30. Viable organism numbers during time Exp: 2 g NZ / 9ml cell suspension in PBS pH 7.3. 25-106 μ m NZ

0 h	Control	Zeolite
-7	65 65x10 ⁷ CFU/ml	72 72x10 ⁷ CFU/ml
-8	7	7
-9	2	1
3 h	Control	Zeolite
-7	106 106x10 ⁷ CFU/ml	43 43x10 ⁷ CFU/ml
-8	8	6
-9	0	4
5h	Control	Zeolite
-7	69 69x10 ⁷ CFU/ml	46 46x10 ⁷ CFU/ml
-8	4	3
-9	0	1
31 h	Control	Zeolite
-5	>300	94 94x10 ⁵ CFU/ml
-6	155 155x10 ⁶ CFU/ml	6
-7	18	4

Effect of Initial afB1 Concentration on Adsorption

There has been increase in removal efficiency even with higher concentration it will be more pronounced (Figure 7.66 and Table 7.31)

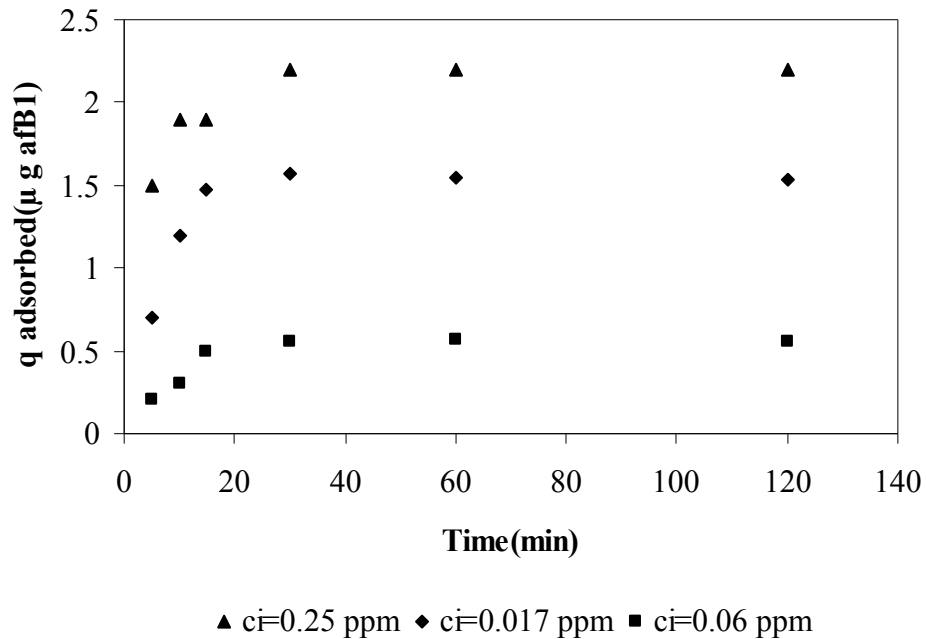


Figure 7.66. Effect of initial afB1 concentration on uptake curves (25 mg PNZ+10¹⁰ cell/10 ml PBS pH 7.3,130 rpm agitation speed , 37 °C, c₀=0.25 ppm).

Table 7.31. Change in afB1 removal percentages with respect to initial afB1 concentration

	%afB1 removal (ci=0.25 ppm)	%afB1 removal (ci=0.17 ppm)	%afB1 removal (ci=0.06 ppm)
probiotic alone	45	50	52
pnz alone	32	35	40
PNZ + lactobacilli	86	90	93

Effect of Temperature on Adsorption

Increase in temperature results in any significant effect in the case of presence of both material together. It can be expected because temperature effect of each material is reverse direction.

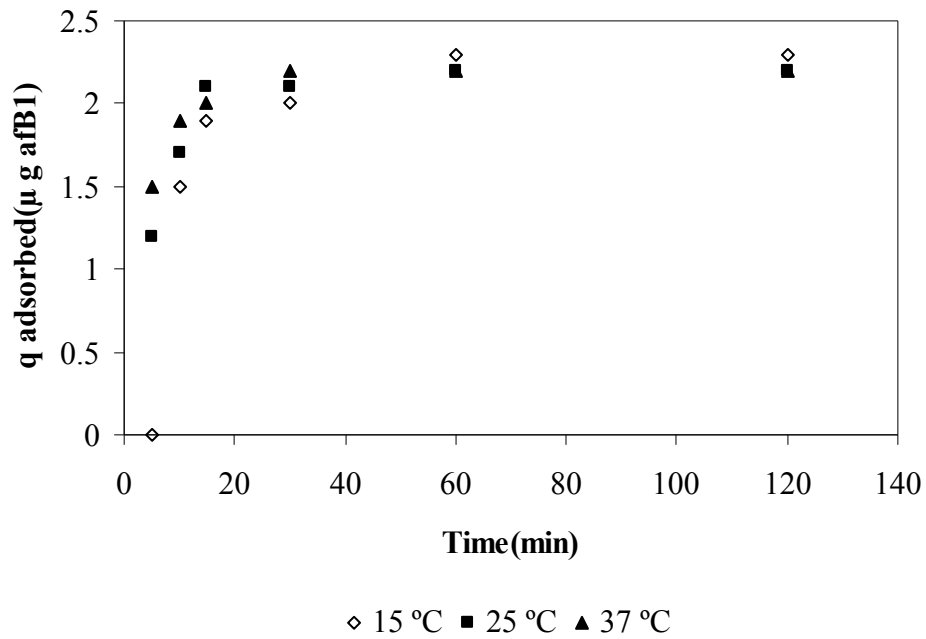


Figure 7.67. Effect of temperature on uptake curves (25 mg PNZ+ 10^{10} cell/10 ml PBS pH 7.3,130 rpm agitation speed , $c_0=0.25$ ppm).

Effect of pH on Adsorption

Increase in pH results in decrease in adsorbed amounts in the case of presence of both materials together. Each material shows similar behaviour within the change in the solution pH.

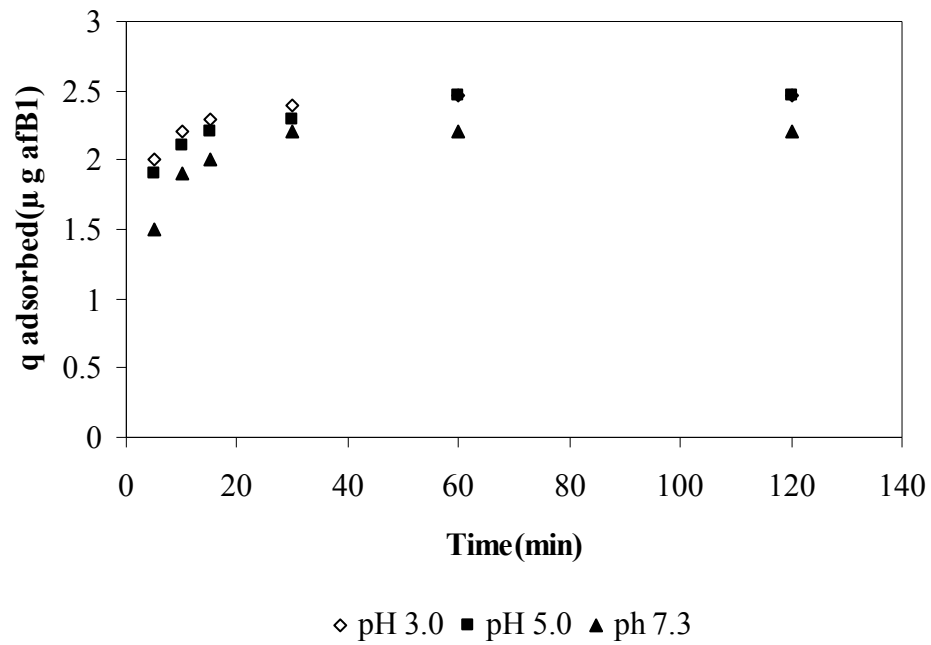


Figure 7.68. Effect of pH on uptake curves (25 mg PNZ+ 10^{10} cell/10 ml PBS,130 rpm agitation speed , 37 °C , $c_0=0.25$ ppm).

CHAPTER 8

CONCLUSION

The present study was designed to determine the removal property of one of the food carcinogen (afB1) by PNZ mineral and *L. plantarum* S2. It has been known that clinoptilolite and probiotic lactic acid bacteria have some common beneficial health effects. The thesis was constructed on this idea and toxin (afB1) removal ability of them was focused. Following the isolation and purification of probiotic lactobacilli; and purification and characterization of clinoptilolite rich mineral they were used in the removal of afB1. The major findings were presented as follow by expressing the contributions to current literature with limitations of the study.

- 110 purified lactobacilli isolated strain were obtained from traditional fermented food products (Boza, fermented cabbage) and stored as glycerol stocks at -80 °C for long term usages. The results indicated that fermented foods have a big probiotic potential and they can be suggested for obtaining new probiotic lactobacilli stains. In the current study, major properties (acid resistance, bile resistance, pancreatic enzyme resistance) were examined due to labor and cost limitations and 15 of lactobacilli isolates were found to have these desirable properties. 3 of them with better properties were chosen and identified at species level as *L. plantarum*. Suggestion of fermented cabbage originated new probiotic strain is one of the significant finding of this study. In the future, 16S R DNA sequence analysis can be suggested to support the identification of this strain at species level. This strain has many potential applications in biomedical, biotechnological and other industrial and scientific areas.
- The results of purification and characterization steps indicated that purified natural mineral has 98% purity and contains toxic elements well below health concerns. This result denoted that our material can be used for various medical applications by considering potential beneficial health effects.
- afB1 adsorption studies indicated that PNZ can adsorp this toxin in the pH range of the gastrointestinal solutions. Kinetic and equilibrium studies showed that experimental data was well represented by Sip's model and adsorption capacity was found as 0.18 µg afB1/mg PNZ at 37°C. Thermodynamic studies implied that afB1

adsorption by PNZ is physical adsorption. Experiments performed at different temperatures also indicated that adsorption is exothermic in nature. There has not been any isotherm modeling study on afB1 adsorption by clinoptilolite rich mineral therefore the results of this part provided important contribution to the current literature. Although capacity is lower than HSCAS and bentonite, considering the cost and health related properties PNZ can be proposed as potential adsorbent in the removal of afB1.

- Modelling of adsorption kinetics for afB1 by PNZ was studied by analyzing controlling mass transfer resistances. It was found that both film diffusion and intra particle diffusion is effective on adsorption kinetics depending on the experimental conditions. Existence of surface resistance rather than external film resistance for well agitated conditions (130-200 rpm) were determined. This part of the study has special contribution to the current literature due to the lack of any kinetic model study on afB1 clinoptilolite rich mineral pairs.
- The afB1 binding ability of probiotic lactobacilli was analysed and afB1 interaction with organism cells were on the cell surface. The dead cells and alive cells showed similar afB1 removal property and this result supports the idea that afB1 removal is not due to the metabolic degradation. afB1 adsorption by *L. plantarum* S2 was analyzed by kinetic and equilibrium studies and it was found equilibrium isotherm data was well represented by Langmuir isotherm and maximum theoretical adsorption capacity was found as 1.3 $\mu\text{g afB1}/10^9$ cell at 37 °C. The effect of temperature on adsorption kinetics was analysed and it was found that adsorption is favorable at higher temperatures and it indicates endothermic nature. Thermodynamic studies implied that it is a physical adsorption. The result of this part might provide special contribution for effective usage of this strain for various afB1 removal applications.
- The experiments with *L. plantarum* S2 cells and PNZ together indicated that they are more effective when they were used together (45% for *L. plantarum* S2, 32% for PNZ, 86% for *L. plantarum* S2 and PNZ together). As a result of this study, new strategies can be developed to manage one of the global unavoidable toxin problem by using these two material together considering health related properties.

REFERENCES

- Al-Ghouti, M.; Khraisheh, M.; A. M., Ahmad, M. N. M.; Allen, S. Adsorption behaviour of methylene blue onto Jordanian diatomite: A kinetic study. *Journal of Hazardous Materials*, 2009, 165, 589–598.
- Anand, S. K.; Srinivasan, R. A.; Rao, L. K. Antibacterial activity associated with *Bifidobacterium bifidum* Cultured Dairy Products *Journal*. 1984, 19, 6-8.
- Anon . Nutritional benefits of yoghurt and other fermented milk products. National Dairy Council Topical Update. 1997, 8, 1-16.
- Ackley, M.; Yang, R.T. Diffusion in Ion Exchanged Clinoptilolites *AIChE Journal*. 1991, 37(11), 1645-1656.
- Akdeniz, Y.; Ülkü, S. Microwave Effect on Ion-Exchange and Structure of Clinoptilolite. *J. Porous Mater.* 2007, 14, 55-60.
- Arvide, M.G.; Velazouez, I.M.A.L.; Dixon, B. Smectite clay adsorption of aflatoxin vs. octahedral composition as indicated by FTIR *Clays and Clay minerals* . 2008, 56(5), 571-578.
- Auerbach , S.M.; Carrado , K. A.; Dutta, P. K. *Handbook of Zeolite Science and Technology*, Section 22, Marcell Dekker Inc., Newyork, 2003.
- Cansever Erdoğan, B.; Ülkü, S. Ammonium sorption by Gördes clinoptilolite rich mineral specimen. *Applied Clay Science*. 2011, 54, 217-255.
- Baup, S.; Jaffre, C.; Wolbert, D.; LaPlanche, A. Adsorption of Pesticides onto Granular Activated Carbon: Determination of Surface Diffusivities Using Simple Batch Experiments. *Adsorption*. 2000, 6, 219-228.
- Barrer, R. M. *Zeolites and Clay Minerals as Sorbents and Molecular Sieves*, Academic Press, New York, 1978.
- Bish, D. L.; Chipera, S. J. Problems and Solutions in Quantitative Analysis of Complex Mixture by X-ray Powder Diffractions. *Adv. X-ray Anal.* 1988, 31, 295-308.
- Blount W. P. Turkey "X" disease. *J Br Turkey Federation* 1961, 1:5162.

- Breck, D. W. *Zeolite Molecular Sieves*, John Wiley and Sons, New York, 1974.
- Bueno, D.,J; Casale, C.H.; Pizoolitto, R. P.;Salvano, M.A.; Oliver, G. Physical adsorption of aflatoxin B1 by lactic acid bacteria and *Saccharamoyces cerevisiae*: A theoretical Model. *Journal Food Protection*. 2007, 70(9), 2148-2154.
- Busby W. F., Jr.; Wogan, G.N. Aflatoxins. In *Chemical Carcinogens*, 2nd Edition (Searle C. E., ed), 9461135. Washington, D.C.: American Chemical Society,1984.
- Boyd, G.E.; Adamson, A. W; Meyers,L. S. *Journal of . American. Chem. Soc.*1947.2836.
- Carnaghan R. B.;Hartley R. D., O'Kelly J. Toxicity and Fluorescence Properties of the Aflatoxins. *Nature*. 1963, 200:1101.
- Cerri, G.; Gennaro, M.; Bonferonc, M. C.; Caramella, C. A. Zeolites in biomedical application: Zn-exchanged clinoptilolite-rich rock as active carrier for antibiotics in anti-acne topical therapy. *Applied Clay Science* .2004, 27, 141-150.
- Chang, Y.; Chu, L.; Tsai, J.; Chiu, S. Kinetic study of immobilized lysozyme on the extrudate-shaped NaY zeolite. *Process Biochemistry*.2006, 41, 1864–1874.
- Crank, J. *The Mathematics of Diffusion*, 2nd ed.; Clarendon Press: Oxford, 1979.
- Çakıcıoğlu-Özkan, F.; Ülkü, S. The Effect of HCl Treatment on Water Vapor Adsorption Characteristics of Clinoptilolite Rich Natural Zeolite. *Microporous Mesoporous Mater.* 2004, 77, 47-53.
- Colella, C. Recent Advances in Natural Zeolite Applications Based on External Surface Interaction with Cations and Molecules. *From Zeolites to Porous MOF Materials – the 40th Anniversary of International Zeolite Conference*. 2007, 2063-2073.
- Concepcion-Rosabal,B.; Rodriguez-Fuentes ,G.; Simon-Carballo,R. Development and featuring of the zeolitic active principle FZ: A glucose adsorbent. *Zeolites*. 1997,19,47-50.

- Dakovic , A.; Tomasevic-Canovic ; M.;Dondur,V.;Vujakovic, A.; Radosevic, P. Kinetics of aflatoxin B1 and G2 adsorption on Ca-Clinoptilolite. J. Serb. Chem.Soc. 2000, 65(1),715-723.
- Dakovic,A.; Tomasevic-Canovic,M.; Dondur, V.; Rottinghaus,G.E.; Vesna Medakovic,V.; Zariic, S. Adsorption of mycotoxins by organozeolites. Colloids and Surfaces B: Biointerfaces .2005, 46,20–25.
- El-Khaiary, M.I ; Gihan F. Malash, G. F. Common data analysis errors in batch adsorption studies. Hydrometallurgy .2011,105, 314–320.
- El-Nezami, H; Kankaapaa,P; Salminen, S.; Ahokasi, J. Ability of dairy strains of Lactic Acid Bacteria to bind a common food carcinogen, aflatoxin B1. Food and Chemical Toxicology.1998, 36, 321-326.
- Ersoy, B.; Çelik, M. S. Electrokinetic Properties of Clinoptilolite with Mono- and Multivalent Electrolytes. Microporous Mesoporous Mater. 2002, 55, 305-312.
- Fariás, T.; Ruiz-Salvador, A. R.; Rivera, A. Interaction Studies Between Drugs and a Purified Natural Clinoptilolite. Microporous Mesoporous Mater. 2003, 61, 117-125.
- Fuller, R. .Probiotics in man and animals. J. Appl. Bact. 1989, 66, 365–378.
- Fooks, L.J.; Fuller, R.; Gibson, G.R. Prebiotics, probiotics and human gut microbiology. International Dairy Journal. 1999,9:53-61.
- Gibson, G. R.; Saavedra, J. M.; Macfarlane, S; Macfarlane, G. T. Gastrointestinal microbial disease. In *R. Fuller, Probiotics 2: application and practical aspects*.1997. 10-39). Andover: Chapman & Hall.
- Grant, P. G.; Phillips, T. D. Isothermal Adsorption of Aflatoxin B1 on HSCAS Clay J. Agric. Food Chem. 1998, 46, 599-605 .
- Grce, M.; Pavelic, K. Antiviral properties of clinoptilolite. Microporous and Mesoporous Materials. 2005, 79, 165–169.
- Goldin, B. R.; Gorbach, S. L. Alterations of the intestinal microflora by diet, oral antibiotics and Lactobacillus: decreased production of free amines from

aromatic nitro compounds, azo dyes and glucorinides. *Journal of the National Cancer Institute*. 1984,73, 689-695.

Göktaş, S.; Ülkü, S.; Bayraktar, O. Clinoptilolite Rich Mineral as a Novel Carrier for the Active Constituents Present in Ginkgo Biloba Leaf Extract. *Applied Clay Science*, 2007, 40, 6-14.

Gottardi, G.; Galli, E. *Natural Zeolites*, Springer-Verlag, Berlin, 1985.

Gu, B.; Schmitt, J.; Chen, Z.; Liang, L.; McCarthy, J. F. Adsorption and Desorption of Natural Organic Matter on Iron Oxide: Mechanisms and Models. *Environ. Sci. Technol.*1994, 28, 38-46.

Guemonde, M.; Salminen, S.. New methods for selecting and evaluating probiotics. *Digestive and Liver Disease*.2006, 38, 242-247.

Hall, K.R.; Eagleton, L.C.; Acrivos, A.; Vermeulen, T. Pore-and Solid-Diffusion Kinetics in Fixed Bed Adsorption Under Constant-Pattern Conditions. *Indian Eng. Chem. Fund.* 1966, 5, 212-223.

Havenaar, R.; Veld, J.H.J. Probiotics: A General View. In *Wood Ed. The Lactic Acid Bacteria* Vol.1 Elsevier Science, Pub. BJB London,1992.

Halpern, G. M.; Vruwink, K. G.; Van de Water, J.; Keen, C. L.; Gershwin, M. E. Influence of long-term yoghurt consumption in young adults. *International Journal of Immunotherapy*.1991, 7, 205-210.

Han, R.; Jingjing Zhang, J; Han, P; Wang, Y; Zhao, Z; Tang. M. Study of equilibrium, kinetic and thermodynamic parameters about methylene blue adsorption onto natural zeolite *Chemical Engineering Journal*.2009,145, 496–504,

Haskard, C. A.; Hani S. El- Nezami, H. S.; Kankaanpaa, P. E.; Salminen, S; Ahokasi, J. T. Surface binding of aflatoxin B1 by Lactic Acid Bacteria *Applied and Environmental Microbiology*. 2001, 3086–3091.

Hassan, N. M.; Rasmussen, P. E.; Dabek-Zlotorzynska, E; Celo, V; Chen, H. Analysis of environmental samples using microwave-assisted acid digestion and inductively coupled plasma mass spectrometry: maximizing total element recoveries. *Water Air Soil Pollut* .2007,178:323–334.

- Hernandez-Mendoza, A; Garcia, H.S; Steele , J.L. Screening of *Lactobacillus casei* strains for their ability to bind aflatoxin B1 Food and Chemical Toxicology.2009, 47, 1064–1068.
- Ho, Y. S. ; McKay, G. Pseudo-second order model for sorption processes Process Biochemistry.1999, 34, 451-465.
- Ho, Y. S.; Ng, J. C.Y.; Mc Kay, G. Kinetics of Pollutant Sorption by Biosorbent:Review. Separation and Purification Methods. 2000, 29, 189-232.
- Ho, Y.S.; McKay, G. A. Comparison of Chemisorption Kinetic Models Applied to pollutant Removal on Various Sorbents. Trans. Inst. Chem. Eng. 1998, 76B,332–340.
- Hoque, M.Z.; Akter,F ; Hossain, K.M. ; Rahman, M.S.M ; Billah , M.M.; Islam, K.M.D. Isolation, Identification and Analysis of Probiotic Properties of *Lactobacillus* Spp. From Selective Regional Yoghurts. World Journal of Dairy & Food Sciences. 2010,5, 39-46.
- Huwig, A.; Freimund, S.; Kappeli, O.; Dutler,H. Mycotoxin Detoxication of Animal Feed by Different Adsorbents. Toxicology Letters. 2001, 122, 179–188.
- Isolauri, E.; Juntunen, M.;Rautanen, T;Sillanaukee, P.; Koivula, T. A. Human *Lactobacillus* strain (*Lactobacillus* GG) promotes recovery from acute diarrhoea in children. Pediatrics, 1991, 88, 90-97.
- Isolauri, E.;Salminen,S.; Ouwehand, A. C. Probiotics. Best practice and Research Clinical Gastroenterology.2004, 18, 299-313.
- Kärger, J.; Ruthven, D. M. *Diffusion in Zeolites and Other Microporous Solids*, JohnWiley and Sons: New York; 1992.
- Kavitha, D.; Namasivayam, C. Experimental and Kinetic Studies on Methylene Blue Adsorption by Coir Pith Carbon. BioresourceTtechnology. 2007, 98(1), 14-21.
- Kennedy, M. J. ; Volz, P. A. Ecology of *Candida albicans* gut colonisation: Inhibition of *Candida* adhesion, colonisation and dissemination from the gastrointestinal tract by bacterial antagonism. Infection and Immunity, 985, 49, 654-663.

- Korkuna, O.; Leboda, R.; Skubiszewska-Zięba, J.; Vrublevska, T.; Gunko, V. M.; Ryzkowski, J. Structural and Physicochemical Properties of Natural Zeolites: Clinoptilolite and Mordenite. *Microporous Mesoporous Mater.* 2006, 87, 243-254.
- Kew M. C. Synergistic interaction between aflatoxin B1 and hepatitis B virus in hepatocarcinogenesis. *Liver Int.* 2003,2,405-409.
- Kinouchi, T.; Kataoka, K.; Ruo Bing, S.; Nakayama, H.; Uejima, M.; Shimono, K.; Kuwahara, T.; Akimoto, S.; Hiraoka, I.; Ohnishi, . Culture supernatants of *Lactobacillus acidophilus* and *Bifidobacterium adolescentis* repress ileal ulcer formation in rats treated with a non-steroidal anti-inflammatory drug by suppressing unbalanced growth of aerobic bacteria and lipid peroxidation. *Microbiology and Immunology.* 1998, 42, 347-355.
- Ko, D.C.K.; Porter, J.F.; Mc Kay, G. Film Pore Diffusion Model For The Fixed-Bed Sorption of Copper and Cadmium Ions onto Bone Char. *Wat.Res.* 2001,35,3876-3886.
- Kulkarni, N.; Reddy, B. S. Inhibitory effect of *Bifidobacterium longum* cultures on the azoxymethane-induced aberrant crypt foci formation and fecal bacterial β -glucuronidase. In *Proceedings of the Society for Experimental Biology and Medicine.* 1994, 207, 278-283.
- Lam, A.; Sierra, L. R.; Rojas, G.; Rivera, A.; Rodriguez-Fuentes, G.; Montero, L. A. Theoretical Study of the Physical Adsorption of Aspirin on Natural Clinoptilolite. *Microporous Mesoporous Mater.* 1998, 23, 247-252.
- Lilley, D.M.; Stilwell, R. H. Probiotics: Growth promoting factors produced by microorganisms. *Science* 1965,147,747-748.
- Lee, Y.K.; El-Nezami, H.; Haskard, C.A.; Puong, S. G. K.Y.; Salminen, S.; Mykkanen, H. Kinetics of Adsorption and Desorption of Aflatoxin B1 by Viable and Nonviable Bacteria. *Journal of Food Protection.* 2003, 66(3), 426-430.
- Lewis, L.; Onsongo, M.; Njapau, H.; Schurz-Rogers, H.; Lubber, G.; Kieszak, S.; Nyamongo, J.; Backer, L.; Dahiye, A. M.; Misore, A.; DeCock, K.; Rubin, C. Aflatoxin Contamination of Commercial Maize Products during an Outbreak of Acute Aflatoxicosis in Eastern and Central Kenya *Environmental Health Perspectives.* 2005, 113(12).

- Maiti, A.; Sharma, H.; Basu J.K.; De, S. Modeling of Arsenic Adsorption Kinetics of Synthetic and Contaminated Groundwater on Natural Laterite. *Journal of Hazardous Material*. 2009, 172, 928-934.
- Martin-Kleiner, I., Flegar-Mestric, Z., Zadro, R., Breljak, D., Janda, S. S., Stockovic,. The effect of zeolite clinoptilolite on serum chemistry and hematopoiesis in mice. *Food and Chemical Toxicology*.2001, 39, 717-727.
- Malash,G. F; El-Khaiaryi M. I. Piecewise linear regression: A statistical method for the analysis of experimental adsorption data by the intraparticle-diffusion models *Chemical Engineering Journal*. 2010, 163, 256–263
- Martin,R.;Jimenez, E.;Olivares,M.; Marin,M.L.; Fernandes,L.;Xaus,J.; Rodriguez, J. M. *Lactobacillus salivarius* CECT 5713, a potential probiotic strain isolated from infant feces and breast milk mother-child pair. *International Journal of Food Microbiology*.2006,112,35-43.
- Mathews, A. P.; Weber, W. J. Effects of external mass transfer and intraparticle diffusion on adsorption rates in slurry reactors.1977, *AICHE symposium series*,91-98.
- McFarland, L. V.;Surawicz, C. M., Greenberg, R. N.; Fekerty, R., Elmer, G. W.; Moyer, K. A. A randomised placebocontrolled trial of *Saccharomyces boulardii* in combination with standard antibiotics for *Clostridium difficile* disease. *Journal of the American Medical Association*.1994, 271, 1913-1918.
- McFarland, L. V.; Surawicz, C. M.; Greenberg, R. N.; Elmer, G. W.; Moyer, K. A.; Melcher, S. A.; Bowen, K. E.; Cox, J. L. .Prevention of b-lactam-associated diarrhoea by *Saccharomyces boulardii* compared with placebo. *American Journal of Gastroenterology*. 1995, 90, 439-448.
- McIntosh, G. H. Probiotics and colon cancer prevention. *Asia Pacific Journal of Clinical Nutrition*, 1996,5, 48-52.
- Miazzo, R; Rosa, C.A.R; Carvalho, E.C.D ; C Magnoli,C ; Chiacchiera, S. M; G Palacio, G ;M Saeuz,M ; Kikot, A ; Baseldella, E;Delcero, A. Efficacy of synthetic zeolite to reduce the toxicity of aflatoxin in broiler chicks *Poultry Sci* 2000, 79,1–6.
- Morata,V. A.;Gusils,C. H.;Gonzalez,S. N.Classification of the Bacteria traditional in *Encyclopedia of Food Microbiology* edited by C. Batt,P. Patel,R.Robinson (Academic Press, United Kingdom).1999,173-183.

- Mourad, K; Karam Nour-Eddine, K. In vitro preselection criteria for probiotic lactobacillus plantarum strains of fermented olives origin. *International Journal of Probiotics and Prebiotics*. 2006, 1, 27-32.
- Mumpton, F. A. *La roca magica: Uses of Natural Zeolites in Agriculture and Industry*. PNAS. 1999, 96, 3463-3470.
- Mumpton, F.A. *Using Zeolites in Agriculture*. Innovative Biological Technologies for Lesser Developed Countries, Washington, DC: U.S. Congress, Office of Technology Assessment, OTA-13P-F-29, July 1985; Elfring C
- Nakamura, T.; Ishikawa, M.; Hiraiwa, T.; Sato, J. X-Ray Diffractometric Determination of Clinoptilolite in Zeolite Tuff using Multiple Analytical Lines. *Anal. Sci*. 1992, 8, 539-543.
- Nassar, M. M.; Magdy. Y. H.; Daifullah. A. H. ; Kelany, H. Mass transfer and adsorption kinetics of phenolic compounds onto activated carbon prepared from rice husk.2008, *Adsorption Science & Technology*,26, 3, 157-167.
- Nair, P.S. ;Surendran, P.K. Biochemical characterization of lactic acid bacteria isolated from fish and prawn.*Journal of Culture Collections*. 2004, 4, 48-52.
- Narin, G. Nitrogen monoxide storage and release properties of local natural zeolite for biological applications. Doctoral Dissertation, Izmir Institute of Technology, 2009.
- Narin,G.;Bulut Albayrak, Ç.; Ülkü, S. Antibacterial and bactericidal activity of nitric oxide-releasing natural zeolite. *Applied Clay Science*.2010, 50: 4, 560-568.
- Nesbit B. F.; O'Kelly J.; Sargeant K.; Sheridan A. Toxic metabolites of *Asergillus flavus*. *Nature*. 1962,195,1062-1063.
- Oguz, H.; Keçeci,T ;Birdane, Y.O; Önder, F; Kurtoğlu, V. Effect of clinoptilolite on serum biochemical and haematological characters of broiler chickens during aflatoxicosis. *Research in Veterinary Science*.2000, 69, 89–93
- Ortatlı, M.; Oğuz, H. Ameliorative effects of dietary clinoptilolite on pathological changes in broiler chickens during aflatoxicosis. *Research in Veterinary Science*, 2001,71, 59-66.

- Ouwehand, A.C.; Kirjavainen, P.V.; Short, C.; Salminen, S. Probiotics: mechanisms and established effects. *International Dairy Journal*. 1999, 43-52.
- Pavelic, K.; Hadzija, M.; Bedrica, L.; Pavelic, J.; Dikic, I.; Katic, M.; Kralj, M.; Bosnar, M. H.; Kapitanovic, S.; Poljak-Blazi, M.; Krizanac, S.; Stojkovic, R.; Jurin, M.; Subotic, B.; Colic, M. Natural Zeolite Clinoptilolite: New Adjuvant in Anticancer Therapy. *J. Mol. Med.* 2001, 78, 708-720.
- Pavelic, K.; Katic, M.; Sverko, V.; Marotti, T.; Bosnjak, B.; Balog, T.; Stojkovic, R.; Radacic, M.; Colic, M.; Poljak-Blazi, M. Immunostimulatory Effect of Natural Clinoptilolite as a Possible Mechanism of Its Antimetastatic Ability. *J. Cancer Res. Clin. Oncol.* 2002, 128, 37-44.
- Papaioannou D., S.; Kyriakis S. C.; Papasteriadis A.; Roubies N., Yannakopoulos A.; Alexopoulos C.. A field study on the effect of in-feed inclusion of a natural zeolite (clinoptilolite) on health status and performance of sows/gilts and their litters. *Research in Veterinary Science*. 2002, 72, 51-59.
- Papaioannou, D. S.; Kyriakis, C. S.; Alexopoulos, C.; Tzika, E. D.; Polizopoulou, Z. S.; Kyriakis, S.C. A field study on the effect of the dietary use of clinoptilolite-rich tuff, alone or in combination with certain antimicrobials, on the health status and performance of weaned, growing and finishing pigs. *Research in Veterinary Science*. 2004, 76, 19-29.
- Pavelic, K.; Hadzija, M.; Bedrica, L.; Pavelic, J.; Dikic, I.; Katic, M. Natural zeolite clinoptilolite: new adjuvant in anticancer therapy. *Journal of Molecular Medicine*. 2001, 78, 708-720.
- Pavelic, K.; Hadzija, M. *Medical Applications of Zeolites*. In S. M. Auerbach, K. A., Carrado, P. K. Duuta (Ed.), *Handbook of Zeolite Science and Technology* (pp. 143; 1174). C.R: Taylor & Francis CRC Press. 2003.
- Peraica M.; Radic B.; Lucic A.; Pavlovic M. Toxic effects of mycotoxins in humans. *Bull World Health Organ* .1999, 77, 754-766.
- Pinto, M.G.V; Franz, C. M.A.P.; Schillinger, U; Holzapfel, W H. Lactobacillus spp. with in vitro probiotic properties from human faeces and traditional fermented products. *International Journal of Food Microbiology* .2006, 109, 205-214.

- Peltonen, D. K.; El-Nezami, H. S.; Salminen, S. J.; Ahokas, J. T. Binding of aflatoxin B1 by probiotic bacteria. *Journal of the Science of Food and Agriculture* 2000, 80, 1942-1945.
- Peltonen, K.; El-Nezami, H.; Haskard, C.; Ahokas, J.; Salminen, S. Aflatoxin B1 binding by dairy strains of Lactic Acid Bacteria and Bifidobacteria. *J. Dairy Sci.* 2001, 84, 2152-2156.
- Pitt J. I. Toxigenic fungi and mycotoxins. *Br Med Bull.* 2000, 56, 184-192.
- Plazinski, W.; Rudzinski, W.; Plazinska, A. Theoretical Models of Sorption Kinetics Including a Surface Reaction Mechanism: A review. *Advances in Colloid and Interface Science.* 2009, 152, 2-13.
- Qiu, H.; Lv, L.; Pan, B.C.; Zhang, Q.J.; Zhang, W.M.; Zhang, Q.X. Critical Review in Adsorption Kinetic Models. *Journal of Zhejiang University-Science A*, 2009, 10 (5), 716-724.
- Petrolekas, P. D.; Maggenakis, G. Kinetic Studies of the Liquid-Phase Adsorption of a Reactive Dye onto Activated Lignite. *Ind. Eng. Chem. Res.* 2007, 46, 1326-1332.
- Reichenberg, D. Properties of ion exchange resins in relation to their structure. III. Kinetics of exchange, *J. Am. Chem. Soc.* 1953, 75, 589-597.
- Reddy, B. S. Prevention of colon cancer by pre- and probiotics: evidence from laboratory studies. *British Journal of Nutrition*, 1998, 80, S219-S223.
- Rivera, A.; Farias, T. Clinoptilolite-surfactant composites as drug support: a new potential application. *Microporous and Mesoporous Materials*, 2005, 80, 337-346.
- Rivera, A.; Farias, T.; Ruiz-Salvador, A. R.; de Menorval, L. C. Preliminary characterization of drug support systems based on natural clinoptilolite. *Microporous and Mesoporous Materials*. 2003, 61, 249-259.
- Rivera, A.; Rodriguez-Fuentes, G.; Altshuler, E. Characterization and neutralizing properties of a natural zeolite/Na₂CO₃ composite material. *Microporous and Mesoporous Materials*. 1998, 24, 51-58.

- Rivera, A.; Rodríguez-Fuentes, G.; Altshuler, E. Time evolution of a natural clinoptilolite in aqueous medium: conductivity and pH experiments. *Microporous and Mesoporous Materials*.2000, 40, 173–179.
- Rivera-Garza, M.; Olgúin, M. T.; García-Sosa, I.; Alcántara, D.; Rodríguez-Fuentes, G. Silver Supported on Natural Mexican Zeolite as an Antibacterial Material. *Microporous Mesoporous Mater.* 2000, 39, 431-444.
- Rodríguez-Fuentes, G.; Barrios, M. A.; Iraizoz, A.; Perdomo, I.; Cedre, B. Enterex: Anti-diarrheic Drug Based on Purified Natural Clinoptilolite. *Zeolites*. 1997, 19, 441-448.
- Rodríguez-Fuentes, G., Rivera, A., Alvarez, M.A.B., Colarte, A.I. Antacid drug based on purified natural clinoptilolite. *Microporous and Mesoporous Materials*. 2006, 94,200–207.
- Rowland, I. R.; Rumney, C. J.; Coutts, J. T.; Lievens, L. C. Effect of *Bifidobacterium longum* and inulin in gut bacterial metabolism and carcinogen-induced aberrant crypt foci in rats. *Carcinogenesis*. 1998,19, 281-285.
- Ruthven, D. M. *Principles of Adsorption and Adsorption Processes*, John Wiley and Sons: New York; 1984.
- Ryan, K.A.; Jayaraman,T.; Daly,P; Canchaya, C.; Curran, S.; Fang, F., Quigley E.M. ;O'Toole, P.W. Isolation of lactobacilli with probiotic properties from the human stomach. *Letters in Applied Microbiology*.2008, 47 (4), 269-274.
- Sağ, Y.,; Aktay, Y. Mass transfer and equilibrium studies for the sorption of chromium ions onto chitin. *Process Biochemistry*.2000, 36, 157-173.
- Salameh,Y; Al-Lagtah, N; Ahmad, M.N.M; Allen, S.J.;Walker, G.M. Kinetic and thermodynamic investigations on arsenic adsorption onto dolomitic sorbents. *Chemical Engineering Journal*. 2010,160, 440–446.
- Sarkar, M., Acharya, P. K. & Bhattacharya, B. Modeling the adsorption kinetics of some priority organic pollutants in water from diffusion and activation energy parameters. *Journal of Colloid and Interface Science*.2003, 266, 28–32.
- Sanders, M.E. Probiotics: Considerations for human health. *Nutr. Rev.*2003, 61,91-99.

- Schaafsma, G.; Meuling, W. J. A.; van Dokkum, W.; and Bouley, C. Effects of a milk product, fermented by *Lactobacillus acidophilus* and with fructo-oligosaccharides added, on blood lipids in male volunteers. *European Journal of Clinical Nutrition*. 1998,52, 436-440.
- Suzuki, M. *Adsorption Engineering*. Elsevier , Tokyo. 1990.
- Surawicz, C. M.; Elmer, L. W.; Speelman, P.; McFarland, L. V., Chinn, J.; van Belle, G. . Prevention of antibiotic-associated diarrhea by *Saccharomyces boulardii*: a prospective study. *Gastroenterology*. 1989, 96, 981-988.
- Sverko, V.; Soboanec, S.;Balog, T.; Colic, M.; Marotti, T. Natural Micronised Clinoptilolite andClinoptilolite Mixtures with *Urtica dioica* L. Extract as Possible Antioxidants. *Food Technology and Biotechnology*.2004, 42 (3) ,189–192.
- Sze, M. F. F.; McKay, G.An adsorption diffusion model for removal of par-chlorophenol by activated carbon derived from bituminous coal*Environmental Pollution* .2010,158, 1669–1674.
- Talarico, T. L.; Dobrogosz, W. J. Chemical characterisation of an antimicrobial substance produced by *Lactobacillus reuteri*. *Antimicrobial Agents and Chemotherapy*.1989, 33,674-679.
- Tateo, F.; Summaa,V.; Bonelli,C. G.;Bentivenga,G Mineralogy and geochemistry of herbalist’s clays for internal use:simulation of the digestive process. *Applied Clay Science*. 2001,20, 97–109.
- Tomoda, T.; Nakano, Y.; Kageyama, T. Variation of intestinal *Candida* of patients with leukaemia and the effect of *Lactobacillus* administration. *Japanese Journal of Medicinal Mycology*. 1983, 24,356- 358.
- Todorov, S. D.; Botes, M.; Guigas,C.; Schillinger, U.; wiid, I.; Wachman,M.B.; Holzaphel,W.H.; Dicks ,L.M.T. Boza ,a natural source of probiotic lactic acid bacteria. *Journal of Food Microbiology*.2008,104, 465-467.
- Tomasevic, M.; Dakovic, M;; Markovic, V.; Stoji, D. The effect of exchangeable cations in clinoptilolite and montmorillonite on the adsorption of aflatoxin B1. *J.Serb.Chem.Soc*. 2001, 66(8),555–561.
- Top, A.; Ülkü, S. Silver, Zinc, and Copper Exchange in a Na-clinoptilolite and Resulting Effect on Antibacterial Activity. *Appl. Clay Sci*. 2004, 27, 13-19.

- Tomasevic-Canovic, M ; Dakovic, A; Markovic ,V; Radosavljevic-Mihajlovic, A; Vukicevic. Adsorption effects of mineral adsorbents; Part III: Adsorption behaviour in the presence of vitamin B6 and microelements J . Acta Veterinaria. 2000, 50, 23–29.
- Tsitsishvili, G. V.; Andronikashvili, T. G.; Kirov, G. N.; Filizova, L. D. *Natural Zeolites*, Ellis Horwood: New York, 1992.
- Türk Gıda Kodeksi Tebliğ . Gıda maddelerinde belirli bulas anların maksimum seviyelerinin bulunması hakkında tebliğ . Resmi gazete, 23 Eylül 2002, sayı: 24885, Ankara, Başbakanlık Basımevi.2002.
- Ülkü, S.A.; Mobedi, M. Adsorption in Energy Storage. In *Energy Storage Systems*; Kakaç, S., Kilkış, B. Eds.; Kluwer Academic Publishers: Netherlands, 1989, p 87-507.
- Ülkü, S. Heat and Mass Transfer in Adsorbent Beds. In *Convective Heat and Mass Transfer in Porous Media*; Kakaç, S., Kilkış, B., Kulakci, F. A., Arınç, F., Eds.; NATO Series; Kluwer Academic Publishers: Dordrecht, 1991, p 695
- Vadivelan, V.; Kumar, V. K. Equilibrium, kinetics, mechanism, and process design for the sorption of methylene blue onto rice husk. *Journal of Colloid and Interface Science*. 2005, 286, 90–100.
- Wang, H.L.; Fei, Z. H.; Chen, J. L.; Zhang, Q. X.; Xu, Y.H. Adsorption thermodynamics and kinetic investigation of aromatic amphoteric compounds onto different polymeric adsorbents *Journal of Environmental Sciences*. 2007, 19, 1298–1304.
- World Health Organization(WHO) Trace Elements in Human Nutrition and Health. 1996, Geneva, 343 pp.
- Wilkin, R. T.; Barnes, H. L. Thermodynamics of Hydration of Na- and K-clinoptilolite to 300 °C. *Phys. Chem. Miner.* 1999, 26, 468-476.
- Williams J. H.; Phillips T. D., Jolly P. E.; Stiles J. K.,; Jolly C. M.,; Aggarwal D. Human aflatoxicosis in developing countries: a review of toxicology, exposure, potential health consequences, and interventions. *Am J Clin Nutr.* 2004, 80, 1106-1122.
- Yang, R. T. *Adsorbents: Fundamentals and Applications* , John Wilwy & Sons Inc., USA., 2003.

Yang, R. T. *Gas Separation by Adsorption Processes*, Imperial College Press: UK, 1997

Zarkovic, N.; Zarkovic, K.; Kralj, M.; Borovic, S.; Sabovlovic, S.; Blazi M. P. Anticancer and antioxidative effects of micronized zeolite clinoptilolite. *Anticancer Research*. 2003, 23, 1589-1596.

APPENDIX A

CHEMICALS

Table A.1. Chemicals used during the study

No	Chemical	Code
1	MRS Broth	Merck 1.10661
2	Bacteriological Pepton	Oxoid LP037
3	Agar	AppliChem A0949
4	D(-) Mannitol	AppliChem A1903
5	D(+) Sucrose	AppliChem A2211
6	Fructose-	AppliChem A3688
7	D(-) Salicin	Fluka 84150
8	Fructose-	AppliChem A3688
9	Mannose	Aldrich 11,258-5
10	(D+) Raffinose	AppliChem A6882
11	Arabinose	Aldrich A,9190-6
12	Trehalose	Merck 1.08216
13	(D-) Ribose	Merck 1.07605
13	L-Arginine hydrochloride	AppliChem A3709
15	D(+) Glucose	AppliChem A3666
16	D(+) Lactose	Sigma L3750
17	D(+) Maltose Monohydrate	AppliChem A3891
18	D(+) Galactose	Aldrich 11259-3
19	D(+) Xylose	Merck 1.08689
20	D(+)Melesitose	Sigma M5375
21	L Rhamnose	AppliChem A4336
22	Melibiose	Sigma M5500
23	Sodium hydroxide	Merck 1.06498
24	Glycerol	AppliChem A2926
25	Potassium iodide	Sigma C6757
26	Bromcresol purple	Merck 1.03025
27	Hyrogen peroxide (%30)	Merck 1.07209
28	Bile salt	Oxoid LP0055

Table A.2. Carbohydrates used in biochemical identification

1. D(+) Xylose
2. D(-) Ribose
3. Melezitose
4. L(+) Arabinose
5. Mannitol
6. D(+) Trehalose
7. Melibiose
8. Raffinose
9. D(+) Galactose
10. Maltose
11. Sucrose
12. D(+) Mannose
13. Fructose
14. Lactose
15. Rhamnose
16. Sorbitol
17. Glucose
18. D(-) Salicin Sugar solution prepared at concentration 5%

APPENDIX B

TEST MEDIA RECIPES

B.1. Test Media for Gas Production from Glucose

Ingredients	g/l
Pepton	10.0
Lab-Lemco meat extract	10.0
Yeast Extract	5.0
D(-) Glucose	20.0
Tween 80	1ml
K ₂ HPO ₄	2
Sodium acetate	5.0
MgSO ₄ .7H ₂ O	0.2
MnSO ₄ .4H ₂ O	0.05
Deionized water	1000ml

All ingredients were dissolved in deionized water and pH was adjusted to 5.6. Medium was dispensed into test tubes and inverted durham tubes were distributed to each test tube, and lastly sterilized by autoclaving at 121°C for 15 min.

B.2. Test media for Growth at Different Temperatures

Ingredients	g/l
Pepton	10.0
Lab-Lemco meat extract	10.0
Yeast Extract	5.0
D(-) Glucose	20.0
Tween 80	1ml
K ₂ HPO ₄	2
Sodium acetate	5.0
Triammonium citrate	2.0
MgSO ₄ .7H ₂ O	0.2
MnSO ₄ .4H ₂ O	0.05
Bromcresol purple	0.04

Deionized water 1000ml

All ingredients were dissolved in deionized water and pH was adjusted to 5.6. Medium was dispensed into test tubes and sterilized by autoclaving at 121°C for 15 min.

B.2. Test Media for Growth at Different NaCl Concentration

Ingredients	g/l
Pepton	10.0
Lab-Lemco meat extract	10.0
Yeast Extract	5.0
D(-) Glucose	20.0
Tween 80	1ml
K ₂ HPO ₄	2
Sodium acetate	5.0
Triammonium citrate	2.0
MgSO ₄ .7H ₂ O	0.2
MnSO ₄ .4H ₂ O	0.05
Bromcresol purple	0.04
NaCl	65 (for NaCl 6.5%)
Deionized water	1000ml

All ingredients were dissolved in deionized water and pH was adjusted to 5.6. Medium was dispensed into test tubes and sterilized by autoclaving at 121°C for 15 min.

B.4. Arginine MRS

Ingredients	g/l
Peptone	10.0
Yeast extract	5.0
Tween 80	1 ml
K ₂ HPO ₄	2
Sodium acetate	5.0
Triammonium citrate	2.0
MgSO ₄ .7H ₂ O	0.2
MnSO ₄ .4H ₂ O	0.05
Arginine	1.5

Deionized water 1000ml

All ingredients were dissolved in deionized water and pH was adjusted to 5.6. Medium was sterilized by autoclaving at 121°C for 15 min.

B.5. Modified MRS for Carbohydrate Fermentations

Ingredients	g/l
Pepton	10.0
Lab-Lemco meat extract	10.0
Yeast Extract	5.0
Tween 80	1ml
K ₂ HPO ₄	2
Sodium acetate	5.0
Triammonium citrate	2.0
MgSO ₄ .7H ₂ O	0.2
MnSO ₄ .4H ₂ O	0.05
Bromcresol purple	0.04
Deionized water	1000ml

All ingredients were dissolved in deionized water and pH was adjusted to 5.6. Medium was sterilized by autoclaving at 121°C for 15 min.

APPENDIX C.

HPLC OPERATION SPECIFICATIONS

Table C.1. Operating conditions and properties of High Performance Liquid Chromatography(HPLC) for Aflatoxin B1 analysis

Property	Values or Attributes
Column type	C18 Hypersil ODS
Column Length	250 mm
Column Diameter	4.6 mm
Particle Size	5 μm
Mobile Phase	Isocratic mobil phase Water:methanol: acetonitrile(60:20:20)
Flow Rate	1 ml/min
Temperature	40 °C
Detector	FLD
Absorbance	Excitation 362 nm Emission 455 nm

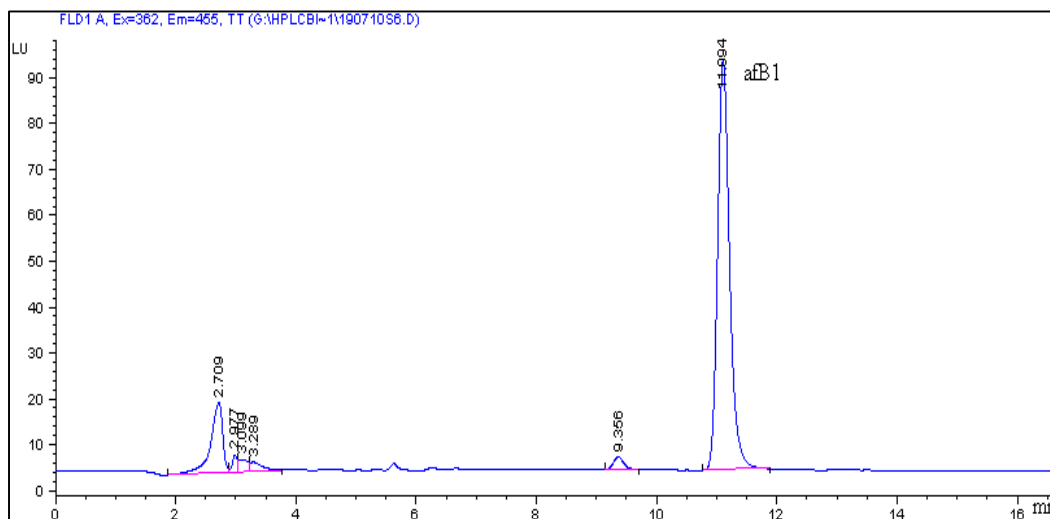


Figure C.1. HPLC chromatogram of the afB1 standard.

APPENDIX D

CALIBRATION CURVES

D.1. Calibration Curve prepared for the Quantitative Mineralogical Analysis for the Nakamura's Method

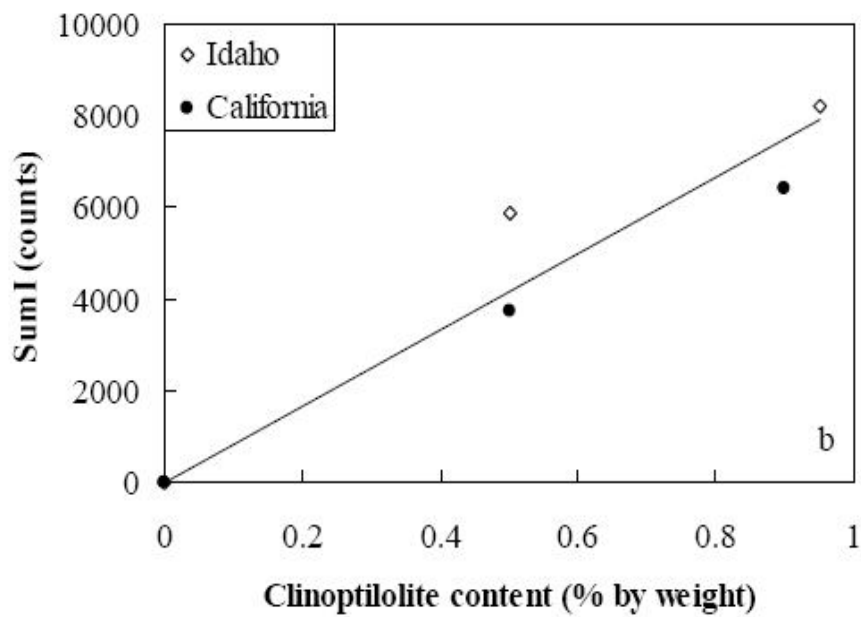


Figure D.1. Calibration curve for quantitative mineralogical analysis by using two reference mineral of the clinoptilolite.(Narin, 2009).

D2. Calibration Curve Prepared for Aflatoxin B1 Analysis by HPLC

Calibration curve of afB1 standards were used for the quantitative analyses . For this purpose, 25 ppm afB1 standard solution in acetonitrile was used and the standard solutions in the concentration of 1.25, 0.625, 0.313, 0.156, 0.078, 0.039 $\mu\text{g}/\text{mL}$ were prepared by using the PBS (pH 7.3) solution .The area versus concentration curve was plotted to form a calibration curve.

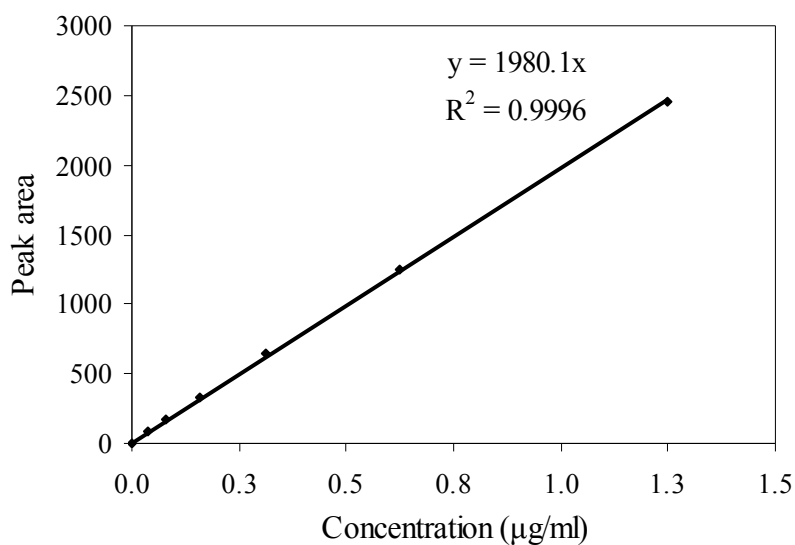


Figure D.2. Calibration curve for afB1 during HPLC analysis.

Çisem BULUT ALBAYRAK

Date of Birth: 05.02.1977

Place of Birth: Manisa

Citizenship: Turkish

EDUCATION

[1993-1998] B.Sc. (Food Engineering)

Ege University

Department of Food Engineering, Izmir, Turkey

Dissertation: Chemical degradations and reactions in fishes

[2000-2003] M.Sc. (Biotechnology Programme)

İzmir Institute of Technology

Department of Food Engineering, İzmir, Turkey

Dissertation: Isolation and molecular characterization of lactic acid bacteria from cheese.

[2003-2012] Ph.D. (Chemical Engineering)

İzmir Institute of Technology

Department of Chemical Engineering, İzmir, Turkey

Dissertation: Adsorptive characteristics of aflatoxin B1 in the presence of purified clinoptilolite rich mineral and *Lactobacillus plantarum* S2.

PUBLICATIONS

Narin,G., Bulut Albayrak, Ç., Ülkü, S."Antibacterial and bactericidal activity of nitric oxide-releasing natural zeolite".Applied Clay Science, 50: 4, 560-568, 2010.

Bulut, C.; Altıok, E.; Bayraktar, O.; Ülkü, S. Antioxidative and Antimicrobial Screening 19 Commercial Essential Oils in Turkey. Proceedings Of The First International Medicinal And Aromatic Plants Conference On Culinary Herbs, 826, 111-116, 2009.

Altıok, E.; Asbagh, L. A., Bulut, Ç.; Ülkü, S.; Bayraktar, O. Antioxidant, Antimicrobial and Cytotoxic Activities of Some Turkish Plant Extracts , Febs. Journal, 273, 371-371, 2006.

Bulut, C., Gunes, H., Okuklu, B., Harsa, S., Kilic, S., Coban, H.S., Yenidunya, A.F. “ Homofermentative Lactic Acid Bacteria of Traditional Cheese, Çömlek Peyniri, from Cappadocia Region” Journal of Dairy Research, 72:1 ,19-24, 2005.

Yavuz, E., Güneş, H., Harsa, Ş., Bulut, Ç. A.F. Yenidünya. “Optimization of pulsed field gel electrophoresis (PFGE) conditions for thermophilic Bacillus.” World Journal Microbiology & Biotechnology, 20: 871–874, 2004.

Yavuz, E., Güneş, H., Bulut, Ç., Harsa, Ş., A.F. Yenidünya Yavuz, E., H. Güneş, Ç. Bulut, Ş. Harsa, A.F. Yenidünya. RFLP of 16 rDNA-ITS region to differentiate Lactobacilli at species level. World Journal of Microbiology & Biotechnology 20, 535-537 ,2004.